ENGINEERING OF A SPECIFIC BINDING SITE FOR PROTEIN LABELLING WITH LUMINESCENT LANTHANIDE COATED NANOPARTICLES: A STUDY OF PROTEIN LABELLING AND NANOPARTICLE-PEPTIDE INTERACTIONS

by

KIMBERLEY ELIZABETH WRIGHT

A thesis submitted to the University of Birmingham for the degree of

DOCTOR OF PHILOSOPHY

PSIBS Doctoral Training Centre

School of Chemistry

College of Engineering and Physical Sciences

University of Birmingham

June 2014

Abstract

The work presented in this thesis investigates the use of new luminescent lanthanide complexes, both free and bound to the surface of gold nanoparticles, for protein labelling. Lanthanide complexes were shown to maintain their luminescence properties when conjugated to proteins and one complex also demonstrated participation in Förster resonance energy transfer when conjugated to a protein in an appropriate system. Furthermore, it was found that bovine serum albumin can act as a vehicle to transport luminescent lanthanide complexes into two human cell lines.

Lanthanide complexes were then used to coat 13 nm gold nanoparticles for protein labelling within cells. The aim was to find a peptide sequence to preferentially bind to gold nanoparticles which could be expressed as part of a protein of interest, acting as a binding site within the cell. The interaction of peptides with gold nanoparticles was examined using several methods and, of the sequences tested, CCPGCC was found to have the highest affinity for the nanoparticles. This peptide was expressed in HeLa cells as part of green fluorescent protein. Co-localisation of the nanoparticles with the protein in cells could not be established through fluorescence microscopy, however, cell lysis revealed green fluorescence protein associated with nanoparticle aggregates.

Acknowledgements

I feel very fortunate to have had the opportunity to conduct a doctoral research project, but I couldn't have done it alone. Firstly, I would like to thank my family for their unwavering support and encouragement throughout my PhD and always. To Mark, I would like to say a massive thank you for believing in me. I am also lucky to have a really great group of friends that were always there to help me let my hair down and forget about my PhD from time to time so thanks for being there for me.

I owe a great deal of gratitude to the entire ZP group and visiting students for offering scientific and practical advice and assistance and for helping me to keep my sanity intact! Dave and Stephen, you showed me the ropes when I arrived and were extremely patient with me which I really appreciated. Alison, Nicola, Richard, Sully, Sam, Sunil, Shiva and Dave, we shared many a good time and I feel lucky to count you amongst my friends. I also had the great opportunity to work as a member of other research groups too so I must also thank the members of both the Hannon and Rappoport groups for welcoming me and helping me out when I needed it. Thanks to Eric, Laura, Sarah and Jeni for giving up their time to show me the practicalities of biological experiments and answer my many questions. Thanks must also go to Gerard Nash and Nik Hodges for allowing me to briefly work in their labs and providing me with cells and to Serascience for allowing me the opportunity to conduct collaborative work involving the antibody FRET system. A big thanks to Pushpa for making all those hours spent sat in the dark running scans enjoyable and for offering advice and support beyond our collaborative work. I must also say how much I enjoyed carrying out my PhD as part of PSIBS, so thanks to both the students and staff because my PhD wouldn't have been the same without you.

There are many talented analytical staff that I owe a great debt of gratitude to for their assistance and support throughout my PhD. I would like to thank Neil Spencer and Peter Ashton for helping me get the best from my mass specs and NMRs and to Graham Burns and Chi Tsang for training me up in HPLC and offering some friendly chit chat to help pass the many weeks I spent in the chromatography lab!

Finally, I want to say thank you to Zoe for allowing me the opportunity to carry out my PhD and to all of my supervisors, Zoe, Mike and Josh, for mentoring me and pushing me to do my best.

Table of Contents

Figures

The following is a list of figures presented in each chapter of this thesis along with their titles and the pages on which they can be found.

Chapter 1

Chapter 2

Chapter 3

Tables

The following is a list of tables presented in this thesis along with their titles and the pages on which they can be found.

Abbreviations

The following is a list of the abbreviations used throughout this thesis along with their explanation and the page on which they are first used.

Abbreviation	Explanation	Page
AuNPs	Gold nanoparticles	1
BSA	Bovine serum albumin	27
CD	Circular dichroism	76
DCC	*N*,*N*′-Dicyclohexylcarbodiimide	98
DLS	Dynamic light scattering	118
DMF	Dimethylformamide	98
DNA	Deoxyribonucleic acid	23
DOTA	1,4,7,10-tetraazacyclododecane-1,4,7,10-tetracarboxylic acid	13
DTPA	Diethylenetriaminepentaacetic	13
ES-TOF	Electrospray - time of flight	89
FLC	Free light chain	46
Fmoc	9-Fluorenylmethoxycarbonyl chloride	119
FRET	Förster resonance energy transfer	4
GFP	Green fluorescent protein	6
HBTU	*N*,*N*,*N*′,*N*′-Tetramethyl-*O*-(1*H*-benzotriazol-1-yl)uronium hexafluorophosphate	147
HPLC	High performance liquid chromatography	51
HRMS	High resolution mass spectrometry	90
HSA	Human serum albumin	20
ICP-MS	Inductively coupled plasma - mass spectrometry	72
ICP-OES	Inductively coupled plasma - optical emission spectrometry	64

ITC	Isothermal titration calorimetry	116
mAb	Monoclonal antibody	46
MALDI-TOF	Matrix assisted laser desorption ionisation - time of flight	86
MeOH	Methanol	89
MRI	Magnetic resonance imaging	10
MS	Mass spectrometry	89
NHS	*N*-hydroxysuccinimide	43
NIR	Near infra-red	12
NMR	Nuclear magnetic resonance	51
PBS	Phosphate buffered saline	61
PMT	Photomultiplier tube	56
SPR	Surface Plasmon resonance	115
TEM	Transmission electron microscopy	25
Trt	Triphenylmethyl	119
UV-Vis	Ultra violet - visible	86
δ	Chemical shift	51
ε	Molar absorption coefficient	89
λ	Wavelength	87
λ_{em}	Emission wavelength	7
λ_{ex}	Excitation wavelength	7
τ	Luminescence lifetime	75
Φ	Luminescence quantum yield	75

1. Introduction

1.1 Background

The focus of this thesis is the exploration of protein labelling strategies *in vitro* and in cells using luminescent probes. Lanthanide complexes offer advantages over many commonly used optical probes, as discussed within this chapter, and as such are employed throughout this research. In addition to the use of lanthanide complexes as individual probes, coating of AuNPs with these complexes allows the delivery of a large number of probes to a protein of interest; the interactions of proteins and peptides with AuNPs was, therefore, also of great interest. Furthermore, the techniques routinely utilised for protein labelling in cells have their drawbacks and may not be applicable for the use of luminescent AuNPs as protein labels in cells, thus adaptation of these techniques was relevant.

1.2 Protein Labelling *In Vitro* and in Cells

Protein labelling has been carried out for many years *in vitro* and in cells with the aim of better understanding phenomena such as protein production, protein folding and protein-protein interactions, which are all of significance when studying overall cell behaviour. More recently, in the field of protein labelling within cells, efforts have been aimed at overcoming the necessity of isolating proteins before labelling and reintroducing them, Scheme 1.1. Up to now, however, the choice of label for protein tagging in cells has been limited with each having disadvantages to overcome.[1]

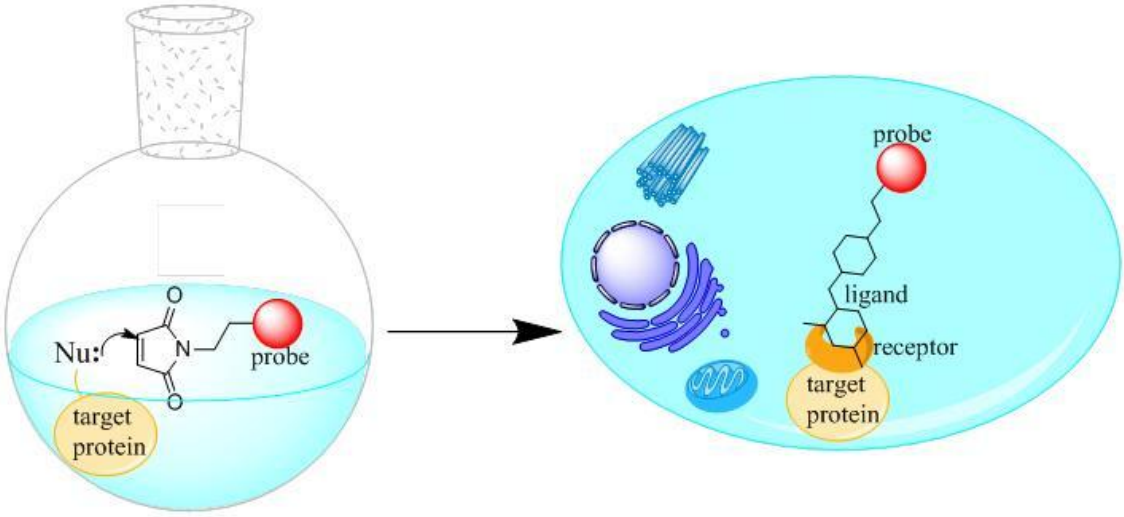

Scheme 1.1 Left: Labelling of isolated protein *in vitro*.
Right: Labelling protein inside the cell.[2]

Protein labelling *in vitro* can provide information about the conformation of a protein and its interaction with other proteins or molecules. One of the key considerations when labelling proteins is that the label, or labelling process, should not affect the structure or function of the protein of interest; in order to achieve this, labelling reactions should take place under mild conditions in aqueous solvent and using reactants that are inert to biological media and are not endogenous to biomolecules in order to prevent unwanted reactions. The advent of bioorthogonal reactions has facilitated the labelling of biomolecules such as proteins within their natural environments and without perturbing their intrinsic nature, Scheme 1.2.[3, 4] Popular chemistries used for bioorthogonal labelling include cycloaddition reactions or polar reactions such as condensation of ketones or aldehydes. Ketones and aldehydes are examples of electrophiles which are not commonly present in biomolecules which means that they can be easily targeted with an appropriate nucleophile such as an aminoxy compound or a hydrazide.[4] Many cycloaddition reactions are employed for bioorthogonal labelling purposes and include variations of Diels-Alder reactions, such as inverse electron-demand Diels-Alder

which can proceed at exceptionally fast rates under biological conditions, and copper-catalyzed azide-alkyne reactions which, unlike the uncatalysed reaction, can proceed in aqueous conditions at room temperature and provide control over the regioisomer produced.

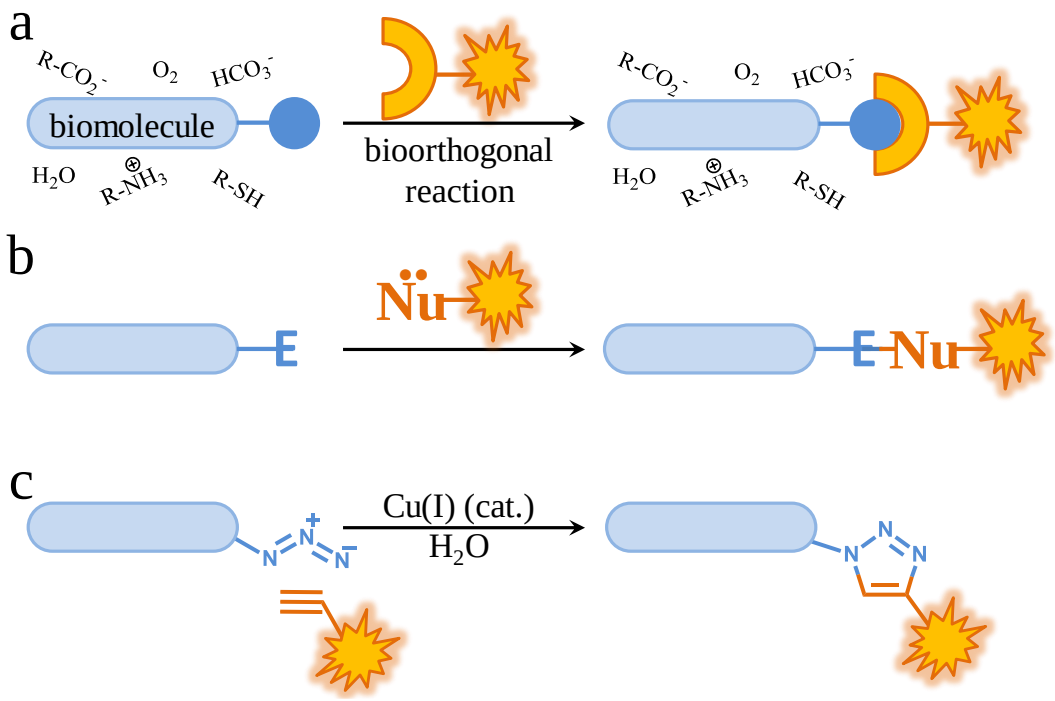

Scheme 1.2 a) Covalent labelling of a biomolecule containing a unique functional group using a complementary probe. Examples of bioorthogonal chemistries b) polar reaction between an electrophile and a nucleophile and c) a cycloaddition represented by a copper-catalyzed azide-alkyne cycloaddition.[4]

1.2.1 Genetic Modification of Proteins for Labelling *In Vitro* and at Cell Surfaces

Copper-catalyzed azide-alkyne cycloadditions, an example of so-called click chemistry, have been widely used in labelling of proteins. The modification of the amino acid pyrrolysine has allowed the utilisation of this reaction to label recombinant proteins *in vitro*. Pyrrolysine is a naturally occurring amino acid and is coded for in some archaea species, but its expression in bacteria, yeast and mammalian cells has now been established. A pyrrolysine variant with an alkyne modification was expressed as part of calmodulin. The alkyne underwent reaction with

azidocoumarin using a copper catalyst *in vitro*.[5] The coumarin dye demonstrated a vast increase in fluorescence after the cycloaddition reaction, and did not show any non-specific interactions with native calmodulin. Additionally, a cysteine residue on the recombinant calmodulin protein was labelled with Alexa Fluor 488 C5-maleimide, a potential FRET partner for the coumarin dye. The FRET efficiency of the pair increased when Ca^{2+} was introduced because the binding of the ion by calmodulin changed the conformation of the protein and reduced the distance between the two dyes, Scheme 1.3.[5]

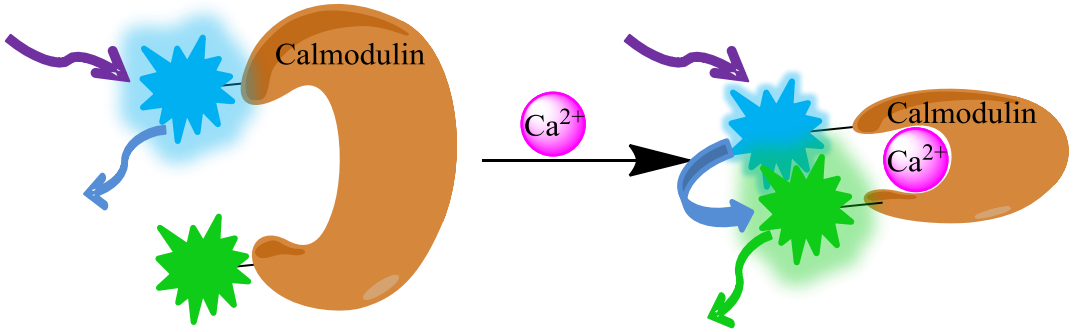

Scheme 1.3 The use of FRET to indicate the binding of Ca^{2+} by calmodulin.

A study using similar chemistry introduced a pyrrolysine residue functionalised with an azide into a protein.[6] The functionalised protein was then labelled with a rhodamine derivative bearing an alkyne group *in vitro* using a copper catalyst. The recombinant protein was also expressed in *Escherichia coli* and labelled with alkyne-coumarin, demonstrating the possibility of using the reaction for labelling proteins inside bacterial cells. Furthermore, the click reaction was used to label a recombinant protein on the surface of embryonic human kidney cells in culture. Whilst the latter study demonstrates the possibility of translating *in vitro* protein labelling techniques to studies within cells, it also highlights an obstacle to achieving this; many protein labels that have been effectively used *in vitro* are not able to

permeate the cell membrane of mammalian cells and as such can only be of use in labelling cell surface proteins unless other methods of introduction are used which may perturb the cells in question.[7]

There have been many examples of labelling cell surface proteins, with a common approach exploiting the expression of a recombinant version of the protein of interest, as used in the two *in vitro* studies described earlier. Another example of this uses peptide sequences containing heptad repeats known to form coiled-coil structures when the appropriate amino acids are present. The peptides used were expected to be unable to permeate the cell membrane due to their net charges and as such were used to label a cell surface receptor.[8] Genetic modification of Chinese hamster ovary cells allowed the expression of one peptide sequence fused to the cell receptor proteins. The complimentary peptide labelled with a fluorophore was then introduced and found to bind selectively to the peptide expressed as part of the receptor, Scheme 1.4. The function of the receptor was not affected by the labelling process and the process was shown to be fully reversible.[8]

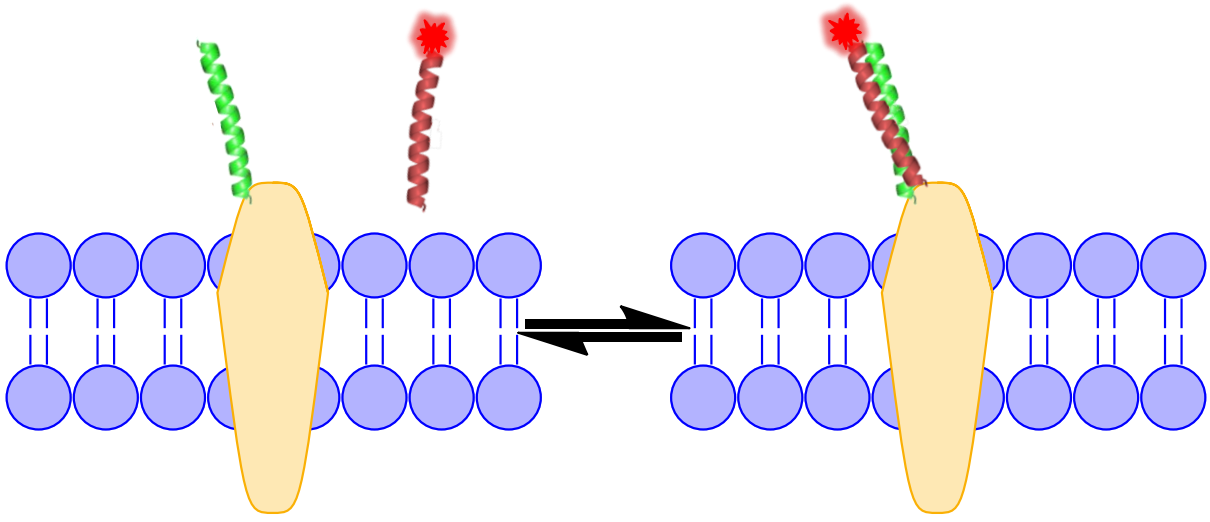

Scheme 1.4 Labelling of a cell surface receptor using coiled-coil peptide interactions.

1.2.2 Genetic Modification of Proteins for Labelling Inside Cells

There have been examples of the genetic modification of endogenous proteins in order to bind a specifically engineered probe that is membrane permeable. However, arguably the most widely used example of genetic modification for protein imaging within cells is the expression of GFP, which requires no probe interaction to generate a response because GFP is itself fluorescent when excited with the appropriate wavelength of light.[9] Furthermore, because the incorporation of GFP into a particular protein is genetically controlled it is specific to the target protein alone. The barrel structure of GFP allows its chromophore some protection from the cellular environment, however, this also prevents GFP from responding effectively to any environmental changes which may be of interest.[10, 11] The large size of GFP, around 235 amino acids, means that it may affect the protein it is incorporated into by altering its function, localisation and overall structure.[10, 12, 13] Another drawback of fluorescent proteins is that they are often spectrally limited and if they are modified in an attempt to alter their spectral properties, their fluorescence is often reduced as a result.[10] Furthermore, GFP has been shown to lose fluorescence as a function of pH, with no fluorescence observed at pH 6.5, and upon exposure to oxyradicals which can be present in large amounts in disease states that may be the focus of an investigation such as diabetes, Alzheimer's disease, cancer, heart disease and Parkinson's disease.[14, 15]

A pioneering technique for fluorescent labelling of recombinant proteins, developed by Roger Tsien's group, is the introduction of tetracysteine motifs into proteins that can bind to membrane-permeable biarsenical probes.[16-18] In addition to the design of an appropriate peptide binding motif it was also necessary to develop an appropriate biarsenical probe that holds the arsenics in the right position for interaction with the cysteine residues, becomes

fluorescent only upon interaction with the peptide, and is able to penetrate the cell membrane. The biarsenical probe first adopted by the group was FlAsH-EDT_2.[17, 18] Analogues of the green emitting FlAsH-EDT_2 (λ_{ex} = 508 nm, λ_{em} = 528 nm), CHOxAsH and ReAsH were later developed to emit in the blue (λ_{ex} = 380 nm, λ_{em} = 430 nm) and red (λ_{ex} = 593 nm, λ_{em} = 608 nm) areas of the spectrum respectively.[16] This approach has been successfully applied to the investigation of many biological phenomena such as connexin trafficking and inhibition of NF-κB activation.[19-21] The former study expressed the tertacysteine motif within the connexin protein, which forms part of the gap junction channels between cells, and labelled the cells first with FlAsH-EDT_2 and later with ReAsH, which was only able interact with the tetracysteine domains not already occupied by FlAsH-EDT_2, in order to see a comparison of the location of older and newer connexin based on their different fluorescent colours. It was found that newer connexin surrounded the older connexin which was in the middle of the gap junction. The study also concluded that the tetracysteine motif did not affect the function of the connexin.[19, 21] The latter study used FlAsH-EDT_2 to fluorescently label the naturally occurring cysteine containing activation loop of IκB catalytic subunits. The purpose of this was to show that the route of toxicity of arsenites is attachment to this particular protein, resulting in its inhibition and subsequently the inhibition of Nf-κB activation, which is a transcription factor. The fluorescence of the biarsenical compound FlAsH-EDT_2 when incubated with the domain of interest *in vitro* showed that arsentites are able to bind to this particular activation loop.[20]

The tetracysteine motif is much smaller than GFP and as such affects the target protein to a lesser extent when fused with it. In addition, the membrane permeable biarsenical compound can be modified to alter its spectral properties allowing it to be compatible with a range of

other cellular stains which may be useful in the case of co-localisation studies, for example, which perhaps presents it as a more flexible fluorescent probe than GFP. Drawbacks of using the tetracysteine motif, however, include the high detection of background, limited use in oxidative environments and the potential toxicity of the biarsenical probes.[7] Furthermore, the biarsenical probes have small Stokes shifts; indeed the emission and excitation spectra of each of the biarsenical derivatives when bound to the peptide overlap, Scheme 1.5, making their use in practice quite difficult due to exclusion of excitation light from detection and self-quenching effects.

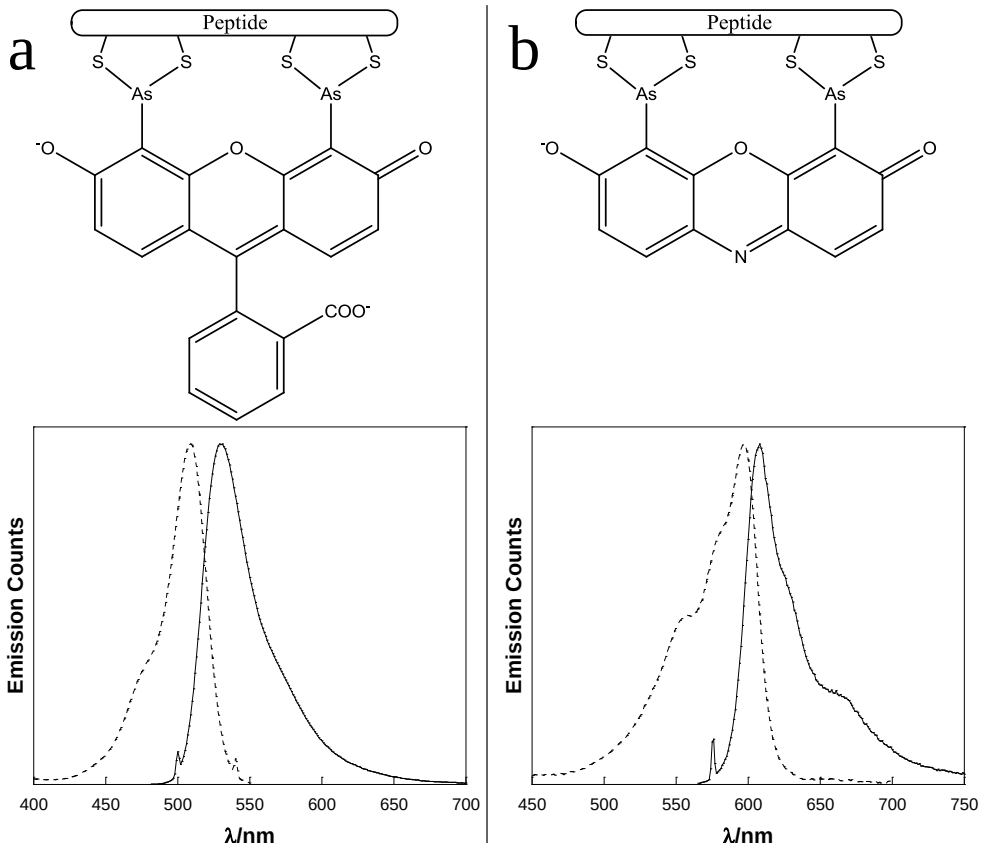

Scheme 1.5 Structure (top) and excitation (---) and emission (—) spectra (bottom) of a) FlAsH and b) ReAsH.

Further research in this field has seen the adaption of a rhodamine-derived bisboronic acid, originally designed as a monosaccharide sensor, to the labelling of recombinant proteins containing a tetraserine motif within cells.[22] Although this probe offers an alternative to biarsenical probes with reduced toxicity, its photophysical properties do not offer much over the biarsenical probes because it also exhibits a small Stokes shift. Alternative genetic modifications have also been developed and used to great effect by the expression of so-called SNAP-tag® or Halo Tag® fusion proteins and subsequent labelling with organic fluorophores.[23, 24]

Another approach that has been explored for protein labelling in cells is devising chemical reactions that will occur at the site of the protein of interest resulting in a detectable signal. This method has been successfully applied to the labelling of carbonic anhydrase enzymes with a ligand complex;[25] the ligand portion of the complex binds to the protein surface, however, the ligand, which is bound to the probe via a phenylsulfonate linkage, is released when tosyl chemistry occurs at the protein surface, leaving only the probe non-covalently linked to the protein surface and is activated upon binding of a particular analyte to the protein, Scheme 1.6. Whilst this technique can boast the advantage of eliminating the need for genetic modification of endogenous proteins, which may be difficult in some cell types, or indeed in whole organisms, it does require that the ligand is specific for a particular protein, and thus must be designed and synthesised for each labelling scenario.

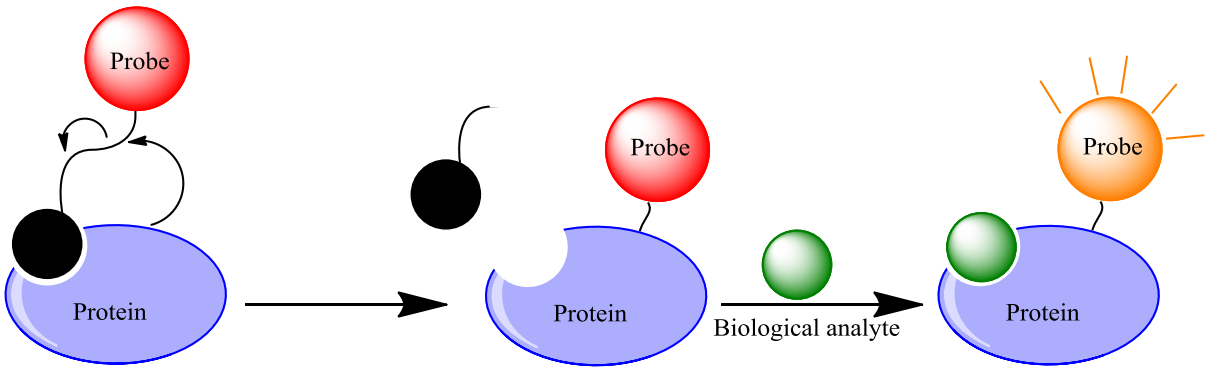

Scheme 1.6 Protein labelling using chemical reactions at the protein surface.

Examples of alternative protein labelling techniques are available in review articles, but it is clear that expression of recombinant proteins is widely used.[1, 2, 7] The extensive adoption in research of genetic modification of the protein of interest and subsequent labelling with a fluorescent probe confirms the suitability of the method to scientific investigations. Having said this, the current use of fluorescent probes within this method could be improved by using lanthanide complexes that offer superior photophysical properties.[26]

1.3 Lanthanide Complexes in Biological Imaging

The paramagnetic properties of gadolinium(III) have seen it become widely used in MRI and research is still continuing to improve the properties of gadolinium complexes for this purpose.[27-35] Aside from this, however, the photophysical differences between lanthanide luminescence and organic fluorescence give lanthanide complexes many advantages when applied to biological imaging techniques such as microscopy. Autofluorescence from biological samples is caused by endogenous organic fluorophores, which, by the nature of organic fluorescence, have small Stokes shifts and short fluorescence lifetimes on the order of nanoseconds. Any applied organic fluorescent labels will, therefore, have similar properties themselves and as such may be masked greatly by background autofluorescence. Lanthanide

complexes, however, are able to overcome this in several ways. Firstly, their effective Stokes shift is so large that it is unlikely that any endogenous species will emit in the same wavelength range as the lanthanide given the far removed excitation used. Secondly, the detection of the lanthanide emission can be time-gated to begin after the decay in fluorescence from organic fluorophores since lanthanide lifetimes are so much longer. Finally, the emission spectrum of the lanthanide can be used to confirm that the lanthanide is the species being detected since its line-like bands of emission are characteristic and unlike the broad emission bands of organic fluorophores, Scheme 1.7.

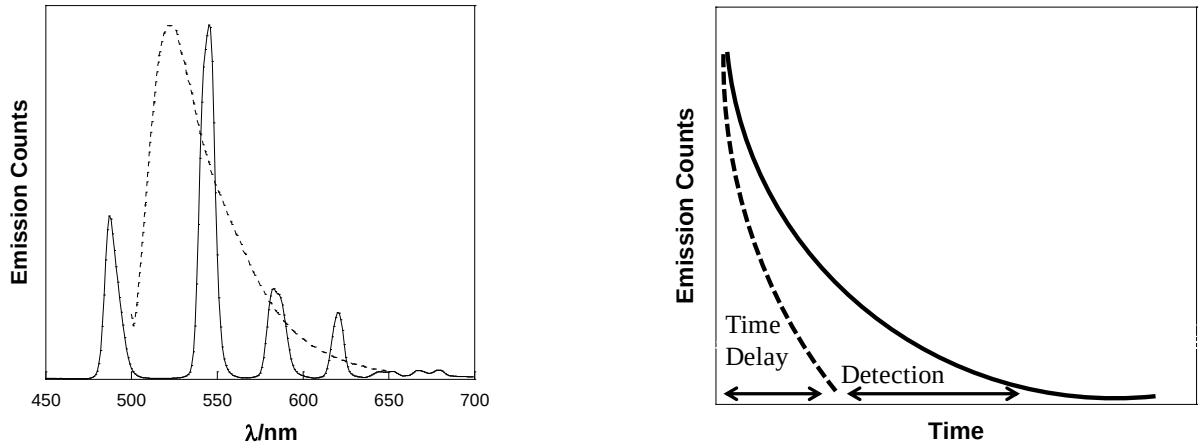

Scheme 1.7 Left: Emission spectra of a Tb^{3+} complex (—) and fluorescein isothiocyanate(---). Right: Principle of time-gated fluorescence demonstrated by the difference in luminescence decay of a lanthanide complex (—) and an organic fluorophore (---).

1.3.1 Luminescence Properties of Lanthanides

Compounds that emit light are usually referred to as fluorescent if the emission is due to a singlet-singlet transition, or phosphorescent if a triplet-singlet transition, requiring a change in spin, results in photon emission. Luminescence, is generally an umbrella term for fluorescence and phosphorescence, but is used in relation to lanthanide emission because their transitions are between states with spin multiplicity and do not involve singlet-singlet or

triplet-singlet transitions. Lanthanide luminescence is a result of the excitation and subsequent relaxation of an f-electron which results in the emission of a photon. The redistribution of electrons within the 4f sub-shell is not allowed according to the Laporté selection rule and as such f-f transitions are parity forbidden. The prohibited nature of these transitions means that the direct excitation of lanthanide ions is very inefficient with molar absorption coefficients typically less than 3 M^{-1} cm^{-1}, however, it also means that once an f-electron has been excited, the relaxation of the electron is equally inefficient resulting in long luminescence lifetimes in the order of milliseconds.[36-38] The luminescence spectra of lanthanides are characterised by narrow, line-like, emission bands resulting from the lack of interaction between the 4f electrons and the external environment. However, interaction with solvent molecules, water in particular, can quench the luminescence by vibrational coupling causing an excited electron to relax via a non-radiative deactivation pathway. The lanthanides display emission across the visible, from thulium, terbium, europium, dysprosium and samarium, and NIR from erbium, neodymium and ytterbium.[26]

1.3.1.1 Lanthanide Sensitisation

Organic chromophores are often included in the structure of lanthanide binding ligands in order to facilitate the luminescence of the lanthanide ion. As previously discussed, the advantageous luminescence properties of the lanthanides, such as their long luminescence lifetimes and characteristic bands of emission, cannot readily be accessed by direct lanthanide excitation, however, an organic chromophore with a high molar absorption coefficient can absorb light easily and can then transfer this energy to the excited state of the lanthanide ion allowing the relaxation to take place through the energy levels of the lanthanide and producing lanthanide luminescence.[26, 36, 37, 39] This is known as the antenna effect and its

principle is demonstrated in Scheme 1.8. Antenna groups usually absorb light in the UV range so when used to sensitise lanthanide emission there is a large effective Stokes shift of up to hundreds of nanometres.

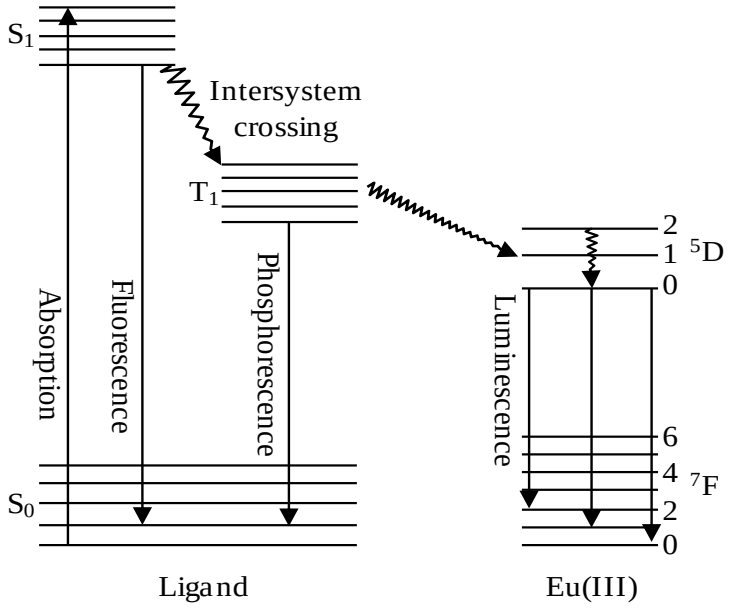

Scheme 1.8 Sensitisation of luminescence from Eu^{3+} by excitation of a ligand bearing an antenna group.

The sensitiser used must be chosen with care with some being more applicable to use with certain lanthanides over others; the antenna must have efficient intersystem crossing capacity and its triplet state should be at least 1850 cm^{-1} higher in energy than the emitting state of the lanthanide in order to prevent repopulation of the triplet state which would not result in lanthanide emission.[39] In some cases the sensitiser group is directly involved in chelating the lanthanide ion, as demonstrated by the cryptand in Figure 1.1, or it may be appended onto the chelating molecule in order to be held in close proximity to the lanthanide centre; DTPA and DOTA are commonly modified to include antenna molecules such as quinoline or azaxanthone.[40, 41]

1.3.2 Lanthanide Coordination

Chelation of lanthanide ions is extremely important if they are to be used in biological systems because lanthanide ions are toxic when free *in vivo* and as such must be incorporated into a complex for *in vivo* or cell based studies. Indeed, the popular use of gadolinium complexes for MRI applications has lead to investigations into the stability of such species due to the fact that free Gd^{3+} forms aggregates in the spleen, bone marrow and liver which can lead to hepatic necrosis.[27, 42] Furthermore, a chelating ligand is able to compete with coordinating solvent reducing the luminescence quenching caused by solvent molecules, and, as discussed previously, a chelating ligand may be comprised of, or introduce, a sensitiser moiety.

Lanthanides are hard Lewis acids and as such demonstrate a preference for coordination with hard donor atoms such as oxygen and nitrogen.[43, 44] Lanthanide ions are most commonly chelated by cryptands, macrocycles and polydentate ligands, containing oxygen and nitrogen donor atoms.

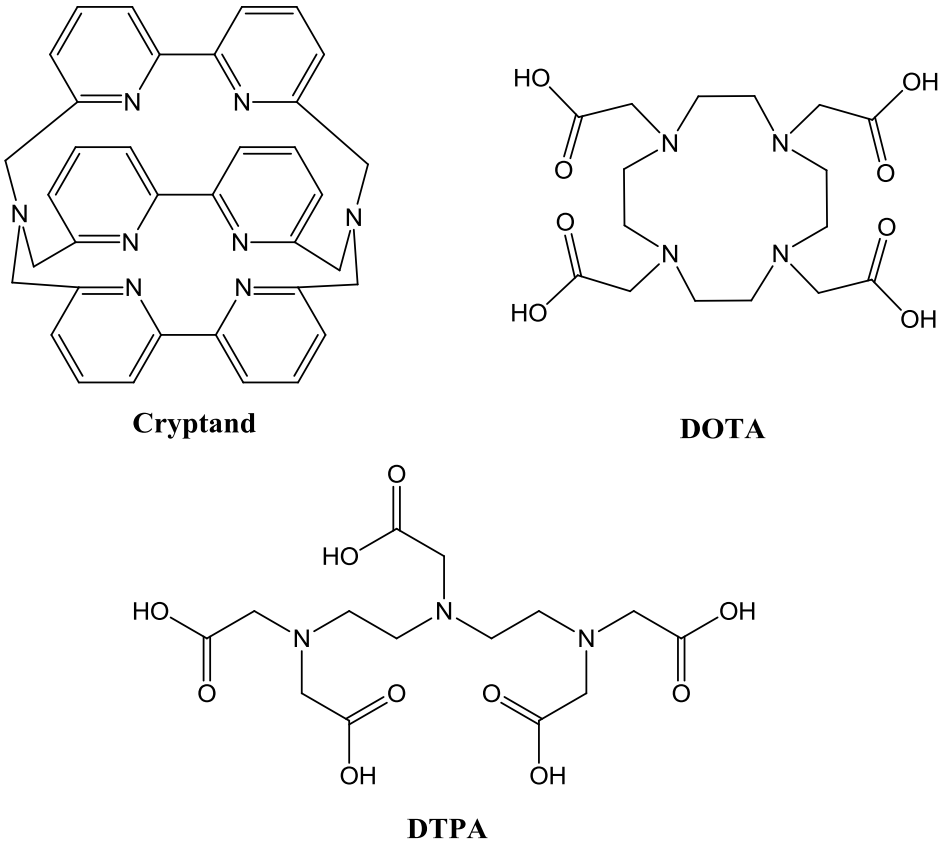

Figure 1.1 Common ligands used to chelate Ln^{3+}. DOTA is an example of a macrocycle, DTPA of a polydentate ligand and the cryptand is taken from work by the Lehn group.[45]

The research of Raymond and Lehn utilises cryptands,[45, 46] Parker and Gunnlaugson employ macrocycles[41, 47] and Pikramenou and Parac-Vogt exploit polydentate ligands for Ln^{3+} chelation.[40, 48] Of course, there is a great interest in the complexation of lanthanide ions and as such these examples are just a few of many as described in review articles.[49-52]

In addition to negating the toxic effects of free lanthanide ions and enhancing the luminescent properties of the lanthanide, chelating ligands can also be functionalised in order to allow the covalent attachment of lanthanide complexes to biomolecules, surfaces or nanoparticles. The use of lanthanide chelating ligands modified with functional groups for attachment to AuNPs and their use in biological assays and cellular studies will be discussed later in this chapter,

whereas the covalent attachment of lanthanide complexes to proteins will be reported in Chapter 2.

1.3.3 Examples of Luminescent Lanthanide Complexes in Cellular Studies

Owing to the advantageous photophysical properties of lanthanide complexes, they have been used in many biological studies, including protein labelling. The development of cell permeable complexes has allowed lanthanides to be utilised as cellular probes, with research aimed at studying and directing cellular localisation of lanthanide complexes.[53] For those complexes requiring some assistance in crossing the cell membrane, peptide sequences known to facilitate cellular uptake, so-called cell penetrating peptides, have been grafted onto the ligands chelating the lanthanide.[54-57]

One of the many reported uses of lanthanide complexes in cells is to act as cellular stains. A range of luminescent lanthanide complexes have been used as general luminescent stains for living cells and fixed tissue samples.[58-61] Specific targeting of cellular receptors have also been reported.[62] Parker and co-workers have demonstrated the use of luminescent lanthanide complexes for cellular staining, previously reporting a terbium complex capable of selectively staining the cell nucleus of dividing HeLa cells, allowing the visualisation of mitotic chromosomes.[63] In this case the lanthanide was chelated by a DOTA based ligand modified with azaxanthone antennas, Figure 1.2a. More recently, however, a series of europium complexes were designed based on a triazacyclononane chelating moiety appended with aryl–alkynyl antennas bearing phosphinate or carboxylate substituents, Figure 1.2b.[64] These complexes were noted for their superior brightness and luminescence quantum yields,

however, not all of the complexes synthesised were soluble in aqueous solution, precluding their use in biological systems.

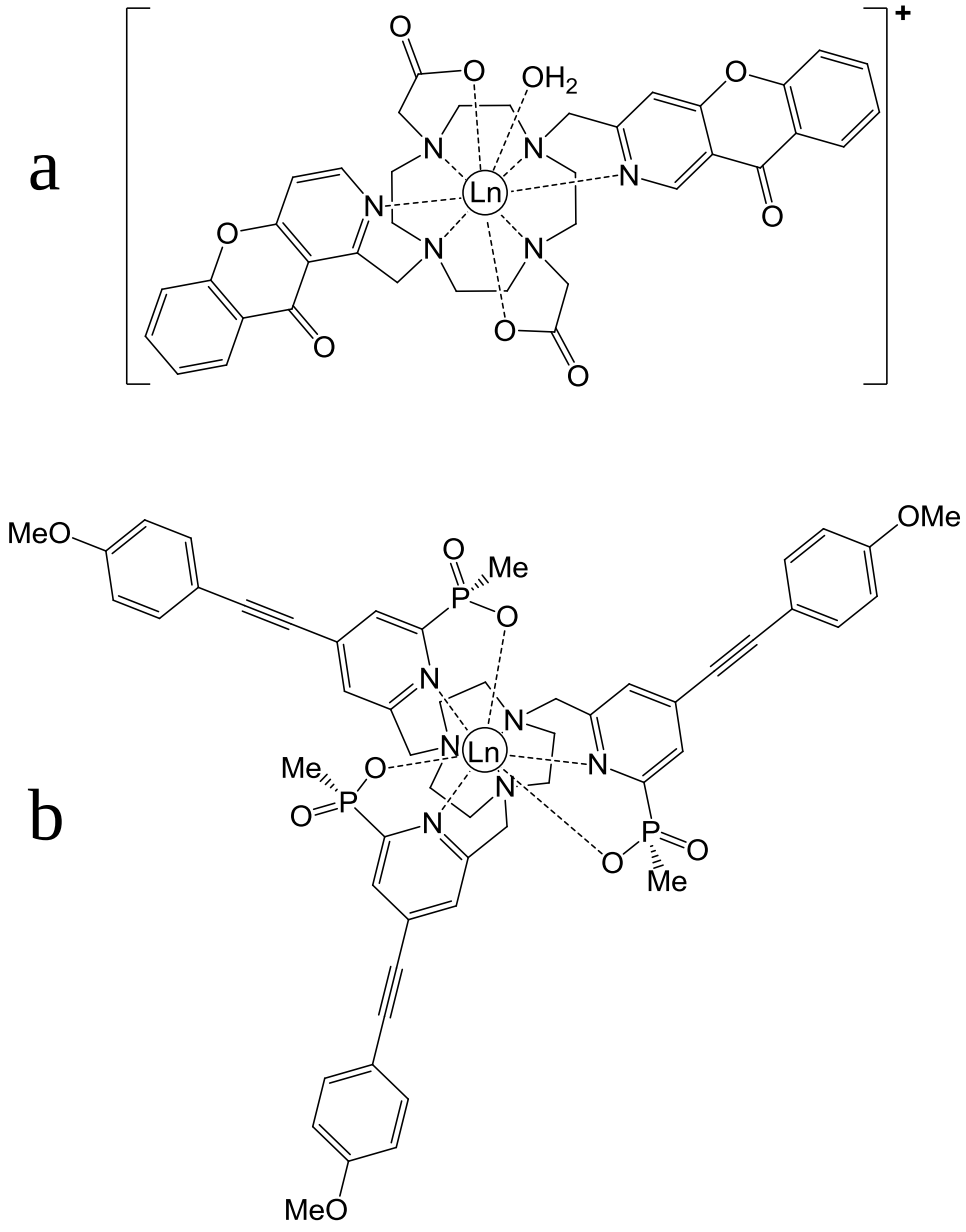

Figure 1.2 Examples of luminescent lanthanide complexes consisting of a) DOTA based ligand modified with azaxanthone antennas and b) triazacyclononane ligand appended with aryl–alkynyl antennas.

The europium complex taken forward for cellular studies was successfully imaged within Chinese hamster ovary cells, human prostate cancer cells and embryonic mouse fibroblast cells and was found to be taken up into cells by macropinocytosis after which selective staining of the mitochondria was observed.[64] In addition to using lanthanide complexes as luminescent stains for mammalian cells, europium analogues of the complexes described above were used to label plant cells and tissues.[65] In all cases the complexes were unable to penetrate the cell walls of healthy cells, with the exception of one complex shown to label the mitochondria of root hairs.[65] It is suggested that the luminescent complexes could be used to study the viability of plant cells because in order for the complexes to penetrate further than the cell wall the cell must either be dying or its cell wall must be compromised.

An alternative approach utilised recently by Yuan and colleagues exploits the encapsulation of a luminescent lanthanide complex by apoferritin for cellular delivery into HeLa cells via endocytosis.[66] Modification of the protein allows the attachment of targeting moieties demonstrated by the attachment of a mitochondrial targeting molecule and subsequent observation of the europium luminescence localised within the mitochondria of HeLa cells.[66]

Another widely exploited use of lanthanide complexes in cells is to act as reporter molecules for species present.[67] The work of Parker and colleagues has explored the use of luminescent lanthanide complexes as cellular reporter molecules.[68] Analytes may alter the coordination environment, allowing reports to be gained by changes in circular polarised luminescence signals or by a change in ratio of two emission bands of the lanthanide centre. DOTA based chelating ligands appended with various sensitiser molecules have been used as cellular sensors for pH and anion concentrations such as carbonate and citrate.[41, 69-72] For example, a

series of complexes of europium and terbium, similar to those used for general cell staining, Figure 1.2a, consisting of a DOTA ligand appended with an azaxanthone antenna were used in a ratiometric manner to determine bicarbonate concentration.[73] It was found that anions are able to displace the coordinated water molecules, thus affecting the circularly polarised luminescence and luminescence intensity of the lanthanide complexes. The emission response of the europium analogue was greater than that of terbium and as such the two signals could be compared in a ratiometric manner to find the concentration of bicarbonate present. The presence of a variety of biologically relevant anions and protein was assessed, however, the ability to sense for bicarbonate remained. The complexes were also incubated with various mammalian cell lines and were subsequently taken up by the cells. Imaging of the cells whilst varying the atmospheric CO_2 caused a response in the signals from the probes as the bicarbonate concentration altered.[73] A similar approach was used to sense for pH changes by conjugating a substituted sulphonamide group onto the ligand able to coordinate the lanthanide centre at certain pH values.[74] Again, the response of europium and terbium analogues differed allowing their emission intensities to be compared in order to measure pH. This was demonstrated by treating various mammalian cell lines with the complexes and monitoring the change in emission intensities of the probes, which were localised within lysosomes, as the pH of the medium was varied.[74] More recently the use of modified versions of the brighter luminescent europium complexes, Figure 1.2b, was reported for bicarbonate quantification in solution.[75] The modified complex has only two appended aryl–alkynyl moieties allowing coordination of water. As before, anions were shown to displace coordinated water from the europium centre affecting the emission profile of the complex. The ratio of the emission bands within the europium spectrum altered with anion concentration and could therefore be used for quantification of the analyte. In this case

alternative anions and HSA were also shown to cause a change in the luminescence measured, however, above a concentration threshold of 10 mM bicarbonate was found to bind selectively to the lanthanide. The luminescent complexes were also found to be taken up in a variety of mammalian cell lines and localised initially in the mitochondria before transport into lysosomes demonstrating the potential use of these complexes for bicarbonate sensing in cells.[75]

Yuan and colleagues have also explored the use luminescent lanthanide species as reporter molecules within cells. A europium complex was developed that was only weakly luminescent until it reacted with nitric oxide under aerobic conditions, upon which a triazole was formed and the luminescence of the europium was effectively "switched on" allowing it to act as a sensor for NO.[76] The initial complex was, however, sensitive to pH changes which affected its ability to act as a sensor, therefore the structure of the complex was modified to allow it to act independently of pH as a selective and rapid NO sensor.[77] The acetoxymethyl ester of the complex was found to be taken up by cells and demonstrated its use as a NO sensor within rat neuronal cells, its luminescence intensity changing as a function of NO concentration.[77] More recently the group have developed a lanthanide complex bearing a 4-hydroxypyridine group which is deprotonated at certain pH values.[78] When deprotonation occurs intramolecular charge transfer arises in the europium analogue, quenching its luminescence, but not in the terbium complex. The two species were, therefore, used to measure pH changes in solution in a ratiometric manner. The probes were also imaged within HeLa cells, however, the measurements taken from cell studies were not ratiometric, but individual species in isolation.[78] Terbium and europium complexes have also been developed

for sensing of thiols in cells, however, the work has only been conducted in extract from cells to date and as such the system must be developed further for use inside living cells.[79]

Alternatively, Nagano and co-workers have used europium complexes with a DTPA based chelating ligand to sense for Zn^{2+} in cells.[80, 81] In this instance the antenna group was based around a quinoline motif with the ability to chelate Zn^{2+}. The binding of the zinc cation induces a change in the photophysical properties of the antenna and the luminescence exhibited by the europium centre is increased, Scheme 1.9. This was successfully used to detect zinc within living cells, however, the probe had to be injected into the cells which is not ideal.

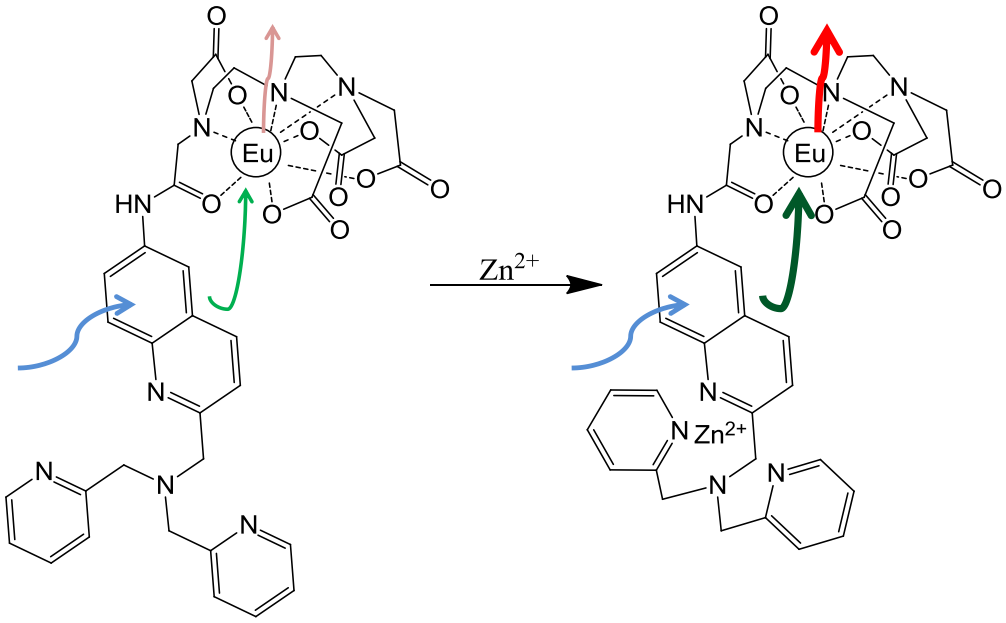

Scheme 1.9 The conformational and photophysical change of a europium complex in the absence and presence of Zn^{2+}.

Luminescent lanthanide complexes have also found use as specific protein labels in cells. One of the many protein labelling techniques explored by Kikuchi includes the labelling of

epidermal growth factor receptor with a luminescent lanthanide complex.[82] In this case a mutant of the β–lactamase enzyme was expressed as part of a recombinant epidermal growth factor receptor protein in embryonic human kidney cells. A europium complex covalently attached to the β-lactam ampicillin was then introduced and was able to label the protein by being held in the enzyme for a prolonged period of time because the mutant enzyme is very slow in releasing the modified substrate, Scheme 1.10.

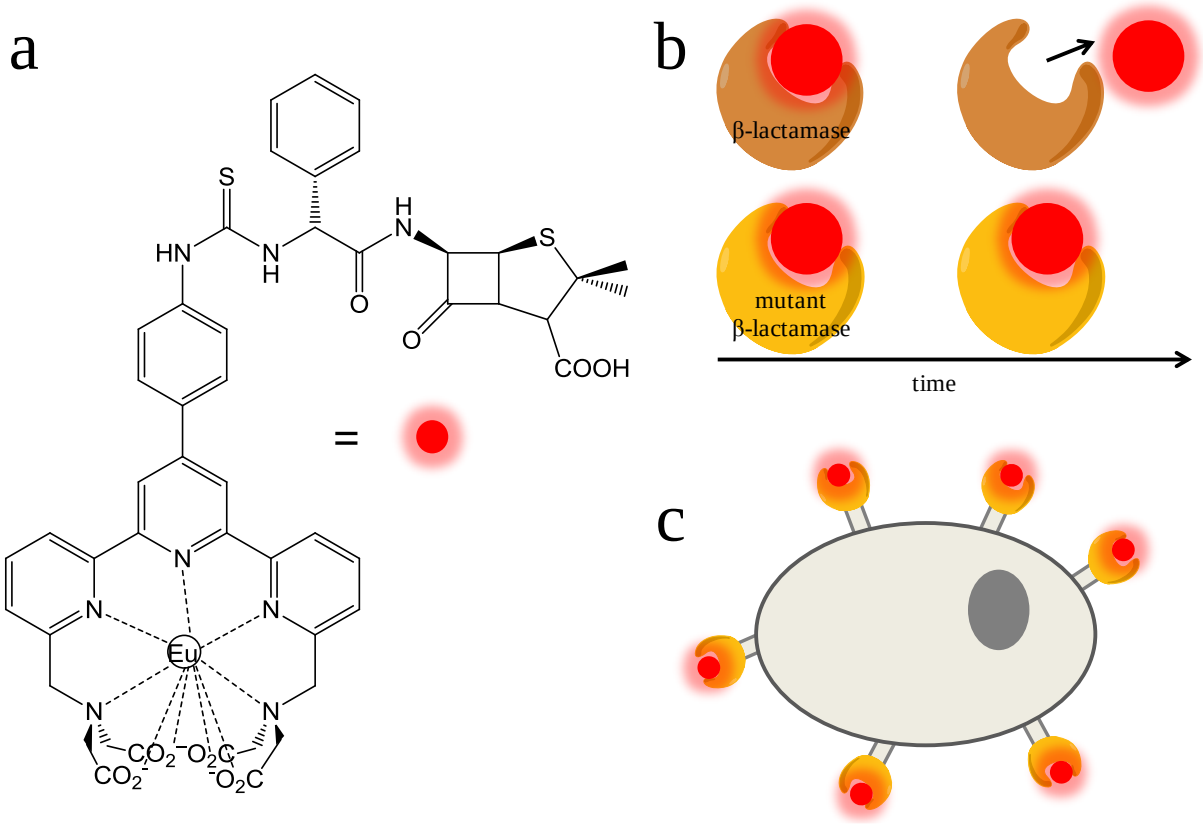

Scheme 1.10 a) Structure of the europium label incorporating ampicillin, b) representation of the retention of the label by β-lactamase and a mutant variant of β-lactamase and c) the expression of the mutant variant of β-lactamase on the cell surface to allow labelling with the europium label.

The long luminescence lifetime of the europium complex was exploited by the use of time resolved microscopy of the labelled cells to reduce background signal. The lanthanide probe

used was limited to labelling proteins on the cell surface because its anionic nature prevented membrane permeation. A similar approach was taken by the Miller group where recombinant cell membrane proteins containing *Escherichia coli* dihydrofolate reductase, which is known to have a high affinity for trimethoprim, were labelled with a commercially available terbium complex grafted to a trimethoprim moiety.[83] The proteins were expressed in embryonic mouse fibroblast cells and were labelled with the terbium complex, however, the membrane permeability of the probe allowed non-specific labelling of other areas of the cell.

1.4. Gold Nanoparticles in Cells

AuNPs have received a great deal of interest in terms of their applications in biology and medicine.[84-94] AuNPs have the potential to deliver drugs, gene regulation agents and imaging agents to cells because of their surface properties that allow for the addition of a range of complexes to their exterior.[84, 86, 95] Furthermore, AuNPs can be used for photothermal therapy due to their rapid conversion of light energy into heat, therefore, if they are modified with antibodies to target cancer cells can facilitate cell death of the cancer by overheating.[84, 96]

The use of AuNPs for biological applications depends on their surface modifications. For instance, the ability of AuNPs to act as gene delivery agents is improved when their surface is functionalised with amines because these groups are positively charged at physiological pH allowing for interaction with negatively charged nucleic acids through electrostatic means. It has been found that using lysine residues, whose side chain terminates in an amine, to modify the AuNP surface results in a more efficient delivery of DNA plasmids than a commercial vector.[86]

Fluorescent AuNPs have been used for a variety of applications. One example reported recently uses 2 nm AuNPs modified with either fluorescein or doxorubicin dyes to examine AuNP uptake and distribution within a tumour model.[97] Both fluorescent molecules were grafted onto the surface of AuNPs using alkane ethers terminated with thiol groups which were able to bind to the gold. The alkane ethers not attached to a dye molecule either all presented an amine or carboxylate group to solution creating AuNPs that were either positively or negatively charged. Fluorescence microscopy and mathematical modelling revealed that the positively charged AuNPs were more effectively taken up by proliferating cells when either fluorescent dye molecule was present, however, negatively charged AuNPs were able to penetrate deeper into the tumour tissue. Research such as this provides insight into the uses of AuNPs as anti-cancer agents.

1.4.1 Gold Nanoparticles - Background

AuNPs are aggregates of Au(0) with dimensions under 100 nm and stabilised by capping ligands on their surface. For example, citrate-stabilised AuNPs can be readily synthesised by the reduction of a gold salt by sodium citrate.[98, 99] This leads to AuNPs with an associated layer of citrate ions on their surface. The size of the nanoparticles can be easily tuned by varying the ratio of gold salt to reducing agent.[100, 101] The citrate capping layer electrostatically stabilises the AuNPs due to the repulsion of the anionic charges, resulting in monodisperse AuNPs in solution. Citrate capping ligands can be easily displaced by other desired species, providing steric stabilisation of the AuNPs, and as such AuNPs can act as carriers to deliver a large payload of cargo to a target destination. Furthermore, because of the large surface area of AuNPs they can be used to carry a variety of ligands allowing them to

act as multi-modal probes, delivering and fluorescently reporting on the location of therapeutics, for example.

AuNPs have interesting optical properties because they are so much smaller than wavelengths of visible light. Valence electrons on the surface of AuNPs will oscillate coherently when a certain wavelength of light is applied, giving rise to a surface plasmon resonance band which is in the visible range for AuNPs; this means that AuNPs have a distinct colour and can be analysed by the measurement of their surface plasmon resonance band in absorption spectroscopy. Furthermore, the density of gold allows AuNPs to be easily imaged through TEM, which they most commonly are. The high scattering properties of AuNPs also allow their detection by dark-field and fluorescence microscopy. In addition to this, when using surface-enhanced Raman scattering to investigate cell samples AuNPs have been used for signal enhancement.[84]

1.4.2 Lanthanide Functionalised Gold Nanoparticles

A large proportion of lanthanide containing nanomaterials consists of quantum dots, polymer based nanoparticles and silica nanoparticles, however, as previously stated, the ligand responsible for chelating a lanthanide ion can also contain functional groups for attachment to AuNPs.[102] Work by the Pikramenou group has described the coordination of Eu^{3+} by a DTPA based ligand containing thiophenol groups for lanthanide sensitisation and attachment of the complex to the surface of AuNPs through creation of a S-Au bond, Scheme 1.11.[103]

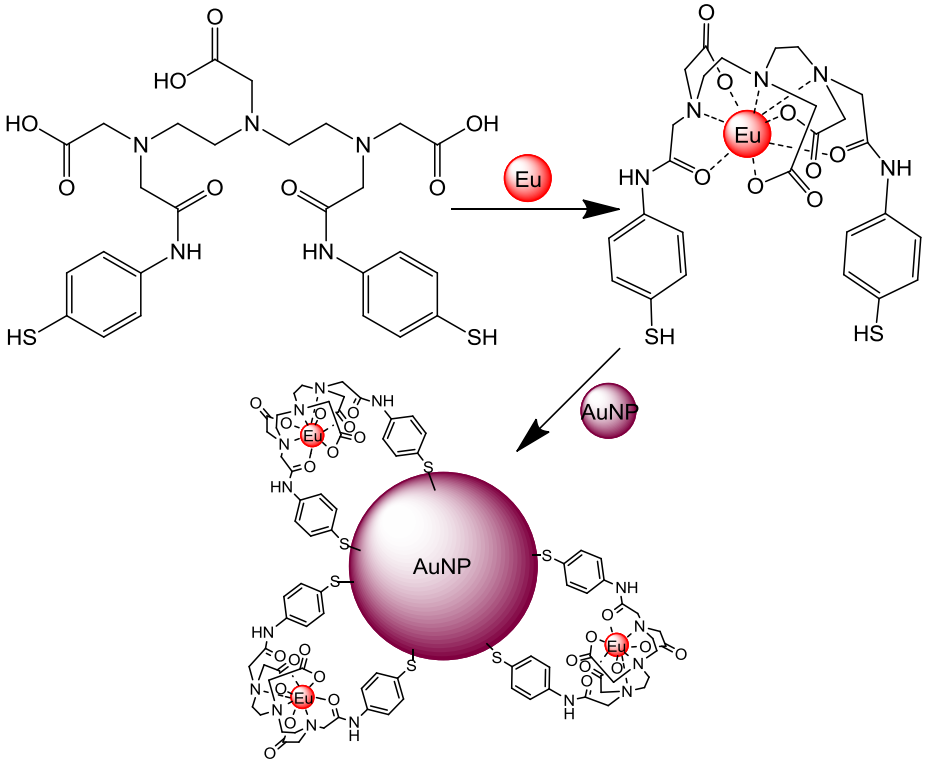

Scheme 1.11 The use of a ligand to coordinate Eu^{3+} and attach the complex to the surface of a gold nanoparticle.

1.4.2.1 Lanthanide Functionalised Gold Nanoparticles in Biological Sensing

The use of AuNPs functionalised with luminescent lanthanide complexes for various sensing applications has been reported by Gunnlaugsson and co-workers. Initially, a europium complex was developed that allowed attachment to the surface of AuNPs using an alkyl thiol group and did not contain an antenna group for the sensitisation of the lanthanide emission.[104] Attachment of the complex to AuNPs resulted in a non-luminescent species, however, when a naphthalene β-diketone antenna was added it was found to coordinate to the lanthanide centre and sensitise its emission, Scheme 1.12.

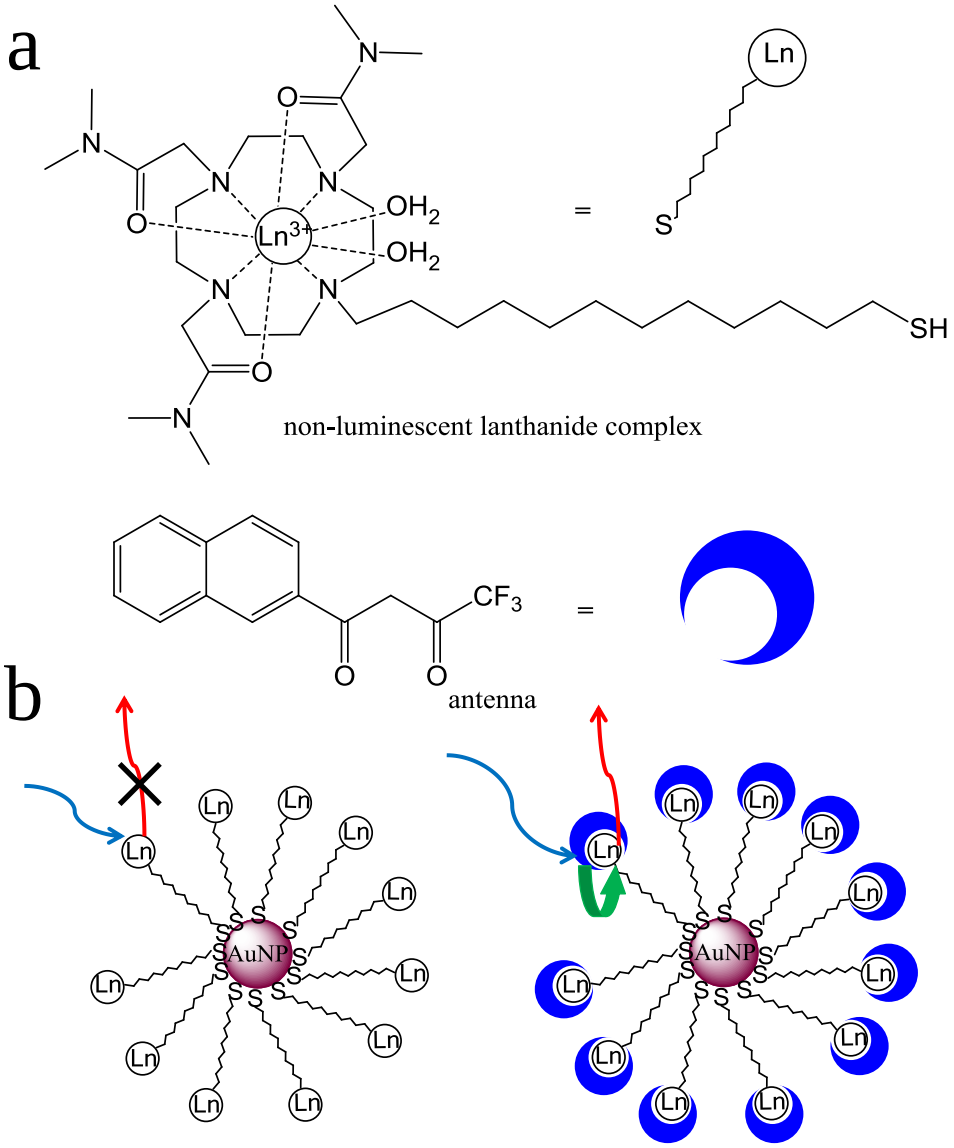

Scheme 1.12 a) Structure of lanthanide complex and β-diketone antenna and b) non-luminescent AuNP capped with lanthanide complex and sensitisation when antenna present.

The displacement of the antenna was then investigated using various biologically relevant anions and was achieved by flavin monophosphate which resulted in complete quenching of the europium luminescence. Alternative anions were found to quench the lanthanide emission to a degree, but no other species offered complete quenching.[104] This displacement assay was the first example of the use of such a system for sensing of biologically relevant species and was further developed by the group. The interaction of the system with BSA was next

explored and it was found that although BSA did not displace the antenna it was able to interact with it in such a way as to quench the europium luminescence.[105] Furthermore, the introduction of ibuprofen, known to bind to site II of BSA, resulted in a recovery of the europium emission leading to the conclusion that BSA interacts with the antenna molecule through its site II region and demonstrating the possibility of sensing for species that bind to BSA. Introduction of warfarin, a site I marker, resulted in a further reduction of the europium emission, but the presence of warfarin did not affect the sensing of ibuprofen.[105] Most recently, a NIR emitting lanthanide, ytterbium, has been attached to the surface of AuNPs and has been used as a pH sensor.[106] In this case the same chelating ligand was used as before with an alkyl thiol group for attachment of the complex to AuNPs, however, xylenol orange was used as the antenna. Xylenol orange is pH sensitive and as such its sensitisation of ytterbium emission is also dependent upon pH. In this case it was found that the luminescence of ytterbium was "switched on" above pH 4, but "switched off" in the range pH 2-4.[106] Although this represents the possibility of using a lanthanide modified AuNP system for pH sensing with NIR emission, modification of the system may be required for use in practice because of the low luminescence quantum yield of the ytterbium centre when attached to AuNPs and sensitised by xylenol orange which was measured to be 0.036%.[106] Currently, however, development of ratiometric sensing using AuNPs co-coated with europium and terbium complexes each with different external antennas and sensing of chiral species, such as amino acids, using AuNPs coated with chiral lanthanide complexes is being pursued.[102] In all cases the assays were carried out in aqueous buffer and as such are relevant for biological systems although the progression from *in vitro* to cellular studies has not been reported to date.

Previous work by Thomas and co-workers demonstrated that AuNPs coated with a derivative of 2,2'-dipyridyl containing a thiol group were able to chelate and sensitise the emission of lanthanide ions.[107] It was found that the ligands chelated the lanthanide ions in a 3:1 stoichiometry which most likely consisted of ligands from more than one AuNP rather than cooperation between the ligands on the surface of a single AuNP. Certainly, the introduction of Cu^{2+} in place of lanthanide ions caused superstructures to be formed by the cooperation of the AuNPs to chelate the metal ions. Both Eu^{3+} and Tb^{3+} were used in the study and it was found that the sensitised luminescence of both species was reduced as other metal cations, such as Ca^{2+} and Zn^{2+}, were introduced due to displacement of the lanthanide ions from the ligands.[107] Although this may be of some use in detecting specific cations, the scope for lanthanide displacement may not extend to molecular ions and certainly the fact that the experiments are carried out in acetonitrile and release free lanthanide ions prevents its use in biological systems.

1.4.2.2 Lanthanide Functionalised Gold Nanoparticles in Cellular Imaging

As previously discussed, complexes of gadolinium are currently used as contrast agents in MRI. However, such contrast agents could be improved by inclusion on nanoparticles. The main advantages of using nanoparticles in MRI is that more gadolinium can be trapped on the nanoparticle surface than a single gadolinium complex and nanoparticles show a longer half-life in the blood stream which means that nanoparticles coated with gadolinium complexes can ultimately deliver more contrast agent to the desired site than traditional compounds. Furthermore, the addition of the gadolinium complex to a larger species will slow its tumbling rate and further improve its contrast properties.[108-111] Moreover, the ability to create multifunctionalised nanoparticles allows for the addition of a targeting moiety which will

allow the nanoparticle to be delivered to the site of interest more effectively. It has also been shown that the AuNP itself can be of use, not in MRI, but as a contrast agent in X-ray computed tomography, with the gold showing a strong X-ray absorption, allowing any gadolinium functionalised AuNPs to be useful contrast agents in two widely used medical imaging techniques.[112]

The modification of AuNPs with luminescent lanthanide complexes and subsequent cellular delivery has also been reported in the literature. Pikramenou and colleagues have described the delivery of AuNPs decorated with luminescent europium complexes into platelet cells.[113] In this instance the AuNPs were also functionalised with a pH responsive peptide capable of inserting itself across a cell membrane at a certain pH, therefore delivering its cargo of nanoparticles inside the platelet cells. The europium luminescence was detected and imaged within the cells demonstrating its use as a biological probe in combination with AuNPs. In an earlier study the location of europium coated AuNPs in human epithelial lung fibroblasts was established through the use of high-resolution synchrotron X-ray fluorescence and they were found able to penetrate the nuclei of the cells.[114]

1.5 Project Overview

The aim of the work in this thesis is to explore methods for protein labelling using luminescent lanthanide complexes and AuNPs modified with these complexes, examining the interaction of these complexes and AuNPs with proteins and peptides in the process. This presents the opportunity to build upon protein labelling techniques that have been developed previously for use *in vitro* and inside live cells, such as the tetracysteine motifs, which could also be used to bind AuNPs *in vivo*, and attempt to address some problems associated with

this approach, as well as offering an alternative to the use of GFP which has been shown to be unstable under certain conditions. Furthermore, although the use of the biarsenical compounds allows for the modification of fluorescence as required, the use of functionalised AuNPs instead allows a truly dual-modal approach to be adopted with the potential to deliver not only luminescent probes to the protein of interest in the first instance, but the possibility of further probe or therapeutic attachment in the future. The use of luminescent lanthanide complexes, both free and attached to AuNPs, have been shown to be of value in biological imaging applications and as such both species will be utilised herein.

The direct labelling of serum albumin with luminescent lanthanide complexes will be described and evaluated in Chapter 2, with an investigation into the possible cellular uptake of fluorescently labelled proteins. Chapter 3 focuses on the binding of several peptide species to AuNPs and their relative binding affinities. The interactions of each peptide with the AuNPs will enable the selection of a binding motif with the potential to bind AuNPs selectively in cells if expressed as part of a protein of interest. Chapter 4 begins by investigating the interaction of AuNPs and lanthanide modified AuNPs with protein *in vitro* before using the expression of fusion protein with the previously identified AuNP binding motif to evaluate the ability of luminescent AuNPs to label a protein of interest within cells.

1.6 References

1. S. Mizukami, Y. Hori and K. Kikuchi, *Acc. Chem. Res.*, 2014, **47**, 247-256.
2. C. Jing and V. W. Cornish, *Acc. Chem. Res.*, 2011, **44**, 784-792.
3. C. R. Bertozzi, *Acc. Chem. Res.*, 2011, **44**, 651-653.
4. D. M. Patterson, L. A. Nazarova and J. A. Prescher, *ACS Chem. Biol.*, 2014, **9**, 592-605.
5. T. Fekner, X. Li, M. M. Lee and M. K. Chan, *Angew. Chem. Int. Ed.*, 2009, **48**, 1633-1635.
6. Z. Hao, Y. Song, S. Lin, M. Yang, Y. Liang, J. Wang and P. R. Chen, *Chem. Commun.*, 2011, **47**, 4502-4504.
7. Z. Wang, X. Ding, S. Li, J. Shi and Y. Li, *RSC Adv.*, 2014, **4**, 7235-7245.
8. Y. Yano, A. Yano, S. Oishi, Y. Sugimoto, G. Tsujimoto, N. Fujii and K. Matsuzaki, *ACS Chem. Biol.*, 2008, **3**, 341-345.
9. M. Fernández-Suárez and A. Y. Ting, *Nat. Rev. Mol. Cell Biol.*, 2008, **9**, 929-943.
10. K. M. Marks and G. P. Nolan, *Nat. Methods*, 2006, **3**, 591-596.
11. R. Y. Tsien, *Annu. Rev. Biochem.*, 1998, **67**, 509-544.
12. Z. Hao, S. Hong, X. Chen and P. R. Chen, *Acc. Chem. Res.*, 2011, **44**, 742-751.
13. C. S. Lisenbee, S. K. Karnik and R. N. Trelease, *Traffic*, 2003, **4**, 491-501.
14. K. M. Alkaabi, A. Yafea and S. S. Ashraf, *Appl. Biochem. Biotechnol.*, 2005, **126**, 149-156.
15. A. A. Alnuami, B. Zeedi, S. M. Qadri and S. S. Ashraf, *Int. J. Biol. Macromol.*, 2008, **43**, 182-186.
16. S. R. Adams, R. E. Campbell, L. A. Gross, B. R. Martin, G. K. Walkup, Y. Yao, J. Llopis and R. Y. Tsien, *J. Am. Chem. Soc.*, 2002, **124**, 6063-6076.
17. B. A. Griffin, S. R. Adams, J. Jones and R. Y. Tsien, in *Applications of Chimeric Genes and Hybrid Proteins - Part B: Cell Biology and Physiology*, eds. J. Thorner, S. D. Emr and J. N. Abelson, Academic Press, San Diego (USA), Editon edn., 2000, vol. 327, pp. 565-578.
18. B. A. Griffin, S. R. Adams and R. Y. Tsien, *Science*, 1998, **281**, 269-272.
19. G. Gaietta, T. J. Deerinck, S. R. Adams, J. Bouwer, O. Tour, D. W. Laird, G. E. Sosinsky, R. Y. Tsien and M. H. Ellisman, *Science*, 2002, **296**, 503-507.

20. P. Kapahi, T. Takahashi, G. Natoli, S. R. Adams, Y. Chen, R. Y. Tsien and M. Karin, *J. Biol. Chem.*, 2000, **275**, 36062-36066.

21. G. E. Sosinsky, G. M. Gaietta, G. Hand, T. J. Deerinck, A. Han, M. Mackey, S. R. Adams, J. Bouwer, R. Y. Tsien and M. H. Ellisman, *Cell Commun. Adhes.*, 2003, **10**, 181-186.

22. T. L. Halo, J. Appelbaum, E. M. Hobert, D. M. Balkin and A. Schepartz, *J. Am. Chem. Soc.*, 2009, **131**, 438-439.

23. A. Keppler, S. Gendreizig, T. Gronemeyer, H. Pick, H. Vogel and K. Johnsson, *Nat. Biotechnol.*, 2003, **21**, 86-89.

24. G. V. Los, L. P. Encell, M. G. McDougall, D. D. Hartzell, N. Karassina, C. Zimprich, M. G. Wood, R. Learish, R. F. Ohana, M. Urh, D. Simpson, J. Mendez, K. Zimmerman, P. Otto, G. Vidugiris, J. Zhu, A. Darzins, D. H. Klaubert, R. F. Bulleit and K. V. Wood, *ACS Chem. Biol.*, 2008, **3**, 373-382.

25. S. Tsukiji, M. Miyagawa, Y. Takaoka, T. Tamura and I. Hamachi, *Nat. Chem. Biol.*, 2009, **5**, 341-343.

26. J.-C. G. Bünzli, *Chem. Rev.*, 2010, **110**, 2729-2755.

27. M. Bellin, *Eur. J. Radiol.*, 2006, **60**, 314-323.

28. P. Caravan, J. J. Ellison, T. J. McMurry and R. B. Lauffer, *Chem. Rev.*, 1999, **99**, 2293-2352.

29. K. W.-Y. Chan and W.-T. Wong, *Coord. Chem. Rev.*, 2007, **251**, 2428-2451.

30. L. Telgmann, M. Sperling and U. Karst, *Anal. Chim. Acta*, 2013, **764**, 1-16.

31. M. R. Berwick, D. J. Lewis, A. W. Jones, R. A. Parslow, T. R. Dafforn, H. J. Cooper, J. Wilkie, Z. Pikramenou, M. M. Britton and A. F. A. Peacock, *J. Am. Chem. Soc.*, 2014, **136**, 1166-1169.

32. P. Caravan, *Acc. Chem. Res.*, 2009, **42**, 851-862.

33. S. Dumas, V. Jacques, W.-C. Sun, J. S. Troughton, J. T. Welch, J. M. Chasse, H. Schmitt-Willich and P. Caravan, *Invest. Radiol.*, 2010, **45**, 600-612.

34. P. D. Garimella, A. Datta, D. W. Romanini, K. N. Raymond and M. B. Francis, *J. Am. Chem. Soc.*, 2011, **133**, 14704-14709.

35. A. M. Nonat, C. Gateau, P. H. Fries, L. Helm and M. Mazzanti, *Eur. J. Inorg. Chem.*, 2012, **2012**, 2049-2061.

36. J.-C. G. Bünzli and C. Piguet, *Chem. Soc. Rev.*, 2005, **34**, 1048-1077.

37. L. J. Charbonnière, *Curr. Inorg. Chem.*, 2011, **1**, 2-16.

38. G. R. Choppin and D. R. Peterman, *Coord. Chem. Rev.*, 1998, **174**, 283-299.

39. E. G. Moore, A. P. S. Samuel and K. N. Raymond, *Acc. Chem. Res.*, 2009, **42**, 542-552.

40. D. J. Lewis, F. Moretta, A. T. Holloway and Z. Pikramenou, *Dalton Trans.*, 2012, **41**, 13138-13146.

41. B. S. Murray, E. J. New, R. Pal and D. Parker, *Org. Biomol. Chem.*, 2008, **6**, 2085-2094.

42. P. Dawson, D. O. Cosgrove and R. G. Grainger, *Textbook of Contrast Media*, ISIS Medical Media Ltd, Oxford, 1999.

43. C. E. Housecroft and A. G. Sharpe, *Inorganic Chemistry*, 2nd edn., Pearson Prentice Hall, Essex, 2005.

44. R. G. Pearson, *J. Am. Chem. Soc.*, 1963, **85**, 3533-3539.

45. B. Alpha, J.-M. Lehn and G. Mathis, *Angew. Chem. Int. Ed. Engl.*, 1987, **26**, 266-267.

46. J. Xu, T. M. Corneillie, E. G. Moore, G.-L. Law, N. G. Butlin and K. N. Raymond, *J. Am. Chem. Soc.*, 2011, **133**, 19900-19910.

47. S. Comby, S. A. Tuck, L. K. Truman, O. Kotova and T. Gunnlaugsson, *Inorg. Chem.*, 2012, **51**, 10158-10168.

48. G. Dehaen, P. Verwilst, S. V. Eliseeva, S. Laurent, L. V. Elst, R. N. Muller, W. M. De Borggraeve, K. Binnemans and T. N. Parac-Vogt, *Inorg. Chem.*, 2011, **50**, 10005-10014.

49. D. Parker, *Chem. Soc. Rev.*, 2004, **33**, 156-165.

50. L. Lattuada, A. Barge, G. Cravotto, G. B. Giovenzana and L. Tei, *Chem. Soc. Rev.*, 2011, **40**, 3019-3049.

51. J.-C. G. Bünzli, *Acc. Chem. Res.*, 2006, **39**, 53-61.

52. D. Parker, R. S. Dickins, H. Puschmann, C. Crossland and J. A. K. Howard, *Chem. Rev.*, 2002, **102**, 1977-2010.

53. E. J. New, A. Congreve and D. Parker, *Chem. Sci.*, 2010, **1**, 111-118.

54. R. Bhorade, R. Weissleder, T. Nakakoshi, A. Moore and C.-H. Tung, *Bioconjug. Chem.*, 2000, **11**, 301-305.

55. S. Mohandessi, M. Rajendran, D. Magda and L. W. Miller, *Chem. – Eur. J.*, 2012, **18**, 10825-10829.

56. P. J. Endres, K. W. MacRenaris, S. Vogt and T. J. Meade, *Bioconjug. Chem.*, 2008, **19**, 2049-2059.

57. J. L. Major and T. J. Meade, *Acc. Chem. Res.*, 2009, **42**, 893-903.

58. A.-S. Chauvin, S. Comby, B. Song, C. D. B. Vandevyver and J.-C. G. Bünzli, *Chem. – Eur. J.*, 2008, **14**, 1726-1739.

59. A.-S. Chauvin, S. Comby, B. Song, C. D. B. Vandevyver, F. Thomas and J.-C. G. Bünzli, *Chem. – Eur. J.*, 2007, **13**, 9515-9526.

60. S. Claudel-Gillet, J. Steibel, N. Weibel, T. Chauvin, M. Port, I. Raynal, E. Toth, R. F. Ziessel and L. J. Charbonnière, *Eur. J. Inorg. Chem.*, 2008, **2008**, 2856-2862.

61. G.-L. Law, K.-L. Wong, C. W.-Y. Man, W.-T. Wong, S.-W. Tsao, M. H.-W. Lam and P. K.-S. Lam, *J. Am. Chem. Soc.*, 2008, **130**, 3714-3715.

62. H. C. Manning, T. Goebel, R. C. Thompson, R. R. Price, H. Lee and D. J. Bornhop, *Bioconjug. Chem.*, 2004, **15**, 1488-1495.

63. G.-L. Law, C. Man, D. Parker and J. W. Walton, *Chem. Commun.*, 2010, **46**, 2391-2393.

64. J. W. Walton, A. Bourdolle, S. J. Butler, M. Soulie, M. Delbianco, B. K. McMahon, R. Pal, H. Puschmann, J. M. Zwier, L. Lamarque, O. Maury, C. Andraud and D. Parker, *Chem. Commun.*, 2013, **49**, 1600-1602.

65. A. J. Palmer, S. H. Ford, S. J. Butler, T. J. Hawkins, P. J. Hussey, R. Pal, J. W. Walton and D. Parker, *RSC Adv.*, 2014, **4**, 9356-9366.

66. L. Tian, Z. Dai, Z. Ye, B. Song and J. Yuan, *Analyst*, 2014, **139**, 1162-1167.

67. A. Thibon and V. C. Pierre, *Anal. Bioanal. Chem.*, 2009, **394**, 107-120.

68. C. P. Montgomery, B. S. Murray, E. J. New, R. Pal and D. Parker, *Acc. Chem. Res.*, 2009, **42**, 925-937.

69. E. J. New, D. Parker, D. G. Smith and J. W. Walton, *Curr. Opin. Chem. Biol.*, 2010, **14**, 238-246.

70. R. Pal and D. Parker, *Chem. Commun.*, 2007, 474-476.

71. R. Pal and D. Parker, *Org. Biomol. Chem.*, 2008, **6**, 1020-1033.

72. J. Yu, D. Parker, R. Pal, R. A. Poole and M. J. Cann, *J. Am. Chem. Soc.*, 2006, **128**, 2294-2299.

73. D. G. Smith, R. Pal and D. Parker, *Chem. – Eur. J.*, 2012, **18**, 11604-11613.

74. D. G. Smith, B. K. McMahon, R. Pal and D. Parker, *Chem. Commun.*, 2012, **48**, 8520-8522.

75. S. J. Butler, B. K. McMahon, R. Pal, D. Parker and J. W. Walton, *Chem. – Eur. J.*, 2013, **19**, 9511-9517.

76. Y. Chen, W. Guo, Z. Ye, G. Wang and J. Yuan, *Chem. Commun.*, 2011, **47**, 6266-6268.

77. M. Liu, Z. Ye, G. Wang and J. Yuan, *Talanta*, 2012, **99**, 951-958.

78. M. Liu, Z. Ye, C. Xin and J. Yuan, *Anal. Chim. Acta*, 2013, **761**, 149-156.

79. Z. Dai, L. Tian, Z. Ye, B. Song, R. Zhang and J. Yuan, *Anal. Chem.*, 2013, **85**, 11658-11664.

80. K. Hanaoka, K. Kikuchi, S. Kobayashi and T. Nagano, *J. Am. Chem. Soc.*, 2007, **129**, 13502-13509.

81. K. Hanaoka, K. Kikuchi, H. Kojima, Y. Urano and T. Nagano, *J. Am. Chem. Soc.*, 2004, **126**, 12470-12476.

82. S. Mizukami, T. Yamamoto, A. Yoshimura, S. Watanabe and K. Kikuchi, *Angew. Chem. Int. Ed.*, 2011, **50**, 8750-8752.

83. H. E. Rajapakse, D. R. Reddy, S. Mohandessi, N. G. Butlin and L. W. Miller, *Angew. Chem. Int. Ed.*, 2009, **48**, 4990-4992.

84. E. Boisselier and D. Astruc, *Chem. Soc. Rev.*, 2009, **38**, 1759-1782.

85. L. A. Dykman and N. G. Khlebtsov, *Chem. Rev.*, 2014, **114**, 1258-1288.

86. D. A. Giljohann, D. S. Seferos, W. L. Daniel, M. D. Massich, P. C. Patel and C. A. Mirkin, *Angew. Chem. Int. Ed.*, 2010, **49**, 3280-3294.

87. N. Khlebtsov and L. Dykman, *Chem. Soc. Rev.*, 2011, **40**, 1647-1671.

88. C. S. Kim, B. Duncan, B. Creran and V. M. Rotello, *Nano Today*, 2013, **8**, 439-447.

89. M. J. Kogan, I. Olmedo, L. Hosta, A. R. Guerrero, L. J. Cruz and F. Albericio, *Nanomed.*, 2007, **2**, 287-306.

90. R. Lévy, U. Shaheen, Y. Cesbron and V. Sée, *Nano Rev.*, 2010, **1**, 4889.

91. Y.-F. Li and C. Chen, *Small*, 2011, **7**, 2965-2980.

92. J. Q. Lin, H. W. Zhang, Z. Chen and Y. G. Zheng, *ACS Nano*, 2010, **4**, 5421-5429.

93. P. Nativo, I. A. Prior and M. Brust, *ACS Nano*, 2008, **2**, 1639-1644.

94. A. S. Thakor, J. Jokerst, C. Zavaleta, T. F. Massoud and S. S. Gambhir, *Nano Lett.*, 2011, **11**, 4029-4036.

95. T. Georgelin, S. Bombard, J. M. Siaugue and V. Cabuil, *Angew. Chem. Int. Ed.*, 2010, **49**, 8897-8901.

96. P. K. Jain, I. H. El-Sayed and M. A. El-Sayed, *Nano Today*, 2007, **2**, 18-29.

97. B. Kim, G. Han, B. J. Toley, C.-k. Kim, V. M. Rotello and N. S. Forbes, *Nat. Nanotechnol.*, 2010, **5**, 465-472.

98. G. Frens, *Nat. Phys. Sci.*, 1973, **241**, 20-22.

99. J. Turkevich, P. C. Stevenson and J. Hillier, *Discuss. Faraday Soc.*, 1951, **11**, 55-75.

100. D. Dixon, I. Mutreja, R. D'Sa, B. J. Meenan and D. Kumar, *Int. J. Nanoscience*, 2012, **11**, 1250023.

101. X. Ji, X. Song, J. Li, Y. Bai, W. Yang and X. Peng, *J. Am. Chem. Soc.*, 2007, **129**, 13939-13948.

102. S. Comby, E. M. Surender, O. Kotova, L. K. Truman, J. K. Molloy and T. Gunnlaugsson, *Inorg. Chem.*, 2014, **53**, 1867-1879.

103. D. J. Lewis, T. M. Day, J. V. MacPherson and Z. Pikramenou, *Chem. Commun.*, 2006, **42**, 1433-1435.

104. J. Massue, S. J. Quinn and T. Gunnlaugsson, *J. Am. Chem. Soc.*, 2008, **130**, 6900-6901.

105. S. Comby and T. Gunnlaugsson, *ACS Nano*, 2011, **5**, 7184-7197.

106. L. K. Truman, S. Comby and T. Gunnlaugsson, *Angew. Chem. Int. Ed.*, 2012, **51**, 9624-9627.

107. B. I. Ipe, K. Yoosaf and K. G. Thomas, *J. Am. Chem. Soc.*, 2006, **128**, 1907-1913.

108. P. J. Debouttière, S. Roux, F. Vocanson, C. Billotey, O. Beuf, A. Favre-Reguillon, Y. Lin, S. Pellet-Rostaing, R. Lamartine, P. Perriat and O. Tillement, *Adv. Funct. Mater.*, 2006, **16**, 2330-2339.

109. H. K. Kim, H. Y. Jung, J. A. Park, M. I. Huh, J. C. Jung, Y. Chang and T. J. Kim, *J. Mater. Chem.*, 2010, **20**, 5411-5417.

110. L. Moriggi, C. Cannizzo, E. Dumas, C. R. Mayer, A. Ulianov and L. Helm, *J. Am. Chem. Soc.*, 2009, **131**, 10828-+.

111. J. A. Park, H. K. Kim, J. H. Kim, S. W. Jeong, J. C. Jung, G. H. Lee, J. Lee, Y. Chang and T. J. Kim, *Bioorg. Med. Chem.*, 2010, **20**, 2287-2291.

112. C. Alric, J. Taleb, G. Le Duc, C. Mandon, C. Billotey, A. Le Meur-Herland, T. Brochard, F. Vocanson, M. Janier, P. Perriat, S. Roux and O. Tillement, *J. Am. Chem. Soc.*, 2008, **130**, 5908-5915.

113. A. Davies, D. J. Lewis, S. P. Watson, S. G. Thomas and Z. Pikramenou, *Proc. Natl. Acad. Sci. U. S. A.*, 2012, **109**, 1862-1867.

114. D. J. Lewis, C. Bruce, S. Bohic, P. Cloetens, S. P. Hammond, D. Arbon, S. Blair-Reid, Z. Pikramenou and B. Kysela, *Nanomed.*, 2010, **5**, 1547-1557.

2. Luminescent Lanthanide Complexes as Covalent Protein Labels

2.1 Introduction

2.1.1 Lanthanide Complexes and Protein Labelling

It is extremely useful to be able to label proteins in order to monitor their behaviour and lanthanide complexes are ideal candidates for such labelling due to their luminescence properties which lend themselves to biological studies, as discussed in Chapter 1. Serum proteins such as BSA and HSA are of interest due to their abundance in the circulatory system of mammals, representing the bulk of protein in the blood plasma, and because of their many important physiological roles such as maintaining the pH of the blood and oncotic pressure and binding molecules such as vitamins, hormones and drugs for transport around the body.[1]

2.1.2 Non-Covalent Protein Labelling

Metal complexes can label proteins through covalent or non-covalent interactions. In the latter case, metal complexes can bind either specifically or non-specifically to proteins and can be engineered in order to exploit these two processes. For example, metal complexes can be synthesised to include molecules such as biotin, known to have high affinity for certain binding sites or receptors such as avidin, thus allowing them to target these receptor sites specifically.[2, 3] Alternatively, there have been many examples of metal complexes interacting with proteins non-specifically, and in many cases the proteins in question have been serum proteins such as HSA and BSA which both present a multitude of binding opportunities. For example, a series of luminescent cyclometalated iridium complexes attached through a spacer to an indole group, Figure 2.1, was bound non-covalently to BSA.

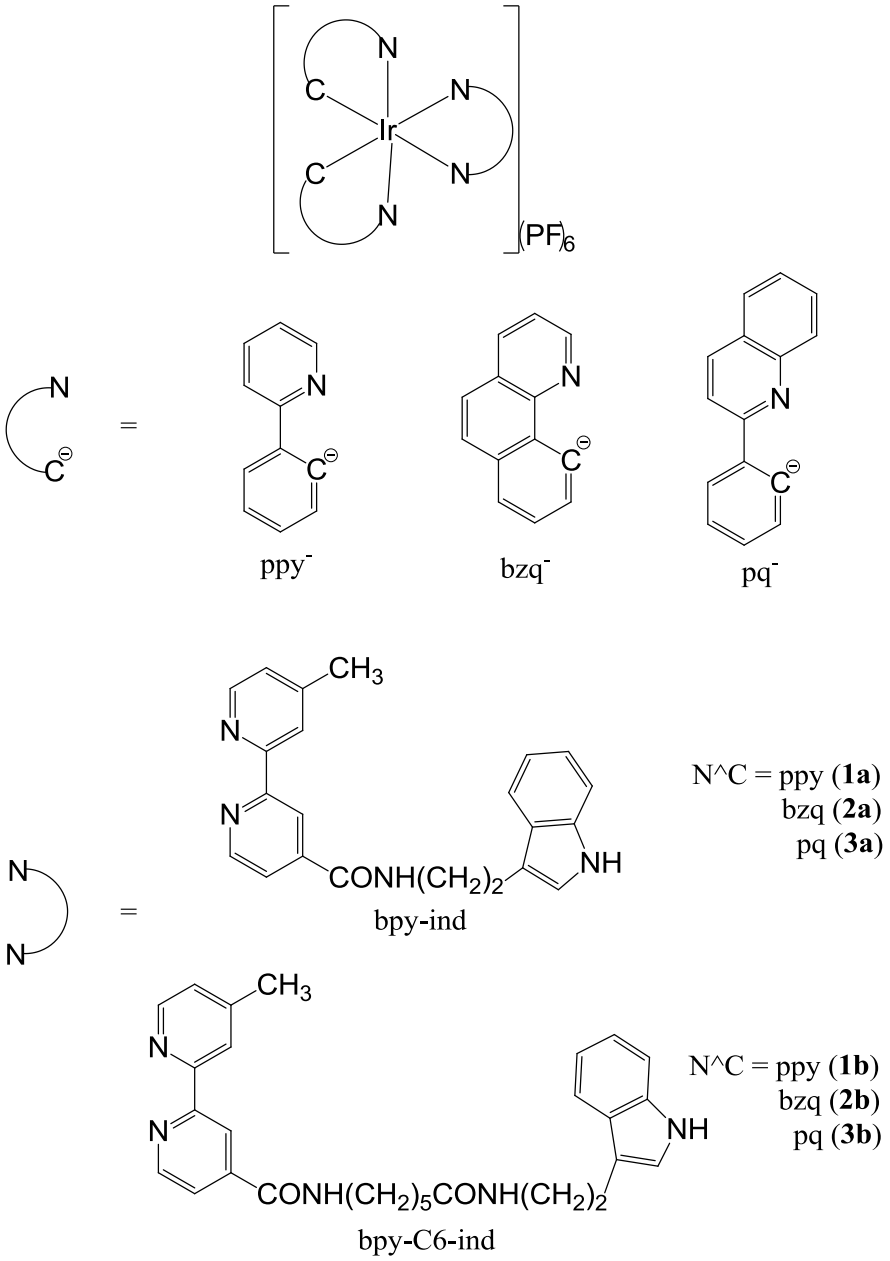

Figure 2.1 Structures of luminescent cyclometalated iridium(III) indole complexes used as non-covalent labels for BSA. The ligands consist of either two phenylpyridine groups (1), two benzoquinoline groups (2), or two phenylquinoline groups (3) in combination with a bipyridine group connected to an indole via a short (a) or long (b) alkane chain.[4]

BSA is a known indole binding protein, and as a result of binding to the protein an increase in the emission and lengthening of the luminescence lifetime of each complex was observed. This was attributed to the protein creating a hydrophobic environment around the complexes

and increased rigidity in the structure of the complexes upon binding.[4] Similarly, a series of luminescent lanthanide complexes utilising the DOTA motif for lanthanide chelation, Figure 2.2, were bound to HSA through non-specific interactions.

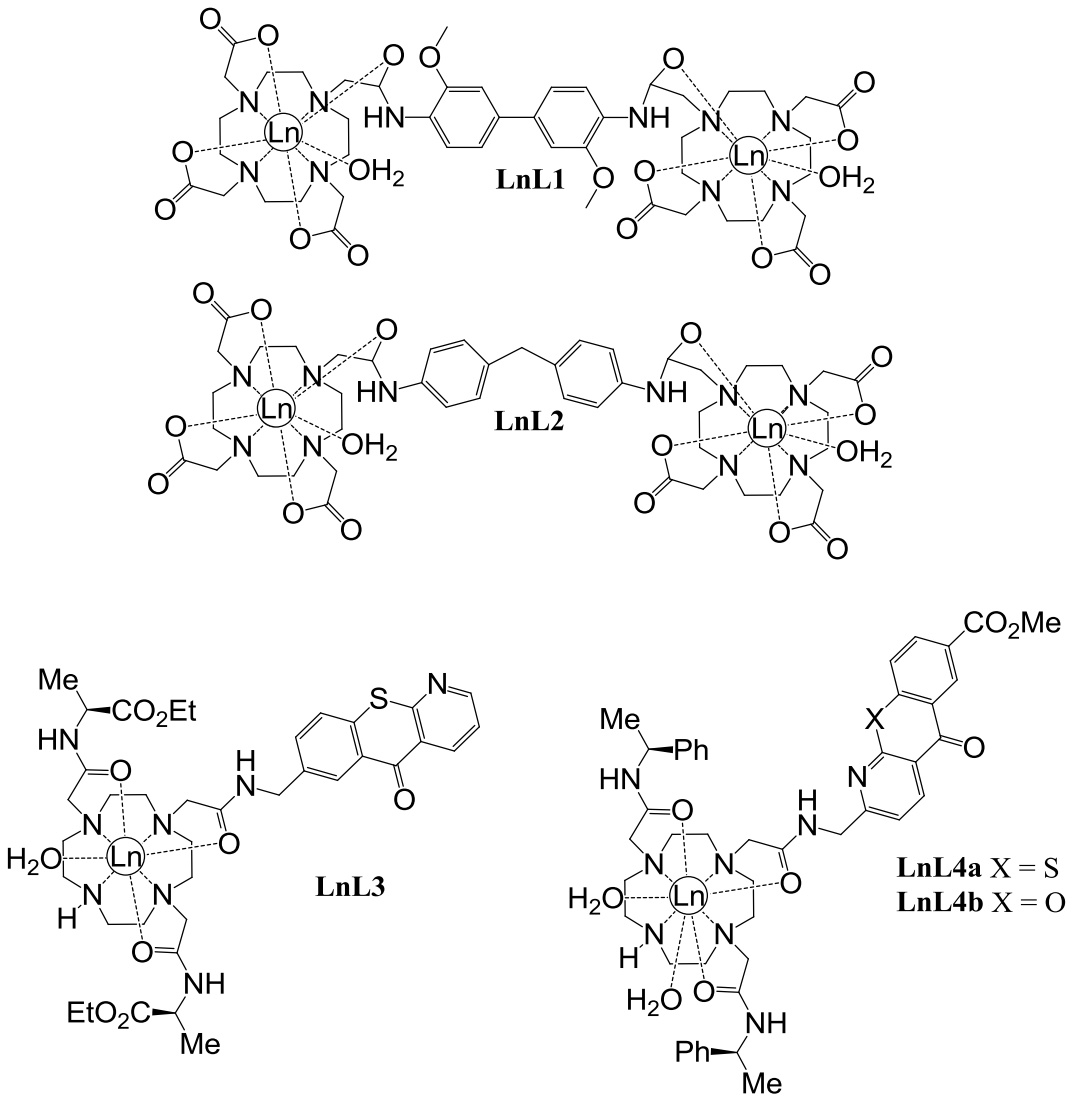

Figure 2.2 Structures of lanthanide complexes used for non-covalent HSA binding. The complexes employ DOTA based chelating ligands and either biphenyl (LnL1), diphenylmethane (LnL2), azathiaxanthone (LnL3 and LnL4a) or azaxanthone (LnL4b) based antennas. In the case of LnL1 and LnL2 the antennas are also used to bridge two DOTA chelated lanthanide centres.[5, 6]

Unlike the cyclometalated iridium(III) complexes, the lanthanide complexes did not all show the same change in photophysical behaviour in the presence of a serum protein. LnL1 showed no change in the emission intensity of either a europium or terbium centre when interacting with HSA, whereas TbL2 showed a small increase in emission intensity after addition of HSA, but greater still was the enhancement of EuL2 emission intensity after addition of HSA.[5] In all cases, for EuL3, EuL4a, EuL4b and TbL4b, the emission intensity of the complexes was reduced upon interaction with HSA, however, the luminescence lifetime of EuL2 showed a decrease where an increase was observed for EuL4a and EuL4b.[6] Additionally, GdL3 demonstrated increased relaxivity when bound to HSA.[6] Indeed, it would be expected that the relaxivity of an MRI contrast agent would be increased through binding to a macromolecule such as HSA because this would slow its tumbling rate and as such non-covalent interactions between gadolinium based MRI contrast agents and serum albumins have been widely studied.[7-18] A caveat of this, however, is that a complex may bind to a hydrophobic pocket of a protein which will exclude solvent molecules thus reducing water exchange at the paramagnetic centre. Non-covalent interactions between lanthanide complexes and proteins can, therefore, offer insight into the potential of a complex to act as a protein label based on its luminescent properties or relaxivity when in the presence of the protein, however, they may also allow dissociation of the lanthanide complex from the protein when other factors are involved such as the presence of alternative proteins or binding site competitors and as such covalent attachment of lanthanide complexes to proteins is the focus of this chapter.

2.1.3 Covalent Protein Labelling

Covalent labelling of proteins can occur through the selective targeting of amino acid side groups such as the primary amine of lysine, which is one of the most commonly targeted groups, the thiol of cysteine, which is one of the most reactive functional groups found within proteins, or the imidazole of histidine. Aldehyde groups, NHS esters and isothiocyanates are often used to form covalent bonds with primary amines, whereas iodoacetamide and maleimide groups are used for targeting thiol groups.[19] Metal complexes coordinated with solvent or Cl^- are able to form bonds with histidine through the replacement of these ligands with the imidazole moiety.[20]

There have been many examples of covalent conjugation of transition metal complexes to serum proteins through specific targeting of the thiol groups,[21-23] or more commonly, the primary amine groups of the proteins.[23-27] In addition to the work with transition metals there is currently much research being carried out into the development of lanthanide complexes to act as biological probes through covalent attachment to proteins. Again, labels are predominately attached through the amine groups of the protein[28-32] most routinely using a complex functionalised with an NHS ester, although maleimide thiol chemistry is also used.[33, 34] As with the study of non-covalent interactions, some of these conjugates were studied for their MRI properties,[29, 30, 33, 34] and others for their photophysical properties.[28, 31, 32] It is interesting to compare two luminescent lanthanide complex designs attached to BSA via an NHS ester reaction, Figure 2.3.

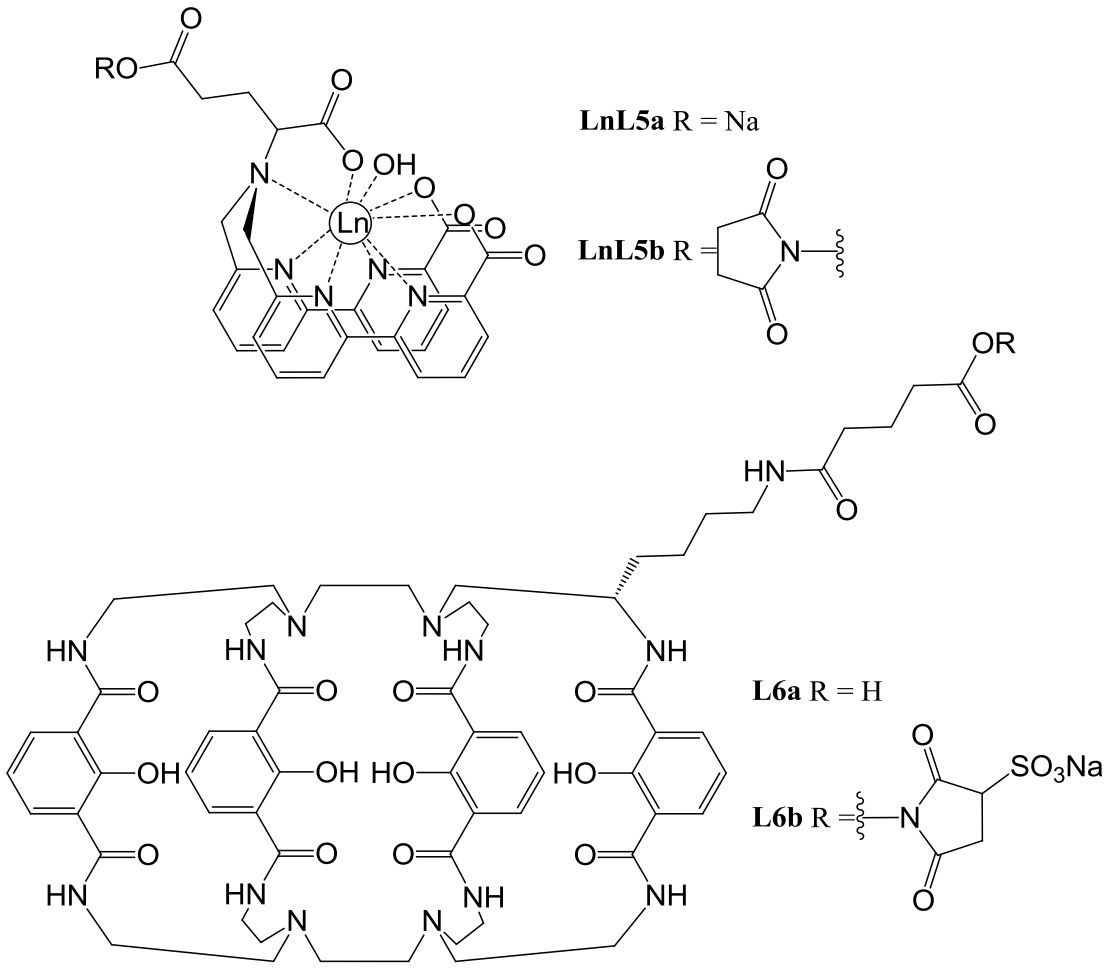

Figure 2.3 Structures of lanthanide chelates used for covalent BSA binding. The ligands consist of either a glutamic acid structure bis-functionalised at its nitrogen atom with bipyridine derivatives (LnL5) or an octadentate macrotricycle bearing phthalamide groups (L6). In both cases the ligands were modified with an NHS ester for covalent attachment to BSA through its primary amine groups (LnL5b and L6b). LnL5 shows the chelation of a lanthanide ion by the ligand whereas L6 shows the ligand only. [28, 31]

It was found that in the case of TbL5b a shortening of the luminescence lifetime of the lanthanide complex was observed after conjugation to BSA in comparison to unbound TbL5a in solution.[31] Similarly, a BSA conjugate of TbL6b demonstrated a shortening of luminescence lifetime and a decrease in luminescence quantum yield when compared with free TbL6a, whereas the europium complex showed the reverse in that the BSA conjugate of EuL6b had a higher luminescence quantum yield and longer luminescence lifetime than free

EuL6a.[28] When comparing the two studies it is interesting to note that where there was an observed increase in luminescence lifetime and quantum yield the lanthanide centre in question was europium, whereas the decreases seen were for terbium complexes. One explanation for this may be that interaction with a serum protein excludes a coordinated water molecule and this would reduce any luminescence quenching caused by the water upon the europium centre which is known to be sensitive to this non-radiative deactivation process, whereas the photophysics of terbium are much more complex and as such the exclusion of coordinating water may not have the same impact as with europium.

2.1.4 Luminescent Protein Conjugates and FRET

In addition to the use of lanthanide complexes simply as protein labels, their luminescence properties and the interaction of proteins with other biomolecules can be utilised to detect such biomolecules via FRET. This has been demonstrated using a terbium complex attached to *Escherichia coli* dihydrofolate reductase as a donor and GFP attached to claudin-1 as an acceptor. In this case the interaction of the two proteins within cells was detected by the FRET interaction of their labels, Scheme 2.1a.[35] More recently a similar approach has been used by the covalent attachment of a terbium complex donor to a specific antibody and a dye acceptor to another antibody both against total prostate specific antigen, Scheme 2.1b. In this case when the two antibodies form an immunocomplex with total prostate specific antigen FRET occurs between terbium and the dye which allows for the detection of total prostate specific antigen, a known marker for prostate cancer.[36]

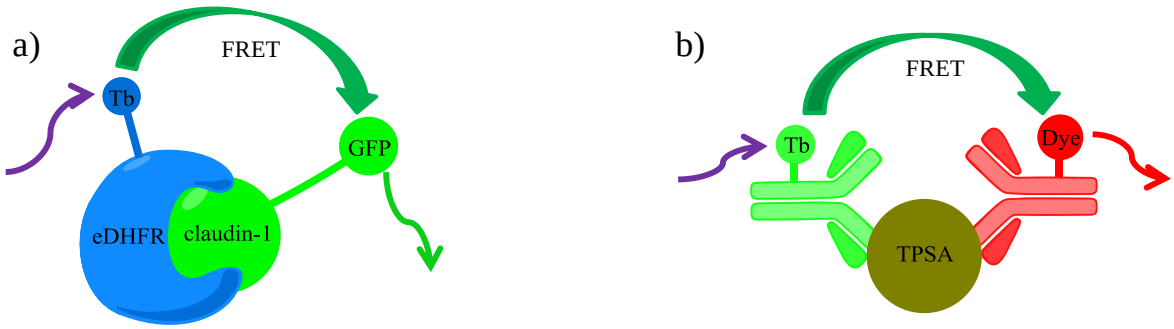

Scheme 2.1 Schematic representation of FRET between a) a terbium complex and GFP when attached to biomolecules where eDHFR = *Escherichia coli* dihydrofolate reductase and b) a terbium complex and a dye attached to antibodies where TPSA = total prostate specific antigen.

2.1.5 Research Aims

The main objective of the work detailed in this chapter is the synthesis of luminescent lanthanide complexes and the investigation into their potential as protein labels. The photophysical properties of these complexes will be compared when free in solution with after protein conjugation in order to assess their suitability for the desired application. The complexes in question, Figure 2.4, employ a ligand that fulfils the criteria of lanthanide chelation and sensitisation as discussed in Chapter 1. Additionally the complexes possess a thiol group which will later be used to anchor the complexes to AuNPs; these functionalised AuNPs will also be used as protein labels and as such the interaction of these complexes directly with proteins observed here will inform further work described in Chapter 4. The proteins selected for conjugation are BSA because of its biological importance and κ FLC which will interact with a labelled anti-κ FLC mAb for FRET applications. All of the complexes synthesised and used in this chapter are shown in Figure 2.4.

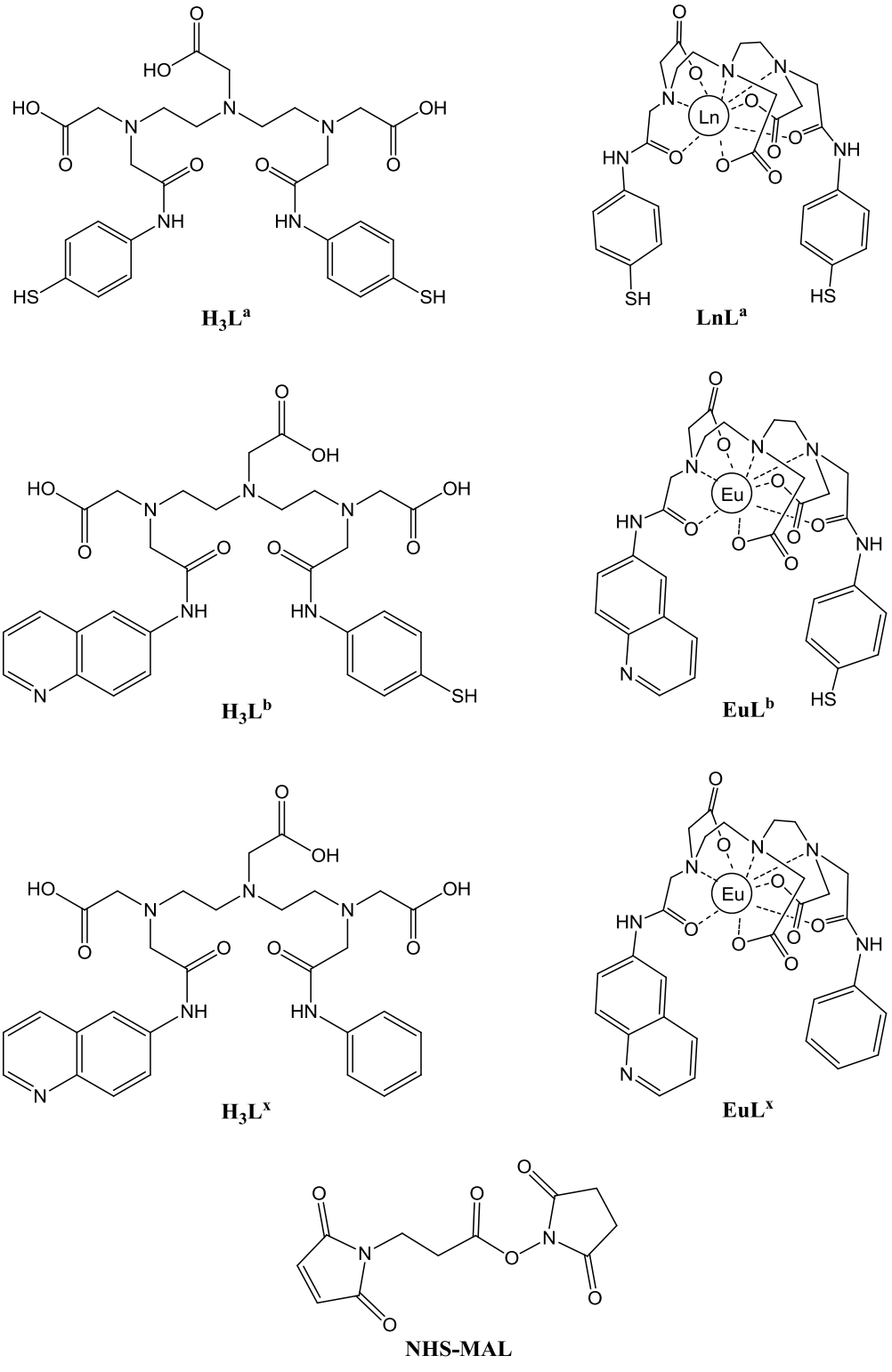

Figure 2.4 Compounds used in this chapter.
Ln = Eu, Tb or Nd.

2.2 Results and Discussion

2.2.1 Syntheses of Compounds Used

2.2.1.1 Synthesis of $\mathbf{H_3L^a}$

Synthesis of $\mathbf{H_3L^a}$ followed that previously reported by the Pikramenou group.[37]

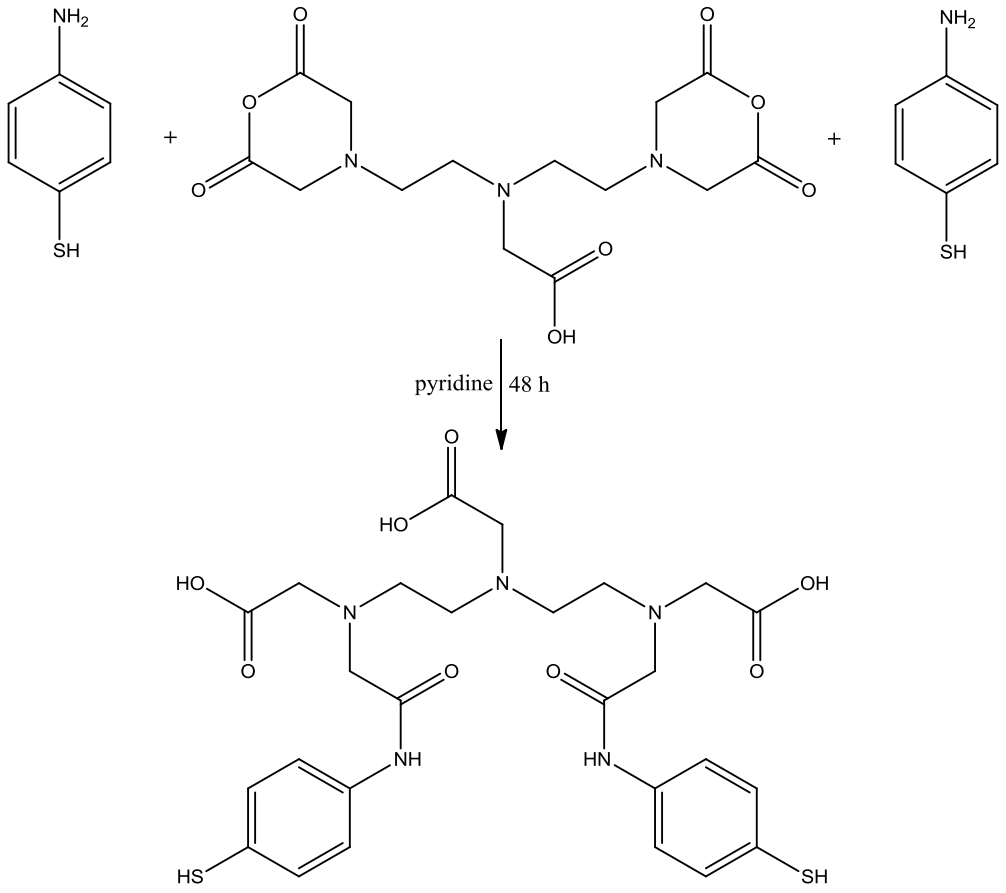

Scheme 2.2 Synthetic route to ligand $\mathbf{H_3L^a}$.

DTPA-bis(anhydride) was subjected to nucleophilic attack by 4-aminothiophenol to give $\mathbf{H_3L^a}$ in 23% yield. Full characterisation of the ligand concurs with that published previously and can be found in the experimental section of this chapter.[37]

2.2.1.2 Synthesis of **LnL^a** (where Ln = Eu, Tb or Nd)

As for the **H$_3$L^a** ligand, the synthesis followed was as previously described by the Pikramenou group.[37]

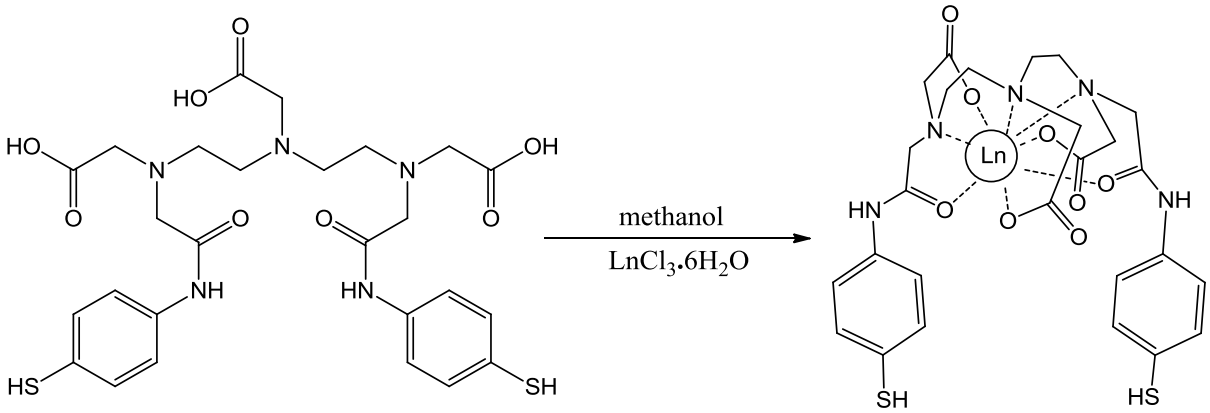

Scheme 2.3 Synthetic route to complexes **LnL^a**
Ln = Eu, Tb or Nd.

The appropriate lanthanide chloride hexahydrate was stirred together with **H$_3$L^a** resulting in the chelation of the lanthanide ion to give LnL^a. The yield of each complex was as follows: **EuL^a** 94%, **TbL^a** 89% and **NdL^a** 97%. Electrospray mass spectrometry of all three lanthanide products confirmed the formation of the complexes.

2.2.1.3 Synthesis of **H$_3$L^b**

This ligand is a modification of the previous **H$_3$L^a** ligand where one of the thiophenol sensitisers is replaced by a quinoline substituent. In this case the remaining thiophenol group possesses a thiol which provides a reactive group for protein conjugation, whereas the quinoline group allows the sensitisation of the lanthanide centre at a longer wavelength than the thiophenol which is more appropriate for studies involving biological materials. The

synthesis carried out here is an adapted version of that established previously by the Pikramenou group.[38]

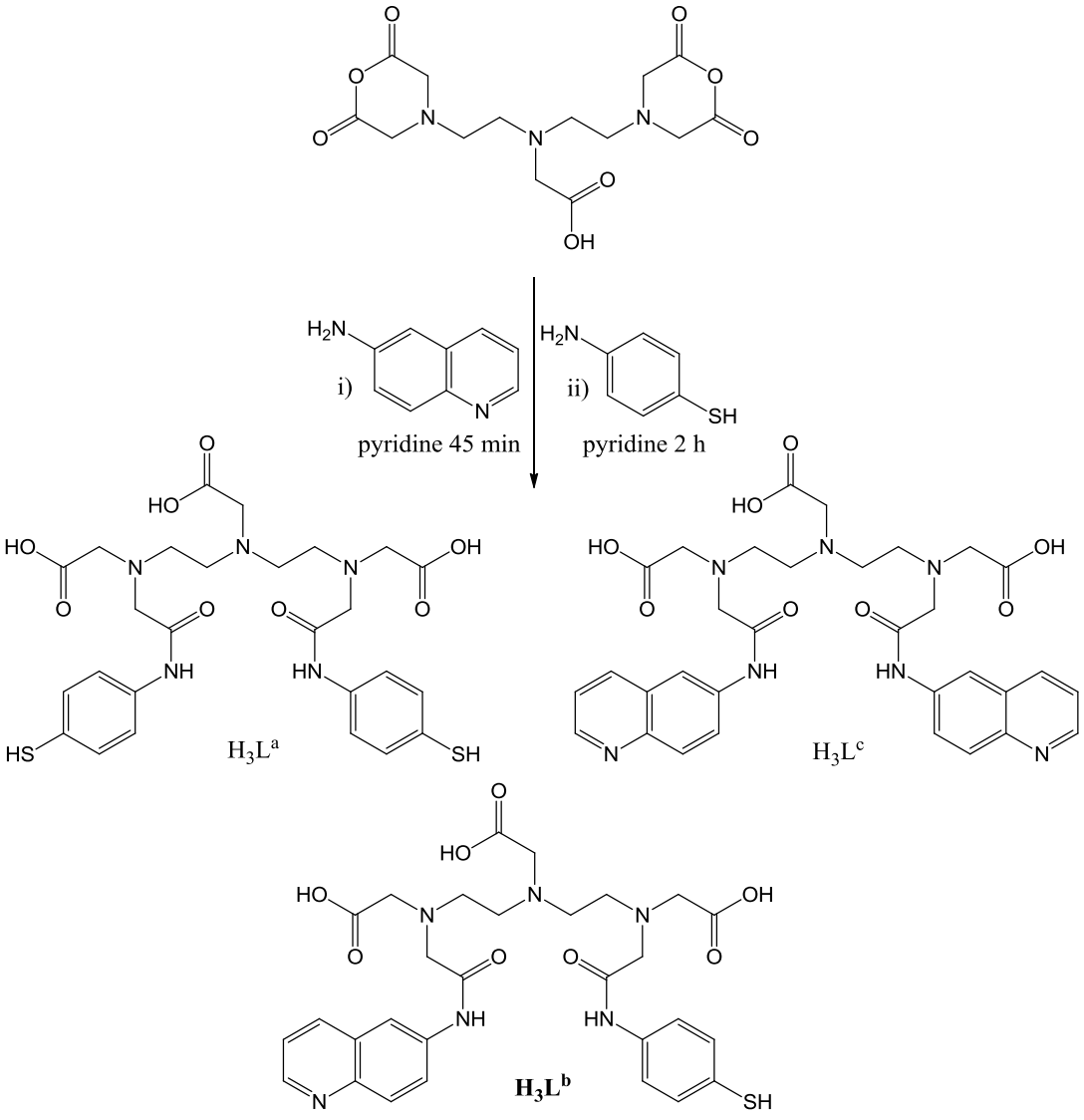

Scheme 2.4 Synthetic route to ligand $\mathbf{H_3L^b}$.

The ligand was formed by nucleophilic attack of DTPA-bis(anhydride), first by 6-aminoquinoline and then 4-aminothiophenol. It was desired that each nucleophile would attack one of the anhydride rings of DTPA-bis(anhydride) to give an asymmetric product, however, it is clearly possible that in some cases the same nucleophile may attack both

anhydride rings leading to the possibility of two unwanted symmetrical products being formed, Scheme 2.4. Indeed, the reaction did yield a mixture of H_3L^a, H_3L^c and the desired species $\mathbf{H_3L^b}$ which were separated by HPLC. The desired asymmetric species, $\mathbf{H_3L^b}$, was isolated in 3% yield. The formation and isolation of $\mathbf{H_3L^b}$ was confirmed by mass spectrometry and the aromatic region of the ^{1}H-NMR spectrum revealed the asymmetric nature of the ligand.

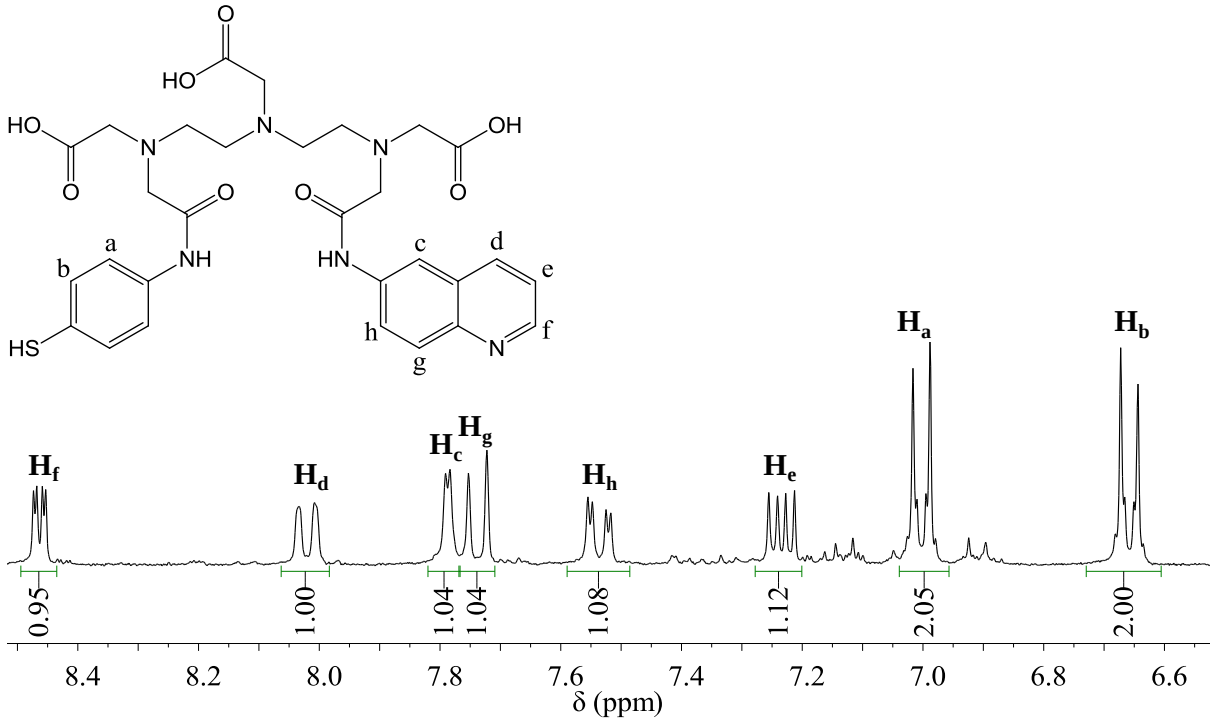

Figure 2.5 Aromatic region of the ^{1}H NMR spectrum of $\mathbf{H_3L^b}$.

The integration of the peaks shown in Figure 2.5 indicate that there are two protons in each of environments *a* and *b* to every proton in environments *c*-*h* which concurs with the intended structure of the ligand. The NMR spectra and other analyses also agree with that observed by David Lewis a previous researcher in the Pikramenou group.[38]

2.2.1.4 Synthesis of **EuL^{b}**

As for the **H$_3$L^{b}** ligand, the synthesis followed was as previously described by a member of the Pikramenou group.[38]

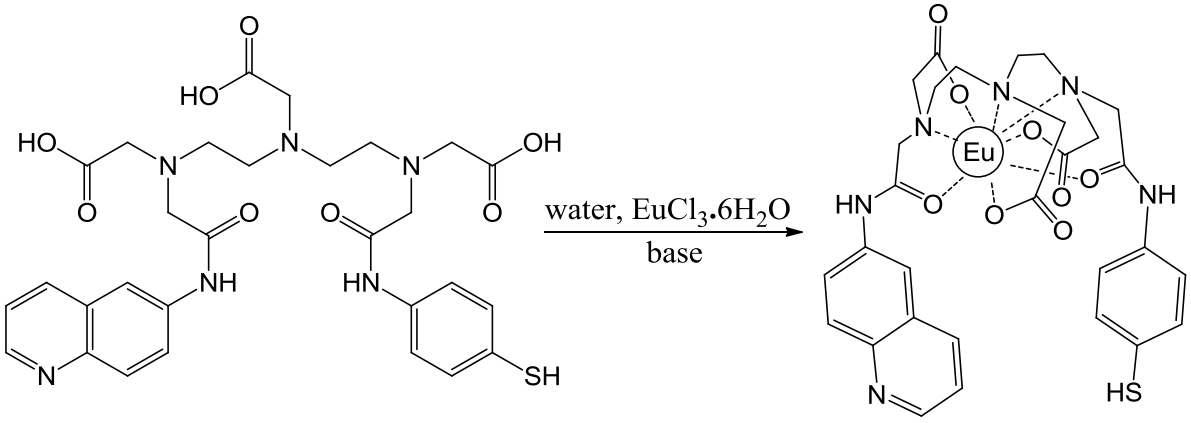

Scheme 2.5 Synthetic route to complex **EuL^{b}**.

Europium chloride hexahydrate was stirred in solution with **H$_3$L^{b}** and the pH of the solution raised by drop-wise addition of aqueous tetrabutylammonium hydroxide. **EuL^{b}** was formed and recovered in 59% yield. The identity of the europium complex was confirmed by mass spectrometry and high resolution mass spectrometry was consistent with the calculated composition of $C_{29}H_{31}EuN_6O_8S$.

2.2.1.5 Synthesis of **H$_3$L^{x}**

The ligand **H$_3$L^{x}** was designed to chelate Eu^{3+} and sensitise its emission. Its resulting lanthanide complex was also indented as a control compound where **EuL^{b}** was used for protein conjugation. The single difference between the two complexes is the absence of the thiol group in **H$_3$L^{x}** which is the group used to attach the complex **EuL^{b}** to proteins.

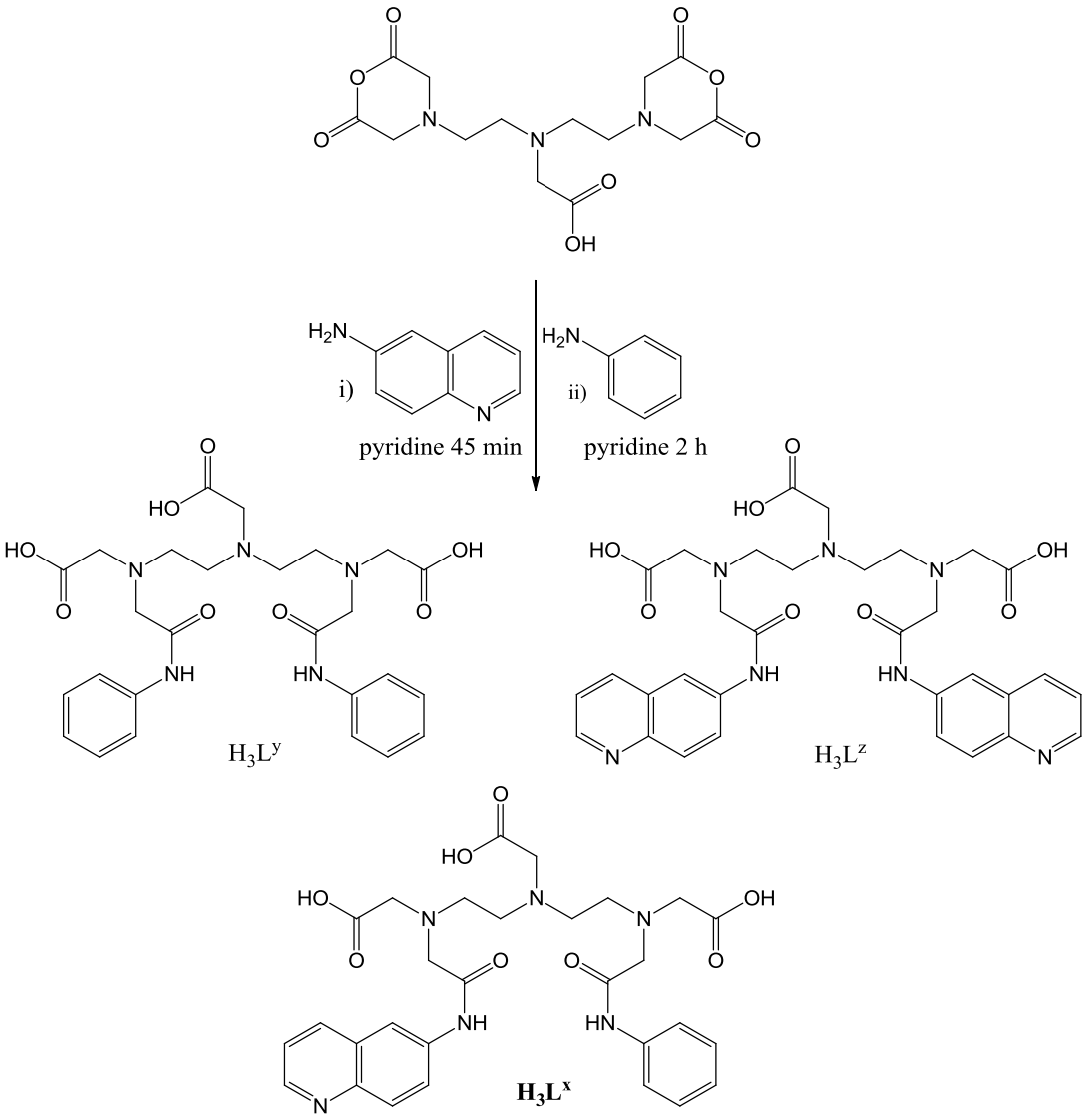

Scheme 2.6 Synthetic route to ligand $\mathbf{H_3L^x}$.

As is evident from Scheme 2.6, the synthesis of $\mathbf{H_3L^x}$ was the same as that for $\mathbf{H_3L^b}$ with the only difference being the replacement of 4-aminothiophenol with aniline in the reaction. HPLC was again used to isolate the asymmetric species to yield $\mathbf{H_3L^x}$ in 6% yield.

2.2.1.6 Synthesis of $\mathbf{EuL^x}$

Due to the similarity of the two ligands, it was possible to chelate europium using $\mathbf{H_3L^x}$ following the same method as that described for the synthesis of $\mathbf{EuL^b}$ in section 2.2.1.4.

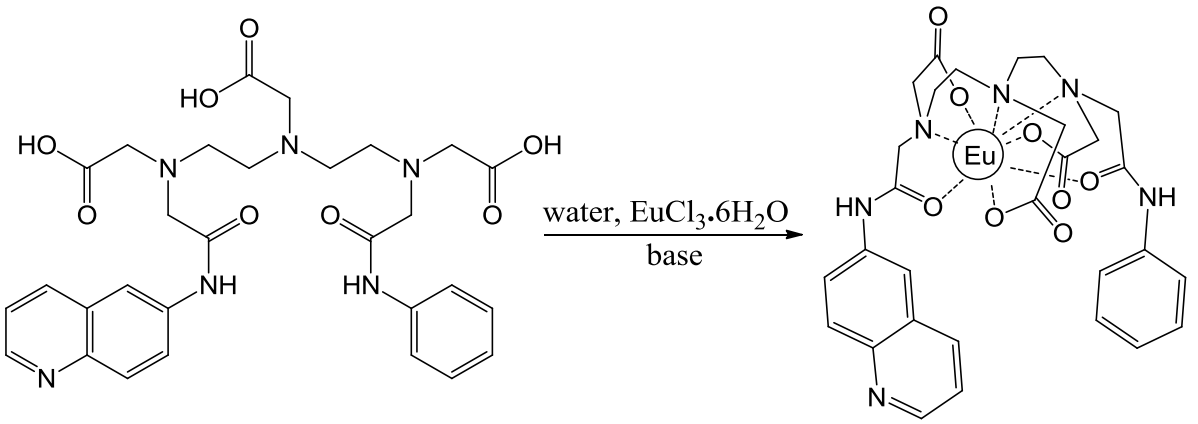

Scheme 2.7 Synthetic route to complex **EuL^{x}**.

EuL^{x} was prepared in 64% yield and its identity confirmed by electrospray mass spectrometry.

2.2.1.7 Synthesis of **NHS-MAL**

The **NHS-MAL** linker is used here to create a covalent link between a luminescent lanthanide complex and a protein molecule. It comprises of an ester of NHS which is a good leaving group thus allowing the formation of a peptide bond between the linker and amines in a protein, such as those found on lysine residues, and maleic anhydride which forms a covalent bond with the sulphur of the lanthanide complex used as the desired protein label. The synthesis followed is that previously described by Buchardt.[39]

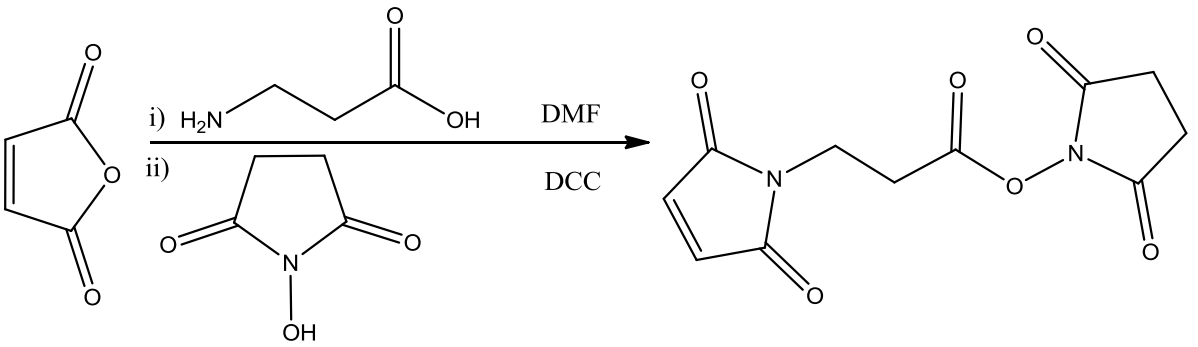

Scheme 2.8 Synthetic route to linker **NHS-MAL**.

Firstly, *β*-alanine underwent a condensation reaction with maleic anhydride at its N-terminal end before esterification at its C-terminal end with NHS to give **NHS-MAL** in 29% yield. Mass spectrometry confirmed the synthesis and isolation of the desired product and the NMR spectra concurred with that previously published.[39]

2.2.2 Examining the Conjugation of **LnL^a** to BSA (where Ln = Eu, Tb or Nd)

2.2.2.1 Preparation of **LnL^a-BSA**

The linker **NHS-MAL** was used to covalently attach **LnL^a** complexes to BSA in a two stage approach where first the linker was attached to BSA and then lanthanide complex was added subsequently.

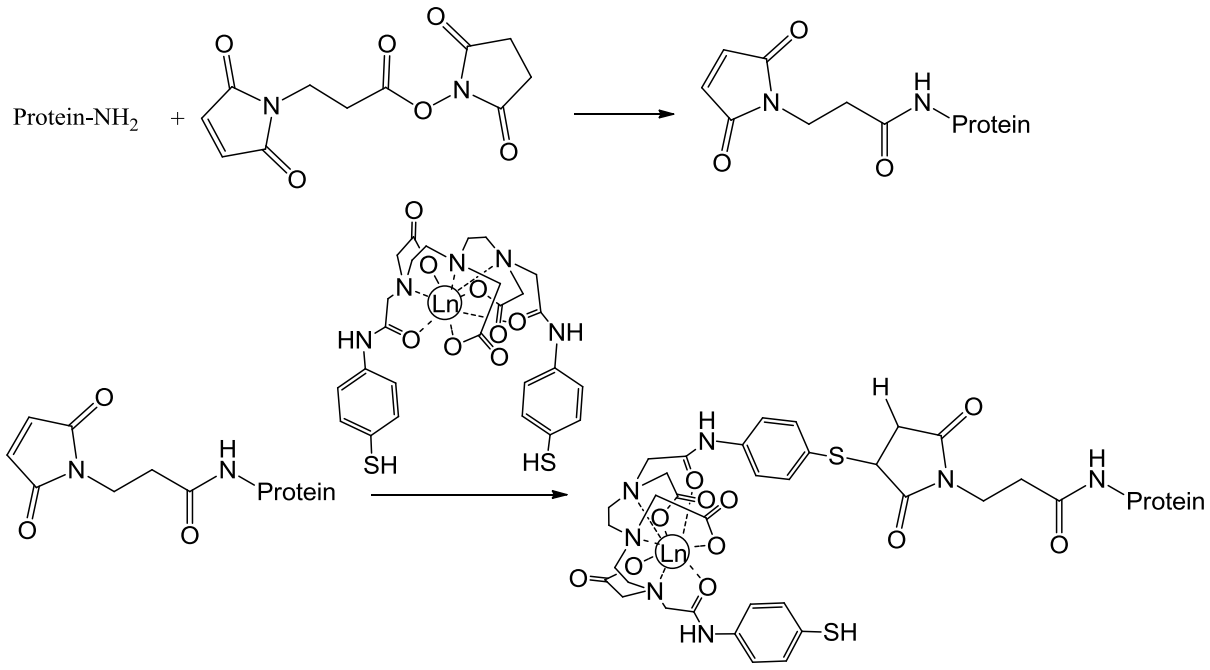

Scheme 2.9 Conjugation of **LnL^a** to the primary amine of a protein.
Ln = Eu, Tb or Nd.

BSA was dissolved in phosphate buffer at pH 7.4 and to this a concentrated solution of **NHS-MAL** was added in thirty times excess. The solution was stirred gently for 1 hour at 37 ºC

before being passed through a Sephadex G-15 size exclusion column to remove any unbound linker. A solution of **LnL^a** in methanol in thirty times excess was then added to the BSA-**NHS-MAL** conjugate collected from the column and gently stirred for 24 hours at room temperature. The solution was again passed through a size exclusion column to remove any free lanthanide complex and the recovered **BSA-LnL^a** conjugate was freeze-dried.

2.2.2.2 Photophysical Characterisation of **LnL^a** and **LnL^a-BSA**

It is worthwhile to compare the luminescent properties of **LnL^a** complexes with those of **LnL^a-BSA** in order to determine whether the photophysical properties of the lanthanide complexes are affected when used as protein labels.

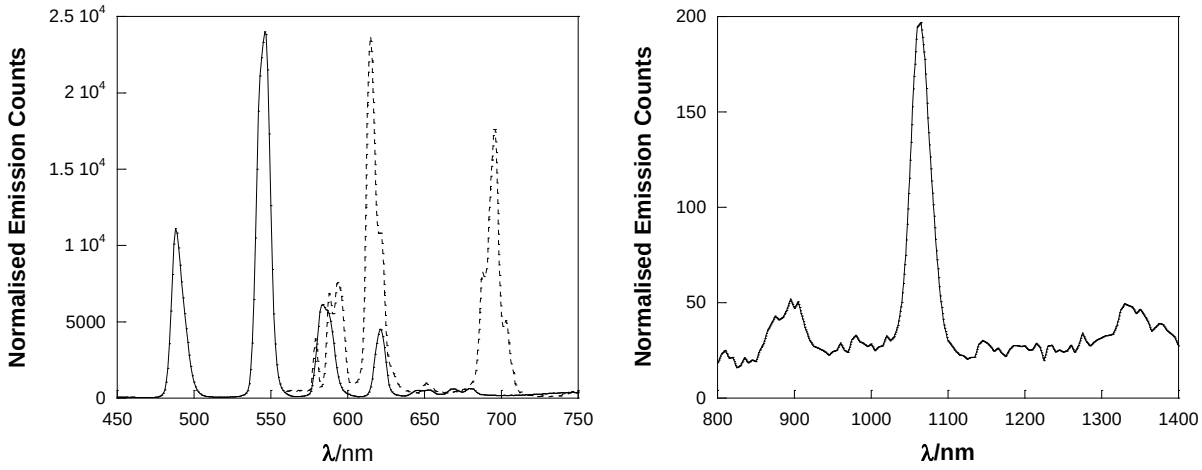

Figure 2.6 Emission spectra of **LnL^a** (Ln = Tb, Eu or Nd). Left: **TbL^a** (—) and **EuL^a** (---) in methanol, λ_{ex} = 266 nm, corrected for PMT response. Right: **NdL^a** (—) in deuterated methanol (CH_3OD), λ_{ex} = 280 nm.

The emission spectra in Figure 2.6 show the characteristic emission peaks expected for each lanthanide ion in question. The results confirm that the **H$_3$L^a** ligand is able to successfully sensitise lanthanide emission because otherwise the emission intensity would be very low if

excited through the lanthanide directly and is not possible at the short wavelengths used for excitation. Although the optimum excitation wavelength for the **LnL^a** complexes is at 266 nm, as shown by the excitation spectra presented in Figure 2.8, a slightly longer excitation wavelength still within the excitation range of the complex, 280 nm, was used to gain an emission spectrum of **NdL^a**; the reason for this is because the intensity of the excitation source used is greater at 280 nm than 266 nm causing a slight improvement in the emission intensity of **NdL^a** which is weak compared to **EuL^a and TbL^a**. Additionally, **NdL^a** was investigated in deuterated solvent to prevent vibrational quenching caused by solvents containing O-H in order to improve its emission intensity, but this was not necessary for **EuL^a** and **TbL^a**. Emission spectra of **LnL^a-BSA** conjugates were then obtained in the same way.

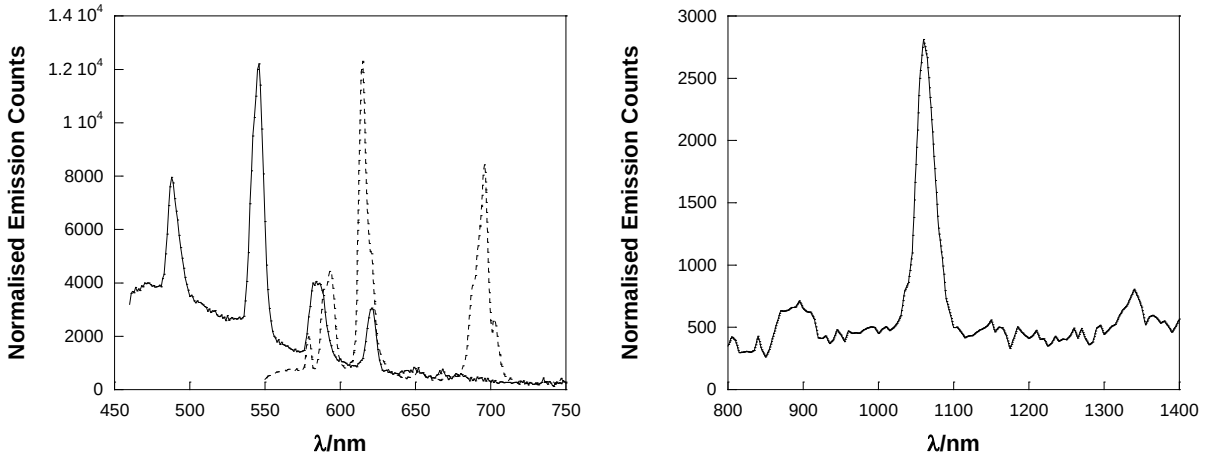

Figure 2.7 Emission spectra of **LnL^a-BSA** (Ln = Tb, Eu or Nd). Left: **TbL^a-BSA** (**—**) and **EuL^a-BSA** (---) in water, λ_{ex} = 266 nm, corrected for PMT response. Right: **NdL^a-BSA** (**—**) in D_2O, λ_{ex} = 280 nm.

The emission spectra in Figure 2.7 indicate that the luminescence of the lanthanide complexes **TbL^a**, **EuL^a** and **NdL^a** is unchanged when conjugated to BSA because the spectra are comparable to those in Figure 2.6 of the free complexes. In each case the characteristic emission peaks of each lanthanide species are present and in the same intensity ratios

displayed for the free complexes which demonstrates that the environment surrounding the lanthanide has changed very little upon conjugation to BSA. The most noticeable difference between the spectra in Figures 2.6 and 2.7 is the appearance of a sloping background to the terbium emission spectrum after conjugation to BSA. This is caused by the emission spectrum of BSA itself which extends into the region collected for terbium emission. An emission spectrum of BSA can be found in the appendix.

Although the appearance of the lanthanide emission spectra has not changed, it would be interesting to ascertain whether the protein itself can have an input into the sensitisation of the lanthanide. In order to do this the excitation spectra of the lanthanide species was measured when conjugated to BSA and when free in solution.

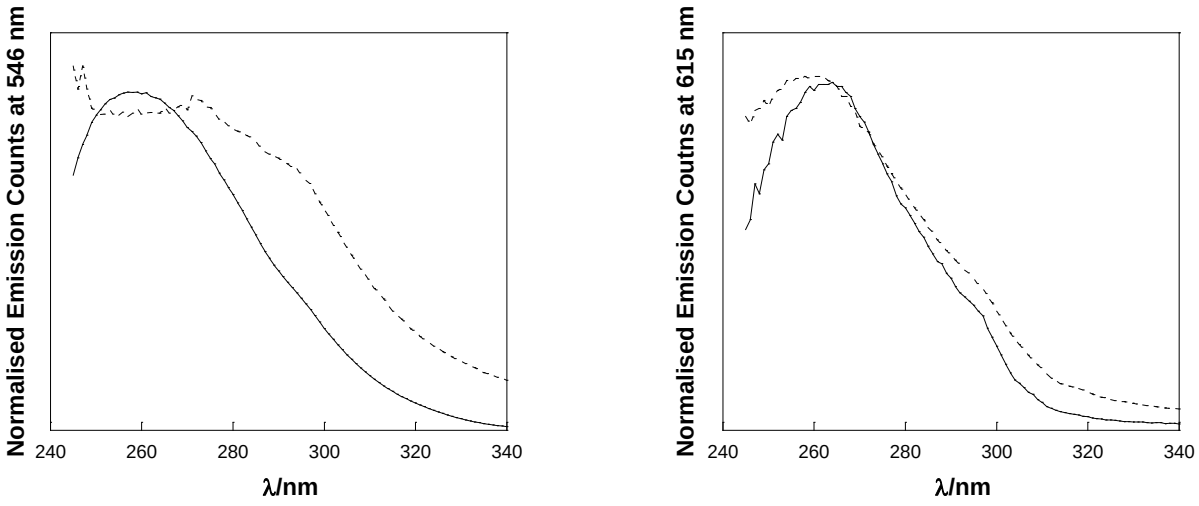

Figure 2.8 Excitation spectra of **LnL^a** in methanol and **LnL^a-BSA** in water. All spectra corrected for lamp intensity. Left: **TbL^a** (—) and **TbL^a-BSA** (---), λ_{em} = 546 nm. Right: **EuL^a** (—) and **EuL^a-BSA** (---), λ_{em} = 615 nm.

The excitation spectra show that the sensitisation of terbium emission does change when **TbL^a** is conjugated to BSA, whereas this is not the case for **EuL^a**. Excitation of the

lanthanide emission through its chelating ligand is centred around 260 nm, however, the excitation broadens in the case of **TbL^{a}-BSA** indicating that the protein, more specifically its tryptophan residues, is able to sensitise terbium emission. The fluorescence of tryptophan is known to be excited in the range of 250-300 nm and it has previously been shown that whilst tryptophan is able to transfer energy more efficiently to Eu^{3+} ions than Tb^{3+} ions, the transfer results in very efficient sensitisation of Tb^{3+} luminescence whereas the transfer to Eu^{3+} results in an almost entirely non-radiative decay.[40] This effect was reported for one previously published study discussed in section 2.1.3; the luminescence lifetime decrease of TbL^{6b}, Figure 2.3, was attributed to the sensitisation of terbium by the protein resulting in a short component to the measured lifetime, however, in this case a europium derivative was not studied.[31] Indeed, there are published reports of the exploitation of tryptophan for sensitised terbium luminescence from terbium complexes without intrinsic antennas or terbium ions for biological assay applications.[41, 42] Another article utilises tryptophan and tryptophan derivatives as antennas attached to a lanthanide chelating moiety; the study found that whilst the luminescence of chelated Tb^{3+} was sensitised by unmodified tryptophan and all tryptophan derivatives, chelated Eu^{3+} displayed sensitised luminescence with only one tryptophan derivative and not unmodified tryptophan. In the case of the modified tryptophan antenna that was able to elicit sensitised Eu^{3+} luminescence its emission was red shifted in relation to unmodified tryptophan.[43]

2.2.2.3 Treatment of Neutrophil Cells with **LnL^{a}-BSA** (Ln = Eu, Tb or Nd)

Previous studies by the Pikramenou group have assessed flow dynamics in channels using luminescent nanoparticles in flow. Where the rheology of blood vessel was of interest these nanoparticles were observed in flow with matter from the blood present in an artificial vessel,

but attempts to label blood cells themselves with lanthanide labels was unsuccessful. As previously discussed, there are many advantages to the use of lanthanide complexes in biological systems, and as such it would be extremely useful to label blood cells with lanthanide labels in order to study their flow in vessels more easily. A possible route to achieve luminescent lanthanide labelling of cells is their treatment with lanthanide labelled BSA. Indeed, serum albumins conjugated to luminescent or radiolabels have been previously shown to be taken up via endocytic pathways by murine macrophage, hepatic and renal cell lines and human cervical and alveolar carcinoma cell lines.[4, 44-46] Having said this, there has not been a report of using lanthanide labelled BSA to stain neutrophil cells in the past. Luminescent europium and terbium complexes have previously been used to specifically label cellular compartments of neutrophils, but in this case the complexes were conjugated to antibodies and the cells were permeabilised using a chemical reagent to allow the conjugated antibodies to access the cellular interior.[47] Labelled cells were imaged using time-gated microscopy techniques allowing the removal of auto-fluorescence from the images and the separation of signal from other probes used. More recently a gadolinium complex, based on a DOTA chelating group, has been attached to a peptide sequence for the specific labelling of receptors on the surface of neutrophils in order that the cells can be tracked by MRI studies, however, no internalisation of the complex was observed.[48] Lanthanide containing KYF_4:Yb,Er nanoparticles have also recently been shown to be taken up by neutrophil cells resulting in bright luminescence images of the cells, however, although BSA was used to coat the nanoparticles, the addition of biotin to the surface of the nanoparticles was deemed to be the most significant factor in terms of cellular uptake.[49]

In this case neutrophils obtained from whole blood were suspended in PBS to give a cell count of 10^8 mL^{-1} and to 100 µL of cells 50 µL of **LnL^a-BSA** was added and the cells incubated with the labelled BSA for 1 hour at 37 ºC. The concentration of labelled BSA was 20 mg mL^{-1} in the case of **EuL^a-BSA** and **NdL^a-BSA** and was 65 mg mL^{-1} in the case of **TbL^a-BSA**. After incubation the cells were collected by centrifugation and the supernatant discarded, the cells were then redispersed in PBS and this process was repeated three times to remove any excess BSA. Finally the cells were centrifuged to form a pellet and were then redispersed in 100 µL of 2% paraformaldehyde. A drop of the treated cells was then placed on a microscope slide with a cover slip on top and epifluorescence microscopy of the samples executed.

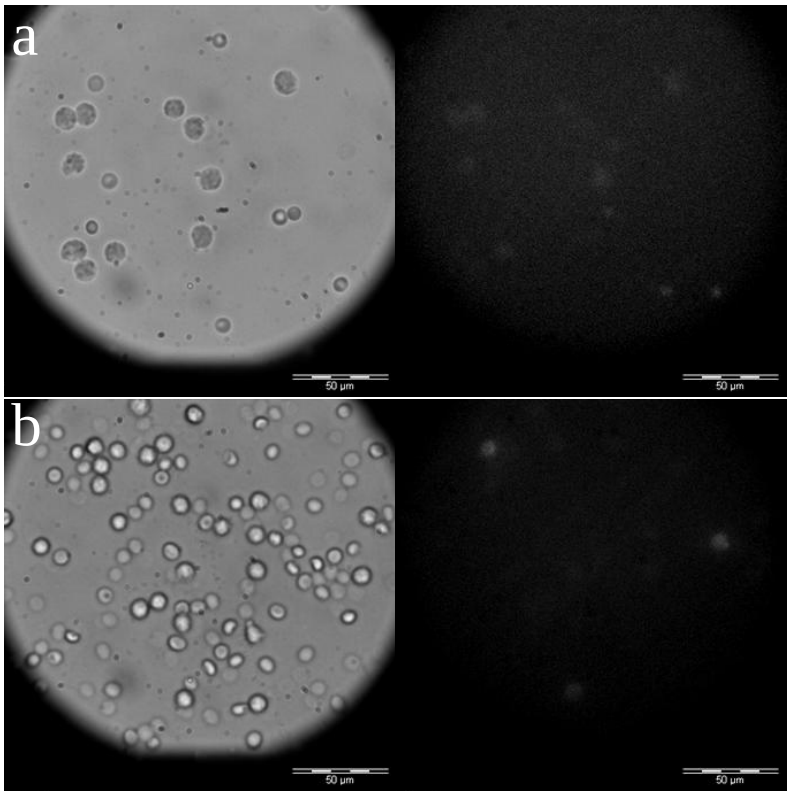

Figure 2.9 Bright field (left) and epiluminescence (right) microscope images of neutrophils treated with a) **TbL^a-BSA**, λ_{ex} = 360 nm and b) **EuL^a-BSA** λ_{ex} = 394 nm. Scale bar = 50 µm.

The microscope images of the cells clearly demonstrates that the neutrophils are luminescent following treatment with **TbL^{a}-BSA** and **EuL^{a}-BSA**, however, it was not possible to gain luminescence images of cells treated with **NdL^{a}-BSA**. To confirm whether the luminescence exhibited by the cells during microscopy was from the **LnL^{a}-BSA** the cells were diluted and a suspension of cells in a cuvette examined in a steady state emission spectrometer.

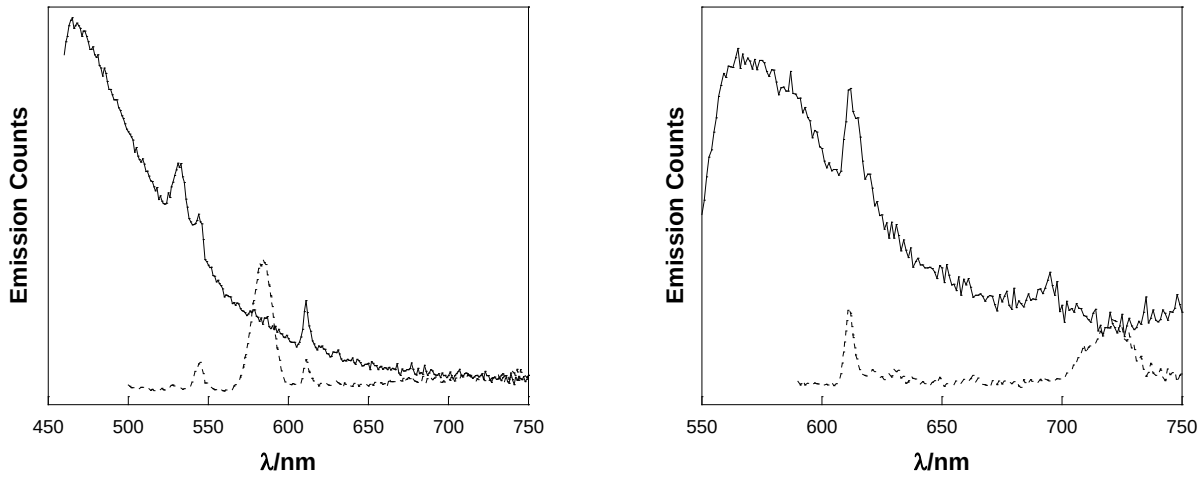

Figure 2.10 Emission spectra obtained from neutrophils treated with **LnL^{a}-BSA**. Left: **TbL^{a}-BSA** where λ_{ex} = 266 nm (—) or 487 nm (---). Right: **EuL^{a}-BSA** where λ_{ex} = 266 nm (—) or 578 nm (---). All spectra corrected for PMT response.

The emission spectra of the neutrophils confirm that their treatment with **LnL^{a}-BSA** has resulted in the uptake of the lanthanide label by the cells. The characteristic luminescence of both **TbL^{a}** and **EuL^{a}** is evident both with a protein fluorescence background when the lanthanide is sensitised through excitation of its chelating ligand at 266 nm and without the protein background when the lanthanide centre is excited directly, although in the latter case the luminescence intensity is understandably lower due to the inefficiency of directly exciting the lanthanide. As with the microscopy **NdL^{a}** emission could not be detected, but this does not necessarily mean that it was not taken up by the cells, rather that the detection of NIR

emission is not as sensitive as that used for visible. The success of luminescently labelling neutrophils with both **TbL^{a}-BSA** and **EuL^{a}-BSA** demonstrates the potential of using BSA covalently linked to luminescent lanthanide labels as a vehicle for label delivery in neutrophil cells.

2.2.2.4 Calculating the Degree of Labelling of **LnL^{a}-BSA**

Attempts were made to obtain mass spectra of the conjugated species, however, all attempts were unsuccessful with all ionisation techniques utilised. It may be the case that in modifying the lysine residues several of the ionisation sites of the protein were blocked preventing the production of a sufficiently charged molecule, but needless to say another method of calculating the degree of labelling was necessary. The first BSA conjugate prepared was **TbL^{a}-BSA** and the degree of labelling in this case was calculated by measuring the absorbance of the protein before and after conjugation. This was not straight forward, however, as the absorbance of BSA and **TbL^{a}** overlap considerably, as shown by their absorption bands in Figure 2.11, and as such the absorbance from the individual species could not be resolved.

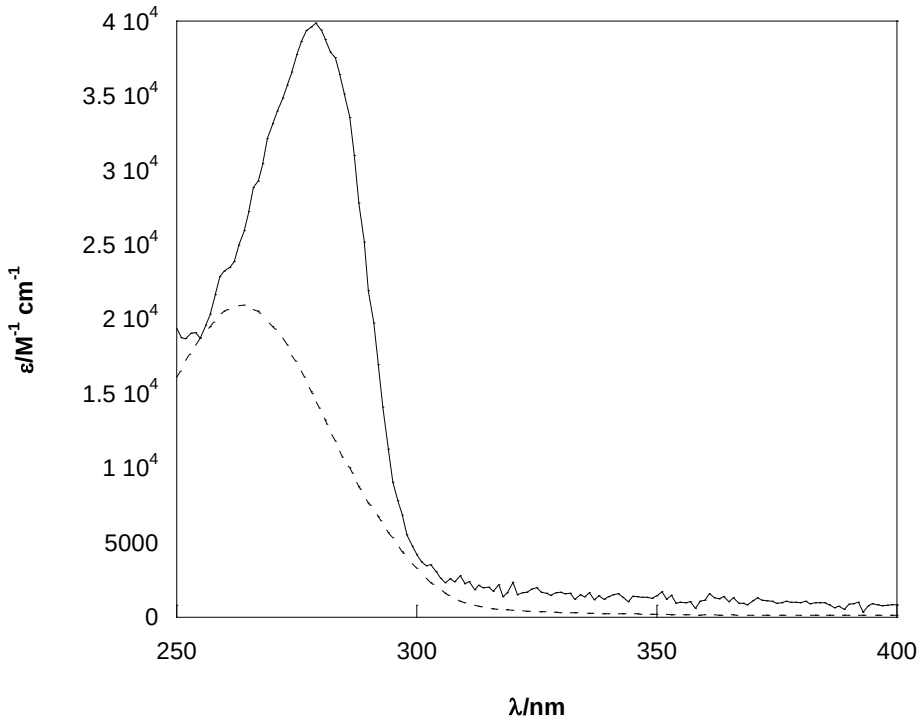

Figure 2.11 Molar absorption coefficient versus wavelength of native BSA in aqueous solution (—) and **TbL^{a}** in 10% methanol in water (---).

Taking into account the estimated dilution of the protein through the purification steps, the increase in absorbance at 278 nm was assumed to be due to the presence of **TbL^{a}**. The amount of 'extra' absorbance measured at 278 nm was then used to calculate the concentration of **TbL^{a}** in the conjugated sample, and thus, in comparison to the concentration of BSA, the degree of labelling. Using this method, there were calculated to be 13 **TbL^{a}** labels per molecule of BSA. However, if the measured molar absorption coefficients of the individual species are combined in a 13:1 ratio the result does not concur with the measured absorbance of the conjugate. This may be due to an inaccurate calculation of the BSA concentration after the conjugation, so in an attempt to confirm the degree of labelling an aliquot of the **TbL^{a}-BSA** conjugate was analysed using ICP-OES for terbium and sulphur. In this case the concentration of terbium should relate to the concentration of label in the sample

and using this the amount of sulphur from the label can be deducted from the total sulphur measured, leaving the sulphur of the protein from which the concentration of BSA can be calculated, however, the measurement of sulphur was too low to be detected and as such this calculation could not be performed.

Another method used to calculate the degree of labelling was to conjugate BSA with $\mathbf{H_3L^a}$, using the same method used for $\mathbf{LnL^a}$, titrate in a lanthanide ion and measure the increase in luminescence until a plateau is reached. Since it is known that each $\mathbf{H_3L^a}$ ligand binds one lanthanide ion, the concentration of lanthanide ion required to reach this plateau should give the concentration of $\mathbf{H_3L^a}$ conjugated to BSA. From the titration results the absorption spectra can be evaluated as before using the known molar absorption coefficients of the individual species to give a degree of labelling. The lanthanide ion chosen for the titration was Eu^{3+} because its emission is more removed from that of BSA which eliminates much of the background fluorescence that would be seen if Tb^{3+} was used and its emission in the visible range which allows for more sensitive detection than if Nd^{3+} was used whose emission is in the NIR. Before the titration was carried out, a titration of Eu^{3+} into a solution of $\mathbf{H_3L^a}$ was conducted as a proof of concept study, the results of which can be found in the appendix. In addition to titrating the Eu^{3+} into conjugated BSA it was also titrated into native BSA as a control study.

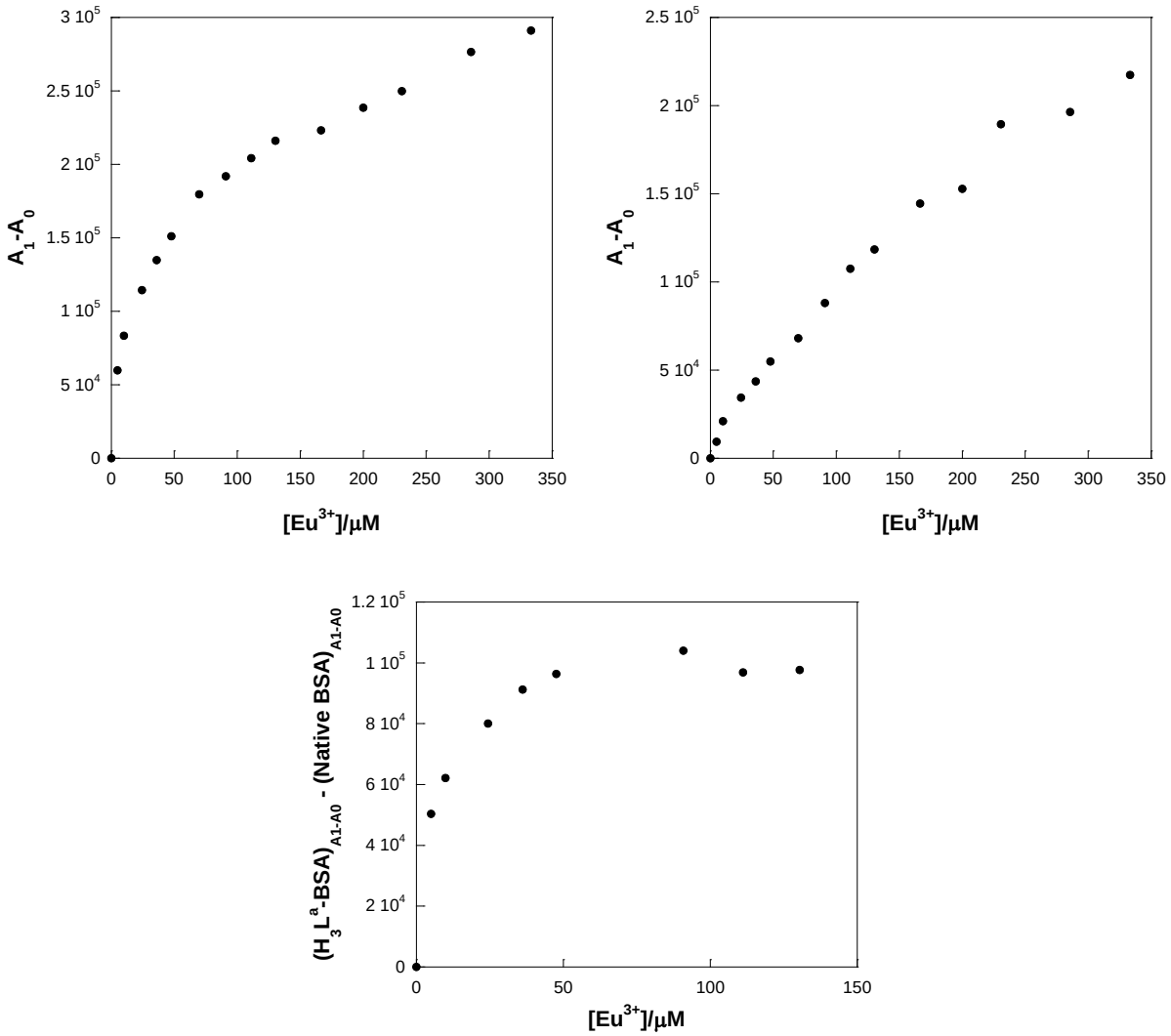

Figure 2.12 Integrated emission signal of **H_3L^a-BSA**, A_0 (top left) or BSA, A_0 (top right) subtracted from integrated emission signal when Eu^{3+} is added, A_1. Integrated emission signal change of native BSA subtracted from integrated emission signal change of **H_3L^a-BSA** (bottom). λ_{ex} = 266 nm, λ_{em} = 550-750 nm. Corrected for PMT response.

If the spectrum on the top left hand side of Figure 2.12 is considered in isolation, the conclusion may be drawn that there is the suggestion of a plateau at a concentration of approximately 150 μM Eu^{3+} after which the emission intensity continues to increase which means that the titration may need to be continued using greater concentrations of Eu^{3+}, however, the titration of Eu^{3+} into native BSA as shown in the top right hand section of Figure 2.12 shows that when **H_3L^a** is not present there is something intrinsic to native BSA that is

able to sensitise Eu^{3+} emission. Indeed, it is not unlikely that Eu^{3+} should bind non-specifically to native BSA given its role of binding ions and molecules within the body, and as previously discussed, the tryptophan residues of native BSA are able to transfer energy to Eu^{3+}. Whilst it was previously shown that the energy transfer of tryptophan to **EuL^{a}** did not sensitise Eu^{3+} emission, this may have been because the sensitisation of the emission was dominated by the chelating ligand, whereas here, in its absence or when all ligands are occupied, the tryptophan sensitisation of Eu^{3+} emission, however weak, is observed. It can be concluded, however, that the binding of Eu^{3+} to **H$_3$L^{a}-BSA** is much stronger than the binding of Eu^{3+} to native BSA. If the change in the integrated emission of native BSA upon addition of Eu^{3+} is subtracted from that of **H$_3$L^{a}-BSA** then a much clearer plateau is seen as shown at the bottom of Figure 2.12. Indeed, the graph at the bottom of Figure 2.12 indicates that all **H$_3$L^{a}** ligands are occupied by europium ions once 50 μM of Eu^{3+} is added. However, if this conclusion is followed through to the say that there must, therefore, be 50 μM of **H$_3$L^{a}** in the **H$_3$L^{a}-BSA** sample, the calculated absorbance of this concentration of ligand based on its molar absorption coefficient is far greater than that measured for the sample prior to the titration. This would suggest that the absorption properties of the two species, **H$_3$L^{a}** and native BSA, at 280 nm do not linearly combine when conjugated to form **H$_3$L^{a}-BSA**, and as such this method of calculating the degree of labelling is precluded.

It is entirely possible that the **H$_3$L^{a}** or **LnL^{a}** is able to cross link two BSA molecules since the ligand bears two thiol groups which could facilitate attachment to two **NHS-MAL** linkers each on different protein molecules. BSA is also known to dimerise naturally, and as such, the dimerisation of the protein, either naturally or through cross linking by the label, may affect the calculation of the degree of labelling.[1]

No further attempts were made to calculate the degree of labelling of **LnL^{a}-BSA** as all stocks of the conjugated samples synthesised had been depleted and plans were made to use an alternative label for future experiments.

2.2.3 Examining the Conjugation of **EuL^{b}** to BSA to give **A-BSA** and **B-BSA**

2.2.3.1 Preparation of **EuL^{b}-BSA** Species **A-BSA** and **B-BSA**

Whilst the experiments with **LnL^{a}-BSA** were successful and interesting, it was decided to begin protein labelling work using **EuL^{b}** for two reasons. Firstly, **EuL^{b}** possesses a quinoline sensitiser facilitating lanthanide sensitisation at 330 nm as opposed to 266 nm used for **LnL^{a}**, which is more appropriate for use with biological materials, and secondly, because only one thiol is present in this molecule compared to the two in **LnL^{a}** which allows a better understanding of the conjugate produced since it may have been possible for **LnL^{a}** to cross link the protein or bind with two linker molecules on a single protein. The conjugation of **EuL^{b}** to BSA was achieved in two ways, firstly, following the same procedure as that described for **LnL^{a}** in section 2.2.2.1 to give the conjugated species **A-BSA**, and secondly using this procedure with minor modification to give the conjugated species **B-BSA**.

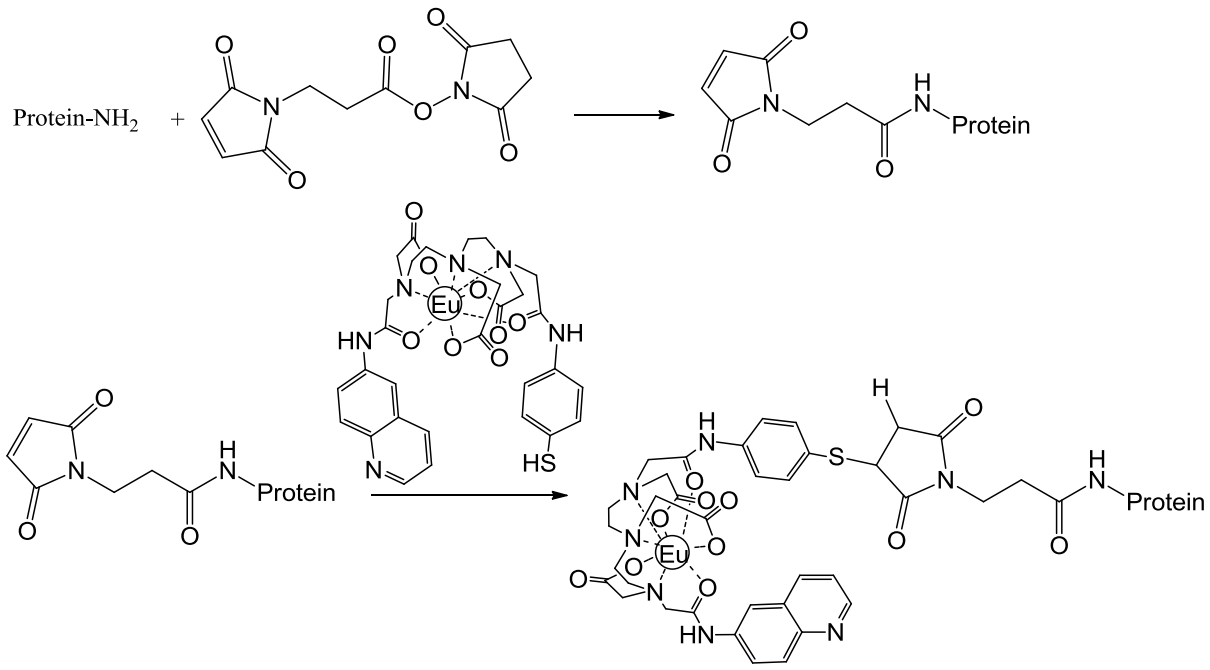

Scheme 2.10 Conjugation of **EuL^{b}** to the primary amine of a protein.

As shown in Scheme 2.10, a two step conjugation was again used, however, in this case an attempt was made to control the degree of labelling of the protein. Two conjugates of **EuL^{b}-BSA** were prepared; **A-BSA**, conjugated as described in section 2.2.2.1, and **B-BSA**, whose conjugation differed by adding at each stage compound in ten times excess compared to a thirty times excess used previously and by drop-wise addition of a dilute solution of **NHS-MAL** over 1 hour compared to a single addition of a concentrated solution. It was anticipated that **A-BSA** should have many lanthanide labels whereas **B-BSA** should have relatively few because of the difference in the amounts of label and linker added in each case. The absorption spectra of the labelled species reveal a possible difference in their degree of labelling.

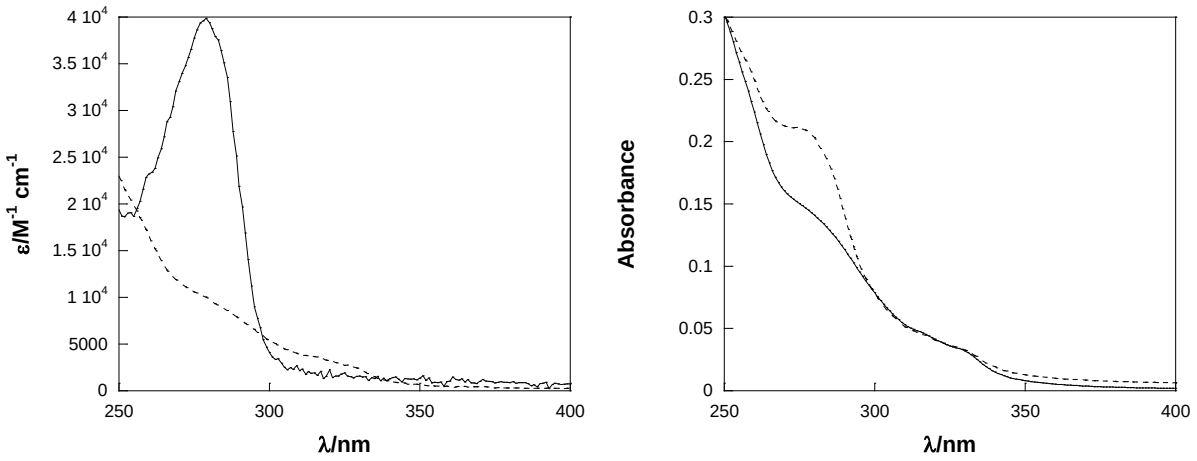

Figure 2.13 Left: Molar absorption coefficient vs wavelength for native BSA in aqueous solution (—) and **EuL^{b}** in 2% methanol in water (---). Right: Absorption spectra of **A-BSA** (—) and **B-BSA** (---) in aqueous solution.

The absorption spectra in Figure 2.13 show that whilst the absorption of both **A-BSA** and **B-BSA** show similarities to that obtained for **EuL^{b}**, the characteristic absorption peak of BSA at around 280 nm is only a feature in the spectrum of **B-BSA** which could indicate that there are considerably more labels in the **A-BSA** conjugate and these labels mask the BSA absorption.

2.2.3.2 Calculating the Degree of Labelling of **EuL^{b}-BSA**

Although overlap at 280 nm in the absorption spectra of the label and the protein still exists as was seen with **LnL^{a}-BSA**, attempts were made to calculate degree of labelling through comparison of absorbance at 280 nm with that at 330 nm since the complex absorbs at 330 nm but the protein does not absorb much at that wavelength, however, the absorption of the protein at 330 nm was sufficient to affect the calculations, as shown on the left hand side of Figure 2.13, so the degree of labelling could still not be calculated in this way.

A Bradford assay was then employed to detect the concentration of BSA of each conjugate.[50, 51] The Bradford assay uses the reagent Coomassie Brilliant Blue G.

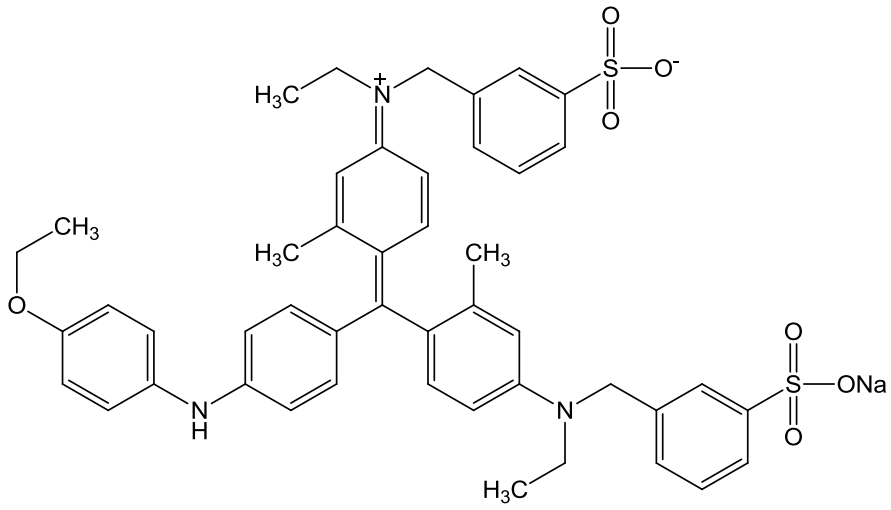

Figure 2.14 Structure of Coomassie Brilliant Blue G.

The Bradford assay relies on the change in absorbance of Coomassie Brilliant Blue G when it binds to protein as opposed to when in is free in solution. The reagent binds to proteins through their arginine and lysine residues and its absorption maxima changes from approximately 450 nm when free in solution to 620 nm when bound to protein, as shown by the spectra on the left hand side of Figure 2.15. The shift in the absorbance of the reagent is due to a change in its charge upon binding. In this case the ratio of absorbance of the dye at 595/450 nm was plotted against known protein concentration in order to achieve a linear calibration curve. Absorption measurements were also taken of Coomassie Brilliant Blue G when mixed with samples of **A-BSA** and **B-BSA** at several dilutions and the results plotted on the calibration curve to find the concentration of BSA in each conjugate sample, as shown on the right hand side of Figure 2.15. The BSA concentration could then be used to calculate the expected absorbance from the protein and as such the measured absorbance of the sample could be used to calculate the concentration of label through its contribution to the measured absorption above that calculated to come from the protein alone.

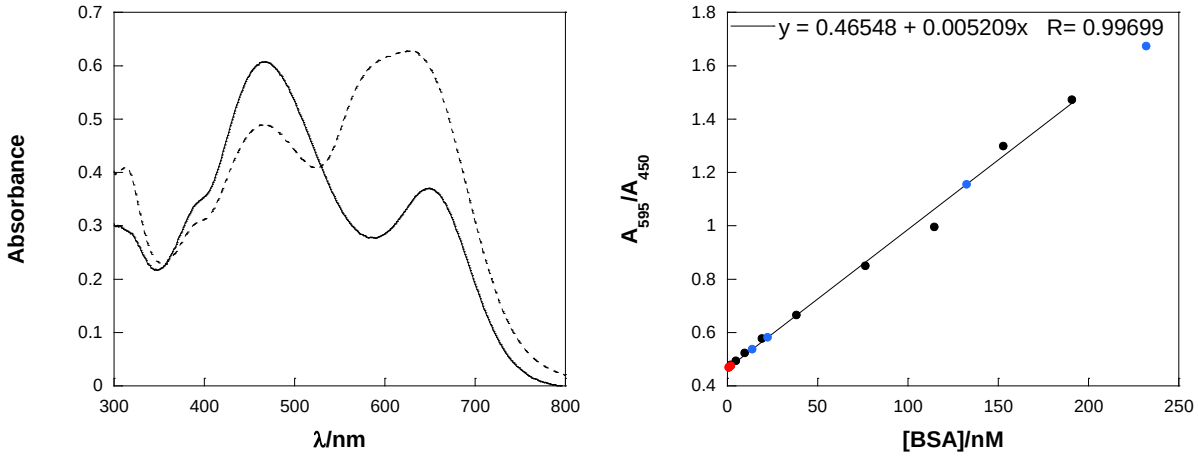

Figure 2.15 Left: Absorption spectra of Brilliant Blue G in the presence of 2.1 nM BSA (—) and 166.4 nM BSA (---). Right: Results of the Bradford Assay for a known amount of native BSA (●), **A-BSA** (●) and **B-BSA** (●).

From the Bradford assay results it was calculated that **A-BSA** contains 122 labels per BSA molecule and that **B-BSA** contains around 4. These results do not seem reliable especially in the case of **A-BSA** because the number of calculated labels is around double the amount of lysine residues present in each molecule of BSA, however, the natural ability of BSA to dimerise may have affected this result.[1] Furthermore, the calculated degree of labelling may be incorrect either because the assumption that the absorbance of the protein and label together is simply a linear combination of the separate species is incorrect, which has already been suggested by previous results, or because Coomassie Brilliant Blue G was affected by the presence of the labels at the lysine residues since it binds to protein through lysine and arginine residues.

ICP-MS was carried out on both conjugates with the aim of detecting the absolute concentrations of europium in the samples. The absorption spectra of the samples was obtained before the samples were digested in acid and diluted. The measured europium concentration was then used to calculate the expected absorbance from the label and as such

this could be subtracted from that measured and from the remaining absorbance the concentration of BSA calculated. The calculation method can be found in the appendix. In this case it was calculated that there are 0.39 labels per BSA molecule in **A-BSA** and 0.13 in **B-BSA**. As with the results from the Bradford assay the calculated degree of labelling seems unlikely. The low levels of labelling in both samples do not concur with the vast difference seen in the absorption spectra of the two species.

Another method to detect the degree of labelling is needed, but as with **LnL^{a}-BSA** mass spectra of **A-BSA** and **B-BSA** could not be obtained and there has not been an attempt to utilise another possible method. Both the Bradford assay and ICP-MS calculations for the degree of labelling are based on the assumption that the absorbance of BSA and **EuL^{b}** is simply cumulative when the two species are conjugated, and perhaps this assumption is incorrect which is why the results are not plausible. This assumption was originally used due to a number of published studies basing their degree of labelling calculations of similar systems around it.[28, 29, 31, 32] However, it may be the case that it is not reliable to do so since the local environments around the chromophores are changed upon conjugation, thus affecting their absorption properties.[52] Although both methods have proved inconclusive, both sets of results confirm that **A-BSA** contains more **EuL^{b}** labels per BSA molecule than **B-BSA** which was the intention of using the different approaches to the conjugation reaction.

2.2.3.3 Photophysical Studies of **EuL^{b}**

The emission spectra of **EuL^{b}**, **A-BSA** and **B-BSA** were measured in order to establish whether the conjugation had affected the luminescence properties of the label.

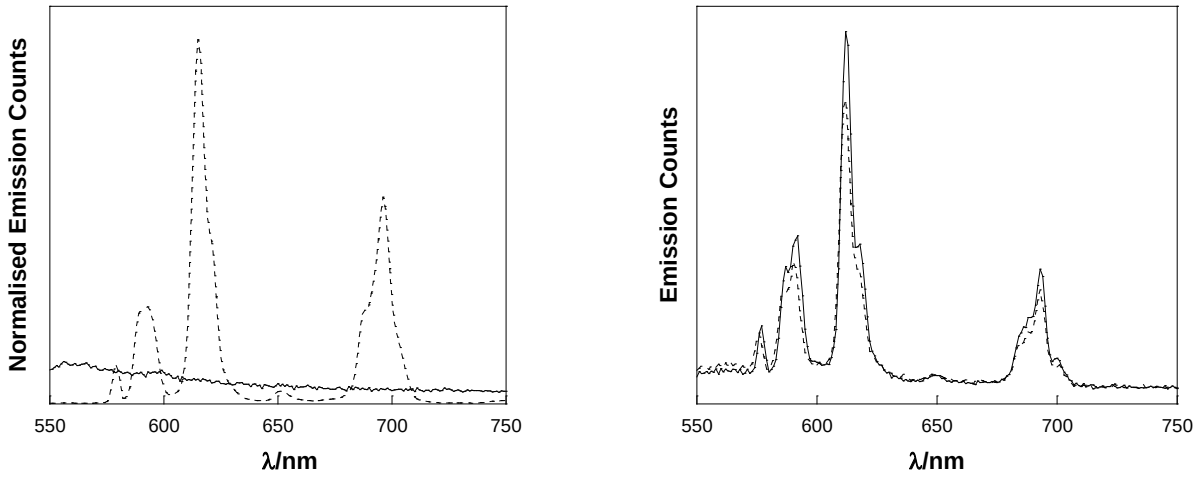

Figure 2.16 Left: Emission spectra of native BSA in aqueous solution (—) and **EuL^{b}** in methanol (---). Right: Emission spectra of **A-BSA** (—) and **B-BSA** (---) in aqueous solution. All spectra λ_{ex} = 330 nm, corrected for PMT response.

As is evident in Figure 2.16, the emission spectra of both **A-BSA** and **B-BSA** show characteristic Eu^{3+} emission that is unchanged from the free complex. In addition to this there appears to be a slight background fluorescence detected for the conjugated species which could be due to the fluorescence of BSA, as demonstrated by the emission spectrum obtained for native BSA, or light scattering caused by particulate matter in solution such as protein aggregates.

Since the luminescent emission peaks of **EuL^{b}** appear unchanged when conjugated to BSA, the luminescence lifetime and quantum yield were also investigated to determine whether conjugation affects these properties.

Sample	Φ/%	τ/μs
EuL^{b} (methanol)	2.60 ± 0.52	798 ± 80
EuL^{b} (aq)	0.86 ± 0.17	416 ± 42
A-BSA (aq)	0.24 ± 0.05	441 ± 44
B-BSA (aq)	0.55 ± 0.11	562 ± 56

Table 2.1 Luminescence quantum yield and lifetime measurements for **EuL^{b}**, **A-BSA** and **B-BSA** in aqueous solution and **EuL^{b}** in methanol. τ measurements obtained at λ_{em} = 615 nm.

The luminescence quantum yield measurements show that the free complex, **EuL^{b}**, in methanol has a greater quantum yield than that of the free complex in water which is similar to the values obtained for the conjugated species, **A-BSA** and **B-BSA**. It must be noted, however, that in order to compare the samples they were made so that all samples had a comparable absorbance at the excitation wavelength used, 330 nm; this means that the comparison of quantum yield measurements between free **EuL^{b}** and conjugated species **A-BSA** and **B-BSA** is unfair due to the absorbance of BSA at this wavelength, as shown in Figure 2.13, which acts as an inner filter of the excitation light applied. It may, therefore, be reasonable to suggest that the quantum yield values of **A-BSA** and **B-BSA** are similar to that of **EuL^{b}** in aqueous solution. As with quantum yield, the luminescence lifetime of the complex is reduced in water compared to methanol, however, the results indicate that the species with fewer labels per molecule of BSA, **B-BSA**, allows some exclusion of water from around the lanthanide label since its lifetime is longer than for the label in **A-BSA** or indeed the free label in water. This may be because when there are fewer labels present the BSA is able to partially shield the label, whereas the conjugation of more labels may alter the conformation of BSA preventing it from behaving in this way. The corresponding luminescence decay curves can be found in the appendix.

2.2.3.4 Study of **EuL^{b}-BSA** (**A-BSA** and **B-BSA**) Protein Conformation

CD spectroscopy was used to assess the protein conformation when in its native form and when conjugated to **EuL^{b}**. A solution of **EuL^{x}** was also titrated into native BSA to examine whether the protein does interact with the label even when there is no potential for covalent conjugation.

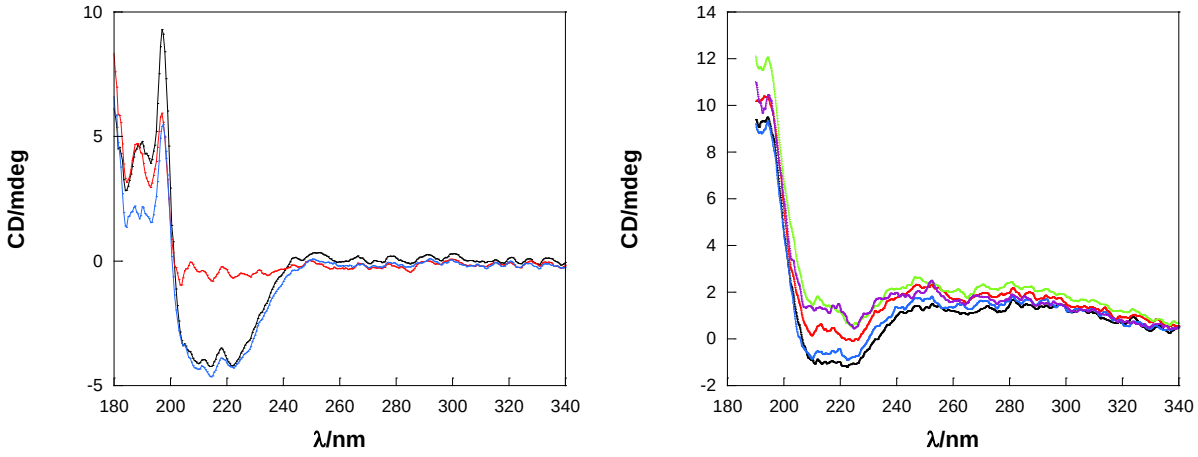

Figure 2.17 Left: CD spectra of native BSA (—), **A-BSA** (—) and **B-BSA** (—). Right: CD spectra of native BSA (—) with titration of 2 equivalents (—), 4 equivalents (—), 6 equivalents (—) and 150 equivalents (—) of **EuL^{x}**. All protein samples in aqueous solution and added **EuL^{x}** in a mix of water and methanol.

It is evident that **B-BSA** has a very similar spectrum to that of native BSA indicating that the structure of BSA is not perturbed with low levels of labelling. The double negative peak between 200-230 nm is typical of α-helical conformation and is caused by the $n \rightarrow \pi^*$ transitions of the amides involved in peptide bonds.[53, 54] **A-BSA** which contains a greater degree of labelling does not show any α-helix characteristics in the spectrum indicating that the higher amount of labels has affected that protein structure. When titrating **EuL^{x}** into BSA, the spectrum of BSA changes significantly with small additions of the complex, with a significant reduction in α-helix content after addition of 6 equivalents of complex and does

not subsequently change even with addition of 150 equivalents of complex. This indicates that the ability to covalently bind to the protein is not necessary for an interaction to occur, however, there is a limited availability for the number of complexes able to interact non-covalently. Previous reports of cationic lanthanide complexes binding to HSA indicate that they are able to bind non-covalently with preference of one complex for a particular binding site within the protein.[16, 17] **EuL^{x}** used here has a neutral charge, however, there is also precedent for neutral lanthanide complexes to bind non-covalently to BSA through either the replacement of coordinated water molecules with carboxylate ions belonging to the protein or the interaction of the aromatic groups of the complex with the protein, as is possible in this case.[18]

2.2.3.5 Treatment of SKOV-3 Cells with **EuL^{b}-BSA** (**B-BSA**)

SKOV-3, a human ovarian cancer cell line, was treated with either **B-BSA**, native BSA, **EuL^{b}** or a mixture of **EuL^{x}** and native BSA. The cells were grown on cover slips in a 6-well plate and were treated in all cases with a sample containing 3.9 μM BSA and/or 25.3 μM europium complex, although these values could only be estimated for **B-BSA**. The treatment was added to the cells in serum free media to discount the interactions of any serum proteins usually found in serum containing media and the cells were incubated for 16 hours at 37 ºC with the applied treatment. The treatment was then removed and the cells washed three times with PBS before the cells were fixed and mounted onto slides for microscopy. Epifluorescence microscopy was then carried out on the cell samples.

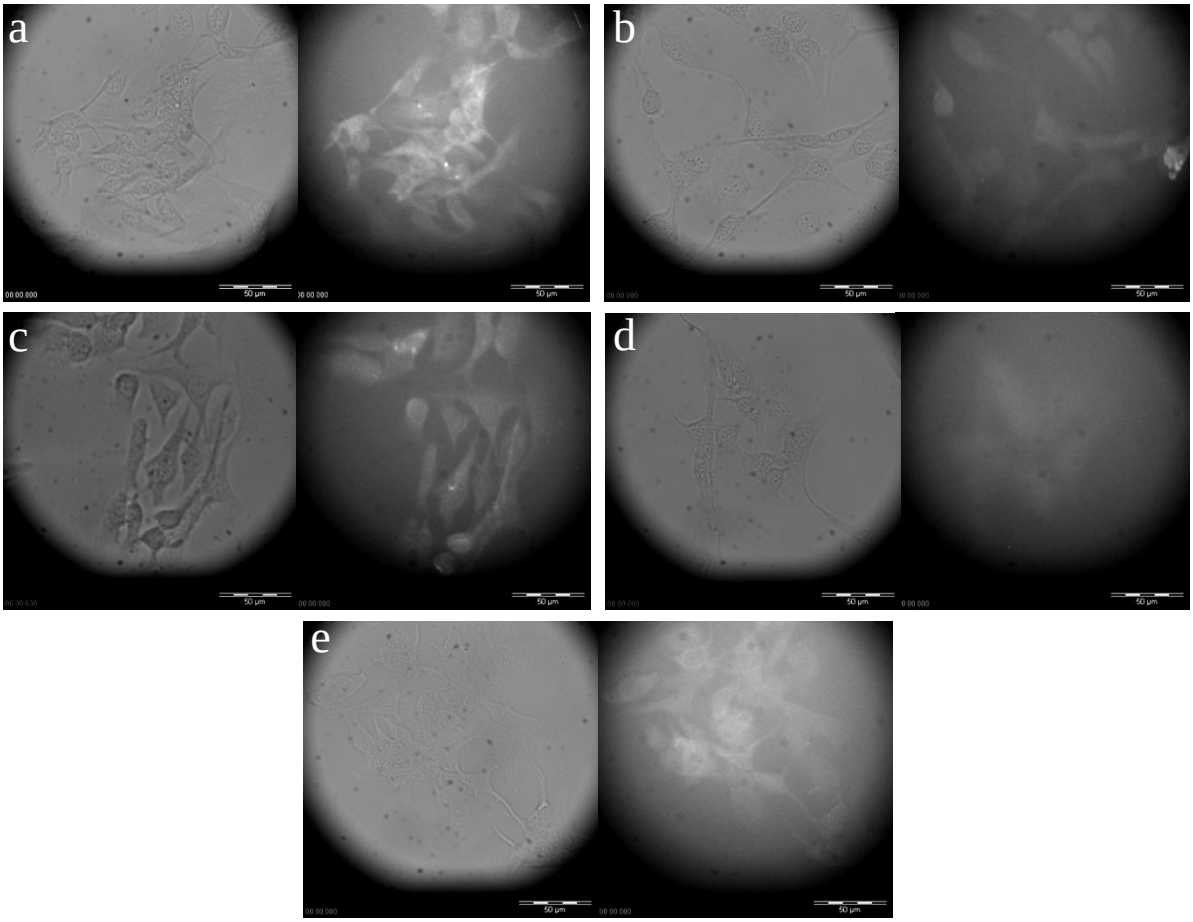

Figure 2.18 Bright field (left) and epiluminescence (right) microscope images of SKOV-3 cells treated with (a) **B-BSA**, (b) **EuL^{b}**, (c) **EuL^{x}** and BSA, (d) native BSA and (e) untreated. In all epiluminescence images λ_{ex} = 330 nm and acquisition time = 100 s. Scale bar = 50 μm.

The microscope images of SKOV-3 cells show that there is rather weak luminescence seen from cells treated with **EuL^{b}** alone, Figure 2.18b, and native BSA, Figure 2.18d, in fact the luminescence is approximately at the same level as the autofluorescence seen from untreated cells. This indicates that **EuL^{b}** is not effectively taken up by the cells when not conjugated to a protein and native BSA alone does not elicit a luminescence increase from the cells. On the other hand, luminescence of the cells treated with the conjugated species **B-BSA**, Figure 2.18a, or a mixture of **EuL^{x}** and BSA, Figure 2.18c, show luminescence greater than the autofluorescence background of untreated cells, Figure 2.18e; this may suggest that the uptake

of lanthanide complex by SKOV-3 cells is facilitated by the presence of BSA. It was previously shown by CD experiments that **EuL^{x}** is able to interact non-covalently with BSA and this interaction may have been sufficient to see it taken up into cells by a similar method to that shown for the covalently conjugated **B-BSA**. The collection of emission spectra from the cells to confirm europium as the origin of the luminescence was not possible due to weak signal. As discussed in section 2.2.2.3, it has been previously demonstrated that covalent attachment of a fluorescent probe to serum albumin can elicit endocytic uptake of the conjugate by mammalian cells.[4, 45, 46]

2.2.4 **EuL^{b}** as a FRET Donor

In order to demonstrate the use of **EuL^{b}** as a luminescent probe for FRET applications it was covalently attached to κ FLC using the method described for **B-BSA** in section 2.2.3.1. The conjugate **κ FLC-EuL^{b}** was intended to act as a donor for FluoProbes 647H, a commercially available protein label, which was conjugated to BUCIS 04 an anti-κ FLC mAb.[55] The mAb labelled with FluoProbes 647H, which will hence forth be referred to as BUCIS 04-FP, and the κ FLC were both supplied by, and experiments carried out in collaboration with, Serascience. The emission and absorbance properties of the FRET pair were measured in order to determine whether FRET should occur if the two proteins were to interact.

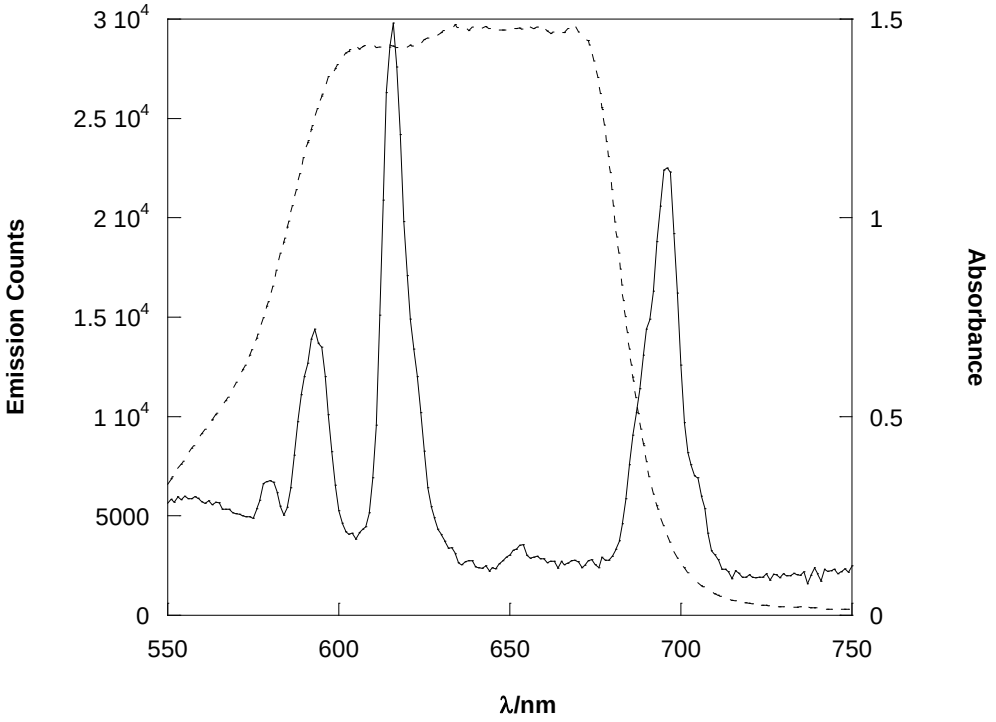

Figure 2.19 Emission spectrum of donor **κ FLC-EuL^{b}** when λ_{ex} = 330 nm (—) and absorption spectrum of acceptor BUCIS 04-FP (---).

As demonstrated in Figure 2.19, when the donor **κ FLC-EuL^{b}** is excited at 330 nm it emits in the range of 550-750 nm which overlaps well with the absorption of the acceptor BUCIS 04-FP. This donor acceptor pair was, therefore, deemed to be successful and as such a FRET experiment was carried out where increasing amounts of BUCIS 04-FP was titrated into 1 μM of **κ FLC-EuL^{b}** and the luminescence lifetime of **κ FLC-EuL^{b}** at 615 nm was measured. It was anticipated that the measurement of the luminescence lifetime of the donor would be more sensitive than the change in emission intensity of either the donor or acceptor.

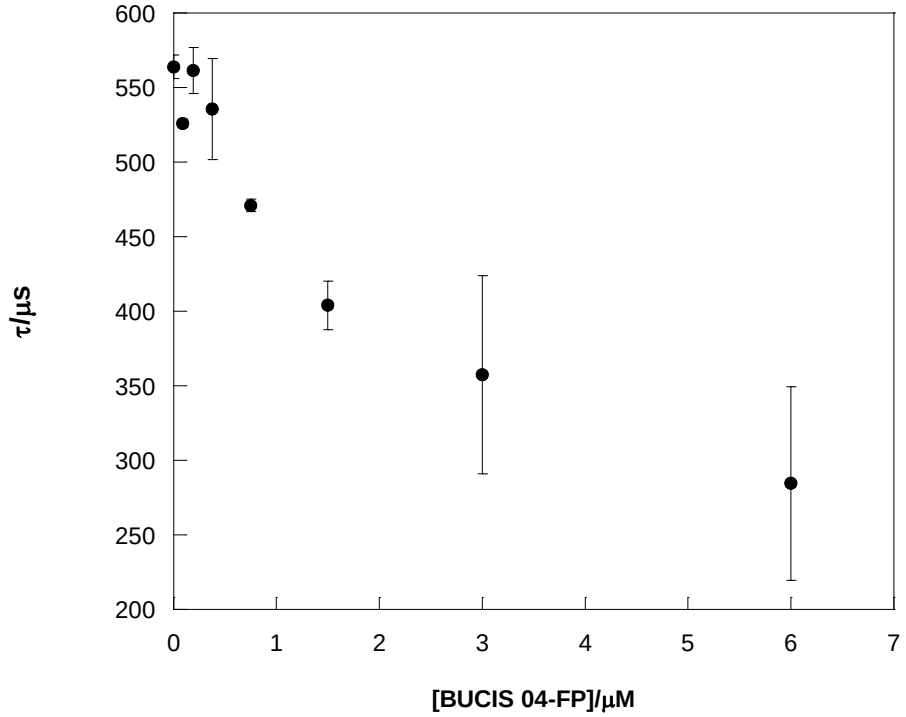

Figure 2.20 Change in luminescence lifetime of 1 μM **κ FLC-EuL^{b}** at 615 nm with additions of BUCIS 04-FP.

The reduction of the luminescence lifetime of **κ FLC-EuL^{b}** with increasing additions of BUCIS 04-FP is attributed to FRET between the two luminophores as their conjugated proteins are interacting.

If the luminescence lifetime of the donor in the absence, τ_D^0, and presence, τ_D, of transfer is known then the distance between the donor and acceptor, *r*, can be calculated using Equation 2.1.

$$r = \frac{R_0}{\left(\frac{\tau_D^0}{\tau_D} - 1\right)^{1/6}}$$

Equation 2.1 Calculation of the distance between the donor and acceptor during FRET.

R_0 is the Förster critical distance for the donor and acceptor in question and can be found in literature. In this case R_0 was estimated to be 7.6 nm based on that of a europium(III) complex/Cy5 system since Cy5 possesses similar photophysical properties to FluoProbes 647H.[55, 56] Using the data collected for the antibody **κ FLC-EuL^{b}**/BUCIS 04-FP system with each protein at equal concentrations r was calculated to be 8.2 nm which is entirely reasonable given the dimensions of the mAb. The mAb is approximately 15 nm from the base of the stem to the top of the fragment antigen-binding region which means that the acceptor must be positioned at least half way along the length of the stem from its base in order to interact with the donor on the κ FLC.[57] In addition to this, the efficiency of the transfer between the donor and acceptor, Φ_T, can be calculated using Equation 2.2.[56]

$$\Phi_T = 1 - \frac{\tau_D}{\tau_D^0}$$

Equation 2.2 Calculation of the transfer efficiency between the donor and acceptor during FRET.

Using the data collected for the **κ FLC-EuL^{b}**/BUCIS 04-FP system, Φ_T was calculated to be 0.37. The transfer efficiency is not surprising given that the distance between the donor and acceptor was calculated to be 8.2 nm which is larger than the Förster critical distance of the pair which is 7.6 nm. By definition, the transfer efficiency at the Förster critical distance is 0.5 and as such an efficiency below this for a pair separated by a larger distance is expected. Recently FRET was observed between a terbium complex and two organic dyes respectively when the antibodies attached to the donor and acceptor came into contact when forming an immunocomplex, Figure 2.1b.[36] The efficiency of transfer in this system was found to be 0.79 when an AlexaFluor647 acceptor was used and 0.68 when a crosslinked allophycocyanin

acceptor was used. Whilst the efficiencies of transfer reported are greater than that found in this project, it must also be noted that the distances between the donor and acceptors were found to be shorter than the Förster critical distance of each pair. Despite achieving a lower transfer efficiency in the system presented here, the results show that the system is still able to perform as intended and, furthermore, has an advantage over the recently published system in that far less of the labelling species, twenty five times less, is needed in order to conjugate the protein successfully.

2.3 Conclusions

This chapter has described the use of two new ligands and four associated lanthanide complexes for protein labelling applications resulting in luminescently labelled proteins emitting in both the visible and NIR. The interactions of the luminescent labels with the proteins were examined in terms of the effect of the conjugation on the photophysical properties of the lanthanide complexes and on the protein structure, the latter of which being omitted from similar studies published previously. The effect of the labelling procedure on the protein is of the utmost importance because its behaviour may change as a result and, therefore, studies of the labelled protein may give misleading results. In this study, where a strategy was employed to obtain a low degree of labelling of the protein, the structure of the protein was unaffected by the conjugation. The lanthanide labels proved to maintain their luminescent properties upon conjugation, providing evidence of their potential to serve as luminescent protein labels. Furthermore, the conjugated species were shown to facilitate the uptake of luminescent lanthanide complexes by neutrophil and ovarian cancer cells which provides a new and alternative route to other disruptive methods for treating cells with membrane impermeable lanthanide complexes. **EuL^{b}** was also shown to not only participate in FRET within an appropriate system, but to respond to acceptor in a concentration dependent manner leading to the opportunity for the development of a bioassay.

Although protein labelling using lanthanide complexes has been shown to be successful, improvements could be made on the work presented here by modifying the lanthanide probe in order to increase luminescence intensity through the utilisation of alternative antenna groups. This would certainly enhance the use of lanthanide complexes and conjugates for microscopy work as it would enable a reduction in the long exposure times currently needed

due to the weak luminescence exhibited **LnL^{a}**, **EuL^{b}** and **EuL^{x}**, thus reducing the potential of cell damage caused by the incident light. Furthermore, it would be beneficial to optimise the method used for conjugation of the lanthanide complexes to proteins in order to reduce the labelling time required which is currently 25 hours in total.

2.4 Experimental

2.4.1 General Considerations

Starting materials were obtained from Sigma Aldrich, Fluka, Fisher Scientific, Invitrogen, Sarstedt or Vector Laboratories and used without further purification unless otherwise stated.

^{1}H NMR were recorded on Bruker AVIII300 and ^{13}C NMR on Bruker AVIII400 spectrometers with $SiMe_4$ as an external reference.

MALDI-TOF mass spectrometry was carried out on a Waters MALDI Micro MX mass spectrometer, using gentisic acid matrix. Electrospray mass spectrometry was carried out on a Micromass LC-TOF.

HPLC was carried out on a Dionex summit system, using a Summit P580 quarternary low pressure gradient pump with built-in vacuum degasser. The detector was a Summit UVD 170s UV-Vis multi-channel detector with a preparative flow cell. The column used was the Phenomenex Luna 10 μm particle size C18 preparative column. All solvents used were HPLC grade solvents, degassed prior to use.

UV-Vis absorption spectra were carried out on Varian Cary 50 or Varian Cary 5000 spectrometers. UV-Vis spectra were taken using 1 cm path length quartz cuvettes.

CD spectra were obtained using a JASCO J180 spectropolarimeter. CD spectra were recorded using 1 cm path length quartz cuvettes.

ICP-OES and ICP-MS analysis were both undertaken at the University of Warwick, UK. ICP-OES was conducted using a Perkin-Elmer 5300DV ICP-OES system. ICP-MS was conducted using an Agilent 7500cx LC-ICP-MS system. PlasmaCal calibration standards for europium, terbium, and sulphur were purchased from SCP science.

Quantum yield measurements were made using the optically dilute relative method and calculated using the following equation[58]:

$$\phi_x = \phi_r \left(\frac{A_r(\lambda_r)}{A_x(\lambda_x)}\right)\left(\frac{I_r(\lambda_r)}{I_x(\lambda_x)}\right)\left(\frac{n_x^2}{n_r^2}\right)\left(\frac{D_x}{D_r}\right)$$

Where *r* denotes reference, *x* denotes sample, Φ = quantum yield, $A(\lambda)$ = absorbance at wavelength used for excitation, $I(\lambda)$ = intensity of excitation light at wavelength used, *n* = refractive index of solvent and *D* = integrated area of emission spectrum. In this case the reference used was a solution of ruthenium(II) tris(bipyridine) dichloride in water.

Elemental analyses were performed by MEDAC Ltd, Surrey, UK. Samples were prepared by drying *in vacuo* using a diffusion pump, however, part of the glass apparatus connected to the pump was broken after the samples were dried allowing the hygroscopic samples to be exposed to the air which may have led to the high water content of the samples. The data was fitted by adding solvent molecules used throughout the syntheses in various combinations until the calculated composition was as close as possible to that measured.

2.4.2 Chemical Syntheses

2.4.2.1 Synthesis of 1,11-(bis(4-amidothiophenol)-1,11-dioxo-3,6,9-triaza-3-6-9,triscarboxymethyl)undecane, **H_3L^a**

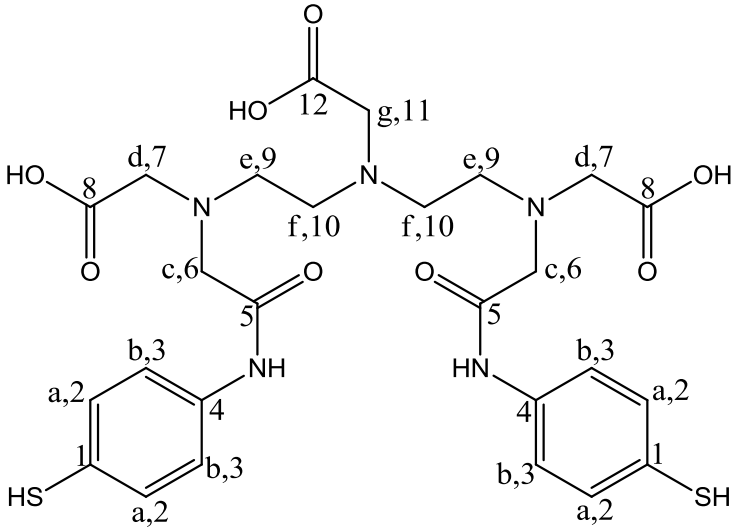

All solvents were degassed before use. DTPA-bis(anhydride) (1.02 g, 2.8 mmol) was stirred in anhydrous pyridine (10 mL) to create a suspension into which 4-aminothiophenol (2.0 g 16 mmol) was added and left to stir under nitrogen for 2 days. The yellow solution was filtered and the filtrate solvent removed *in vacuo* to give a thick yellow oil. Water (~20 mL) was added to dissolve the oil which dissolved upon stirring to give a dark yellow solution. To the stirring solution, which was at pH 5, conc. HCl was added drop-wise under a stream of nitrogen until pH 3 was reached at which point the solution became clear and colourless and a sticky yellow solid formed at the bottom of the flask. The solid was washed with water (10 mL) and acetonitrile (2 x 25 mL). Acetonitrile (50 mL) was added to the solid and stirred under nitrogen overnight to yield a white powder. The solid was allowed to settle and most of the acetonitrile decanted off before a further 40 mL was added and stirred under nitrogen for a further 1.5 h. The solid was collected by suction filtration under nitrogen and washed with acetonitrile (2 x 10 mL) and diethyl ether (2 x 20 mL). The fine white powder was dissolved in anhydrous pyridine (20 mL) to give a yellow solution to which hydrazine monohydrate (3

mL) was added drop-wise. Solvent was removed *in vacuo* leaving a yellow oil. Water (10 mL) was added to dissolve the oil to give a cloudy solution which was filtered under nitrogen. HCl was added drop-wise to the solution until pH 3 was reached, at which point the solution became clear and colourless leaving a white solid at the bottom of the flask. The water was removed and solid allowed to stir under nitrogen in acetonitrile for 1h. The solid was allowed to settle and the acetonitrile decanted before the solid was washed with acetonitrile (2 x 15 mL) and left to stir under nitrogen in acetonitrile (50 mL) overnight. The white powder formed was collected by vacuum filtration under nitrogen and washed with acetonitrile (2 x 10 mL) and diethyl ether (2 x 20 mL). The resulting white powder was dried under vacuum to give $\mathbf{H_3L^a}$ (0.4 g, 23% yield). ^{1}H NMR (300 MHz, MeOH-d_4), δ ppm: 7.42 (4H, d, ^3J = 9.0 Hz, H_b); 7.15 (4H, d, ^3J = 9.0 Hz, H_a); 4.19 (2H, s, H_g); 3.64 (4H, s, H_d); 3.61 (4H, s, H_c); 3.52 (4H, t, ^3J = 5.6 Hz, H_e); 3.26 (4H, t, ^3J = 5.6 Hz, H_f). ^{13}C NMR {^{1}H} PENDANT (400 MHz, D_2O), δ ppm: 174.7 (1C, C_{12}); 171.5 (2C, C_8); 168.3 (2C, C_5); 132.5 (2C, C_4); 130.8 (4C, C_2); 123.8 (2C, C_1); 122.0 (4C, C_3); 58.0 (1C, C_{11}); 56.2 (2C, C_7); 55.2 (2C, C_6); 54.6 (2C, C_9); 54.2 (2C, C_{10}). MS (ES-TOF$^+$): *m/z* 608 $\{M + H\}^+$, 630 $\{M + Na\}^+$, 670 $\{M + Cu\}^+$. UV-Vis (MeOH) λ_{max} nm (log ε): 264 (4.4). All data agree with that previously published and as such no further analysis was required.[37]

2.4.2.2 Synthesis of **LnL^a** where Ln = Eu, Tb or Nd.

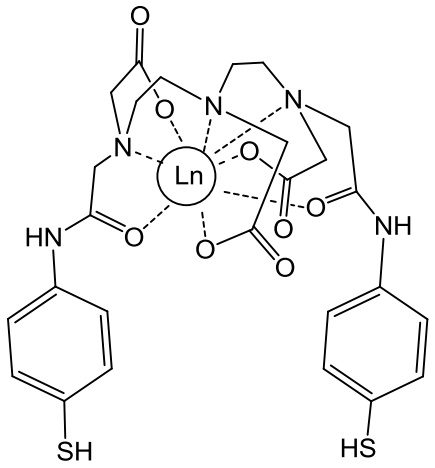

2.4.2.2.1 Synthesis of **EuL^a**

All solvents were degassed prior to use. Europium chloride hexahydrate (0.06 g, 0.16 mmol) was dissolved in methanol (3 mL). H_3L^a (0.1 g, 0.16 mmol) was added to the solution and sonicated until all of the ligand had dissolved. Acetonitrile (30 mL) was added to the solution to yield a white solid which was collected by suction filtration under nitrogen and washed with acetonitrile and diethyl ether. The isolated solid was dried under vacuum to give **EuL^a** (114 mg, 94% yield). MS (ES-TOF$^+$): *m*/*z* 758 $\{M + H\}^+$. HRMS (ES-TOF) calc. for $C_{26}H_{27}EuN_5O_8S_2$: 754.0513. Found: 754.0510. UV-Vis (MeOH) λmax nm (log ε): 266 (4.4). All data agree with that previously published and as such no further analysis was required.[37]

2.4.2.2.2 Synthesis of **TbL^a**

All solvents were degassed prior to use. Terbium chloride hexahydrate (0.12 g, 0.32 mmol) was dissolved in methanol (3 mL). H_3L^a (0.2 g, 0.33 mmol) was added to the solution and sonicated until all of the ligand had dissolved. Acetonitrile (30 mL) was added to the solution to yield a white solid which was collected by suction filtration under nitrogen and washed with acetonitrile and diethyl ether. The isolated solid was dried under vacuum to give **TbL^a**

(224 mg, 89% yield). MS (ES-TOF$^-$): *m*/*z* 762 {M – H}$^-$. UV-Vis (MeOH) λmax nm (log *ε*): 266 (4.7). All data agree with that previously published and as such no further analysis was required.[37]

2.4.2.2.3 Synthesis of **NdL^a**

All solvents used were degassed prior to synthesis. Neodymium chloride hexahydrate (34 mg, 0.1 mmol) was dissolved in methanol (3 mL). H_3L^a (58 mg, 0.01 mmol) was added to the solution and sonicated until all of the ligand had dissolved. The solution was added drop-wise to ice cold acetonitrile (30 mL) to yield a white solid which was collected by suction filtration under nitrogen and washed with acetonitrile and diethyl ether. The isolated solid was dried under vacuum to give **NdL^a** (67 mg, 97%). MS (ES-TOF$^+$): *m*/*z* 749 {M + H}$^+$. UV-Vis (MeOH) λmax nm (log *ε*): 266 (4.3). All data agree with that previously published and as such no further analysis was required.[37]

2.4.2.3 Synthesis of **H_3L^b**

2.4.2.3.1 Preparation of Crude **H_3L^b**

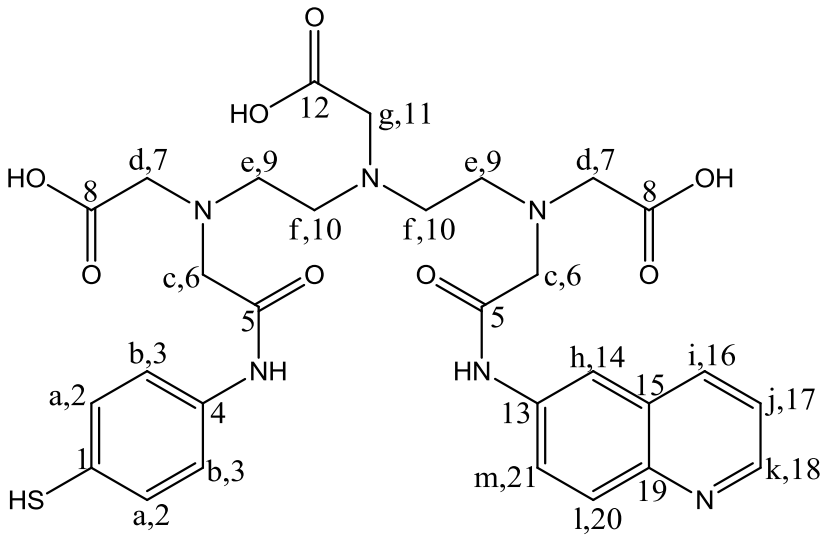

All solvents were degassed before use. 4-aminothiolphenol was distilled at 200 °C at high pressure using Kugelrohr distillation to yield an off white solid (1.5 g) which was stored under nitrogen at -20 °C until use.

DTPA-bis(anhydride) (4.3 g, 12 mmol) was stirred in anhydrous pyridine (100 mL) to create a suspension into which 6-aminoquinoline (1.7 g, 11.9 mmol) was added and left to stir under nitrogen for 45 min. 4-aminothiolphenol (1.5 g, 12.3 mmol) was added to the solution and stirring continued under nitrogen for a further 2 h. Water (80 mL) was added to quench the reaction and the solution stirred for 30 min under nitrogen. The solvent was removed *in vacuo* to give a sticky orange solid to which water (~150 mL) was added before the mixture was filtered under gravity to give a clear yellow solution. Conc. HCl was added drop-wise to the solution under a stream of nitrogen until pH 3 was reached at which point a yellow precipitate was formed. The clear yellow aqueous layer was decanted to leave a yellow solid that was washed with water (50 mL) and acetonitrile (50 mL) before being triturated in acetonitrile for two days under nitrogen. A bright yellow powder was formed and was collected by suction filtration and washed with acetonitrile (2 x 50 mL) and diethyl ether (2 x 50 mL). The resulting yellow powder was dried under vacuum to give a mixture, Scheme 2.4, of H_3L^a, H_3L^c and the desired species H_3L^b (2 g, 27%). MS (ES-TOF$^+$): *m*/*z* 608 $\{H_3L^a + H\}^+$, 627 $\{H_3L^b + H\}^+$, 630 $\{H_3L^a + Na\}^+$, 646 $\{H_3L^c + H\}^+$, 649 $\{H_3L^b + Na\}^+$, 668 $\{H_3L^c + Na\}^+$.

2.4.2.3.2 Isolation of **H_3L^b**

The asymmetric species H_3L^b was separated from the symmetric species, H_3L^a and H_3L^c using HPLC. Prior to injection onto the column the sample was dissolved in tetrahydrofuran/water (1:1) and an excess of tris(2-carboxyethyl)phosphine hydrochloride was added to reduce any

disulphide bonds. The optimum set up for separation was found to be injection of a 1 mL aliquot of 100 mg/mL reduced sample onto a preparative HPLC system using a Luna C_{18} reverse phase column running a water/acetone gradient (0-75% acetone over 30 mins) at 8 mL/min. Solvents used contained 0.05% trifluoroacetic acid. Monitoring the absorbance at 210 nm and 336 nm allowed detection of each species as eluted. After a complete run the column was washed with acetone and water before injection repeated. Three peaks eluted, peak 1 at 11 min, peak 2 at 17 min and peak 3 at 25 min and were identified using mass spectrometry (MALDI-TOF$^+$). **H_3L^b** was contained in peak 2 (*m/z* 626 $\{M + H\}^+$), peak 1 contained H_3L^c (*m/z* 646 $\{M + H\}^+$) and peak 3 contained H_3L^a (*m/z* 608 $\{M + H\}^+$). Peak 2 was collected and solvent removed *in vacuo* to afford a yellow solid that was dried further *in vacuo* to yield **H_3L^b** (60 mg, 3%). ^{1}H NMR (300 MHz, D_2O), δ ppm: 8.46 (1H, dd, ^3J = 4.4 Hz, ^4J = 1.6 Hz, H_k); 8.02 (1H, m, H_i); 7.79 (1H, d, ^4J = 2.3 Hz, H_h); 7.74 (1H, d, ^3J = 9.1 Hz, H_l); 7.54 (1H, dd, ^3J = 9.1 Hz, ^4J = 2.3 Hz, H_m); 7.23 (1H, m, H_j); 7.00 (2H, d, ^3J = 8.5 Hz, H_b); 6.66 (2H, d, ^3J = 8.5 Hz, H_a); 3.18 (2H, s, H_c); 3.08 (2H, s, H_c); 2.95-2.91 (6H, comp, $H_{d,g}$); 2.52 (8H, t, ^3J = 11.0 Hz, $H_{e,f}$). ^{13}C NMR {^{1}H} PENDANT (400 MHz, MeOH-*d_4*), δ ppm: 179.5 (1C, C_{12}); 173.6 (2C, C_8); 172.3 (2C, C_5); 149.4 (1C, C_{18}); 144.1 (1C, C_{19}); 142.5 (1C, C_{13}); 141.9 (1C, C_4); 137.2 (1C, C_{16}); 135.3 (1C, C_{21}); 133.0 (1C, C_{15}); 130.4 (2C, C_2); 128.3 (1C, C_1); 124.8 (1C, C_{20}); 121.9 (2C, C_3); 121.6 (1C, C_{14}); 117.9 (1C, C_{17}); 59.5 (3C, $C_{7,11}$); 59.2 (2C, C_6); 58.8 (2C, C_9); 58.3 (2C, C_{10}). MS (MALDI-TOF$^+$): *m/z* 626 $\{M + H\}^+$. UV-Vis (MeOH) λ_{max} nm (log ε) 248 (4.7), 330 (3.6). All data agree with that previously reported and as such no further analysis was required.[38]

2.4.2.4 Synthesis of **EuL^{b}**

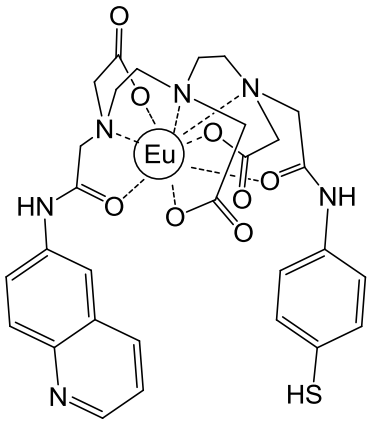

All solvents were degassed prior to use. Europium chloride hexahydrate (23 mg, 0.06 mmol) was added to a stirring solution of H_3L^b (23 mg, 0.06 mmol) in water (5 mL). The pH of the solution was raised to pH 5 by drop-wise addition of aqueous tetrabutylammonium hydroxide (40% w/v) solution under a stream of nitrogen. The volume of the solution was reduced *in vacuo* to <1 mL and acetonitrile was added (30 mL) to yield a precipitate. The solid was recovered by suction filtration under nitrogen and washed with acetonitrile (2 x 10 mL) and diethyl ether (2 x 10 mL). The resulting off white powder was dried *in vacuo* to yield **EuL^{b}** (29 mg, 59%). MS (MALDI-TOF^{+}) *m/z* 776 $\{M + H\}^{+}$, 798 $\{M + Na\}^{+}$. HRMS (ES-TOF) calc. for $C_{29}H_{31}EuN_6O_8S$: 776.1137. Found: 776.1149. UV-Vis (MeOH) λ_{max} nm (log ε) 247 (4.5), 328 (3.5). All data agree with that previously reported and as such no further analysis was required.[38]

2.4.2.5 Synthesis of $\mathbf{H_3L^x}$

2.4.2.5.1 Preparation of Crude $\mathbf{H_3L^x}$

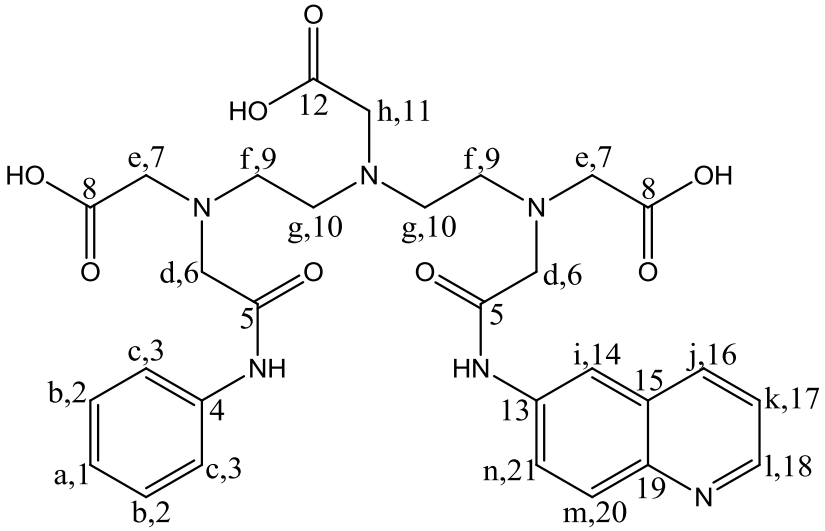

DTPA-bis(anhydride) (0.99g, 2.8 mmol) was stirred in anhydrous pyridine (100 mL) to which 6-aminoquinoline (0.4 g, 2.8 mmol) was added and stirring continued for 45 min under nitrogen. Aniline (0.26 g, 2.7 mmol) was then added to the cloudy yellow solution and stirred for 2 h under nitrogen. Water (80 mL) was added to quench the reaction and the solution stirred for 30 min under nitrogen. Solvent was then removed *in vacuo* to give a sticky orange solid that was dissolved in water (~100 mL) and pH lowered to pH 3 by drop-wise addition of conc. HCl. The volume of the solution was reduced *in vacuo* before addition of acetonitrile (100 mL) which produced a bright yellow precipitate. Once the precipitate had settled the acetonitrile was decanted before addition of fresh acetonitrile and the solid was triturated for several hours under nitrogen. Solid was isolated by suction filtration, washed with acetonitrile (2 x 25 mL) and diethyl ether (2 x 25 mL). The resulting yellow powder was dried under vacuum to give a mixture, Scheme 2.6, of H_3L^y, H_3L^z and the desired species H_3L^x (0.87 g, 54%). MS (MALDI-TOF$^+$): *m/z* 544 $\{H_3L^y + H\}^+$, 566 $\{H_3L^y + Na\}^+$, 582 $\{H_3L^y + K\}^+$, 595 $\{H_3L^x + H\}^+$, 617 $\{H_3L^x + Na\}^+$, 633 $\{H_3L^x + K\}^+$, 646 $\{H_3L^z + H\}^+$, 668 $\{H_3L^z + Na\}^+$, 684 $\{H_3L^z + K\}$+.

2.4.2.5.2 Isolation of **H_3L^x**

The asymmetric species H_3L^x was separated from the symmetric species, H_3L^y and H_3L^z using HPLC. The optimum set up for separation was found to be injection of a 1 mL aliquot of 100 mg/mL sample in tetrahydrofuran/water (1:1) onto a preparative HPLC system using a Luna C_{18} reverse phase column running a water/acetone gradient (0-75% acetone over 30 mins) at 8 mL/min. Solvents used contained 0.05% trifluoroacetic acid. Monitoring the absorbance at 210 nm and 336 nm allowed detection of each species as eluted. After a complete run the column was washed with acetone and water before injection repeated. Three peaks eluted, peak 1 at 13 min, peak 2 at 17 min and peak 3 at 25 min and were identified using mass spectrometry (MALDI-TOF$^+$). H_3L^x was contained in peak 2 (*m/z* 595 $\{M + H\}^+$), peak 1 contained H_3L^z (*m/z* 646 $\{M + H\}^+$) and peak 3 contained H_3L^y (*m/z* 544 $\{M + H\}^+$). Peak 2 was collected and solvent removed *in vacuo* to give a yellow oil that was dissolved in water. Aqueous tetrabutylammonium hydroxide solution (40% w/v) was added drop-wise until the solution reached pH 3. Volume reduced *in vacuo* and ice cold acetone (~100 mL) added to produce a precipitate that was collected by suction filtration, washed with acetone (2 x 25 mL) and diethyl ether (2 x 25 mL) to afford the off white powder **H_3L^x** (97 mg, 6%). ^{1}H NMR (300 MHz, D_2O), δ ppm: 8.39 (1H, dd, ^3J = 4.4 Hz, ^4J = 1.6 Hz, H_l); 7.91 (1H, d, ^3J = 8.2 Hz, H_j); 7.71 (1H, d, ^4J = 2.3 Hz, H_i); 7.61 (1H, d, ^3J = 9.0 Hz, H_m); 7.45 (1H, dd, ^3J = 9.0 Hz, ^4J = 2.3 Hz, H_n); 7.17 (1H, m, H_k); 6.99 (2H, m, H_c); 6.84 (3H, m, $H_{a,b}$); 3.12 (2H, s, H_d); 3.04 (2H, s, H_d); 3.02-2.79 (6H, comp, $H_{e,h}$); 2.51 (8H, br t, $H_{f,g}$). ^{13}C NMR {^{1}H} PENDANT (400 MHz, D_2O), δ ppm: 179.3 (1C, C_{12}); 173.3 (2C, C_8); 172.7 (2C, C_5); 149.1 (1C, C_{18}); 143.9 (1C, C_{19}); 141.7 (1C, C_{13}); 137.1 (1C, C_4); 136.4 (1C, C_{16}); 136.1 (1C, C_{21}); 128.9 (1C, C_{15}); 128.4 (2C, C_2); 128.2 (1C, C_1); 125.1 (1C, C_{20}); 121.8 (2C, C_3); 121.1 (1C, C_{14}); 117.7 (1C, C_{17}); 59.5 (1C, C_{11}); 59.1 (2C, C_7) 58.9 (2C, C_6); 58.8 (2C, C_9); 58.3 (2C, C_{10}). MS

(MALDI-TOF$^+$): *m/z* 595 {M + H}$^+$. UV-Vis (MeOH) λ_{max} nm (log ε) 247 (4.6), 332 (3.5). Anal. calc. for $C_{29}H_{34}N_6O_8(H_2O)_{2.8}$ C: 54.0; H: 6.2; N: 13.0. Found C: 54.2; H: 5.7; N: 12.6.

2.4.2.6 Synthesis of **EuL^x**

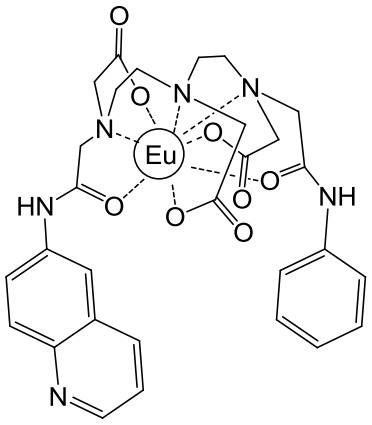

H_3L^x (50 mg, 0.08 mmol) was added to a stirring solution of europium chloride hexahydrate (28.4 mg, 0.08 mmol) in water (3 mL). The pH of the solution was raised to pH 5 by drop-wise addition of aqueous tetrabutylammonium hydroxide (40% w/v). The volume of the solution was reduced *in vacuo* to <1 mL to which ice cold acetone was added (30 mL) to yield a precipitate. The solid was recovered by suction filtration and washed with acetone (2 x 10 mL) and diethyl ether (2 x 10 mL). The resulting off white powder was dried *in vacuo* to yield **EuL^x** (37 mg, 64%). MS (ES-TOF$^+$) *m/z* 767 {M + Na}$^+$. UV-Vis (MeOH) λ_{max} nm (log ε) 246 (4.5), 329 (3.3). Anal. calc. for $C_{29}H_{31}EuN_6O_8(H_2O)_{11.6}$ C: 36.6; H: 5.7; N: 8.8. Found C: 36.2; H: 4.4; N: 8.2.

2.4.2.7 Synthesis of **NHS-MAL**

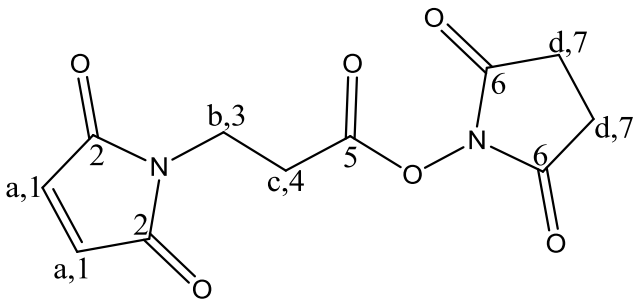

Maleic anhydride (1.01 g, 10 mmol) and *β*-alanine (0.91 g, 10 mmol) were added to degassed DMF (10 mL) and heated until all solid had dissolved to give a yellow solution before stirring at room temperature for 1 h. The solution was cooled in an ice bath and *N*-hydroxysuccinimide (1.45 g, 13 mmol) and DCC (4.12 g, 20 mmol) added and the solution stirred in the ice bath for a further 4 min. The ice bath was then removed and the solution stirred at room temperature for 4 h, during which time the cloudy yellow solution became very thick and had to be manually stirred periodically to release the stirrer bar. The solution was filtered under gravity and washed with DMF. The yellow/brown filtrate was mixed with water and an extraction with dichloromethane (2 x 50 mL) performed. The solution was dried with Na_2CO_3 and filtered under gravity. The volume of the filtrate was reduced *in vacuo* to give a brown oil. The oil was dissolved in dichloromethane and added drop-wise to petroleum ether 40 °C – 60 °C causing the product to precipitate as a white solid which was collected by filtration under gravity. The resulting off-white solid was dried under vacuum to give **NHS-MAL** (0.8g, 29%). ^{1}H NMR (300 MHz, $CHCl_3$-*d*), δ ppm: 6.75 (2H, s, H_a); 3.95 (2H, t, ^3J = 6.9 Hz, H_c); 3.02 (2H, t, ^3J = 7.0 Hz, H_b); 2.80 (4H, s, H_d). ^{13}C NMR {^{1}H} PENDANT (400 MHz, DMSO-*d6*), δ ppm: 171.0 (2C, C_2); 170.4 (2C, C_6); 167.2 (1C, C_5); 135.1 (2C, C_1); 33.2 (1C, C_3); 29.5 (1C, C_4); 25.8 (2C, C_7). MS (ES-TOF$^+$): *m*/*z* 289 {M + Na}$^+$. UV-Vis (MeOH) λ_{max} nm (log ε) 262 (3.0). All data agree with that previously published and as such no further analysis was required.[39]

2.4.3 Conjugation of **LnL** Labels to Proteins

2.4.3.1 Conjugation of **LnL^{a}** to BSA

BSA (2 mg, 32 nmol) was dissolved in NaCl/Na_2HPO_4 buffer (1 mL) at pH 7.4. To this a solution of **NHS-MAL** in dimethyl sulphoxide (30 μL, 102 mM) was added and the reaction mixture stirred gently for 1 h at 37 ºC. The solution was then passed through a Sephadex G-15 size exclusion column and the fraction containing BSA collected and confirmed via UV-Vis. The BSA containing fraction was then stirred with a solution of **LnL^{a}** in methanol (150 μL, 10 mM) for 24 h at room temperature. The solution was then passed through a Sephadex G-15 size exclusion column and the fraction containing the **LnL^{a}-BSA** was identified using UV-Vis, collected and lyophilised.

2.4.3.2 Conjugation of **EuL^{b}** to BSA (**A-BSA**)

BSA (0.66 mg, 10 nmol) was dissolved in NaCl/Na_2HPO_4 buffer (0.5 mL) at pH 7.4. To this a solution of **NHS-MAL** in dimethyl sulphoxide (3 μL, 102 mM) was added and the reaction mixture stirred gently for 1 h at 37 ºC. The solution was then passed through a HiTrap column and the fraction containing BSA collected. The BSA containing fraction was then stirred with a solution of **EuL^{b}** in methanol (750 μL, 13 mM) for 24 h at room temperature. The volume of the solution was then reduced to <2 mL *in vacuo* and passed through a HiTrap column and the fraction containing the **A-BSA** was collected and lyophilised.

2.4.3.3 Conjugation of **EuL^{b}** to BSA (**B-BSA**)

BSA (2 mg, 32 nmol) was dissolved in NaCl/Na_2HPO_4 buffer (0.5 mL) at pH 7.4. To this a solution of **NHS-MAL** in 0.3% dimethyl sulphoxide (1 mL, 0.3 mM) was added drop-wise to the BSA solution as it was gently stirred over 1 h at 37 ºC. The solution was then passed

through a HiTrap column and the fraction containing BSA collected. The BSA containing fraction was then stirred with a solution of **EuL^{b}** in methanol (250 μL, 13 mM) for 24 h at room temperature. The volume of the solution was then reduced to <2 mL *in vacuo* and passed through a HiTrap column and the fraction containing the **B-BSA** was collected and lyophilised.

2.4.3.4 Conjugation of **EuL^{b}** to κ FLC

A solution of κ FLC in PBS (250 μL, 0.04 mM) was sterile filtered (0.2 μm) and added to a round bottom flask. To this a sterile filtered (0.2 μm) solution of **NHS-MAL** in 0.3% dimethyl sulphoxide (1 mL, 0.3 mM) was added drop-wise to the κ FLC solution as it was gently stirred over 1 h at 37 ºC. The solution was then passed through a HiTrap column and the fraction containing κ FLC collected. The κ FLC containing fraction was then stirred with a sterile filtered (0.2 μm) solution of **EuL^{b}** in methanol (8 μL, 36 mM) for 24 h at room temperature. The solution was passed through a HiTrap column and the fraction containing the **κ FLC-EuL^{b}** was collected.

2.4.4 Cell Studies

2.4.4.1 Neutrophil Studies

2.4.4.1.1 Collection of Neutrophil Cells

Neutrophils were collected by the research group of Professor Gerard Nash, University of Birmingham, UK, as described previously.[59] Neutrophil cells were isolated from a sample of whole human blood collected in ethylenediaminetetraacetic acid coated tubes. Histopaque 1119 (2.5 mL) was added to a 10 mL tube onto which Histopaque 1077 (2.5 mL) was added before gently layering blood (5 mL) on top. The tube was centrifuged at 700 x g for 50 min at

room temperature. The layer containing neutrophils was recovered and washed twice by centrifugation at 250 x g for 5 min. The cells were counted and the cell viability established via tryptan blue exclusion. Neutrophil cells were then redispersed in PBS to give 10^8 cells mL^{-1}.

2.4.4.1.2 Treatment of Neutrophil Cells

To each of three separate sample tubes neutrophil cells (100 μL) were added. To one tube a solution of **EuL^a-BSA** in PBS (50 μL, 20 mg mL^{-1}) was then added, to another a solution of **NdL^a-BSA** in PBS (50 μL, 20 mg mL^{-1}) was added and to the remaining tube a solution of **TbL^a-BSA** in PBS (50 μL, 65 mg mL^{-1}) was added. Following the addition of **LnL^a-BSA** the cells were incubated for 1 h at 37 ºC.

2.4.4.1.3 Preparation of Neutrophil Cells for Microscopy

Following treatment the cells were isolated by centrifugation before being redispersed in PBS and the process repeated three times to wash the cells. A pellet of cells was then collected by centrifugation and redispersed in a solution of 2% paraformaldehyde to fix the cells. A drop of fixed cells was added to a glass slide and a cover slip placed on top.

2.4.4.1.4 Microscopy of Neutrophil Cells

Epiluminescence microscopy was carried out using an Edinburgh Instruments fluorescence system, FLSPM920, with a 450 W xenon arc lamp excitation source coupled to an Olympus IX71 inverted microscope with a LUCPLFLN 40 x 0.60 NA objective. A Hamamatsu EMCCD C9100-13 detected luminescence images and all images were obtained using Olympus Soft Imaging Solutions GmBH Cell^M 3.2 software.

Luminescence images of cells treated with **EuL^{a}-BSA** were gained by excitation of the sample with 394 nm light and 5000 ms exposure time. Luminescence images of cells treated with **TbL^{a}-BSA** were gained by excitation of the sample with 360 nm light and 10000 ms exposure time.

2.4.4.2 SKOV-3 Studies

2.4.4.2.1 SKOV-3 Cell Culture Maintenance

SKOV-3 cells were grown in complete media (5 mL) in T25 flasks with vented caps in an incubator at 37 ˚C containing 5% CO_2. Complete media consisted of Roswell Park Memorial Institute-1640 Medium supplemented with foetal bovine serum (10%), L-glutamine (1%) and streptomycin/penicillin (1%). Cell passage was carried out every 3-4 days by washing with PBS and detachment using trypsin followed by dilution in complete media and adding to either a fresh T25 flask or 6-well plates.

2.4.4.2.2 Treatment of SKOV-3 Cells

3 mL of cell solution after passage was added to each well of a 6-well plate also containing a glass cover slip and cells incubated at 37 ˚C in a 5% CO_2 atmosphere for 24 h prior to further treatment. The media was then removed from the wells and the cells washed with PBS before addition of sample solutions (2 mL) to each well. Sample solutions were made by dissolving the desired sample in serum-free media containing L-glutamine (1%) and streptomycin/penicillin (1%). Treatments consisted of **B-BSA** (0.56 mg, 7.8 nmol, [Eu] ~ 50 nmol), native BSA (0.52 mg, 7.8 nmol), **EuL^{b}** (0.04 mg, 50 nmol) or a mixture of native BSA (0.52 mg, 7.8 nmol) and **EuL^{x}** (0.04 mg, 50 nmol). As a control serum free media alone was also added to separate wells. The cells were then returned to incubate at 37 ºC for 16 h.

2.4.4.2.3 Fixing and Mounting SKOV-3 Cells

Once treatments were complete media was removed from the cells and cells washed with PBS. Ice cold methanol (1 mL) was added to each well and cells kept at -20 ºC for 10 min. Methanol was then removed and cover slips were placed cells down onto a drop of VectaMount mounting medium on a glass slide. The slides were sealed with varnish, refrigerated flat and protected from light for at least 24 h prior to imaging.

2.4.4.2.4 Microscopy of SKOV-3 Cells

Epiluminescence microscopy was carried out using an Edinburgh Instruments fluorescence system, FLSPM920, with a 450 W xenon arc lamp excitation source coupled to an Olympus IX71 inverted microscope with a LUCPLFLN 40 x 0.60 NA objective. A Hamamatsu EMCCD C9100-13 detected luminescence images and all images were obtained using Olympus Soft Imaging Solutions GmBH Cell^M 3.2 software.

Luminescence images of SKOV-3 cells were gained by excitation of the sample with 330 nm light and 100000 ms exposure time.

2.4.5 Luminescence Spectroscopy

Luminescence experiments were carried out using an Edinburgh Instruments fluorescence system, FLSPM920. The illumination source uses a 450 W xenon arc lamp. The detection system used was a Hamamatsu R928 PMT for visible and Hamamatsu R5509 PMT cooled to -80 ºC for NIR. The emission monochromator is fitted with two interchangeable gratings blazed at 500 nm and 1200 nm. Luminescence studies were carried out using quartz cuvettes

with four transparent polished faces and 1 x 1 cm path length. F900 spectrometer analysis software was used to record the data.

2.4.5.1 Terbium Emission

Luminescence spectra of **TbL^{a}** containing samples were gained by excitation of the complex at 266 nm, detection of emission in the range 455-750 nm and employing a 455 nm long pass filter. Where the lanthanide centre was excited directly excitation at 487 nm was used in conjunction with a 495 nm long pass filter end emission detected in the range 500-750 nm. Typically a 0.2 s dwell time and a 1 nm step size were employed with excitation and emission slits set to 5 nm and 3 nm respectively.

2.4.5.2 Europium Emission

Luminescence spectra of **EuL^{a}** containing samples were gained by excitation of the complex at 266 nm, detection of emission in the range 550-750 nm and employing a 550 nm long pass filter. Where the lanthanide centre was excited directly excitation at 578 nm was used in conjunction with a 590 nm long pass filter end emission detected in the range 590-750 nm. Luminescence spectra of **EuL^{b}** and **EuL^{x}** containing samples were gained by excitation of the complex at 330 nm, detection of emission in the range 550-750 nm and employing a 550 nm long pass filter. Typically a 0.2 s dwell time and a 1 nm step size were employed with excitation and emission slits set to 5 nm and 3 nm respectively.

2.4.5.3 Neodymium Emission

Luminescence spectra of **NdL^{a}** containing samples were gained by excitation of the complex at 280 nm, detection of emission in the range 800-1400 nm and employing a 715 nm long

pass filter. A 0.5 s dwell time and a 1 nm step size were employed and scans were repeated three times to record a cumulative spectrum. Excitation and emission slits set to 15 nm.

2.4.5.4 BSA Emission

In order to gain details of how the tail of the BSA emission peak may create a background in the emission spectra of **EuL^{b}** containing samples native BSA was also examined under the conditions described for **EuL^{b}**.

2.4.5.5 Excitation Spectra

For **EuL^{a}** containing samples emission was detected at 615 nm with a 550 nm long pass filter and for **TbL^{a}** containing samples emission was detected at 546 nm with a 455 nm long pass filter. Excitation wavelengths in the range 200-350 nm were used. In both cases excitation and emission slits were set to 3 nm and 5 nm respectively with a 0.5 s dwell time and a 1 nm step size.

2.4.5.6 Luminescence Lifetime Measurements

Luminescence lifetimes were measured using the spectrophotometer described in section 2.4.5 with a 100 W μF920H lamp illumination source. In the case of **EuL^{b}** containing samples excitation was at 330 nm, emission at 615 nm and a 550 nm long pass filter used. Excitation and emission slits set to 5 nm and 3 nm respectively. Emission was detected over an 8 ms range for 120 s with a 0.1 ms lamp trigger delay.

2.5 References

1. T. Peters Jr., *All About Albumin: Biochemistry, Genetics and Medical Applications*, Academic Press, San Diego (USA), 1996.

2. K. K. W. Lo, W. K. Hui, C. K. Chung, K. H. K. Tsang, T. K. M. Lee, C. K. Li, J. S. Y. Lau and D. C. M. Ng, *Coord. Chem. Rev.*, 2006, **250**, 1724-1736.

3. K. K.-W. Lo, K. Y. Zhang, S.-K. Leung and M.-C. Tang, *Angew. Chem. Int. Ed. Engl.*, 2008, **47**, 2213-2216.

4. J. S.-Y. Lau, P.-K. Lee, K. H.-K. Tsang, C. H.-C. Ng, Y.-W. Lam, S.-H. Cheng and K. K.-W. Lo, *Inorg. Chem.*, 2009, **48**, 708-718.

5. Y. O. Fung, W. Wu, C.-T. Yeung, H.-K. Kong, K. K.-C. Wong, W.-S. Lo, G.-L. Law, K.-L. Wong, C.-K. Lau, C.-S. Lee and W.-T. Wong, *Inorg. Chem.*, 2011, **50**, 5517-5525.

6. B. S. Murray, E. J. New, R. Pal and D. Parker, *Org. Bio. Chem.*, 2008, **6**, 2085-2094.

7. V. V. Martin, W. H. Ralston, M. R. Hynes and J. F. W. Keana, *Bioconjug. Chem.*, 1995, **6**, 616-623.

8. M. Giardiello, M. Botta and M. Lowe, *J. Inclusion Phenom. Macrocyclic Chem.*, 2011, **71**, 435-444.

9. R. N. Muller, B. Raduchel, S. Laurent, J. Platzek, C. Pierart, P. Mareski and L. Vander Elst, *Eur. J. Inorg. Chem.*, 1999, 1949-1955.

10. P. Caravan, N. J. Cloutier, M. T. Greenfield, S. A. McDermid, S. U. Dunham, J. W. M. Bulte, J. C. Amedio, R. J. Looby, R. M. Supkowski, W. D. Horrocks, T. J. McMurry and R. B. Lauffer, *J. Am. Chem. Soc.*, 2002, **124**, 3152-3162.

11. J. Kotek, P. Lebduskova, P. Hermann, L. V. Elst, R. V. Muller, C. Geraldes, T. Maschmeyer, I. Lukes and J. A. Peters, *Chem. – Eur. J.*, 2003, **9**, 5899-5915.

12. T. N. Parac-Vogt, K. Kimpe, S. Laurent, L. Vander Elst, C. Burtea, F. Chen, R. N. Muller, Y. C. Ni, A. Verbruggen and K. Binnemans, *Chem. – Eur. J.*, 2005, **11**, 3077-3086.

13. C. Henoumont, V. Henrotte, S. Laurent, L. V. Elst and R. N. Muller, *J. Inorg. Biochem.*, 2008, **102**, 721-730.

14. P. Caravan, *Acc. Chem. Res.*, 2009, **42**, 851-862.

15. C. Henoumont, L. V. Elst, S. Laurent and R. N. Muller, *J. Phys. Chem. B*, 2010, **114**, 3689-3697.

16. G. Dehaen, P. Verwilst, S. V. Eliseeva, S. Laurent, L. V. Elst, R. N. Muller, W. M. De Borggraeve, K. Binnemans and T. N. Parac-Vogt, *Inorg. Chem.*, 2011, **50**, 10005-10014.

17. D. M. Dias, J. M. C. Teixeira, I. Kuprov, E. J. New, D. Parker and C. F. G. C. Geraldes, *Org. Bio. Chem.*, 2011, **9**, 5047-5050.

18. A. M. Nonat, C. Gateau, P. H. Fries, L. Helm and M. Mazzanti, *Eur. J. Inorg. Chem.*, 2012, **2012**, 2049-2061.

19. M. Brinkley, *Bioconjug. Chem.*, 1992, **3**, 2-13.

20. D.-L. Ma, W.-L. Wong, W.-H. Chung, F.-Y. Chan, P.-K. So, T.-S. Lai, Z.-Y. Zhou, Y.-C. Leung and K.-Y. Wong, *Angew. Chem. Int. Ed. Engl.*, 2008, **47**, 3735-3739.

21. J. D. Dattelbaum, O. O. Abugo and J. R. Lakowicz, *Bioconjug. Chem.*, 2000, **11**, 533-536.

22. K. K. W. Lo, W. K. Hui, D. C. M. Ng and K. K. Cheung, *Inorg. Chem.*, 2002, **41**, 40-46.

23. K. M.-C. Wong, W.-S. Tang, B. W.-K. Chu, N. Zhu and V. W.-W. Yam, *Organometallics*, 2004, **23**, 3459-3465.

24. E. M. Ryan, R. O'Kennedy, M. M. Feeney, J. M. Kelly and J. G. Vos, *Bioconjug. Chem.*, 1992, **3**, 285-290.

25. M. Salmain, M. Gunn, A. Gorfti, S. Top and G. Jaouen, *Bioconjug. Chem.*, 1993, **4**, 425-433.

26. M. Salmain, K. L. Malisza, S. Top, G. Jaouen, M. C. Senechaltocquer, D. Senechal and B. Caro, *Bioconjug. Chem.*, 1994, **5**, 655-659.

27. P.-K. Lee, H.-W. Liu, S.-M. Yiu, M.-W. Louie and K. K.-W. Lo, *Dalton Trans.*, 2011, **40**, 2180-2189.

28. N. Weibel, L. J. Charbonnière, M. Guardigli, A. Roda and R. Ziessel, *J. Am. Chem. Soc.*, 2004, **126**, 4888-4896.

29. S. Claudel-Gillet, J. Steibel, N. Weibel, T. Chauvin, M. Port, I. Raynal, E. Toth, R. F. Ziessel and L. J. Charbonnière, *Eur. J. Inorg. Chem.*, 2008, **2008**, 2856-2862.

30. O. Vasalatiy, P. Zhao, M. Woods, A. Marconescu, A. Castillo-Muzquiz, P. Thorpe, G. E. Kiefer and A. Dean Sherry, *Bioorg. Med. Chem.*, 2011, **19**, 1106-1114.

31. J. Xu, T. M. Corneillie, E. G. Moore, G.-L. Law, N. G. Butlin and K. N. Raymond, *J. Am. Chem. Soc.*, 2011, **133**, 19900-19910.

32. L. Zhang, Y. J. Wang, Z. Q. Ye, D. Y. Jin and J. L. Yuan, *Bioconjug. Chem.*, 2012, **23**, 1244-1251.

33. P. F. Sieving, A. D. Watson and S. M. Rocklage, *Bioconjug. Chem.*, 1990, **1**, 65-71.

34. P. D. Garimella, A. Datta, D. W. Romanini, K. N. Raymond and M. B. Francis, *J. Am. Chem. Soc.*, 2011, **133**, 14704-14709.

35. H. E. Rajapakse, N. Gahlaut, S. Mohandessi, D. Yu, J. R. Turner and L. W. Miller, *Proc. Natl. Acad. Sci. U. S. A.*, 2010, **107**, 13582-13587.

36. K. Nchimi-Nono, K. D. Wegner, S. Linden, A. Lecointre, L. Ehret-Sabatier, S. Shakir, N. Hildebrandt and L. J. Charbonnière, *Org. Bio. Chem.*, 2013, **11**, 6493-6501.

37. D. J. Lewis, P. B. Glover, M. C. Solomons and Z. Pikramenou, *J. Am. Chem. Soc.*, 2011, **133**, 1033-1043.

38. D. J. Lewis, thesis, University of Birmingham, 2006.

39. O. Nielsen and O. Buchardt, *Synthesis*, 1991, 819-821.

40. W. D. Horrocks and W. E. Collier, *J. Am. Chem. Soc.*, 1981, **103**, 2856-2862.

41. C. L. Davies, N. G. Housden and A.-K. Duhme-Klair, *Angew. Chem. Int. Ed. Engl.*, 2008, **47**, 8856-8858.

42. A. K. di Gennaro, L. Gurevich, E. Skovsen, M. T. Overgaard and P. Fojan, *Phys. Chem. Chem. Phys.*, 2013, **15**, 8838-8844.

43. J. D. Brennan, A. Capretta, K. Yong, D. Gerritsma, K. K. Flora and A. Jones, *Photochem. Photobiol.*, 2002, **75**, 117-121.

44. Y. Iwao, M. Hiraike, U. Kragh-Hansen, K. Mera, T. Noguchi, M. Anraku, K. Kawai, T. Maruyama and M. Otagiri, *Biochim. Biophys. Acta.*, 2007, **1774**, 1582-1590.

45. D. J. Weaver, A. Cherukuri, J. Carrero, T. CoelhoSampaio, G. Durack and E. W. Voss, *Biol. Cell.*, 1996, **87**, 95-104.

46. R. Yumoto, S. Suzuka, K. Oda, J. Nagai and M. Takano, *Drug Metab. Pharmacokinet.*, 2012, **27**, 336-343.

47. A. E. Soini, A. Kuusisto, N. J. Meltola, E. Soini and L. Seveus, *Microsc. Res. Tech.*, 2003, **62**, 396-407.

48. G. J. Stasiuk, H. Smith, M. Wylezinska-Arridge, J. L. Tremoleda, W. Trigg, S. K. Luthra, V. M. Iveson, F. N. E. Gavins and N. J. Long, *Chem. Commun.*, 2013, **49**, 564-566.

49. I. C. Serrano, A. M. Adams, R. Palankar, G. Stoica, E. Palomares and M. Delcea, *RSC Adv.*, 2014, **4**, 15040-15047.

50. M. M. Bradford, *Anal. Biochem.*, 1976, **72**, 248-254.

51. N. J. Kruger, in *The Protein Protocols Handbook*, ed. J. M. Walker, Humana Press Inc., Moscow, 2003, pp. 15-21.

52. R. F. Chen, *Arch. Biochem. Biophys.*, 1969, **133**, 263-276.

53. S. Beychok, *Science*, 1966, **154**, 1288-1299.

54. A. Rogozea, I. Matei, I. M. Turcu, G. Ionita, V. E. Sahini and A. Salifoglou, *J. Phys. Chem. B*, 2012, **116**, 14245-14253.

55. Innova Biosciences Ltd, *Lightning-Link® FluoProbes®647H*, http://www.innovabiosciences.com/antibody-labeling-kits/fluorescent-dye-labeling-kits/lightning-link-fluoprobes-647h.html, Accessed 22nd January, 2014.

56. B. Valeur and M. N. Berberan-Santos, in *Molecular Fluorescence: Principles and Applications*, Wiley-VCH Verlag GmbH & Co. KGaA, Weinheim (Germany), Editon edn., 2012, pp. 213-261.

57. L. F. Pease, J. T. Elliott, D.-H. Tsai, M. R. Zachariah and M. J. Tarlov, *Biotechnol. Bioeng.*, 2008, **101**, 1214-1222.

58. G. A. Crosby and J. N. Demas, *J. Phys. Chem.*, 1971, **75**, 991-1024.

59. S. M. Buttrum, R. Hatton, G. B. Nash, *Blood*, 1993, **82**, 1165-1174.

3. Design of a Specific Peptide Binding Site for Luminescent Gold Nanoparticles

3.1 Introduction

3.1.1 Applications of Peptides and Nanoparticles

Since the advent of nanomaterial research, nanoparticles at the biological interface has been a topic of great interest. The effect of nanomaterials on biological species is a key area of research, but in addition to this the benefits of combining nanomaterials with biological matter has been widely investigated. Peptides in particular have been added to the surface of nanoparticles to stabilise the nanoparticles, to act as sensors and to act as a targeting moiety to deliver nanoparticles with a beneficial payload to a particular cell or cellular compartment.[1] There have been extensive studies of so called cell penetrating peptides which usually contain several arginine or lysine residues which facilitate the peptide crossing the cell membrane. Previous research has shown that cell penetrating peptides are able to facilitate nuclear localisation of AuNPs in cells such as human fibroblast cells, human cervical cancer cells, human epithelial cancer cells and African green monkey kidney cells.[2-5] There have also been studies that suggest that the cellular fate of AuNPs may depend on the AuNP size in addition to the cell penetrating peptide sequence used.[4-6] It may be of interest to examine the mode of attachment of these peptides to AuNPs in order to better understand the use of attachment methods in biological applications. In all but one of the studies referenced here, the peptides were attached to the AuNPs by a Au-S bond, either using a thiol contained within the peptide sequence, or attaching the peptide to a linker possessing a thiol terminus.[2-5] The study that did not exploit the high affinity of sulphur for gold did use peptides terminating in cysteine residues which contain a thiol group, but used this thiol to attach the peptides to BSA which then coated the AuNPs, presumably through electrostatic means.[6] In all cases where the

peptide was attached to the AuNPs via a Au-S bond, the peptide modified AuNPs were found to locate in different areas of the cell to unmodified AuNPs, thus demonstrating the localisation effect of the peptides used and confirming their presence at the surface of the AuNPs.[2-5] AuNPs modified with BSA-peptide conjugates were subject to protein displacement studies which revealed that up to 30% of the BSA-peptide conjugates were displaced from the surface of the AuNPs over four hours when in the presence of cell culture medium containing foetal bovine serum.[6] Since the studies utilising Au-S chemistry did not quantitatively explore the displacement of the peptides from the surface of the AuNPs when in biological systems it is hard to compare their stability to the BSA-peptide modified AuNPs, however, it was noted that the final cellular localisation of the BSA-peptide modified AuNPs was dependent upon the peptide sequence used, demonstrating the presence of the BSA-peptide conjugate at the surface of the AuNPs after administration to cells.[6]

3.1.2 Covalent Attachment of Peptides to AuNPs

In addition to the studies involving cell penetrating peptides, much research has been carried out into the modification of AuNP surfaces by peptides with a large number of papers describing the use of cysteine residues for the attachment of peptides to the AuNPs because of the affinity of its thiol side group for the gold surface.[1, 7-11] Experiments to find alternative gold binding peptides have used libraries of peptides displayed on cell surfaces. These studies have found that although cysteine is the dominant binding residue when present, combinations of other residues bearing functional groups such as carboxyls can interact with gold and, when considered cumulatively, in comparable strength to the gold-sulphur bond.[10-12] The option of using combinations of amino acids to obtain a comparable binding affinity to gold to that achieved with a single thiol group obviously limits the number of peptides or

additional molecules of interest able to bind to the surface of the AuNPs. This is because the binding peptide will take up a larger amount of surface space to enable binding through several residues compared to one cysteine residue. It is for this reason that peptide sequences containing one or more cysteine residues will be explored for binding AuNPs in this chapter; the overall scope of the project, as described in Chapter 4, involves peptides binding to AuNPs already modified with luminescent molecules and, as such, it would be preferable for the peptide to bind strongly to the AuNPs through a minimal number of residues.

In addition to peptides binding to formed AuNPs, it is possible to include peptides in the synthesis of AuNPs. In this case peptides are used to reduce gold salts and form the final surface layer capping the AuNPs.[13, 14] For example, the synthesis of 10 nm AuNPs was achieved by using a polypeptide containing lysine residues, whose amine side groups were converted to nitrite by oxidation induced by the gold ions. The polypeptide capped AuNPs were stabilised by the repulsion of the positively charged polypeptides. The charged polypeptides were also able to bind to negatively charged DNA allowing gene delivery by the AuNPs to embryonic mouse fibroblast cells.[14] Similarly, peptide sequences containing residues for reducing gold salts and a molecular recognition sequence were used to synthesise 13 nm AuNPs. In this case tyrosine was thought to be the residue responsible for gold reduction and the molecular recognition sequence was shown to attach the AuNPs to surfaces displaying antibodies against the sequence.[13] Whilst these interactions of peptides with AuNPs may be of interest in some applications, they will not be the focus of this chapter. Again, this is because a strong bond is needed between the peptide and AuNPs that have already been prepared and modified in order to fulfil the applications of the AuNPs as discussed in Chapter 4.

A peptide with the sequence CALNN is an example of a peptide that attaches to AuNPs through the thiol of its cysteine residue and has been shown to stabilise AuNPs in solution and in cells.[9, 15, 16] The ability of CALNN to stabilise AuNPs in aqueous solution is thought to be because it presents a hydrophobic environment close to the AuNP surface with a hydrophilic portion of the peptide containing asparagine residues exposed to solution. The amino acids also possess side chains of increasing size from cysteine to asparagine, sterically promoting the formation of a monolayer on the curved surface of AuNPs, Scheme 3.1. In order to increase the affinity of a peptide for a gold surface, it is also possible to replace the cysteine residue with a group such as a thioctic acid which has the potential to be reduced at the surface of the AuNP and thus present two sulphur atoms through which to create bonds with the AuNP surface.[17] Previous research by the Pikramenou group has shown the attachment of a variant of CALNN, where the cysteine residue has been replaced by a thioctic acid group, to AuNPs and the subsequent ability of the peptide to bind lanthanide ions.[17] As a starting point for designing the peptide binding motif in this project, variants of CALNN will be used, with additional cysteine sites to present the potential for a greater binding affinity between the peptide and the AuNPs.

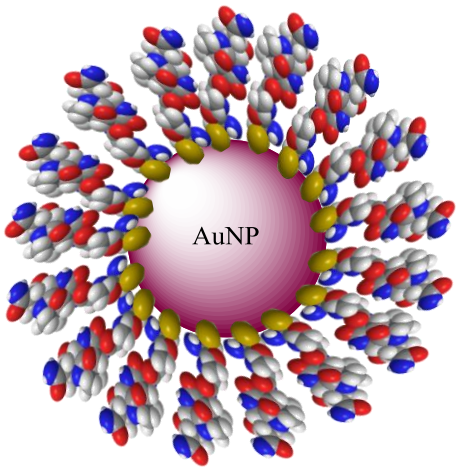

Scheme 3.1 Schematic representation of CALNN surface coverage of AuNPs.

Another possible AuNP binding peptide may be found when considering the work of Roger Tsien's group where tetracysteine motifs were introduced into proteins to bind biarsenical probes.[18, 19] The use of cysteine residues in this case was because of their affinity for arsenic and because other reactive amino acids such as glutamates or lysines were considered too abundant in natural proteins, thus limiting the specificity of the interaction between the probe and the designed peptide. The initial tetracysteine containing peptide domain developed had the sequence WEAAAREACCRECCARA which included both an EAAAR repeat, which is known to form α-helices, and cysteine residues in the positions *i*, *i*+1, *i*+4 and *i*+5 allowing the formation of dithiol interactions at each trivalent arsenic contained within the biarsenical compound, Scheme 3.2.

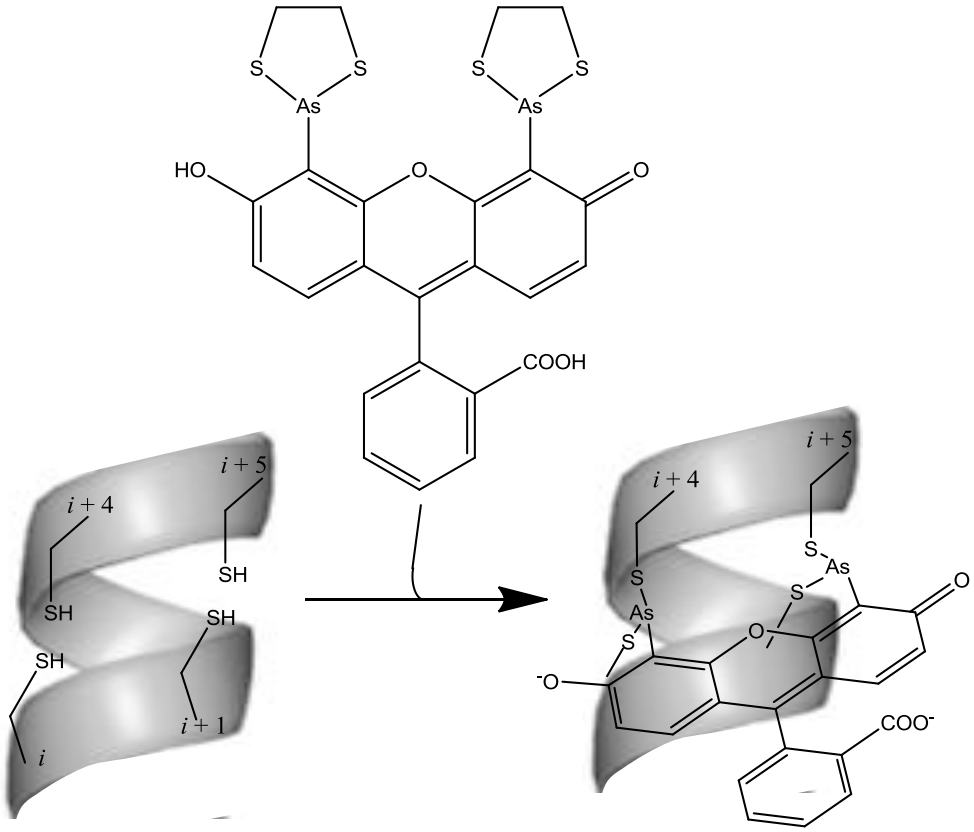

Scheme 3.2 Interaction of a biarsenical compound with the tetracysteine motif contained within a helix formation.

Further research suggested that including proline and glycine between the two double cysteines creates a hairpin conformation rather than an α-helix and produces a greater affinity for the biarsenical probe.[18] The ability of the hairpin tetracysteine motif to bind the biarsenical probe may also be applicable to binding AuNPs and this will be explored in this chapter.

3.1.3 Measuring Peptide – AuNP Interactions

AuNPs display an SPR band in their absorption spectra which is caused by the coherent oscillation of free electrons across the surface of the nanoparticles when a particular wavelength of light is applied. This phenomenon is typically in the visible region for gold nanoparticles and is indicative of both size and shape of the nanoparticles. The SPR peak in the absorption spectrum can be used to monitor the modification of the surface of AuNPs because it should change as molecules adsorb to the nanoparticles. This technique has been previously used to measure peptide attachment to AuNPs.[1, 17, 20] For example, a modified peptide sequence, thioctic acid-ALNN, induced a 2 nm bathochromic shift in the SPR absorption peak of 13 nm citrate-stabilised AuNPs.[17] The position of the SPR peak in the absorption spectrum gradually shifted with small additions of the peptide species before remaining constant at a 2 nm change for several peptide additions indicating no further change at the surface and thus the saturation of the surface of the AuNPs with the peptide. Similarly, UV-Vis absorption spectroscopy was used to monitor the addition of a disulphide containing peptide to the surface of 13 nm citrate-stabilised AuNPs and it was found that the peptide induced a 5 nm bathochromic shift in the SPR peak of the AuNPs.[20] Since the change in SPR position in the absorption spectrum of AuNPs changes gradually and finally reaches a plateau when peptides are titrated into a solution of AuNPs, it may be possible to plot a curve

of change in the SPR band as a function of peptide concentration and fit the curve to find information about the strength of binding.

The binding constant of peptides to AuNPs can also be measured using ITC which measures changes in the temperature of a solution of AuNPs as peptides are added. ITC can give information about the enthalpy and entropy change, number of binding sites and the binding constant of a particular peptide-AuNP interaction. One study used ITC to determine the binding constant of anionic peptides to surface modified 2 nm cationic AuNPs to be in the range of 10^6 M^{-1} by titrating a solution of AuNPs into a solution of peptide.[21] Another study titrated a peptide solution into a solution of 5 nm AuNPs to find a binding constant in the region of 10^5 M^{-1}.[22] In both cases ITC data was fit using a one-site binding model because, although AuNPs contain many possible binding sites for the peptide, each site can be considered equal and independent.[21, 22]

3.1.4 Research Aims

The main objective of this chapter is to identify a peptide capable of binding strongly to AuNPs. Three peptide sequences will be used, two based around the CALNN motif and the other a tetracysteine motif CCPGCC. A variety of techniques will be used to determine the binding affinity of each peptide to AuNPs. The work outlined here will inform the utilisation of the peptide binding sequence in Chapter 4 where luminescent AuNPs will be employed. The effect of peptide on the luminescent properties of lanthanide coated AuNPs will, therefore, also be explored.

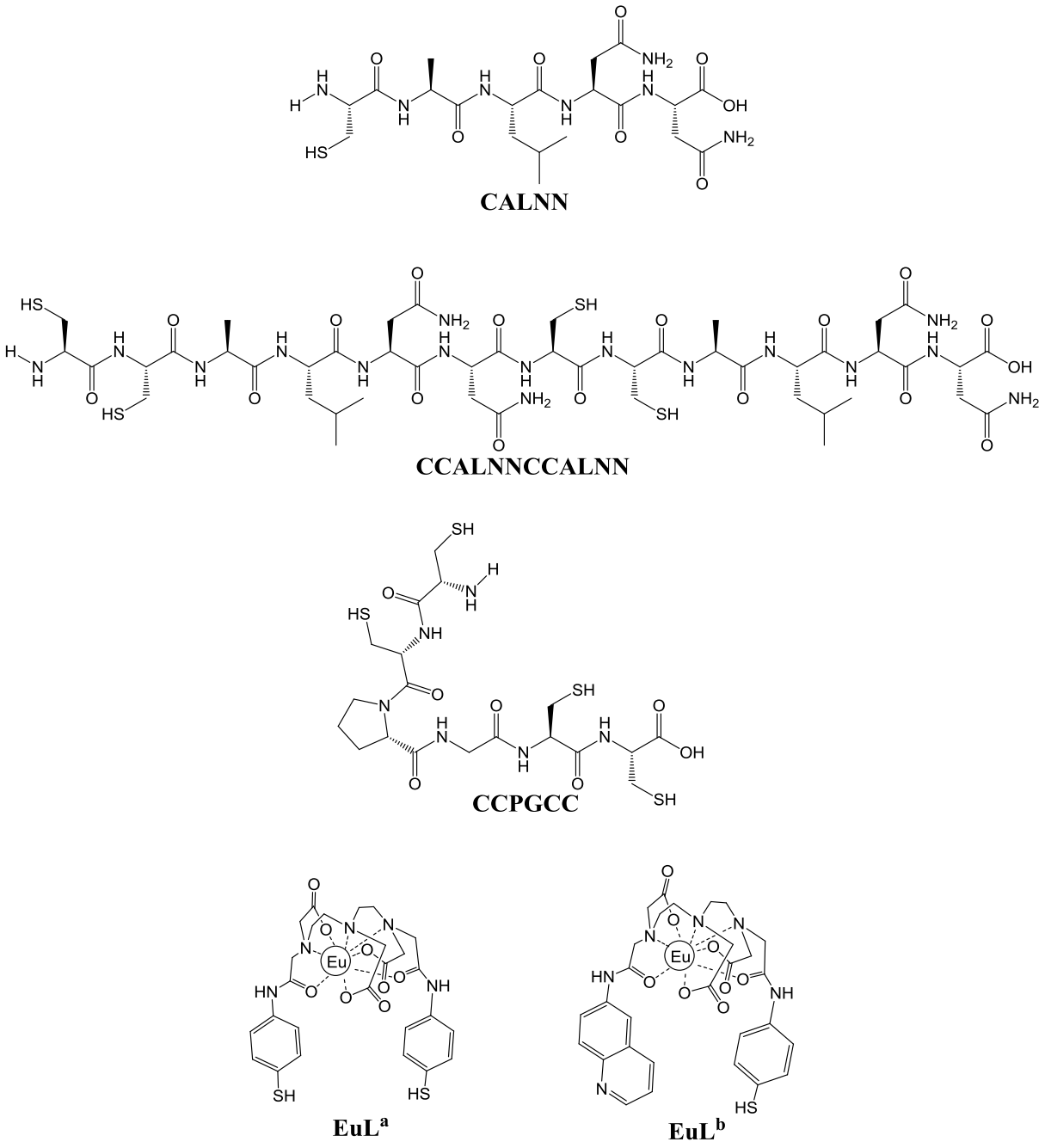

Figure 3.1 Peptides and luminescent europium complexes used in this chapter.

3.2 Results and Discussion

3.2.1 Synthesis of **Citrate-AuNPs**

The preparation of citrate-stabilised gold nanoparticles was based upon a well known synthesis which uses the reduction of Au(III) by citrate ions resulting in a nanoparticle core of Au(0) capped with citrate ions.[23] The resulting 13 nm **Citrate-AuNPs** were characterised by UV-Vis spectroscopy, DLS and ζ-potential measurements. The hydrodynamic diameters reported throughout this chapter are taken from the number distribution data obtained from DLS measurements, however, both number and intensity distribution graphs are available in the appendix.

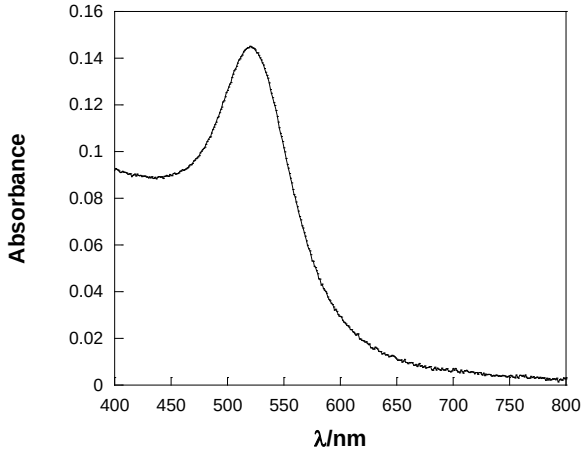

Figure 3.2 UV-Vis absorption spectrum of 0.47 nM **Citrate-AuNPs**.

Hydrodynamic Diameter/nm	ζ-potential/mV
13 ± 2	-33 ± 2

Table 3.1 DLS and ζ-potential measurements of **Citrate-AuNPs**.

The UV-Vis absorption spectrum of **Citrate-AuNPs** shows the characteristic SPR band at 520 nm. The DLS measurements of **Citrate-AuNPs** reveals a hydrodynamic diameter of around 13 nm which indicates that the nanoparticles do not have any large molecules associated with their surface because this is the same diameter calculated in literature using

TEM, for AuNPs prepared using this method, which will only give information about the gold core of the nanoparticles.[23] **Citrate-AuNPs** exhibit a ζ-potential of -33 mV which indicates that they are stable in solution since their surface charge is sufficient for the nanoparticles to repel one another, preventing aggregation of the nanoparticles. The ζ-potential is also negative as would be expected due to the citrate ions capping the surface of the nanoparticles.

3.2.2 Preparation of Peptides

The preparation of **CCALNNCCALNN** followed that of solid phase peptide synthesis using Fmoc protected amino acids and Fmoc-Asn(Trt)-Wang resin in a Liberty 1 CEM Microwave Peptide Synthesizer. The preparation was carried out on a 0.1 mmol scale with five-fold excess of each amino acid used. The desired peptide was isolated using HPLC and identified using MALDI mass spectrometry and characterised by UV-Vis spectroscopy.

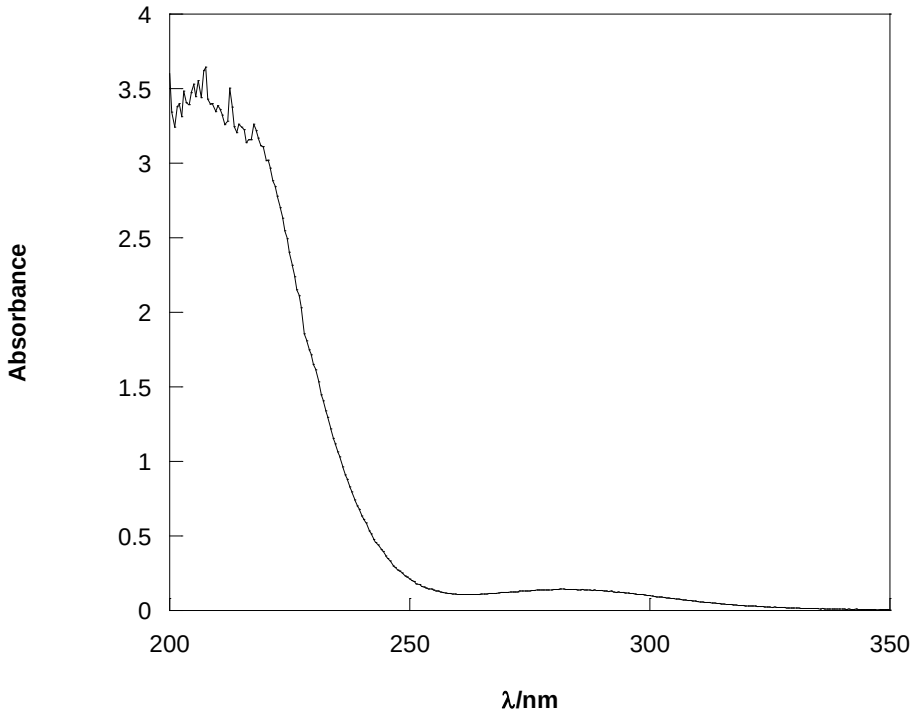

Figure 3.3 Absorption spectrum of 1 mM **CCALNNCCALNN** in water.

The absorption spectrum of **CCALNNCCALNN** shown in Figure 3.3 is typical of what would be expected for a peptide molecule with this sequence. The large absorption, with a molar absorption coefficient of 3500 M^{-1} cm^{-1}, at around 205 nm is attributed to the peptide bond $\pi \rightarrow \pi^*$ transition with some possible contribution from its $n \rightarrow \pi^*$ transition.[24] Peptides containing residues with aromatic side chains would usually exhibit absorption around 280 nm with high molar absorption coefficients, however, in this case no such residues are present. A small absorption, ε = 140 M^{-1} cm^{-1}, at 280 nm for this peptide is most likely to arise from the presence of disulphide bonds which must have formed either intra- or inter-molecularly.[25]

3.2.3 Interaction of CALNN with **Citrate-AuNPs**

The peptide with the sequence CALNN is known within literature to bind to and impart great stability to citrate coated AuNPs.[9, 15] It is also important to investigate the interaction of peptides with **Citrate-AuNPs** rather than lanthanide coated ones since the surface modifications of the AuNPs may differ depending on their application.

3.2.3.1 Preparation of **CALNN-AuNPs**

The absorption spectrum of **Citrate-AuNPs** was measured as a solution of CALNN was titrated into the nanoparticles. Since the SPR band in the absorption spectrum of AuNPs is sensitive to their surface modification, monitoring this should allow information to be gathered about the displacement of citrate on the surface of **Citrate-AuNPs** by CALNN.

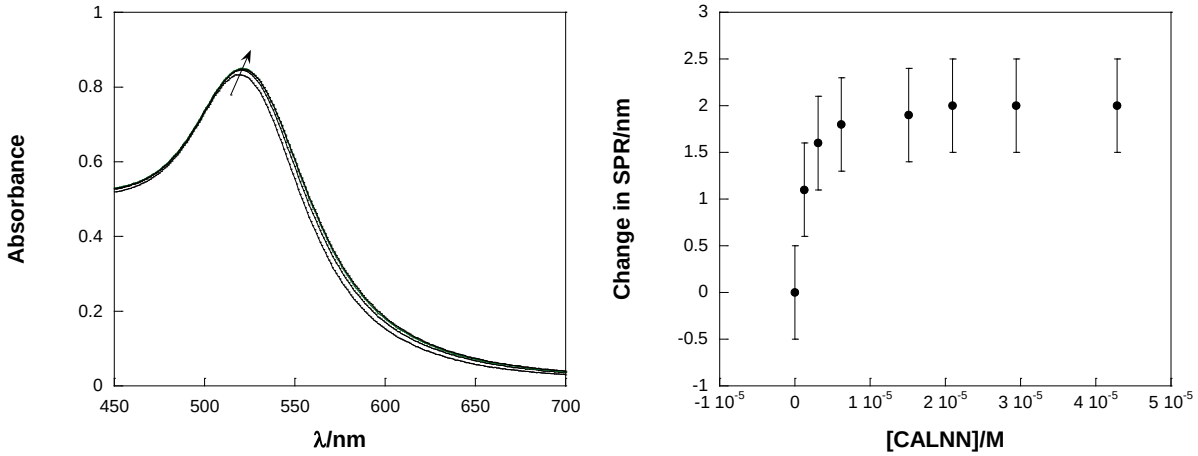

Figure 3.4 Left: Absorption spectra of 3 nM **Citrate-AuNPs** with microlitre additions of a 0.5 mM solution of CALNN. Right: Change in SPR position of 3 nM **Citrate-AuNPs** with titration of CALNN.

As CALNN was titrated into **Citrate-AuNPs** a bathochromic shift of the SPR band was observed indicating a change at the surface of the AuNPs likely to be the displacement of citrate ions by peptide molecules binding to the gold. The 2 nm shift in SPR position concurs with that achieved in the literature following mixing of peptide and AuNP solutions.[9, 26] The newly formed **CALNN-AuNPs** were centrifuged to form a pellet, the supernatant discarded and the pellet redispersed in deionised water before the process was repeated to remove any unbound peptide species. The position of the SPR peak in the UV-Vis absorption spectrum was unchanged by washing and centrifugation of the AuNPs. A solution of isolated **CALNN-AuNPs** were then analysed by DLS measurements.

Sample	Hydrodynamic Diameter/nm
Citrate-AuNPs	13 ± 2
CALNN-AuNPs	12 ± 3

Table 3.2 Hydrodynamic diameters of **Citrate-AuNPs** and **CALNN-AuNPs** measured by DLS.

After addition of CALNN to **Citrate-AuNPs** there is no real change observed in the hydrodynamic diameter of the AuNPs. A previously published study reports that on addition of CALNN to 9.3 nm citrate-stabilised AuNPs, an increase in hydrodynamic diameter of 1.2 nm is observed.[26] An increase of 1.2 nm is within the measured range recorded in this instance and as such the similarity between the hydrodynamic diameters of the two AuNP species is not unexpected. It has been previously hypothesised that the N-terminal cysteine residue binds to the surface of the AuNPs while the rest of the peptide molecule points outwards towards the solvent because the two C-terminal asparagine residues are hydrophilic and are relatively bulky which may encourage their projection towards the surrounding solvent.[9] The approximate length of the peptide is 1.5 nm and as such would be expected to add 3 nm to the hydrodynamic diameter of the AuNPs if it were to bind in the fashion described previously, however, such an increase is not observed and as such it may be possible that the peptide is held more closely to the surface of the AuNPs than expected.

3.2.3.2 Measurement of CALNN Binding to **Citrate-AuNPs**

The possibility of using CALNN as a specific binding site for AuNPs was assessed by measuring the binding constant of the peptide to the AuNP surface. The binding constant was investigated using ITC which measures the heat change as the peptide is titrated into **Citrate-AuNPs** which can then be fit to find K_a. It is important with this technique that **Citrate-AuNPs** and CALNN are in the same solvent as mixing of solvents can cause a heat change and, for this reason, **Citrate-AuNPs** were centrifuged to form a pellet before being redispersed in deionised water and the process repeated to ensure there were no excess ions from their synthesis in solution. CALNN was also dissolved in deionised water. This is in

contrast to the titration monitored via UV-Vis spectroscopy where **Citrate-AuNPs** were used as synthesised with potential excess ions present in the aqueous solution.

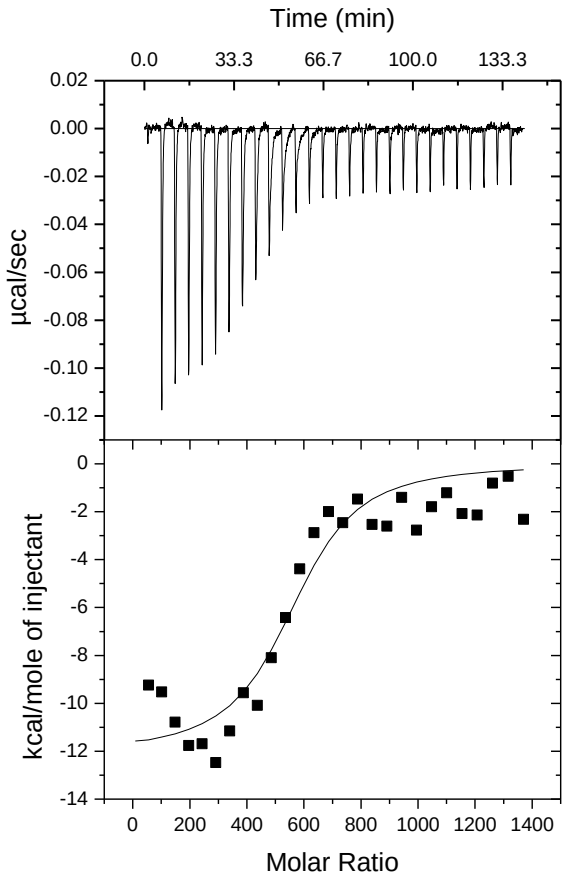

Figure 3.5 ITC data for the titration of 0.03 mM CALNN into 4.5 nM **Citrate-AuNPs**. Top: change in heat measured over time as CALNN is added at specific time intervals. Bottom: integrated area of peaks shown in the top graph to give energy change at each addition of peptide against molar ratio of the two species with the fit shown as a line through the data points.

The ITC results were analysed using Origin 7.0 software and the data fit using a 1:n binding model which is appropriate in this case because although there are multiple binding sites on the AuNP surface for the peptide to bind, the degree of cooperation between these sites is negligible and the peptide is present in high excess which drives a 1:1 interaction between peptide and AuNP binding site. The peptide is added in such excess that overall binding is

observed and analysed as opposed to individual events. Similarly, if the peptide binds sequentially through one thiol and then another group, such as an amine, this technique will not resolve such changes and as such only the overall binding of the peptide to AuNPs is considered. The fit achieved, however, does not capture the data well which may suggest that the experimental parameters could be optimised in the future if the experiment were to be repeated. For example, using different concentrations of the substrates might result in a neater curve and a better fit of the data. To date the concentrations used to produce the results in Figure 3.5 provided the best results, however, in comparison to results reported later, Figure 3.8, it is evident that the signal detected in this case is weak which may have hampered the fitting of the data. Nevertheless, since additional techniques will be used to find the binding constant of this system these results will be corroborated.

Here the change in heat of the system is measured, therefore, it is not just K_a that can be calculated from the results. The equation used to fit the data can be found in the appendix.

Parameter	Calculated Value
K_a	$9.14 \times 10^6 \pm 4.40 \times 10^6$ M^{-1}
Number of binding sites	564 ± 28.5
ΔH	$-1.208 \times 10^4 \pm 821.8$ cal mol^{-1}
ΔS	-8.67 cal mol^{-1} K^{-1}

Table 3.3 Calculated values for the parameters K_a, number of binding sites, ΔH and ΔS from ITC data measured for the titration of CALNN into **Citrate-AuNPs**.

The binding of CALNN to **Citrate-AuNPs** is found by ITC measurement to be an exothermic process which is spontaneous if not entropically favoured. The spontaneity of the reaction can be calculated using the above parameters in the equation below.

$$\Delta G = \Delta H - T\Delta S$$

Equation 3.1 Calculation of the Gibbs free energy of a reaction.

Using Equation 3.1 and the results in Table 3.3 with the knowledge that the reaction was carried out at 298 K, ΔG was found to be -9496 cal mol^{-1} which indicates a spontaneous reaction because of its negative value. It is not surprising that the reaction is not entropically favoured as the peptide molecules, although displacing citrate from the AuNP surface, will become more ordered in binding to the gold surface and perhaps will create increased order within the solvation sphere surrounding each peptide coated AuNP. Importantly, K_a was found to be in the range of 10^6 M^{-1} indicating strong binding. The number of binding sites calculated relates to 1.2 peptides per nm^2, which is slightly lower than the 1.67-1.93 peptides per nm^2 reported previously for CALNN coverage of 12.3 nm AuNPs.[9] Treating the 13 nm AuNPs as spheres, their surface area can be calculated and, since the size of gold atoms is known, the number of gold atoms at the surface of the AuNPs can also be calculated; using this method, the AuNPs here are found to have 9004 gold atoms at their surface.[27] Assuming that the number of binding sites calculated from the ITC data is equal to the number of surface gold atoms occupied the peptide interacts with just 6% of the available surface. Of course, the footprint of the peptide molecule and its ability to pack on the surface will also influence the surface coverage as well as its binding affinity, but the number of binding sites calculated here directly relates to the ratio of peptide to AuNPs during the titration.

Another, perhaps simpler, way to gain an estimation of the binding constant is to apply a fit to the titration curve shown in Figure 3.4 in order to find K_a. In this case a regime is used to fit a 1:n binding event. The equation used is shown in the experimental section and the curve fit can be found in the appendix.

System Examined	K_a/M^{-1}
Citrate-AuNPs + CALNN	$1.4 \times 10^6 \pm 2.3 \times 10^5$

Table 3.4 K_a calculated upon fitting the curve of change in SPR absorption maximum position of **Citrate-AuNPs** with titration of CALNN.

Fitting the data from the titration reveals a binding constant for CALNN onto AuNPs in the range of 10^6 M^{-1} which concurs with the results from ITC analysis, demonstrating the use of this method as a simple way to gain an estimate of binding information.

In addition to ITC measurements and UV-Vis absorption titrations, the binding of CALNN to gold was measured by SPR spectroscopy. A gold surface, similar to AuNPs, can exhibit an SPR when incident light hits the surface at the resonant angle. The resonant angle needed to create an SPR changes upon modification of the gold surface and as such can be used to measure the binding of molecules to gold. In this case solutions of CALNN in water at various concentrations were flowed over a gold chip and the SPR response measured.

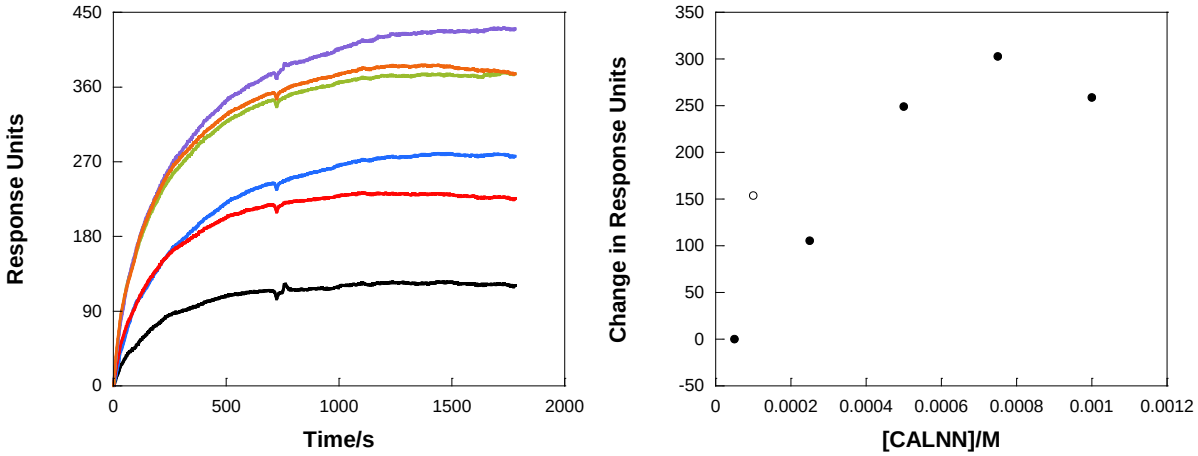

Figure 3.6 Left: Sensorgrams of response units over time for 0.05 mM (—), 0.1 mM (—), 0.25 mM (—), 0.5 mM (—), 0.75 mM (—) and 1 mM (—) CALNN flowing over a gold SPR chip corrected against a blank. Right: Response units taken from the peak of each sensorgram plotted against peptide concentration.

It can be seen from the sensorgrams that as the concentration of the peptide increases the response units measured increase as would be expected, however, there are some anomalies in this general trend. The response units recorded at the top of each curve were plotted against the corresponding peptide concentration to give a curve from which K_a could be found using the same regime used to fit the UV-Vis absorption titration data.

System Examined	K_a/M^{-1}
Gold chip + CALNN	$1.0 \times 10^6 \pm 3.4 \times 10^7$

Table 3.5 K_a calculated upon fitting the curve of change in SPR response maximum of a gold chip with addition of CALNN.

The data point on the right-hand graph of Figure 3.6 represented by an open circle was not used in the data fitting as it was seen to be anomalous. The binding constant was again found to be in the order of 10^6 M^{-1}, however, the error relating to this value is extremely high which

means that the results are inconclusive. It may be noted that the binding constant calculated for CALNN binding to a gold surface is comparable to the peptide binding to AuNPs which may indicate that the binding interaction is not influenced to any great extent by the surface topology, such as its curvature, but due to the large error in the binding constant calculated further studies would be required to confirm this. SPR experiments require considerably more peptide than ITC and UV-Vis absorption titrations and as such were not used for binding studies with other peptides.

3.2.4 Interaction of CCPGCC with **Citrate-AuNPs**

The peptide sequence CCPGCC when part of a larger peptide chain has previously been shown through NMR studies to position all four thiol groups towards one face of the peptide sequence allowing interaction of all four cysteine side chains with an external substance.[28] The positioning of the thiol groups is due to the hairpin structure caused by the steric restrictions of the proline residue. The CCPGCC sequence when part of a larger recombinant protein has previously been shown to bind to AuNPs of various sizes in an oriented manner.[29]

3.2.4.1 Preparation of **CCPGCC-AuNPs**

As described previously, a solution of CCPGCC in water was titrated into a solution of **Citrate-AuNPs** and the titration monitored via the absorption spectra of the AuNPs in solution. In this case a small amount of hydrazine monohydrate was added to the peptide solution to reduce any possible disulphide bonds.

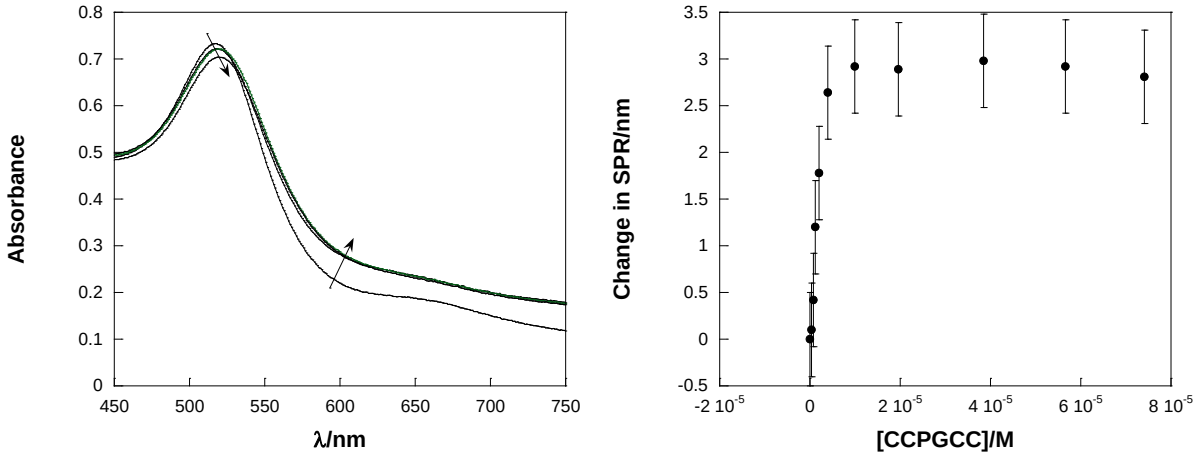

Figure 3.7 Left: Absorption spectra of 3 nM **Citrate-AuNPs** with microlitre additions of a 1 mM solution of CCPGCC. Right: Change in SPR position of 3 nM **Citrate-AuNPs** with titration of CCPGCC.

As CCPGCC was titrated into **Citrate-AuNPs** a bathochromic shift was observed for the SPR peak in the absorption spectrum of the AuNPs, indicating that the peptide was binding to the surface of the AuNPs. Absorbance above ~600 nm also increased over the course of the titration which may indicate flocculation of the AuNPs, however, no aggregation was observed. The newly formed **CCPGCC-AuNPs** were passed through a Sephadex G-15 size exclusion column to remove unbound peptide species and subsequently characterised by DLS measurements. The position of the SPR peak in the UV-Vis absorption spectrum was unchanged by isolation of the **CCPGCC-AuNPs**.

Sample	Hydrodynamic Diameter/nm
Citrate-AuNPs	13 ± 2
CCPGCC-AuNPs	26 ± 7

Table 3.6 Hydrodynamic diameters of **Citrate-AuNPs** and **CCPGCC-AuNPs** measured by DLS.

CCPGCC forms a hairpin structure due to the rigid structure of its cyclic proline residue, Figure 3.1, and as such should be able to present all four cysteine residues to the surface of the AuNPs without the need for additional adjustment of its conformation. The height of the peptide from the AuNP surface should be around 1.5 nm if it was indeed attached through all four cysteine residues, however, if it were to bind through only one end of the peptide chain the height of the peptide from the AuNP surface would still be around 1.5 nm. In each case it would, therefore, be expected that the increase in hydrodynamic diameter of the AuNPs after CCPGCC binding should be approximately 3 nm. The larger increase in hydrodynamic diameter may be due to the association of solvent molecules with the peptide, or possibly, in this case, the peptide may be cross-linking two AuNPs which may, in part, explain the growth in absorption seen at above 600 nm during the titration.

3.2.4.2 Measurement of CCPGCC Binding to **Citrate-AuNPs**

Firstly, the binding constant was investigated using ITC measurements. As before, **Citrate-AuNPs** were isolated and redispersed in deionised water and the peptide also dissolved in deionised water. A solution of 0.2 mM CCPGCC was titrated into 4.5 nM **Citrate-AuNPs**.

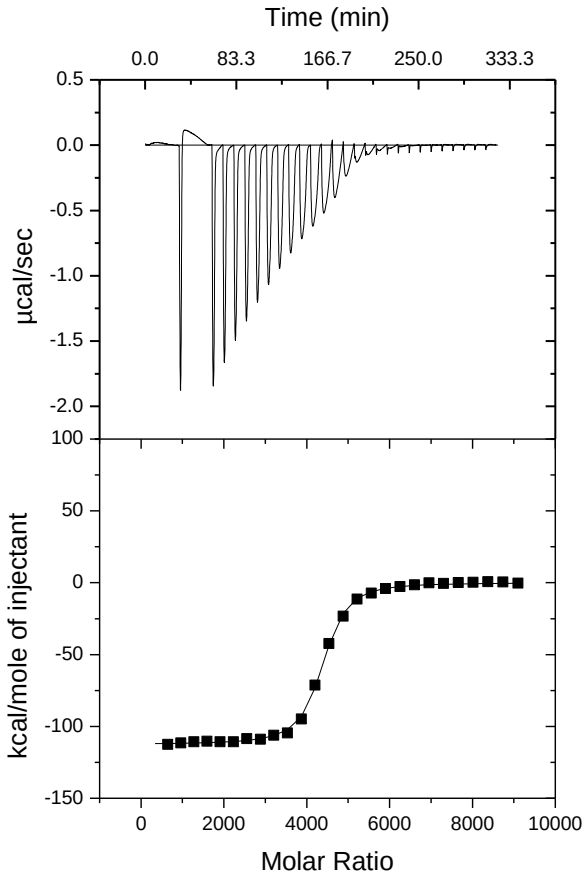

Figure 3.8 ITC data for the titration of 0.2 mM CCPGCC into 4.5 nM **Citrate-AuNPs**. Top: change in heat measured over time as CCPGCC is added at specific time intervals. Bottom: integrated area of peaks shown in the top graph to give energy change at each addition of peptide against molar ratio of the two species with the fit shown as a line through the data points.

The ITC results were analysed using Origin 7.0 software and the data fit using a 1:n binding model. Fitting the data also revealed additional parameters of the system.

Parameter	Calculated Value
K_a	$1.19 \times 10^7 \pm 7.09 \times 10^5$ M^{-1}
Number of binding sites	$4.26 \times 10^3 \pm 9.22$
ΔH	$-1.126 \times 10^5 \pm 421.5$ cal mol^{-1}
ΔS	-345 cal mol^{-1} K^{-1}

Table 3.7 Calculated values for the parameters K_a, number of binding sites, ΔH and ΔS from ITC data measured for the titration of CCPGCC into **Citrate-AuNPs**.

As with the binding of CALNN to AuNPs, the binding of CCPGCC to AuNPs was found to be spontaneous, but not entropically favoured, with a Gibbs free energy of -9790 cal mol^{-1} calculated using Equation 3.1. The binding constant in this case was found to be in the order of 10^7 M^{-1}. In this instance the number of binding sites occupied by the peptide is much higher than that measured for CALNN. Using the number of binding sites calculated from the ITC data, and assuming that this equals the number of gold atoms involved in binding, CCPGCC is found to bind to 47% of the surface of the AuNPs, 41% more than CALNN.

The K_a for CCPGCC binding to AuNPs was also calculated by fitting the UV-Vis absorption titration data in the same way as for CALNN titrations and the fit can be found in the appendix.

System Examined	K_a/M^{-1}
Citrate-AuNPs + CCPGCC	$1.2 \times 10^7 \pm 1.4 \times 10^7$

Table 3.8 K_a calculated upon fitting the curve of change in SPR absorption maximum position of **Citrate-AuNPs** with titration of CCPGCC.

Fitting of the titration data revealed a K_a in the order of 10^7 M^{-1} which does concur with the value for K_a calculated from the ITC data, however, the error in the value is very high which means that no conclusions can be drawn from this result. It may have been the case that the concentration of peptide added during the titration was too high, resulting in a sharp curve that was difficult to fit. If the titration were to be repeated using a lower concentration of peptide a shallower curve may result allowing a fit to be applied with less error.

3.2.5 Interaction of **CCALNNCCALNN** with **Citrate-AuNPs**

As previously discussed, it is known that the peptide sequence CALNN is able to coat AuNPs and stabilise them effectively.[9, 15] It was, therefore, attempted to further investigate the affinity of the peptide for AuNPs by addition of an extra cysteine residue into the sequence and then duplicating the sequence to give **CCALNNCCALNN**. This sequence should allow evaluation of the effects of amino acid sequence and number of cysteine residues on binding to AuNPs.

3.2.5.1 Computer Modelling of **CCALNNCCALNN**

CCALNNCCALNN in aqueous solution was modelled using AMBER software utilised through the BlueBEAR facility at the University of Birmingham, UK.

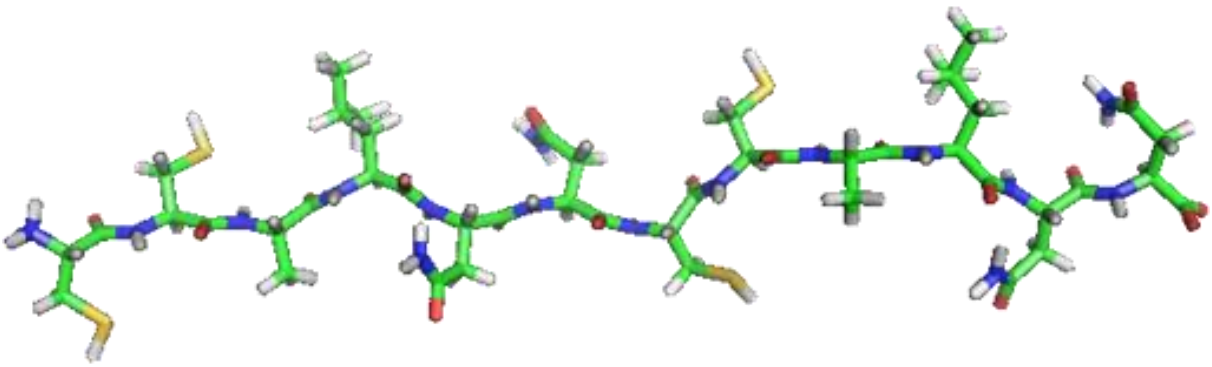

Figure 3.9 Computer model of **CCALNNCCALNN** in water.

The computer model of the peptide shows that the conformation of **CCALNNCCALNN** does not adhere to any organised secondary structure, which is perhaps not unexpected due to its short length. How **CCALNNCCALNN** interacts with AuNPs is not intuitive based on its structure.

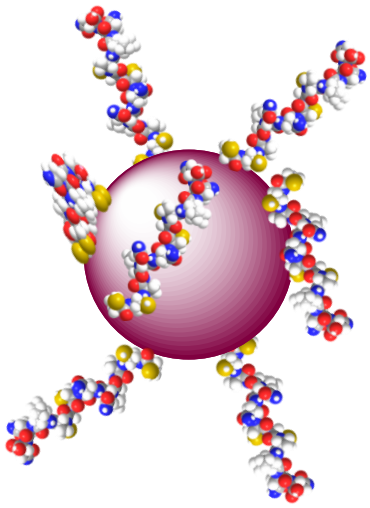

Scheme 3.3 Schematic representation of the interaction of **CCALNNCCALNN** with AuNPs.

The thiol groups of the peptide are most likely to bind to the surface of the AuNP due to the affinity of sulphur for gold, however, the peptide may fold to allow all cysteine residues access to the AuNP surface, or may wrap around part of the AuNP surface for the same reason, or perhaps only the two terminal cysteine residues will bind to the gold surface with possible stabilising interactions with neighbouring peptides.

3.2.5.2 Preparing **CCALNNCCALNN-AuNPs**

As with the other peptides used, a solution of **CCALNNCCALNN** in water was titrated into a solution of **Citrate-AuNPs** and the titration monitored by UV-Vis absorption spectroscopy. A small amount of hydrazine monohydrate was added to the peptide solution prior to the

titration to reduce any disulphide bonds which could affect the interaction of the peptide with the AuNPs.

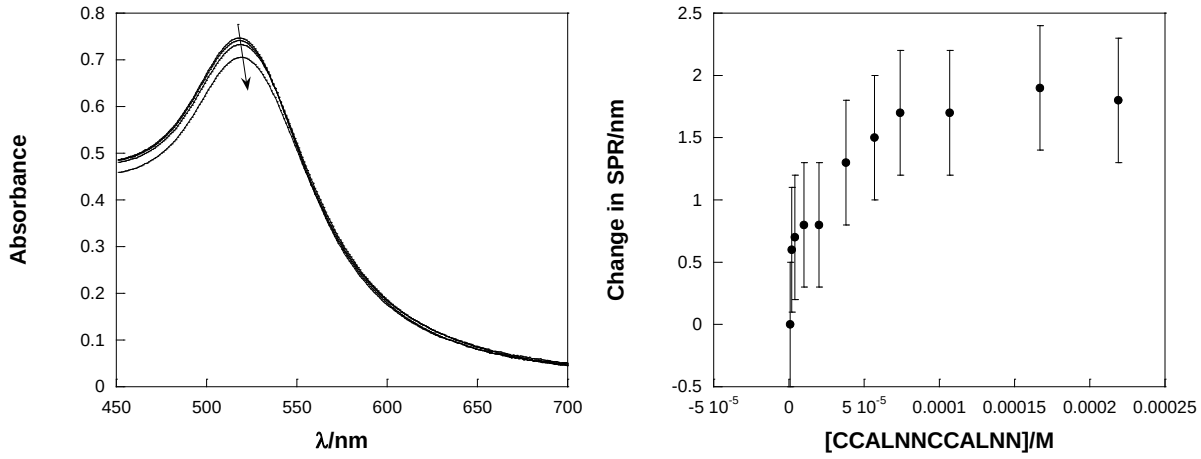

Figure 3.10 Left: Absorption spectra of 3 nM **Citrate-AuNPs** with microlitre additions of a 1 mM solution of **CCALNNCCALNN**. Right: Change in SPR position of 3 nM **Citrate-AuNPs** with titration of **CCALNNCCALNN**.

The binding of **CCALNNCCALNN** to the surface of AuNPs elicits a bathochromic shift in the SPR peak in the absorption spectra relative to **Citrate-AuNPs**. DLS was used to assess the change in hydrodynamic diameter of the AuNPs. Unlike with the other peptide coated AuNPs, **CCALNNCCALNN-AuNPs** were not isolated before further analysis because attempts to do so led to particle aggregation.

Sample	Hydrodynamic Diameter/nm
Citrate-AuNPs	13 ± 2
CCALNNCCALNN-AuNPs	12 ± 3

Table 3.9 Hydrodynamic diameters of **Citrate-AuNPs** and **CCALNNCCALNN-AuNPs** measured by DLS.

The hydrodynamic diameter of the AuNPs is unchanged after addition of the peptide. The length of the peptide when in the conformation shown in Figure 3.9 is approximately 4 nm which is not reflected in the measured hydrodynamic diameter of the peptide coated AuNPs. This may indicate that the peptide binds to the AuNPs along its length rather than through terminal residues. This would potentially allow the interaction of all four cysteine residues with the surface of the AuNPs.

3.2.5.3 Measurement of **CCALNNCCALNN** Binding to **Citrate-AuNPs**

In this case, only fitting of the UV-Vis absorption titration was used to find the binding constant of the peptide to AuNPs since it has been previously demonstrated to give K_a values comparable to those obtained by other methods. The binding constant, K_a, may also help to confirm which mode of binding the peptide uses since the strength of binding should be suggestive of the number of thiol groups binding to the surface of the AuNPs, however, the interaction of other amino acids with gold, through amines for example, cannot be discounted.[11]

System Examined	K_a/M^{-1}
Citrate-AuNPs + **CCALNNCCALNN**	$2.1 \times 10^4 \pm 9.6 \times 10^3$

Table 3.10 K_a calculated upon fitting the curve of change in SPR absorption maximum position of **Citrate-AuNPs** with titration of **CCALNNCCALNN**.

The fit of the binding curve has revealed a binding constant of around 10^4 M^{-1} for **CCALNNCCALNN** binding to **Citrate-AuNPs**. In order to draw any conclusions about the

strength of this binding event and the information it can reveal about the method of binding, it was decided pertinent to execute a comparison to CALNN and CCPGCC binding data.

3.2.6 Comparison of Peptide Binding to **Citrate-AuNPs**

The binding of CALNN, CCPGCC and **CCALNNCCALNN** to AuNPs has been analysed and can be compared on their measured K_a and their UV-Vis absorption titration curves.

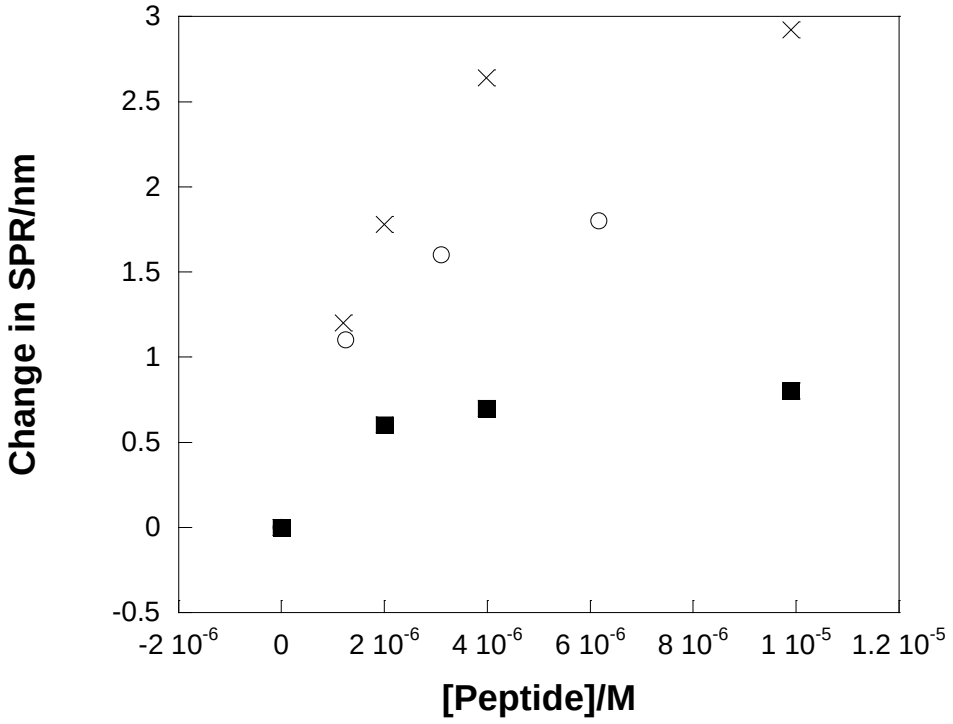

Figure 3.11 Change in SPR position of 3 nM **Citrate-AuNPs** with titration of solutions of 1 mM CCPGCC (×), 0.5 mM CALNN (○) and 1 mM **CCALNNCCALNN** (■).

Of the three peptides CCPGCC demonstrates the highest affinity for AuNPs with **CCALNCCALNN** displaying the lowest affinity; this is reflected in their respective titration curves, Figure 3.11, with CALNN producing the sharpest change in AuNP SPR and **CCALNNCCALNN** the smallest change. It is interesting that CALNN should have a higher

binding constant than **CCALNNCCALNN** because it has fewer thiol groups for binding to AuNPs, however, it must be the case that the structure of **CCALNNCCALNN** somehow prevents it from binding efficiently to the surface of AuNPs as opposed to CALNN which binds more strongly. Certainly, the binding constants measured are not simply related to the number of cysteine residues contained within each peptide sequence, therefore, the structure and conformation and the interaction between peptides on the surface of the AuNPs must also have an impact on their binding.[8, 30]

The difference in the number of binding sites calculated from ITC data for CALNN and CCPGCC is also reflected in their binding constants; CALNN occupies 6% of the surface of AuNPs, whereas CCPGCC occupies 47%, a difference of 41%. The binding constant of CCPGCC to AuNPs is around 41% greater than that found for CALNN.

Since the purpose of these experiments is to find a peptide capable of specifically binding AuNPs only CCPGCC and CALNN were taken forward into further experiments due to their higher affinity for AuNPs.

3.2.6.1 CALNN and CCPGCC Competition Experiments

In order to probe the binding behaviour of the two peptides on AuNPs further, a 0.5 mM solution of one peptide was titrated into a 3 nM solution of **Citrate-AuNPs** until the maximum change in SPR band position in the absorption spectrum was seen and then a 1 mM solution of the other peptide was titrated in to see whether a further shift in the SPR band was observed.

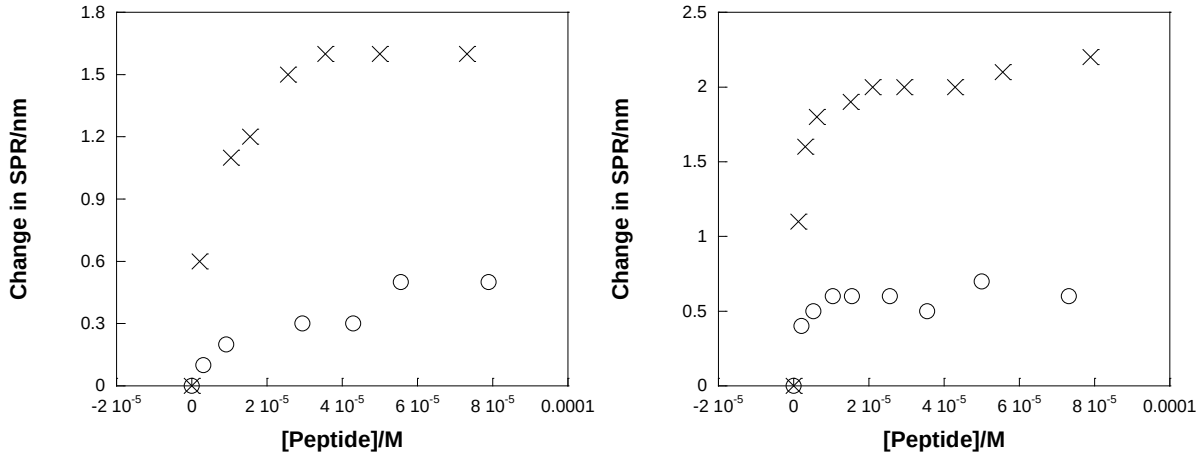

Figure 3.12 Change in SPR peak position when the first 0.5 mM peptide solution is added in microlitre aliquots to 3 nM **Citrate-AuNPs** and then subsequent change of SPR position when the second 1mM peptide solution is added in microlitre aliquots. Left: CCPGCC (○) added first then CALNN (×). Right: CALNN (×) added first then CCPGCC (○).

The results indicate that in each case the peptide added second is able to affect the SPR band of the AuNPs. Certainly in each case, the concentration of peptide bound to the surface of the AuNPs, as calulated from the number of binding sites revealed by ITC, is not comparable with the peptide added afterwards which is in great excess, possibly driving the reaction towards displacement at the surface. Previous experiments to find the binding constant of the two peptides on AuNPs have shown that CCPGCC has a higher affinity for AuNPs than CALNN, which means another hypothesis may be that CCPGCC is able to displace CALNN and in the case where CCPGCC is added first, it could bind through only two thiols leaving two free to futher interact with CALNN causing the subsequent SPR shift upon its addition. From these results it is difficult to confirm this hypothesis, therefore, a further study to elucidate the number of thiols used in binding to AuNPs was executed.

3.2.6.2 Sensing for Zn^{2+} and Ni^{2+} using **Peptide-AuNPs**

Solutions of **CALNN-AuNPs** and **CCPGCC-AuNPs** were prepared as previously described and the AuNPs collected as a pellet by centrifugation and redispersed in deionised water several times to ensure no unbound peptides were present in solution. To the AuNPs solutions of $ZnCl_2$ or $NiCl_2$ were added and the resulting change in the SPR peak measured by UV-Vis absorption spectroscopy.

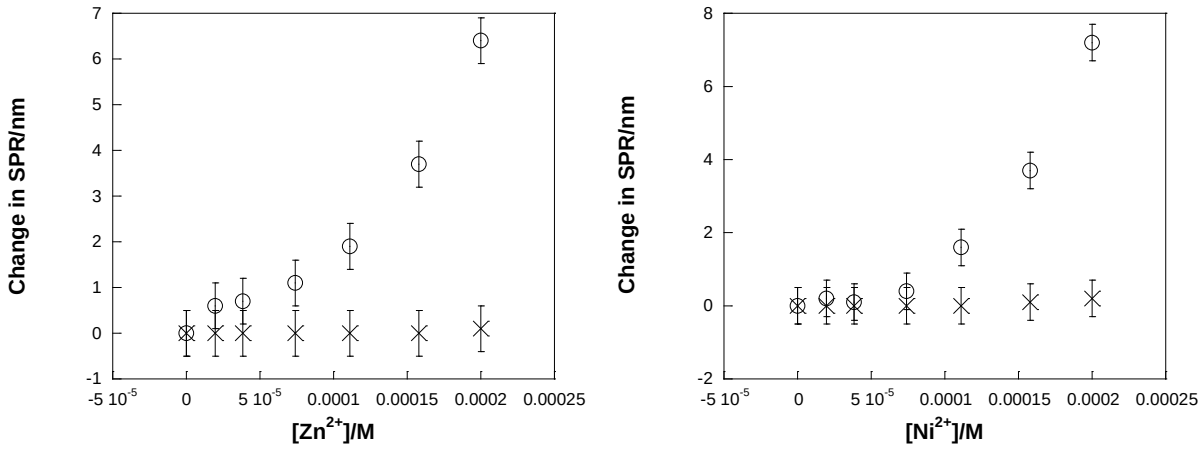

Figure 3.13 Change in SPR peak position of 41 pM **CCPGCC-AuNPs** (○) and 41 pM **CALNN-AuNPs** (×) with titration of 1 mM Zn^{2+} solution (left) or 1 mM Ni^{2+} solution (right).

The change in SPR peak position of the peptide-AuNPs indicates that the addition of a metal cation causes a change at the surface of **CCPGCC-AuNPs** but not **CALNN-AuNPs**. Since Ni^{2+} is a relatively soft cation and Zn^{2+} is a borderline cation it would be reasonable to suggest that they are bound by the sulphurs of CCPGCC, indicating that not all of the cysteine residues of CCPGCC are used in binding to the surface of AuNPs. CALNN does not display any indication of binding the metal cations which serves to act as a control since its only cysteine group should be occupied in binding to the surface of the AuNPs. It may also be suggested that other residues present in CALNN may interact with the metal cations, and as

such it is unexpected not to see an interaction, however, in naturally occurring metal binding proteins containing asparagine residues (N), the asparagine residue is never the residue responsible for coordinating the metal.[31]

Looking towards sensing applications, the results show that for **CCPGCC-AuNPs** there is a range where the SPR of the AuNPs does not change, after which the SPR changes linearly with increasing Zn^{2+} or Ni^{2+} concentration. In both cases it could be argued that **CCPGCC-AuNPs** could be used to sense for Zn^{2+} or Ni^{2+} over a linear range, however, this experiment does not confirm whether this behaviour is also demonstrated for other metals or the range of the linear response and as such if the applications of these AuNPs to sensing is to be explored further experiments are needed.

3.2.7 The Effect of CCPGCC on Luminescent AuNPs

CCPGCC was identified as the best candidate for specific binding to AuNPs, however, it has been examined in terms of its intereaction with **Citrate-AuNPs**. The application of the peptide to further work will require its interaction with luminescent AuNPs and as such its effect on the luminescence of these AuNPs was assessed.

3.2.7.1 Preparation of Luminescent AuNPs and Addition of CCPGCC

1 mM solutions of luminescent lanthanide species **EuL^{a}** and **EuL^{b}**, Figure 3.1, whose syntheses are described in Chapter 2, were titrated into solutions of 3 nM **Citrate-AuNPs** until a plateau was reached in the change of the SPR peak, as measured by UV-Vis absorption spectroscopy, to give **EuL^{a}-AuNPs** and **EuL^{b}-AuNPs** respectively. Following this a 1 mM solution of CCPGCC was added until a peptide concentration of 17 μM was reached and a

further shift in the SPR peak was measured indicating interaction of the peptide with the luminescent AuNPs. The AuNPs were then isolated as pellets by centrifugation before being redispersed in deionised water and the process repeated to remove any unbound species, or, indeed, any luminescent europium complexes that may have been displaced by the binding of the peptide to the AuNPs.

3.2.7.2 Luminescent Properties of **EuL-AuNPs** with CCPGCC

The luminescence emission properties of the luminescent AuNPs were measured before and after the addition of peptide.

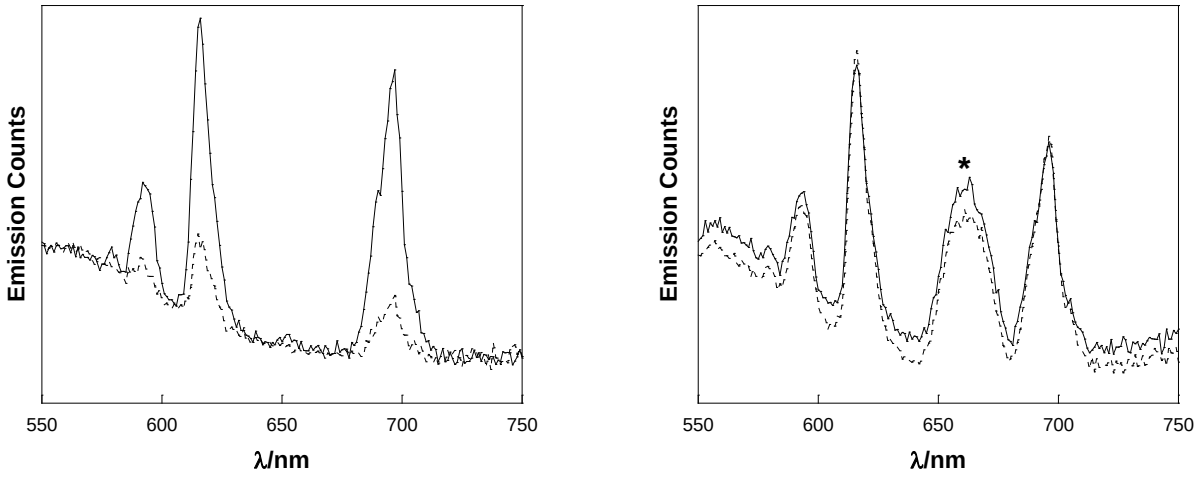

Figure 3.14 Emission spectra of **EuL^{a}-AuNPs**, λ_{ex} = 266 nm (left) and **EuL^{b}-AuNPs**, λ_{ex} = 330 nm (right) with (---) and without (—) addition of CCPGCC. Spectra corrected for PMT response and absorbance of comparable samples equal at λ_{ex} and λ_{em} (615 nm) respectively. * indicates scattering at double the excitation wavelength which is seen in the right hand spectra and not the left due to the difference in excitation wavelengths used for the complexes.

The emission spectrum of **EuL^{a}-AuNPs** after the addition of CCPGCC is reduced in intensity compared to that measured without peptide present. This may be indicative of displacement of **EuL^{a}** molecules from the surface of AuNPs by CCPGCC. In contrast to this, the emission

spectrum of **EuL^{b}-AuNPs** is largely unchanged before and after addition of CCPGCC. The luminescence lifetime of the observed emission was also measured and their corresponding spectra can be found in the appendix.

Sample	τ/μs
EuL^{a}-AuNPs	524 ± 52
EuL^{a}-AuNPs + CCPGCC	341 ± 34
EuL^{b}-AuNPs	550 ± 55
EuL^{b}-AuNPs + CCPGCC	548 ± 55

Table 3.11 Luminescence lifetime measurements of luminescent AuNPs in the presence and absence of CCPGCC. For all samples λ_{em} = 615 nm, **EuL^{a}-AuNPs** λ_{ex} = 266 nm, **EuL^{b}-AuNPs** λ_{ex} = 330 nm.

The luminescence lifetime of **EuL^{a}-AuNPs** decreases after addition of CCPGCC in comparison to the lifetime before its addition. This may suggest that the emission of the lanthanide complex is quenched by the peptide rather than the peptide displacing it from the AuNPs as was thought as a result of the emission spectra. This could be due to the large solvation sphere of the peptide, as indicated by the DLS data in Table 3.4, bringing a higher concentration of water molecules to the proximity of the europium centre. This is clearly not the case with **EuL^{b}-AuNPs** since the luminescence lifetime is not changed when CCPGCC is added much like the emission spectra, which could indicate that the slight difference in the structure of the complex prevents the peptide from binding as closely to **EuL^{b}** as it does for **EuL^{a}**. For this reason, and for the fact that **EuL^{b}-AuNPs** can be excited at a longer wavelength than **EuL^{a}-AuNPs** which is more applicable to biological studies, **EuL^{b}-AuNPs** will be taken forward for use as protein labels in cells in the next chapter.

3.3 Conclusions

The aim of this chapter, which was to identify a peptide sequence capable of specifically binding luminescent AuNPs within cells, has been achieved by measuring the binding affinity of three candidate peptides to AuNPs using a variety of techniques and comparing the results obtained for each peptide. It was found that the number of cysteine residues contained within the peptide sequence was not the deciding factor on the strength of binding to AuNPs as was predicted to be the case. Indeed, CCPGCC was found to have the highest binding constant when binding to AuNPs, but it was revealed that not all of its cysteine residues are occupied in binding to AuNPs since the peptide was able to bind to free transition metal cations. Nevertheless, CCPGCC was selected as the optimum AuNP binding peptide and it was shown not to affect the luminescence properties of luminescent **EuL^{b}-AuNPs** and as such will be taken forward with these AuNPs for further experiments in the next chapter.

3.4 Experimental

3.4.1 General Considerations

Starting materials were obtained from Sigma Aldrich, Fluka, Fisher Scientific or AGTC Bioproducts and used without further purification.

MALDI-TOF mass spectrometry was carried out on a Waters MALDI Micro MX mass spectrometer, using α-cyano-4-hydroxycinnamic acid matrix.

HPLC was carried out on a Dionex summit system, using a Summit P580 quarternary low pressure gradient pump with built-in vacuum degasser. The detector was a Summit UVD 170s UV-Vis multi-channel detector with a preparative flow cell. The column used was the Phenomenex Luna 10 μm particle size C18 semi-preparative column. All solvents used were HPLC grade solvents, degassed prior to use.

UV-Vis absorption spectra were carried out on Varian Cary 50 or Varian Cary 5000 spectrometers. UV-Vis spectra were taken using 1 cm path length quartz cuvettes.

All ITC measurements were carried out using a MicroCal VP-ITC system at 25 ºC. Origin 7 MicroCal Software was used to record and analyse the data.

SPR spectroscopy measurements were achieved using a Reichert Life Sciences SR7000DC SPR spectrometer equipped with a SR7300 semi-automatic valve.

3.4.2 Chemical Syntheses

3.4.2.1 Synthesis of Citrate-Stabilised AuNPs: **Citrate-AuNPs**

All glassware was cleaned in aqua regia ($HCl:HNO_3$, 3:1), rinsed with deionised water and dried in a hot oven prior to use. Hydrogen tetrachloroaurate (0.08 g, 0.2 mmol) was dissolved in water (200 mL), stirred vigorously and heated under reflux until a rolling boil was reached. To the boiling solution sodium citrate (0.22 g, 0.8 mmol) in water (20 mL) was added which turned the solution from colourless to dark red. The solution was allowed to boil for a further 10 min before being removed from the heat and stirred for a further 15 min. The solution was then left to cool to room temperature. UV-Vis (H_2O) λ_{max} nm: 520.

3.4.2.2 Synthesis of **CCALNNCCALNN**

The peptide was synthesised using a solid phase technique on a 0.1 mmol scale, with a five-fold excess of each amino acid used. Liberty 1 CEM Microwave Peptide Synthesizer was used for the synthesis therefore the solutions needed were made up in advance and loaded into the synthesizer. The amino acid solutions were made as detailed in the following table:

Compound	Molecular Mass/g mol^{-1}	Mass Used/g	Moles Used/mmol	Dissolved in/mL
Fmoc-Asn(Trt)-OH	354.4	0.95	2.68	8 DMF
Fmoc-Leu-OH	353.4	0.42	1.19	6 DMF
Fmoc-Ala-OH	311.3	0.37	1.19	6 DMF
Fmoc-Cys(Trt)-OH	585.7	1.29	2.20	11 DMF

Deprotection solution was made by dissolving 1-hydroxybenzotriazole (3.8 g, 24.8 mmol) in a solution of 20% piperidine in DMF (250 mL). The activator solution was made by

dissolving HBTU (8.5 g, 22.4 mmol) in DMF (50 mL). Activator base solution was made by adding diisopropylethylamine (17.5 mL, 100 mmol) to *N*-methylpyrrolidone to make a solution with a total volume of 50 mL. DMF was used for washing the resin in between synthesis steps. Fmoc-Asn(Trt)-Wang resin (0.208 g) was added to the microwave reaction vessel and the program allowed to run to synthesise the peptide. The synthesis program consisted of single coupling reactions with cysteine couplings at 50 °C and the remaining amino acids at 75 °C. When the peptide was complete the final amino acid was deprotected, but no capping was carried out. The resin was removed from the synthesizer and rinsed with dichloromethane (5 x 7 mL) followed by diethyl ether and left to dry. Cleavage of the peptide from the resin support was achieved by stirring at room temperature for 2 h in a cleavage cocktail comprised of trifluoroacetic acid (9 mL), thioanisole (0.5 mL), 1,2-ethanedithiol (0.3 mL) and anisole (0.2 mL). The resin was then filtered and washed with a few millilitres of trifluoroacetic acid and the filtrate was reduced in volume under nitrogen gas. The peptide solution was added drop-wise to a 10-fold excess of cold diethyl ether upon which the peptide precipitated from solution and was collected via filtration to give an off-white solid. The crude product was then desalted by passing it through a Sephadex G-10 size exclusion column using 20% acetic acid. Any potential disulfide bonds were reduced by dissolving the peptide in a degassed aqueous solution of N-ethylmorpholine (10 mL, 0.05 M) and adding dithiothreitol (0.077 g, 0.5 mmol) and stirring under nitrogen at room temperature for 4 h. The solution was then taken to pH 3 using 10% trifluoroacetic acid solution and the solvent removed *in vacuo* to give an orange oil. The oil was dissolved in degassed water and purified by HPLC using a semi-preparative C-18 reversed phase column and an isocratic method of 20% acetonitrile and 80% water for 30 min at 3 mL/minute. Solvents contained 0.05% trifluoroacetic acid. The peptide was found to elute from the column after 8 min and was

collected and lyophilised. MS (MALDI-TOF$^+$): *m*/*z* 1278 $\{M + Na\}^+$. UV-Vis (H_2O) λ_{max} nm (log ε): 205 (3.6), 280 (2.1).

3.4.3 CALNN and CCPGCC Peptides

CALNN and CCPGCC were both purchased in 95% purity from Alta Biosciences, University of Birmingham UK and were used without any further purification.

3.4.4 Luminescence Spectroscopy

Luminescence experiments were carried out using an Edinburgh Instruments fluorescence system, FLSPM920. The illumination source uses a 450 W xenon arc lamp. The detection system used was a Hamamatsu R928. The emission monochromator is fitted with two interchangeable gratings blazed at 500 nm and 1200 nm. Luminescence studies were carried out using quartz cuvettes with four transparent polished faces and 1 x 1 cm path length. F900 spectrometer analysis software was used to record the data.

3.4.4.1 Europium Emission

Luminescence spectra of **EuL^a** containing samples were gained by excitation of the complex at 266 nm, detection of emission in the range 550-750 nm and employing a 550 nm long pass filter. Luminescence spectra of **EuL^b** containing samples were gained by excitation of the complex at 330 nm, detection of emission in the range 550-750 nm and employing a 550 nm long pass filter. A 1 s dwell time and a 1 nm step size were employed with excitation and emission slits set to 10 nm and 5 nm respectively. Emission scans were repeated three times to produce a cumulative emission spectrum.

3.4.4.2 Luminescence Lifetime Measurements

Luminescence lifetimes were measured using the spectrophotometer described in section 3.4.4 with a 100 W μF920H lamp illumination source. In the case of **EuL^{a}** containing samples excitation was at 266 nm, whereas for samples containing **EuL^{b}** excitation was at 330 nm. Emission was detected at 615 nm and a 550 nm long pass filter used. Excitation and emission slits were set to 10 nm. Emission was detected over an 8 ms range for 300 s with a 0.1 ms lamp trigger delay.

3.4.5 DLS and ζ-potential Measurements

Measurements were obtained using a Beckman-Coulter Delsa Nano C particle analyser and data was recorded and analysed using Delsa Nano software.

3.4.5.1 DLS Measurements

Samples were analysed using quartz cuvettes with four transparent polished faces and 1 x 1 cm path length. Measurements were taken over 70 accumulations through a 50 μm pinhole. Data were analysed using a CONTIN method.

3.4.5.2 ζ-potential Measurements

Samples were analysed using a quartz flow cell purchased form Beckman-Coulter. Measurements were taken over 10 repeats at a 15º scattering angle through a 50 μm pinhole. The Smoluchowski conversion equation was used to analyse the data.

3.4.6 Fitting of UV-Vis and SPR Titration Data

$$y = \frac{B_{max}}{2[x]} 0.5 \left(\left([h] + [x] + \frac{1}{K_a} \right) - \sqrt{\left([h] + [x] + \frac{1}{K_a} \right)^2 - 4[x][h]} \right)$$

This equation, where $[x]$ is the concentration of the added species, $[h]$ is the concentration of the host species and B_{max} is the point where maximum change of the observed parameter is measured, can be used to find the binding constant of a system when the concentration of both species is known and there is a measured change upon binding. The equation was converted to a format accepted by the graphing software KaleidaGraph and this software used to fit the data curves. The equation was derived by a previous member of the Pikramenou group.[32]

3.5 References

1. M. J. Kogan, I. Olmedo, L. Hosta, A. R. Guerrero, L. J. Cruz and F. Albericio, *Nanomed.*, 2007, **2**, 287-306.

2. J. M. de la Fuente and C. C. Berry, *Bioconjug. Chem.*, 2005, **16**, 1176-1180.

3. B. Kang, M. A. Mackey and M. A. El-Sayed, *J. Am. Chem. Soc.*, 2010, **132**, 1517-1519.

4. E. Oh, J. B. Delehanty, K. E. Sapsford, K. Susumu, R. Goswami, J. B. Blanco-Canosa, P. E. Dawson, J. Granek, M. Shoff, Q. Zhang, P. L. Goering, A. Huston and I. L. Medintz, *ACS Nano*, 2011, **5**, 6434-6448.

5. L. L. Sun, D. J. Liu and Z. X. Wang, *Langmuir*, 2008, **24**, 10293-10297.

6. A. G. Tkachenko, H. Xie, Y. L. Liu, D. Coleman, J. Ryan, W. R. Glomm, M. K. Shipton, S. Franzen and D. L. Feldheim, *Bioconjug. Chem.*, 2004, **15**, 482-490.

7. Ž. Krpetić, P. Nativo, F. Porta and M. Brust, *Bioconjug. Chem.*, 2009, **20**, 619-624.

8. J. M. Lee, H. K. Park, Y. Jung, J. K. Kim, S. O. Jung and B. H. Chung, *Anal. Chem.*, 2007, **79**, 2680-2687.

9. R. Lévy, N. T. K. Thanh, R. C. Doty, I. Hussain, R. J. Nichols, D. J. Schiffrin, M. Brust and D. G. Fernig, *J. Am. Chem. Soc.*, 2004, **126**, 10076-10084.

10. J. M. Slocik and R. R. Naik, *Chem. Soc. Rev.*, 2010, **39**, 3454-3463.

11. A. Vallee, V. Humblot and C. M. Pradier, *Acc. Chem. Res.*, 2010, **43**, 1297-1306.

12. C. Tamerler, M. Duman, E. E. Oren, M. Gungormus, X. R. Xiong, T. Kacar, B. A. Parviz and M. Sarikaya, *Small*, 2006, **2**, 1372-1378.

13. J. M. Slocik, M. O. Stone and R. R. Naik, *Small*, 2005, **1**, 1048-1052.

14. X. H. Yan, J. Blacklock, J. B. Li and H. Mohwald, *ACS Nano*, 2012, **6**, 111-117.

15. R. Lévy, *Chembiochem*, 2006, **7**, 1141-1145.

16. P. Nativo, I. A. Prior and M. Brust, *ACS Nano*, 2008, **2**, 1639-1644.

17. A. C. Savage and Z. Pikramenou, *Chem. Commun.*, 2011, **47**, 6431-6433.

18. S. R. Adams, R. E. Campbell, L. A. Gross, B. R. Martin, G. K. Walkup, Y. Yao, J. Llopis and R. Y. Tsien, *J. Am. Chem. Soc.*, 2002, **124**, 6063-6076.

19. B. A. Griffin, S. R. Adams and R. Y. Tsien, *Science*, 1998, **281**, 269-272.

20. A. Davies, D. J. Lewis, S. P. Watson, S. G. Thomas and Z. Pikramenou, *Proc. Natl. Acad. Sci. U. S. A.*, 2012, **109**, 1862-1867.

21. Y. Fillon, A. Verma, P. Ghosh, D. Ernenwein, V. M. Rotello and J. Chmielewski, *J. Am. Chem. Soc.*, 2007, **129**, 6676-6677.

22. S. C. Wagner, M. Roskamp, M. Pallerla, R. R. Araghi, S. Schlecht and B. Koksch, *Small*, 2010, **6**, 1321-1328.

23. K. C. Grabar, R. G. Freeman, M. B. Hommer and M. J. Natan, *Anal. Chem.*, 1995, **67**, 735-743.

24. A. Hofmann, in *Principles and Techniques of Biochemistry and Molecular Biology*, eds. K. Wilson and J. Walker, Cambridge University Press, New York; Cambridge, 2010, pp. 477-519.

25. D. Creed, *Photochem. Photobiol.*, 1984, **39**, 577-583.

26. J. Cortez, E. Vorobieva, D. Gralheira, I. Osório, L. Soares, N. Vale, E. Pereira, P. Gomes and R. Franco, *J. Nanopart. Res.*, 2010, **13**, 1101-1113.

27. D. J. Lewis, T. M. Day, J. V. MacPherson and Z. Pikramenou, *Chem. Commun.*, 2006, **42**, 1433-1435.

28. F. Madani, J. Lind, P. Damberg, S. R. Adams, R. Y. Tsien and A. O. Gräslund, *J. Am. Chem. Soc.*, 2009, **131**, 4613-4615.

29. A. M. W. Reed and S. J. Metallo, *Langmuir*, 2010, **26**, 18945-18950.

30. M. Hnilova, E. E. Oren, U. O. S. Seker, B. R. Wilson, S. Collino, J. S. Evans, C. Tamerler and M. Sarikaya, *Langmuir*, 2008, **24**, 12440-12445.

31. A. Passerini, M. Punta, A. Ceroni, B. Rost and P. Frasconi, *Proteins: Struct. Funct. Bioinf.*, 2006, **65**, 305-316.

32. J. M. Haider, thesis, University of Edinburgh, 2001.

4. Luminescent Nanoparticles for Protein Labelling in Cells

4.1 Introduction

4.1.1 Luminescent Nanoparticles and Proteins

As the interest in the use of nanoparticles increases, so does the research into the interaction of nanoparticles with biological molecules such as proteins. Studies focussing on the effect of protein interaction with nanoparticles on the conformation of the protein are numerous, as are the studies into the binding interactions that facilitate protein adsorption onto nanoparticle surfaces.[1-13] Unmodified nanoparticles have not been the only topic of research, with the effect of nanoparticle surface modification on protein adsorption also a key area of interest.[14-19] Nanoparticles offer a vehicle for the delivery of a large payload of luminescent material to a protein for imaging purposes and, where luminescent compounds are decorating the surface of the nanoparticles, they may also affect the interaction of the nanoparticle with the protein of interest. Indeed, when labelling a protein in order to study its role and function, it is important that the label employed, be it a nanoparticle or molecular probe, does not affect the conformation of the protein as this may in turn change or eliminate its inherent function.

4.1.2 Understanding Nanoparticle – Protein Interactions

It is well known that proteins adsorb onto the surface of nanoparticles to form a corona.[3, 6, 7, 20-24] The corona is divided into the hard corona, which contains proteins that are immediately surrounding the nanoparticles and dissociate over a large timescale of hours or days, if at all, and the soft corona which is the outer protein layer that changes comparatively quickly by exchange with other protein species from the surrounding environment. For example, a study investigating the interaction between α-synuclein, an amyloid protein, and AuNPs found that

the protein forms a hard corona through strong electrostatic interactions with the surface of the AuNPs, whereas further away from the surface the protein is involved in weaker protein-protein interactions and is in constant exchange with free protein.[12] In this case a combination of spectroscopic and light scattering techniques were used to examine the interaction between the protein and the AuNPs, however, a range of alternative and complimentary techniques are available to investigate the interaction of proteins with nanoparticles and the formation of the corona.

4.1.2.1 Examining Protein Adsorption Mechanisms

Several approaches are used to determine the affinity of proteins to nanoparticles and include ITC, SPR, DLS, affinity capillary electrophoresis, quartz crystal microbalance and fluorescence and UV-Vis spectroscopies.[2, 14, 20, 22] For example, Brewer *et al.* measured the interaction of BSA with 10 nm citrate-stabilised AuNPs using a quartz crystal microbalance and found the binding constant to be 1 μM^{-1} at pH 7.[2] It was proposed that the interaction is electrostatic in nature because, whilst both the AuNPs and BSA are negatively charged at pH 7, the lysine groups of BSA are positively charged allowing the interaction to take place, Scheme 4.1. Furthermore, the analysis was used to measure the amount of BSA adsorbed and, when taking into account the dimensions of the protein, it was calculated that BSA must bind to citrate coated AuNPs by an 'end-on' mechanism, i.e. the portion of BSA exposed to the AuNP surface is that of the shortest length allowing more BSA molecules to interact with the AuNP surface than if the BSA bound through its largest surface.

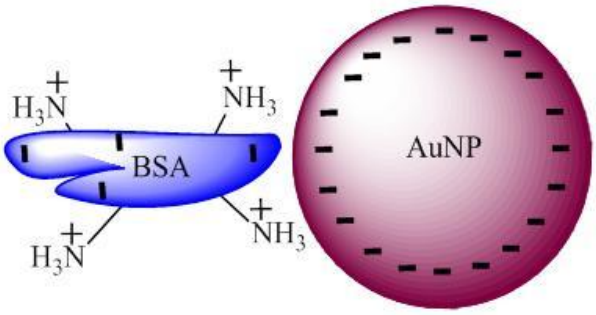

Scheme 4.1 Schematic representation of BSA and a AuNP at pH 7.

An alternative approach examined the formation of a protein corona around citrate-stabilised AuNPs that were exposed to cell culture medium containing 10% foetal bovine serum.[3] In this study UV-Vis spectroscopy and light scattering techniques were used to measure the formation of the protein corona over time. It was found that the protein corona was loosely attached to the AuNPs at first, but over time became irreversibly attached, suggesting an electrostatic mechanism as opposed to a covalent mechanism of interaction which would form a strong interaction more quickly.

A more recent study used alternative techniques to examine the interactions between BSA and citrate capped AuNPs and also suggests that it is of an electrostatic nature.[5] In this research light scattering was used to measure the diffusion time of the AuNPs in the absence and presence of protein and this was used to calculate the thickness of the protein corona because the increased dimensions of the AuNPs caused by adsorbed protein should affect their diffusion. AuNPs were exposed to BSA at concentrations equal to that of serum found in human blood. AuNPs of 51, 70 and 93 nm were used in the experiments and it was found that the size of the AuNPs did not impact on the adsorption of the protein which was found to form a monolayer across the surface of all of the AuNPs; this conclusion was based on the known dimensions of the protein and the measured 5 nm increase in the radii of the AuNPs of

all sizes. The magnitude of the negative ζ-potential of the citrate-stabilised AuNPs was reduced upon BSA adsorption which is suggested to be indicative of electrostatic interactions between the anionic citrate and cationic lysine side chains as opposed to displacement of the citrate by the one thiol group found on the surface of BSA. Interestingly, poly(ethylene glycol) coated AuNPs of 56 nm diameter did not display any protein adsorption which may confirm the electrostatic interaction between BSA and citrate ions since the poly(ethylene glycol) layer was attached using sulphur-gold chemistry which would have displaced the citrate ions and reduced the surface charge of the AuNPs, as confirmed by ζ-potential measurements, eliminating the opportunity for BSA to adsorb electrostatically. Having said this, the poly(ethylene glycol) layer may be up to 5 nm if fully extended and as such could sterically prevent BSA from binding to the surface of the AuNPs through its thiol group if this is indeed the mechanism through which it adsorbs.

Tsai and co-workers, however, conclude that BSA covalently binds to AuNPs through its one surface available thiol.[11] This conclusion is based upon the measured affinity of the protein for AuNPs of 10, 30 and 60 nm diameters which is suggested to be high and, therefore, indicative of covalent binding. DLS, infra-red spectroscopy and asymmetric-flow field flow fractionation were combined to assess the formation of a protein corona in the presence of BSA over a range of protein concentrations. The surface change of the AuNPs was plotted as a function of protein concentration and the data fit to find the equilibrium binding constant which, for the systems explored, was found to be in the range of 0.51 - 1.65 μM^{-1}.

4.1.2.2 The Effect of Nanoparticle Surface Chemistries on Protein Adsorption

Proteins may react in different ways to nanoparticles comprised of different materials which is not unexpected.[16] Proteins may also interact differently with nanoparticles of the same material, but with differing surface chemistries. For example, Boulos and co-workers examined the interaction of BSA with AuNPs of various sizes and surface charges.[14] Fluorescence quenching of the BSA when in the presence of the AuNPs was measured in addition to the employment of affinity capillary electrophoresis and it was found that, although BSA demonstrated a similar affinity for all AuNPs tested, there was a faster adsorption of BSA onto positively charged AuNPs in comparison to those with a negative surface charge. Zeng and colleagues also used capillary electrophoresis to measure the interaction of β-casein with AuNPs possessing two different surface chemistries.[19] The AuNPs were of identical shape and dimensions, however, one sample had 100% coating with carboxyl terminated polyhistidine, whereas the other was only 95% coated with this and the remaining 5% surface coverage was provided by polyhistidines with an amide blocking their terminal carboxyl. Both sets of AuNPs displayed very similar properties such as ζ-potential and mobility, however, the small change in surface chemistry meant that β-casein displayed an affinity that was five times greater in the case of the AuNPs with 95% carboxyl terminated polyhistidine coating than AuNPs with 100% coating by the same ligands. It was suggested that this small change in surface chemistry of the AuNPs reduced the repulsion between the carboxyl groups and the acidic protein leading to a stronger interaction.

Alternatively, DLS and TEM have been used to investigate the effect of the surface chemistry of AuNPs on the adsorption of serum proteins.[15] AuNPs of 39 nm diameter were either citrate-stabilised or coated with thioglycolic acid, cysteine or poly(ethylene glycol). The

serum proteins used in the experiments were BSA, transferrin and fibrinogen. The results show that the capping of AuNPs with poly(ethylene glycol) prevents protein adsorption, with longer chain lengths prohibiting BSA adsorption completely. Fibrinogen caused aggregation of AuNPs with all surface coatings except poly(ethylene glycol), whereas BSA and transferrin formed mono or bilayer coronas of 6 - 8 nm around citrate and thioglycolic acid capped AuNPs. The dissociation constants of BSA and transferrin with citrate and thioglycolic acid coated AuNPs were found to be in the range of 10^{-8} - 10^{-6} M.

4.1.2.3 Examining the Effect of Adsorption on Protein Conformation

Alternative methods are often used for the exploration of how interaction with nanoparticles affects the structure of the protein. These techniques include spectroscopic methods such as CD, fluorescence, Fourier transform infrared and NMR.[4, 7, 8, 10, 22, 25] For example, a recent study found that when polymer nanoparticles were exposed to serum containing cell growth media BSA was the most abundant protein in the resulting corona. Further investigations involving the titration of nanoparticles into a BSA solution showed, through CD measurements, that the structure of BSA was altered upon interaction with the nanoparticles.[25] A previous study into AuNPs of various sizes with a range of common blood proteins used CD analysis to find that, generally, the structure change in proteins is small and localised when interacting with AuNPs and that the effect on structure is greater with larger particles, however, it was concluded that it was not possible to find overall trends since the nature of the protein change was different for each protein examined.[7] Recently, the interaction of α-synuclein with 20 nm cationic poly(allylamine hydrochloride) coated AuNPs was examined through CD measurements.[13] The CD spectra of the protein revealed that, although the protein

is naturally unstructured, interaction with AuNPs was able to increase the β-sheet content and reduce the α-helix content of the protein.

Whilst there are a range of techniques available to assess nanoparticle-protein interactions, it is fair to conclude that the best analysis will encompass more than one technique. Indeed, much of the research found in literature does not rely on a single method, possibly because of the effect of nanoparticles within the analysis. Certainly, the presence of noble metal nanoparticles can affect spectroscopy data due to inner filter effects.

4.1.3 Nanoparticle Protein Corona and Cells

The formation of a protein corona around nanoparticles upon mixing with biological fluids alters the surface of the nanoparticle and how it appears to tissues, cells and receptors. A recent study investigated the loading of substances such as doxorubicin into agglomerates of lysozyme and citrate AuNPs and subsequent coating with serum albumin, Scheme 4.2.[26]

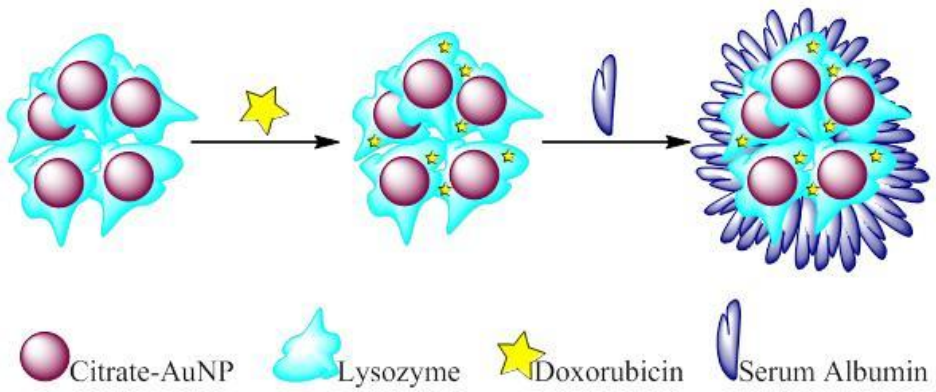

Scheme 4.2 Schematic representation of loading of doxorubicin into AuNP-lysozyme agglomerates and subsequent coating with serum albumin.

In this case the motivation for employing serum albumin was to stabilise the agglomerates and because it was suspected its presence may facilitate cell uptake. Indeed, BSA was shown to prevent alteration in the absorption spectra of the agglomerates after centrifugation and redispersion and the albumin coated agglomerates were taken up by human cervical cancer cells allowing the release and toxic effects of doxorubicin to ensue.[26]

Several other recent publications have also reported the effect of protein corona on the cellular uptake of nanoparticles. In comparison to the delivery of bare nanoparticles, where the presence of a protein corona was avoided by use of serum free cell growth media, it was found that the protein corona reduced uptake of unmodified silica and carboxylated polystyrene nanoparticles by human lung cancer cells by limiting their adhesion to the cell membrane.[27] In this case the nanoparticles were fluorescently labelled and as such the number of nanoparticles internalised per cell could be measured directly using flow cytometry. The adhesion of the nanoparticles to the cell membrane was examined by initial incubation of the cells with nanoparticles at 4 ºC, preventing active uptake of the nanoparticles, and subsequent washing of the cells and incubation with nanoparticle free media at 37 ºC, allowing internalisation of any nanoparticles adhered to the cell surface, before flow cytometry analysis. Similarly, the protein corona of the same types of nanoparticles was found to affect cellular uptake in addition to thrombocyte activation, haemolysis and endothelial cell death.[24] Investigating the protein corona of polymer nanoparticles, another study found that BSA was the most abundant protein in the corona when the nanoparticles were introduced to serum containing cell growth media. The identities of the proteins in the corona were revealed by their isolation and subsequent separation by sodium dodecyl sulphate polyacrylamide gel electrophoresis. CD analysis showed that BSA was denatured upon interaction with

nanoparticles and this led to decreased adhesion to the cell membrane and a reduction in the efficiency of uptake by human monocytic cells. In contrast, the protein corona coated nanoparticles were found to trigger receptor-mediated phagocytosis in differentiated macrophage-like cells, but in this case without affecting uptake efficiency. The cell adhesion and uptake of the nanoparticles was again investigated using flow cytometry as described for the previous study discussed.[25]

A recent study examined the biodistribution of AuNPs in mice after intra-venous administration.[28] Citrate-stabilised AuNPs and AuNPs coated with HSA or apolipoprotein E, which are both proteins found in the blood, were compared in terms of their accumulation in certain organs. In this case the AuNPs were radio-labelled with ^{198}Au and the proteins labelled with fluorescent dyes. Gamma spectroscopic radio analysis of tissue sections and fluorescence analysis of histology sections were used to quantify AuNP uptake. It was found that after 19 and 48 hours the accumulation of 15 nm citrate capped AuNPs was greater than 95% in the liver whereas only 52% of 15 nm AuNPs coated with HSA and 72% of 15 nm AuNPs coated with apolipoprotein E accumulated in the liver. In comparison to 15 nm citrate capped AuNPs, 15 nm protein conjugated AuNPs displayed increased accumulation in the spleen, with 18% of HSA coated AuNPs also accumulating in the lungs. Evidence of HSA coated 15 nm AuNPs was also found in brain tissue. The protein modification of 80 nm AuNPs, however, did not affect biodistribution in comparison to citrate-stabilised AuNPs of the same size. This demonstrates the use of protein modification of 15 nm AuNPs for organ targeting and increased exposure to the systemic system in mice which may be of use for therapeutic applications.

4.1.4 Nanoparticles for Cell and Protein Labelling

The possible negative effect of nanoparticles on protein structure may be seen as a disadvantage of their use; however, as discussed previously, nanoparticles can be used effectively to deliver therapies into cells, therefore presenting the opportunity for delivery of other species such as imaging agents. Research by the Pikramenou group has demonstrated the use of luminescent europium coated 13 nm AuNPs attached to a cell penetrating peptide for labelling of human platelets, which do not respond to alternative labelling methods such as microinjection or transfection. The platelets were imaged using luminescence microscopy which detected emission from the europium delivered using the AuNPs.[29] Further to this, human lung cancer cells were labelled with luminescent ruthenium coated AuNPs of 13 and 100 nm without any observed toxicity, and, in the latter case, the ruthenium luminescence showed the AuNPs were co-localised with chromatin, a complex of protein and DNA.[30]

In addition to general cellular labelling, nanoparticles have also been shown to be useful in the fluorescent labelling and detection of proteins. One example uses AuNPs coated with GFP for detection of an array of serum proteins *in vitro*.[31] In this case GFP fluorescence is quenched by its electrostatic interaction with AuNPs, but is observed after displacement of the GFP from the AuNPs by other proteins. A signature response to individual serum proteins is reported. Another study uses the absorption profile of 18 and 33 nm AuNPs to detect HSA.[32] AuNPs were coated with HSA and when a polyclonal antibody was introduced it became bound to the HSA coated AuNPs changing their absorption profile. The use of this system in human urine samples allows the free HSA contained within the sample to compete with the HSA coated AuNPs for binding to the antibody; thus, the absorption response can be used to calculate the concentration of HSA contained within the sample.

Whilst the discussed research is extremely useful for protein labelling and detection *in vitro*, nanoparticles have the potential to label proteins in cells which would allow the investigation of protein interactions and function within cells. Research combining cellular targeting of luminescent nanoparticles and protein labelling using fluorescent nanoparticles is needed.

4.1.5 Research Aims

The main objective of the research in this chapter is to explore the possibility of specific and selective labelling of a protein within cells using luminescent nanoparticles, Scheme 4.3. The luminescent nanoparticles consist of a gold core decorated with luminescent lanthanide complexes; the luminescence properties of the lanthanide complexes when in contact with proteins were established in Chapter 2. The labelling of a particular protein involves genetic engineering to induce the expression of the protein of interest with the addition of a nanoparticle binding motif, as designed in Chapter 3. Initial studies will demonstrate the interaction of nanoparticles with protein *in vitro* before proceeding to investigate the ability of the nanoparticles to label proteins in cells.

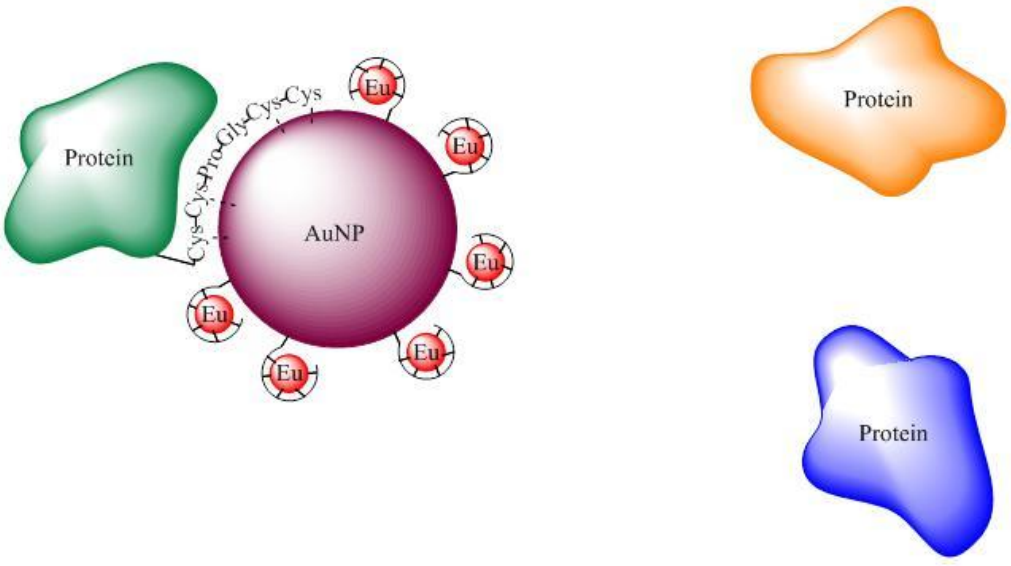

Scheme 4.3 Schematic representation of specific labelling of a recombinant protein with luminescent AuNPs.

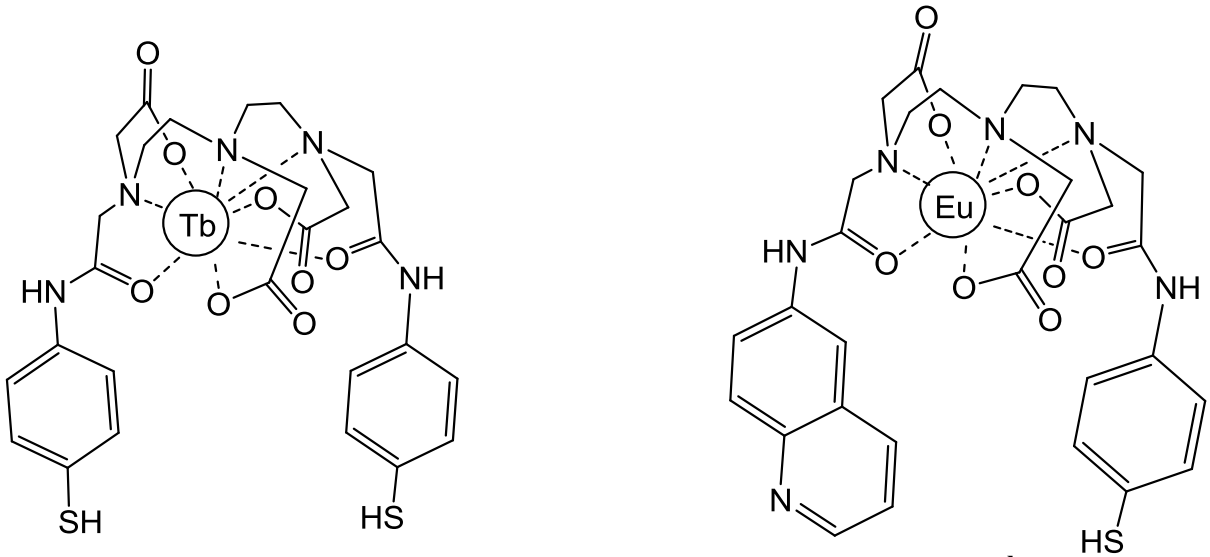

TbL[a] **EuL[b]**

Figure 4.1 Luminescent lanthanide complexes used in this chapter.

4.2 Results and Discussion

4.2.1 Citrate-Stabilised AuNPs and Protein

In order to investigate the interaction of proteins with citrate-stabilised AuNPs (**Citrate-AuNPs**) *in vitro*, BSA was chosen as a model protein. BSA is widely available and there is a wealth of comparable publications describing the interactions of BSA with nanoparticles of various materials, shapes and with a range of surface modifications. Unmodified citrate-AuNPs were first investigated for their interactions with BSA before continuing experiments with luminescent AuNPs in order to assess whether surface modification affects the interaction. The synthesis of **Citrate-AuNPs** can be found in Chapter 3.

4.2.1.1 Surface Coverage of **Citrate-AuNPs** by BSA

As previously discussed, the unique surface properties of AuNPs gives rise to a UV-Vis absorption band which changes as a result of surface modification or aggregation of the AuNPs. UV-Vis spectroscopy was, therefore, used to examine the interaction of BSA with the surface of AuNPs.

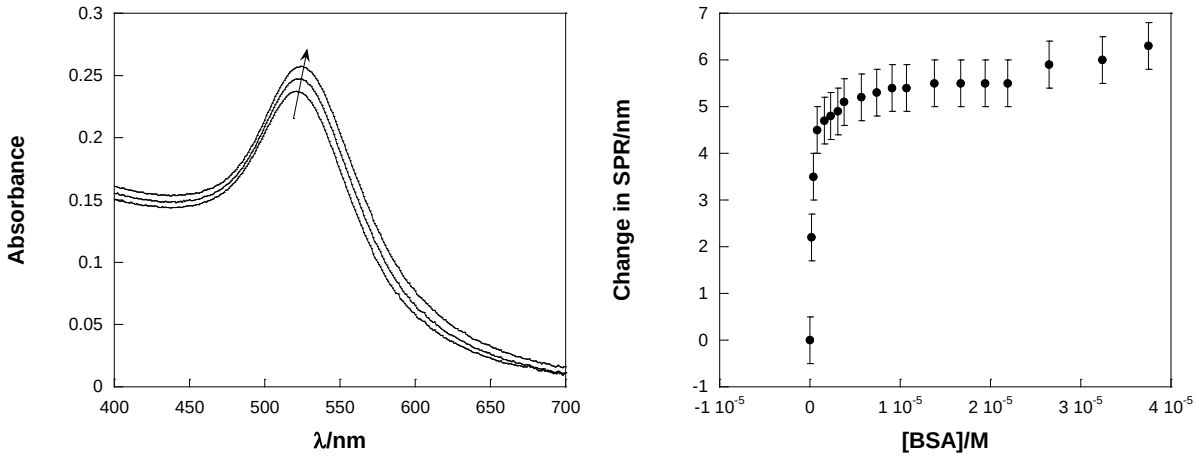

Figure 4.2 Left: Absorption spectra of 1 nM **Citrate-AuNPs** with microlitre additions of 0.1 mM BSA in water. Right: Change in SPR position of 1 nM **Citrate-AuNPs** with titration of BSA.

It is clear from the change in the SPR absorption peak of the **Citrate-AuNPs** that BSA is able to interact with the surface of the AuNPs. Although both the **Citrate-AuNPs** and BSA are negatively charged, the interaction is not unexpected because the surface of BSA has many lysine residues which, at pH 7, are positively charged and can, therefore, initiate an electrostatic interaction with the **Citrate-AuNPs**.[2, 3, 5] In order to elucidate more information about this interaction, BSA solutions of different concentrations were titrated into **Citrate-AuNPs**. The UV-Vis spectra were collected and analysed as seen in Figure 4.2 and the results are shown in Figure 4.3.

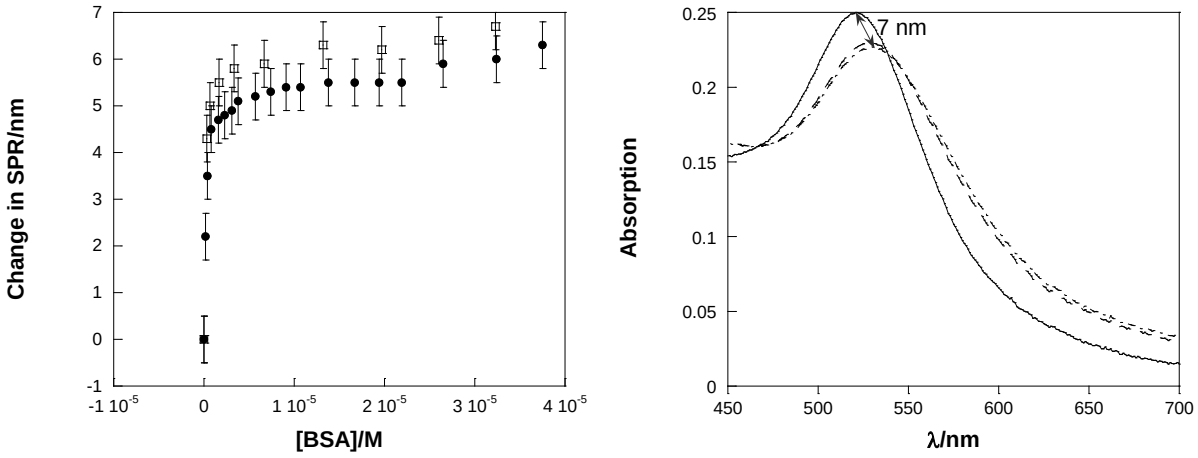

Figure 4.3 Left: Change in SPR position of 1 nM **Citrate-AuNPs** with titration of BSA in water at a concentration of 0.1 mM (●) and 0.8 mM (□). Right: Absorption spectra of 1 nM **Citrate-AuNPs** (—) with a single 1 mL addition of 0.8 mM BSA (- -) and 10 mins after protein addition (-·-).

The results in Figure 4.3 show that the change at the surface of the AuNPs is the same, within experimental error, when BSA of different concentrations is titrated into a solution of **Citrate-AuNPs**. A previous study has observed higher binding constants for initial BSA addition to citrate coated gold surfaces than for subsequent BSA binding; this is because the initial BSA added is able to spread on the surface and mask its negative charge from the

positive lysine residues of incoming BSA.[2] The same conclusion, however, cannot be drawn from the results here because of the lack of difference in surface modification of the AuNPs between the different concentrations of BSA added. It may be the case that at both concentrations used, the initial protein additions are able to coat the surface of the AuNPs and prevent the adsorption of subsequently added protein. The addition of 0.8 mM BSA in a single 1 mL addition, rather than through titrations of microlitre quantities, resulted in the same shift in the SPR of the AuNPs as seen for the titrations. This indicates that within the concentration range used here the adsorption of BSA onto the surface of AuNPs does not differ depending on the ratio of BSA to AuNPs since at the beginning of the titrations there was much less BSA present and yet this did not affect the attainment of the ~7 nm shift in SPR position. The absorption spectra on the right of Figure 4.3 also demonstrates the stability of BSA coated AuNPs because their absorption profile does not change with time.

The interaction of BSA with AuNPs can also be investigated by examining the fluorescence of the protein.

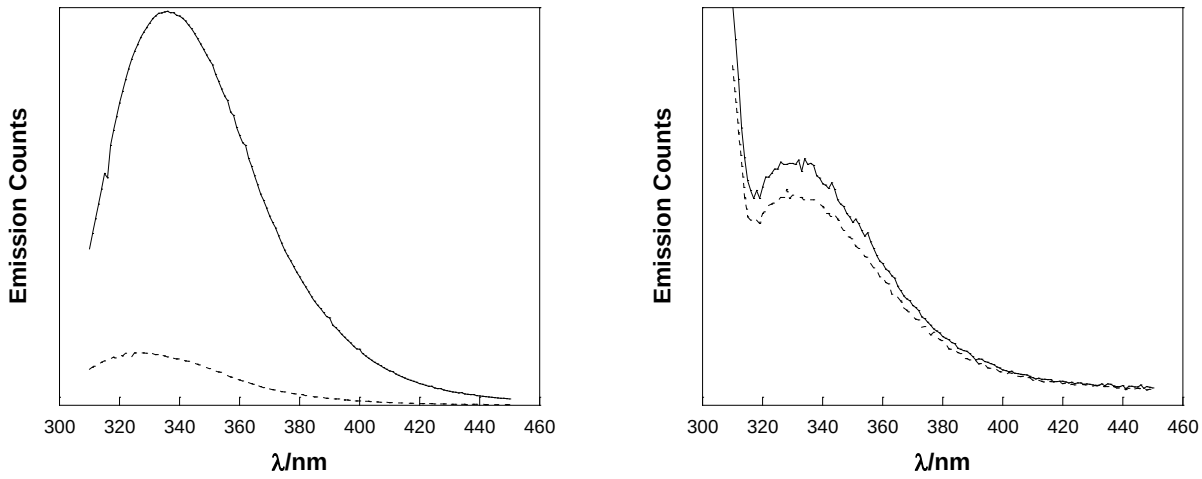

Figure 4.4 Left: Emission spectra of 2 μM BSA in water in the absence (—) and presence of 1 nM **Citrate-AuNPs** (---), λ_{ex} = 290 nm. Right: Emission spectra of 0.3 μM **TbL^{a}-BSA** in water in the absence (—) and presence of 0.2 nM **Citrate-AuNPs** (---), λ_{ex} = 279 nm. All spectra corrected for PMT response.

BSA contains two tryptophan residues that give a fluorescence peak at ~340 nm when excited in the range 250-300 nm. It has previously been demonstrated that adsorption of BSA onto the surface of noble metal nanoparticles results in quenching of the fluorescence by the metal surface. Quenching of the fluorescence form BSA can, therefore, indicate adsorption of the protein onto the nanoparticles.[7, 9, 14] In the case of native BSA, the emission spectra shown in Figure 4.4 show a clear quenching of protein based fluorescence indicating adsorption onto the surface of **Citrate-AuNPs** and confirming the interaction seen in the UV-Vis results. It is interesting to compare this to the change in fluorescence seen for lanthanide labelled BSA, **TbL^{a}-BSA** which is synthesised and characterised in Chapter 2, because the quenching effect of the **Citrate-AuNPs** on the protein fluorescence is much less pronounced. In both samples the ratio of protein to AuNPs is roughly equal which means the difference in quenching between the two proteins must be due to the modification of the protein with the lanthanide complex. It could be said that the process of labelling BSA with the lanthanide complex has affected its conformation and, therefore, its ability to adsorb onto the AuNPs, but it may also be the case that the lanthanide label, which also absorbs in the same range as BSA, may be absorbing some of the excitation light which means that the fluorescence of BSA is not as intense as would be expected even before the addition of AuNPs. Certainly, in both cases **Citrate-AuNPs** are able to act as an inner filter by increasing the absorption of the sample and scattering light. In addition to indicating the interaction between BSA and AuNPs, the fluorescence quenching may arise from a change in the environment of the tryptophan residues which would occur if the protein had changed conformation when adsorbing onto **Citrate-AuNPs**. In order to confirm whether a change in protein conformation has occurred a further technique is required.

4.2.1.2 Effect of **Citrate-AuNPs** on Protein Conformation

CD analysis was used to investigate the change in the conformation of BSA in solution when **Citrate-AuNPs** are titrated into it.

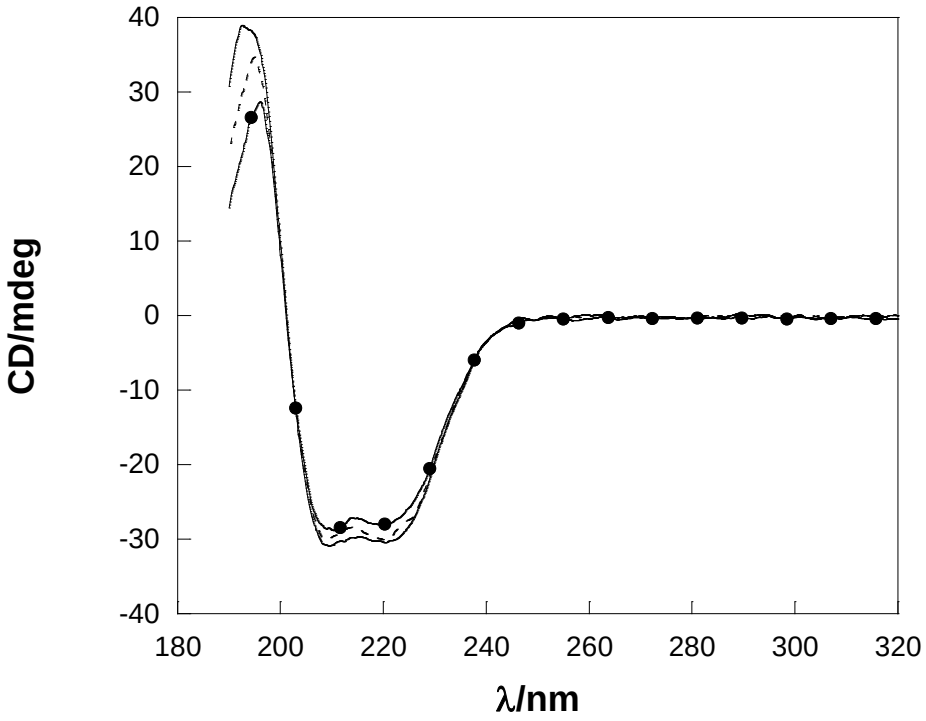

Figure 4.5 CD spectra of 0.1 μM BSA (—), 0.1 μM BSA + 31 pM **Citrate-AuNPs** (---) and 0.1 μM BSA + 124 pM **Citrate-AuNPs** (-●-). All samples in water.

The concentration of BSA required to obtain a good CD profile is much lower than the concentration of BSA used in the UV-Vis absorption titrations, therefore, the concentration of **Citrate-AuNPs** used was also lower. In this experiment the ratio of BSA to AuNPs is much lower than used for the UV-Vis titrations, which would allow the BSA to spread across the surface of the AuNPs if, indeed, that is the mechanism of the interaction. The negative ellipticity of BSA at 209 and 220 nm is indicative of its α-helical content and shows a small decrease as higher amounts of **Citrate-AuNPs** are added. The small decrease in ellipticity

observed does not indicate any spreading or denaturing of BSA on the surface of the AuNPs, but a small local change in the structure of the protein. This is in agreement with previous studies of serum albumins on AuNPs of various sizes and in a range of concentration ratios.[4, 7, 8] This confirms that the interaction of BSA with **Citrate-AuNPs** does not alter its conformation significantly. Since this indicates that BSA does not spread across the surface of AuNPs it also confirms the suggestion that the small differences in the SPR shift of the AuNPs observed in the UV-Vis titration experiments when varying concentrations of BSA are present, Figure 4.3, are not caused by BSA adsorbing by spreading across the surface of the AuNPs in one case and tightly packing on the surface without spreading in another, but instead can be attributed to experimental error since the SPR changes in each case are within the experimental error of ± 0.5 nm.

4.2.2 Luminescent AuNPs and Protein

AuNPs coated with luminescent lanthanide complexes were chosen as imaging agents for protein labelling. The interaction of protein with lanthanide coated AuNPs was, therefore, investigated in order to assess the effect of the interaction on both the luminescence properties of the nanoparticles and the structure of the protein. It will be interesting to compare the effect on the protein to those observed with **Citrate-AuNPs** because any differences will be caused by the modification of the surface of the AuNPs. BSA was again used as a model protein. During the course of this work Gunnlaugsson and colleagues have published an investigation into the binding of BSA to AuNPs coated with a europium complex.[33] In this case the europium was chelated by a DOTA type ligand and attached to the surface of AuNPs via an alkyl thiol group. The complex was not luminescent, but was able to interact with a β-diketonate antenna upon which europium luminescence was observed. Interaction of the

luminescent AuNPs with BSA caused quenching of the europium luminescence, thus presenting the potential of the system as a sensor for BSA. Subsequent introduction of ibuprofen, which binds to site II of BSA, resulted in a recovery of europium emission leading to a further possibility of the system acting as a sensor for molecules that bind to site II of BSA when BSA is present.[33]

4.2.2.1 Surface Coverage of **TbL^{a}-AuNPs** by BSA

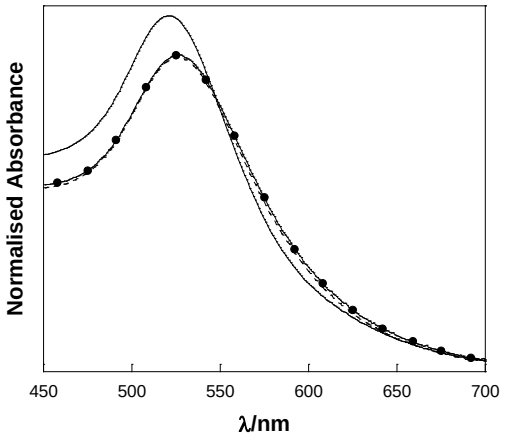

Figure 4.6 Absorption spectra of **Citrate-AuNPs** (—), **TbL^{a}-AuNPs** (---) and **TbL^{a}-AuNPs** + BSA (-●-).

Sample	SPR Band Position/nm[a]
Citrate-AuNPs	520
TbL^{a}-AuNPs	526
TbL^{a}-AuNPs + BSA	526

Table 4.1 λ_{max} of SPR band of 13 nm AuNPs with different surface modifications. [a] ± 0.5 nm

After the addition of **TbL^{a}** to the AuNPs the sample was passed through a Sephadex G-15 size exclusion column to remove any unbound lanthanide complex before BSA was added. It is apparent that the surface environment of the **Citrate-AuNPs** is modified upon addition of **TbL^{a}** but that no further change in at the surface is detected after addition of BSA which leads to the assumption that BSA does not interact with **TbL^{a}-AuNPs**.

The interaction of BSA with partially coated **TbL^{a}-AuNPs** was also assessed by UV-Vis spectroscopy.

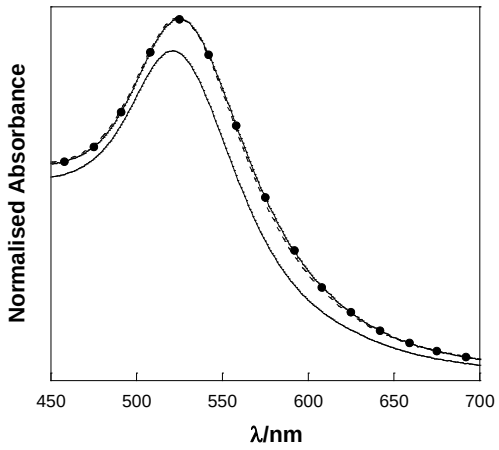

Figure 4.7 Absorption spectra of **Citrate-AuNPs** (—), **pTbL^{a}-AuNPs** (---) and **pTbL^{a}-AuNPs** + BSA (-●-).

Sample	SPR Band Position/nm[a]
Citrate-AuNPs	520
pTbL^{a}-AuNPs	523
pTbL^{a}-AuNPs + BSA	523

Table 4.2 λ_{max} of SPR band of 13 nm AuNPs with different surface modifications. [a] ± 0.5 nm

The shift in the SPR band of **Citrate-AuNPs** after addition of **TbL^{a}** is approximately half of the maximum shift that can be achieved when adding this complex to 13 nm **Citrate-AuNPs**, as seen previously, indicating that the surface of the AuNPs is not fully coated by the lanthanide complex.[34] The partially coated AuNPs are denoted as **pTbL^{a}-AuNPs**. The AuNPs were then passed through a Sephadex G-15 size exclusion column to remove any unbound **TbL^{a}**, after which the SPR position was unchanged. Subsequent addition of BSA, however, does not have a further effect of the position of the SPR band of the AuNPs, which may mean that the protein is not able to interact with the surface of the AuNPs when their surface is even partially coated by **TbL^{a}**. The AuNPs with each surface coating were analysed by measuring their ζ-potentials.

Sample	ζ-potential/mV
Citrate-AuNPs	-33 ± 0.5
BSA-AuNPs	-44 ± 0.2
pTbL^{a}-AuNPs	-25 ± 2.0
pTbL^{a}-AuNPs + BSA	-16 ± 0.7

Table 4.3 ζ-potential measurements of 13 nm AuNPs with various surface modifications.

The ζ-potential measurements reveal that **Citrate-AuNPs** have a negative surface charge which would be expected due to the presence of the anionic citrate at their surface. The magnitude of the negative charge is sufficient to stabilise the AuNPs because of their repulsion of one another preventing aggregation. After addition of BSA to **Citrate-AuNPs**, the magnitude of the negative charge is increased which, may be expected due to the overall negative charge of the protein, however, this does not concur with previous reports that found that the negative value obtained for citrate-stabilised AuNPs was slightly reduced after addition of BSA.[2, 5] When **TbL^{a}** is added to **Citrate-AuNPs** the magnitude of the negative surface charge is reduced which is due to the displacement of anionic citrate from the surface of the AuNPs by neutral **TbL^{a}**. The most interesting result, however, is the ζ-potential measurement of **pTbL^{a}-AuNPs** after addition of BSA. In this case the negative surface charge of the AuNPs is further reduced to the point where the AuNPs may become unstable and susceptible to aggregation. This result is somewhat counterintuitive because, firstly, the absorption results show no change to the surface environment of the AuNPs which leads to the assumption of no BSA interaction, which would mean no change in the ζ-potential, and secondly, if there is an interaction BSA is negatively charged and so should increase the surface charge of the AuNPs as seen with fully coated BSA-AuNPs. This may be because the interaction of BSA with **pTbL^{a}-AuNPs** is weak and that the displacement of the citrate

anions by **TbL^{a}** has reduced the interaction of the AuNPs with the cationic surface groups of BSA, allowing these to present towards the solution, reducing the negativity of the ζ-potential of the **pTbL^{a}-AuNPs**.

The effect of the interaction between BSA and **pTbL^{a}-AuNPs** was also probed by measuring the fluorescence of BSA.

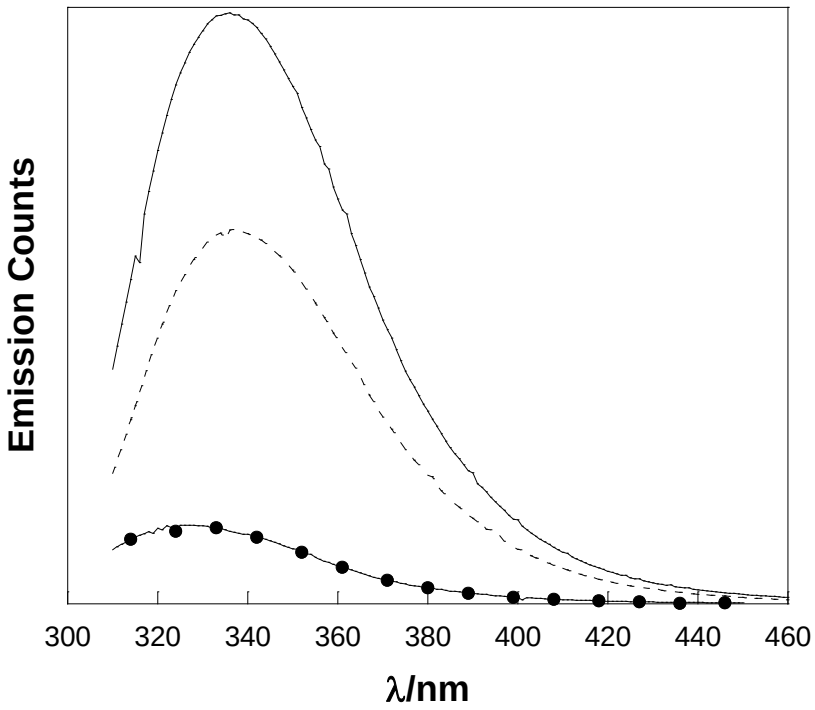

Figure 4.8 Emission spectra of 2 μM BSA in water in the absence of any AuNPs (—), in the presence of 1 nM **pTbL^{a}-AuNPs** (---), and in the presence of 1 nM **Citrate-AuNPs** (-●-). λ_{ex} = 290 nm. All spectra corrected for PMT response.

The fluorescence of BSA is quenched upon interaction with **pTbL^{a}-AuNPs**, indicating that some adsorption onto the AuNPs has taken place. The quenching effect of **Citrate-AuNPs**, however, is far greater than that of **pTbL^{a}-AuNPs** which may suggest that the interaction between BSA and **pTbL^{a}-AuNPs** is not as strong as that between BSA and **Citrate-AuNPs**.

This may explain why the UV-Vis absorption experiments were able to characterise the interaction between BSA and **Citrate-AuNPs** well, but not that of BSA and **pTbL^{a}-AuNPs**.

4.2.2.2 Effect of Luminescent AuNPs on Protein Conformation

CD measurements were used to assess the effect of BSA conformation as a result of interaction with luminescent AuNPs. In this case 0.1 μM BSA was in solution with 42 pM of either **Citrate-AuNPs** or **pTbL^{a}-AuNPs**.

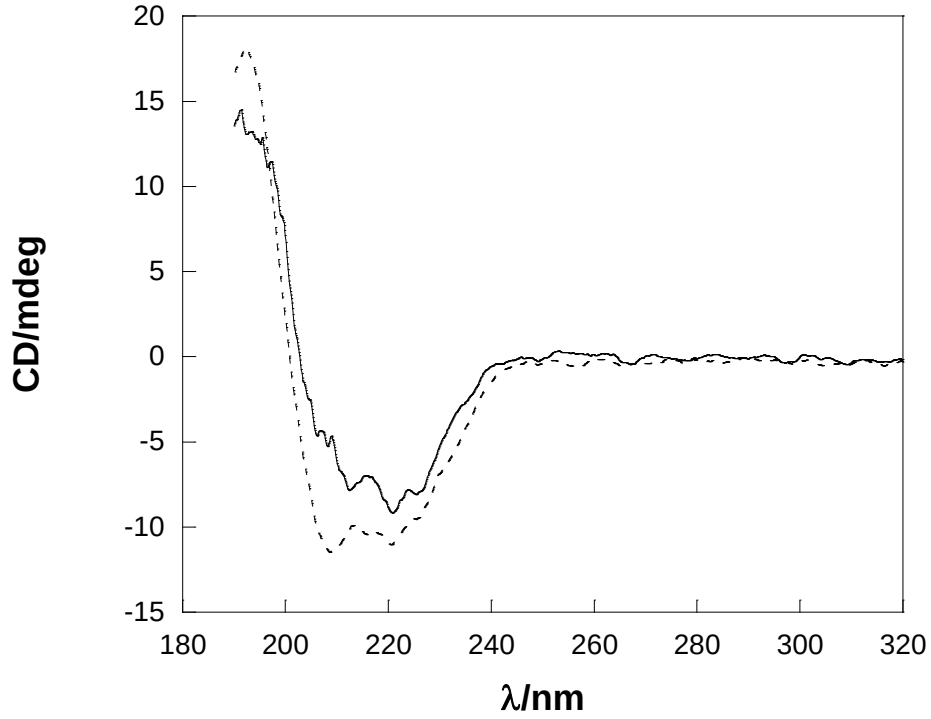

Figure 4.9 CD spectra of 0.1 μM BSA in the presence of 42 pM **Citrate-AuNPs** (—) or 42 pM **pTbL^{a}-AuNPs** (---).

The CD spectra of BSA in Figure 4.9 indicate that the conformation of the protein is less perturbed by the presence of **pTbL^{a}-AuNPs** than **Citrate-AuNPs** due to the higher magnitude of the negative α-helical peaks in the former case. This may mean that BSA is able

to interact to a greater extent with **Citrate-AuNPs** than **pTbL^{a}-AuNPs**; it is fair to conclude that due to the electrostatic nature of the interaction of BSA with **Citrate-AuNPs**, the displacement of the citrate by charge neutral **TbL^{a}** would reduce this interaction.

4.2.2.3 Emission Properties of Luminescent Nanoparticles with Protein

The emission properties of the lanthanide nanoparticles were assessed by taking **TbL^{a}-AuNPs** with and without the presence of protein and recording steady state emission spectra of the lanthanide luminescence. In all cases the concentration of **TbL^{a}-AuNPs** was approximately 1 nM. A solution of BSA in water was added to **TbL^{a}-AuNPs** to reach a final BSA concentration of 3.3 μM. Emission of BSA alone in solution is also presented for comparison and has been normalised to match the emission counts of **TbL^{a}-AuNPs** with BSA.

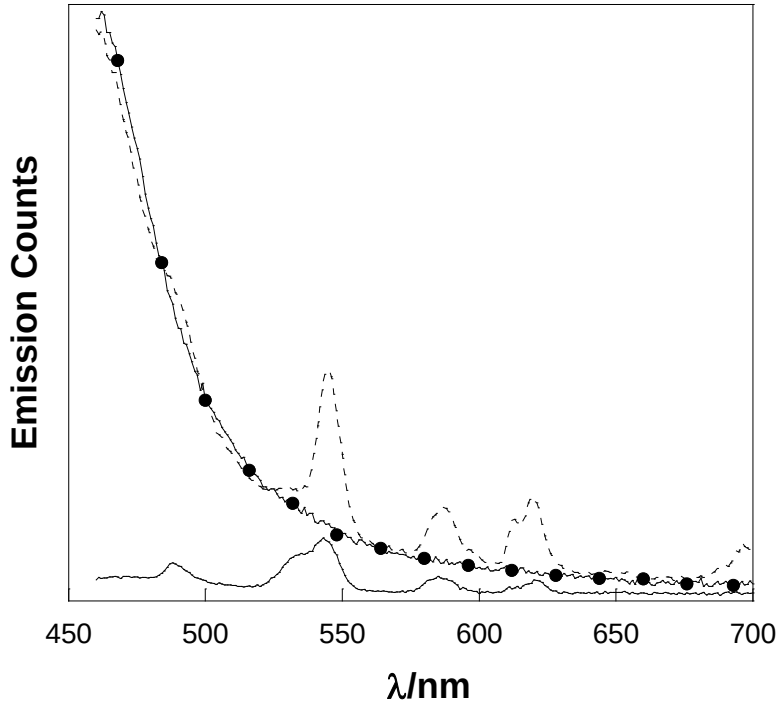

Figure 4.10 Emission spectra of 1 nM **TbL^{a}-AuNPs** (—), 1 nM **TbL^{a}-AuNPs** + 3.3 μM BSA (---) and 11 μM BSA (-●-) normalised to **TbL^{a}-AuNPs** + BSA. λ_{ex} = 266 nm, corrected for PMT response.

The emission spectra demonstrate that the characteristic Tb^{3+} emission is seen when **TbL^a-AuNPs** are in solution with and without BSA. There is a background observed when BSA is present and this is caused by the fluorescence of BSA itself, as demonstrated by the emission spectrum of BSA. The emission results indicate that the luminescent nanoparticles are appropriate for protein labelling due to the preservation of their luminescent properties when in the presence of protein.

4.2.2.4 Emission Properties of Luminescent Nanoparticles with Cell Growth Media

As discussed within the literature, it is well known that proteins found within cell growth media readily form a corona around nanoparticles.[3, 25] It was thought prudent, therefore, to examine the properties of the luminescent AuNPs when suspended in the cell growth media that will be used for cell studies. In this case **EuL^b-AuNPs** were examined in serum containing Dulbecco's Modified Eagle's Medium. The synthesis and characterisation of **EuL^b** can be found in Chapter 2. **EuL^b-AuNPs** were made by titrating a solution of **EuL^b** into **Citrate-AuNPs** until the SPR peak of the AuNPs stopped shifting; excess **EuL^b** was then removed by centrifugation. 100 μL **EuL^b-AuNPs** were suspended in either complete media or distilled water to give a total volume of 1 mL. The absorption spectra of the samples were recorded before and after isolating the AuNPs by centrifugation, discarding the supernatant and re-suspending in distilled water and repeating to wash the AuNPs. It was reasoned that if the protein corona was able to displace any lanthanide complex from the surface of the AuNPs then the wash steps would remove the unbound lanthanide complex. The wash steps were also carried out on the **EuL^b-AuNPs** in water for consistency in case the washing process itself affected the **EuL^b-AuNPs**. The emission spectra of the samples were then recorded.

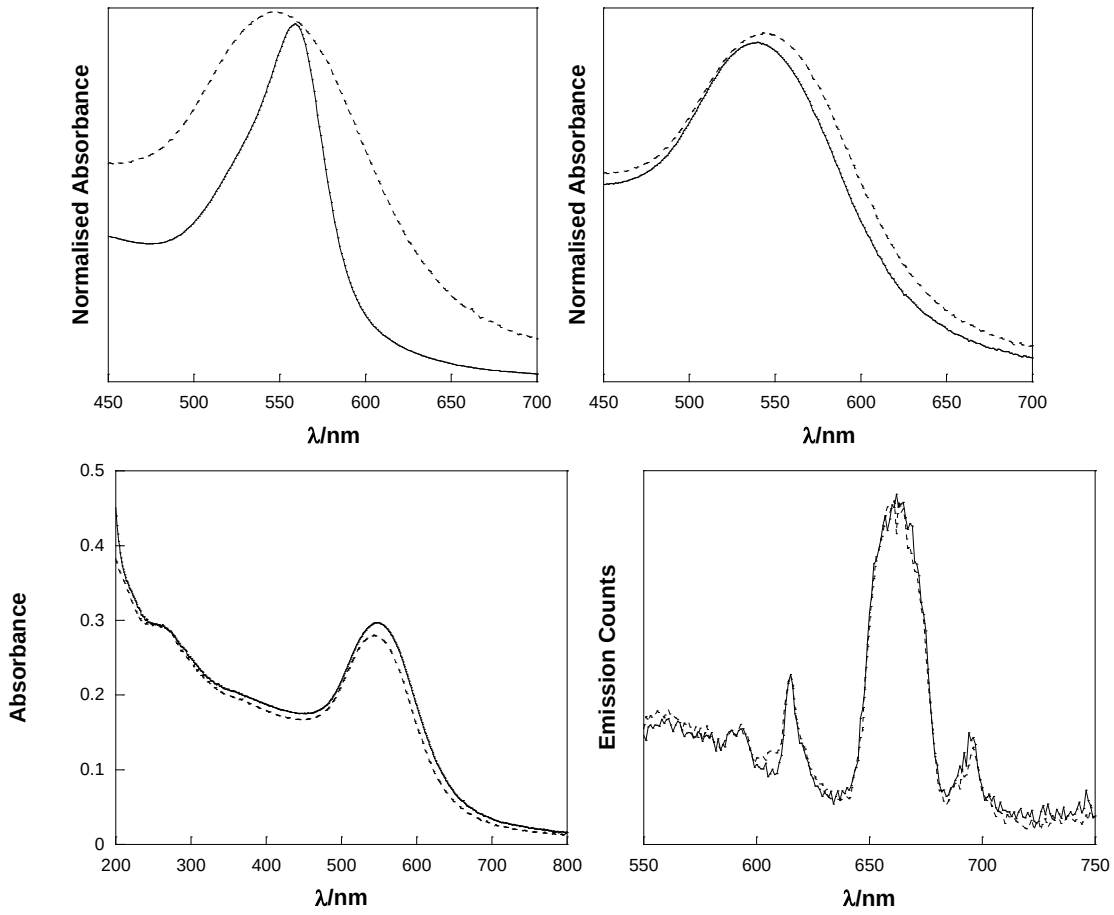

Figure 4.11 Top left: Absorption spectra of **EuL^{b}-AuNPs** diluted in media before (—) and after (---) washing. Top right: Absorption spectra of **EuL^{b}-AuNPs** diluted in water before (—) and after (---) washing. Bottom left: Absorption spectra of **EuL^{b}-AuNPs** diluted in media (—) or water (---) both after washing. Bottom right: Emission spectra of **EuL^{b}-AuNPs** diluted in media (—) or water (---) both after washing. λ_{ex} = 330 nm, corrected for PMT response.

The absorption spectra of the AuNPs in Figure 4.11 show that those originally dispersed in media suffered some changes during the washing steps, with a possible indication of some flocculation, although no aggregation was apparent. The AuNPs dispersed in water throughout show a broader SPR band than those in media from the beginning, but this does not change after washing. The differences in the SPR bands may be due to the difference in dielectric constant of the surrounding media given that all samples, once in water, give a similar SPR peak, whereas only those dispersed in cell culture media display a different

curve.[35, 36] Indeed the SPR curve of the AuNPs originally dispersed in cell culture media matches those of AuNPs in water once isolated and redispersed in water. Both samples of **EuL^{b}-AuNPs** after wash steps have very similar absorbance arising from the AuNPs at ~520 nm and from the **EuL^{b}** complex at ~330 nm which means that they are comparable for emission studies. The emission spectra of both samples are remarkably similar and clearly show the characteristic emission peaks of Eu^{3+}. The emission spectra confirm that any protein corona formed when **EuL^{b}-AuNPs** are suspended in media does not affect their luminescence properties, further reinforcing their suitability for protein labelling in cells.

4.2.3 **EuL^{b}-AuNPs** as Protein Labels in Cells

4.2.3.1 Target Protein and Its Expression in HeLa Cells

As discussed in Chapter 3, of the peptides studied CCPGCC showed the greatest affinity for AuNPs and as such will be used as the binding motif for the luminescent AuNPs. In order to label a protein of interest the binding motif will need to be expressed in cells as part of a recombinant protein. In this case enhanced GFP was chosen as the target protein to be labelled in cells because it is fluorescent and as such should allow co-localisation with the **EuL^{b}-AuNPs** to be established through fluorescence microscopy. More specifically, the recombinant protein has the binding motif contained within the peptide sequence FLNCCPGCCMEP which is fused to the C-terminal of enhanced GFP. The recombinant protein will henceforth be referred to as GFP-4C. Previously published work has established the ability of a similar recombinant protein of enhanced GFP and CCPGCC to bind to AuNPs *in vitro* in an oriented fashion through the tetracysteine motif.[37] Furthermore, the recombinant protein was found to have strong affinity for AuNPs of a range of sizes and a recombinant protein with the dicysteine motif, as opposed to the tetracysteine, did not have any higher

affinity for AuNPs than native enhanced GFP.[37] This research confirms the possibility of using the tetracysteine motif CCPGCC as a binding sequence for AuNPs when fused to a protein of interest.

A plasmid expressing GFP-4C was transformed into *Escherichia coli* and amplified. The amplified plasmid was harvested and purified before being used to transfect HeLa cells, a human cervical cancer cell line.

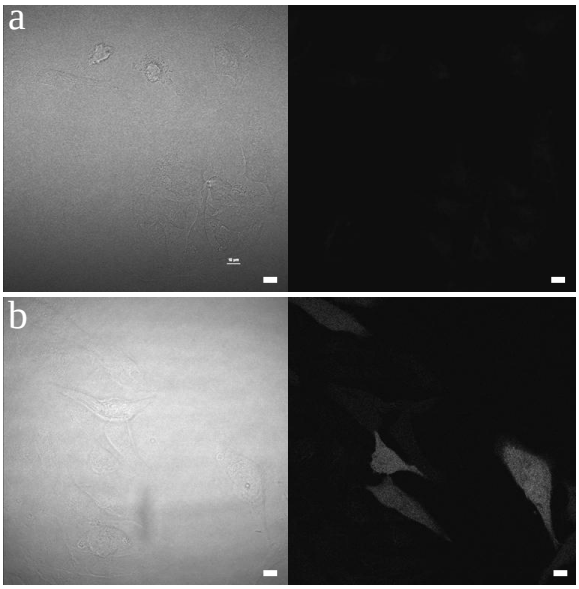

Figure 4.12 Confocal microscopy images of (a) HeLa cells and (b) HeLa cells transfected for 24 h to express GFP-4C. Left: bright field and Right: Fluorescence where λ_{ex} = 488 nm and λ_{em} = 500-550 nm. Scale bar = 10 μm.

The images in Figure 4.12 reveal the success of the transfection of HeLa cells to express GFP-4C. The untreated HeLa cells display some autofluorescence, however, the signal is much lower than that exhibited by the transfected cells, indicating that the fluorescence does indeed originate from GFP-4C. It is not uncommon to see autofluorescence from HeLa cells examined under these conditions originating from molecules such as flavin adenine

dinucleotide.[38] The fluorescence of the transfected cells is diffuse across the cells which means that GFP-4C is located throughout the cell cytoplasm.

4.2.3.2 Treatment of HeLa Cells with **Citrate-AuNPs**

After establishing the success of transfecting HeLa cells to express GFP-4C, the uptake of AuNPs by HeLa cells was then examined. Firstly, HeLa cells both expressing and not expressing GFP-4C were treated with **Citrate-AuNPs** for 24 hours. Transfected HeLa cells either had the transfection media removed after 24 hours and prior to the addition of **Citrate-AuNPs**, which were incubated with the cells for a further 24 hours, or were treated with transfection media for 48 hours with the **Citrate-AuNPs** being added to the transfection media for the final 24 hours.

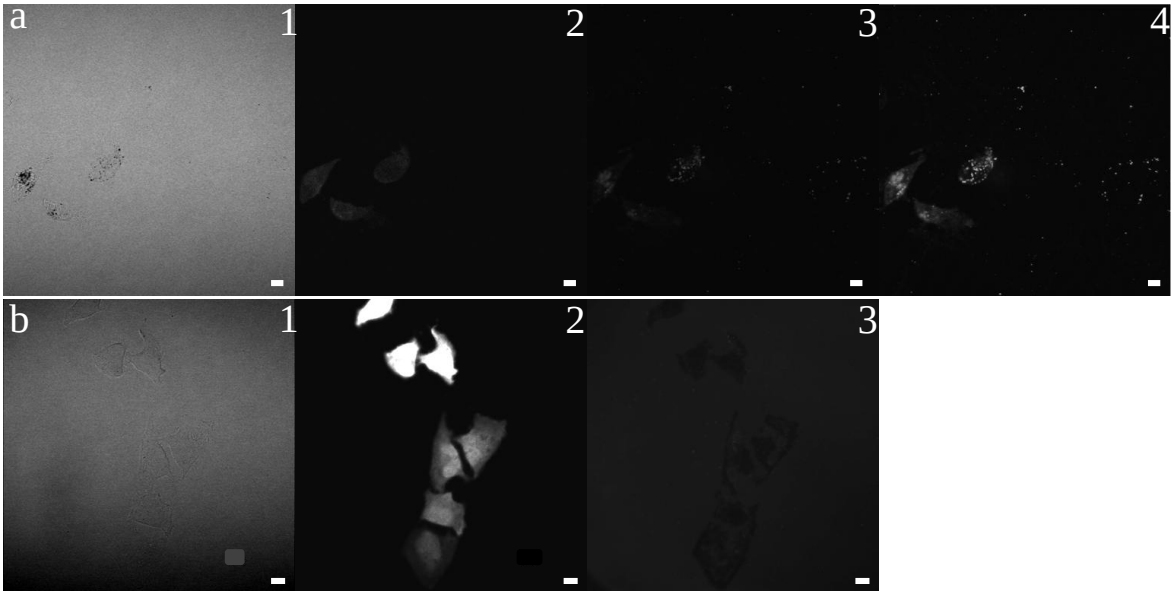

Figure 4.13 Confocal microscopy images of (a) HeLa cells transfected for 24 h to express GFP-4C with subsequent treatment with 0.9 nM **Citrate-AuNPs** for 24 h after the removal of Lipofectamine 2000 and (b) HeLa cells transfected for 48 h to express GFP-4C with treatment with 0.9 nM of **Citrate-AuNPs** for the final 24 h in the presence of Lipofectamine 2000. 1) bright field, 2) fluorescence where λ_{ex} = 488 nm and λ_{em} = 500-550 nm, 3) reflectance where λ_{ex} = 637 nm and λ_{em} = 400-700 nm and 4) overlay of fluorescence and reflectance images. Scale bar = 10 μm.

Transfection factors have previously been used for cellular delivery of AuNPs and other luminescent nanoparticles.[39-41] In this case it would seem that the presence of the transfection factor Lipofectamine 2000 is affecting the uptake of the **Citrate-AuNPs** because large aggregates are seen in both the bright field and reflectance images where the transfection factor is not present, Figure 4.13a, but not when the transfection factor is present, Figure 4.13b. Typically AuNPs are observed as dark objects in bright field images and bright spots in reflectance images if their dimensions make them large enough to be detected.[42] Reflectance imaging can typically detect AuNPs with diameters above 30 nm, and particles with diameters of 30 - 40 nm offer good signal to noise ratio in bright field imaging.[42, 43] It is, therefore, assumed that the dark objects in the bright field images and the corresponding bright spots in the reflectance images are clusters of **Citrate-AuNPs** since individual particles are likely to be too small to be detected. The apparent presence of AuNP clusters indicates aggregated AuNPs; in contrast, the lack of these features when the transfection factor is present does not necessarily mean that AuNPs are not present, but perhaps that the transfection factor has aided their delivery without aggregation which would mean that they are small enough to go undetected by these microscopy techniques. It is clear that where AuNPs are visible, Figure 4.13a, that they could possibly be in the vicinity of a discrete amount of GFP-4C, however, since the fluorescence of the protein is diffuse it is difficult to conclude whether the this is, in fact, due to interaction. In order to gain more information about the localisation of the **Citrate-AuNPs** within the cells, TEM was used to gain images of the cells after transfection and treatment with **Citrate-AuNPs** over two timeframes with transfection factor present.

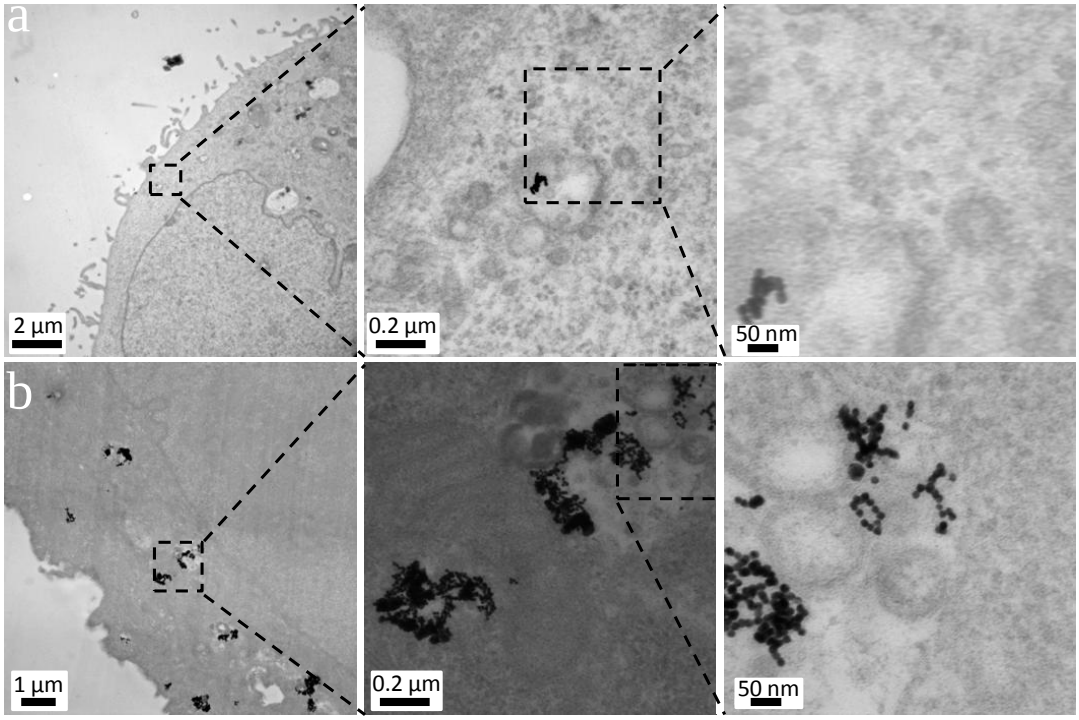

Figure 4.14 TEM micrographs of HeLa cells treated with **Citrate-AuNPs** for a) 30 min and b) 24 h. Both treatments in the presence of Lipofectamine 2000.

The TEM micrographs clearly show that when the **Citrate-AuNPs** treatment has been applied for only 30 minutes, Figure 4.14a, the **Citrate-AuNPs** are transported into the cells in a small tightly packed cluster, with a diameter of 75 nm, across its longest dimension, contained within an endosome. On the other hand, **Citrate-AuNPs** incubated with HeLa cells for 24 hours, Figure 4.14b, contain larger, more diffuse collections of AuNPs, with dimensions up to 400 nm, within the cell with evidence that they have escaped the endosome. If the **Citrate-AuNPs** are free within the cytoplasm then it may be possible for them to interact with GFP-4C, which would not be possible if they were trapped within endosomes. In order to see if the cellular uptake of luminescent AuNPs followed similar mechanisms, these experiments were repeated using **EuL^{b}-AuNPs**.

4.2.3.3 Treatment of HeLa Cells with **EuL^{b}-AuNPs**

Administration of **Citrate-AuNPs** to HeLa cells transfected to express GFP-4C revealed that the presence of transfection factor seemed to be advantageous for the uptake of AuNPs by the cells without significant aggregation and allowed some endocytic uptake in as little as 30 minutes. With these results in mind **EuL^{b}-AuNPs** were administered to HeLa cells either for the final 30 minutes or 24 hours of a 48 hour transfection to express GFP-4C. The cells were then imaged using confocal microscopy.

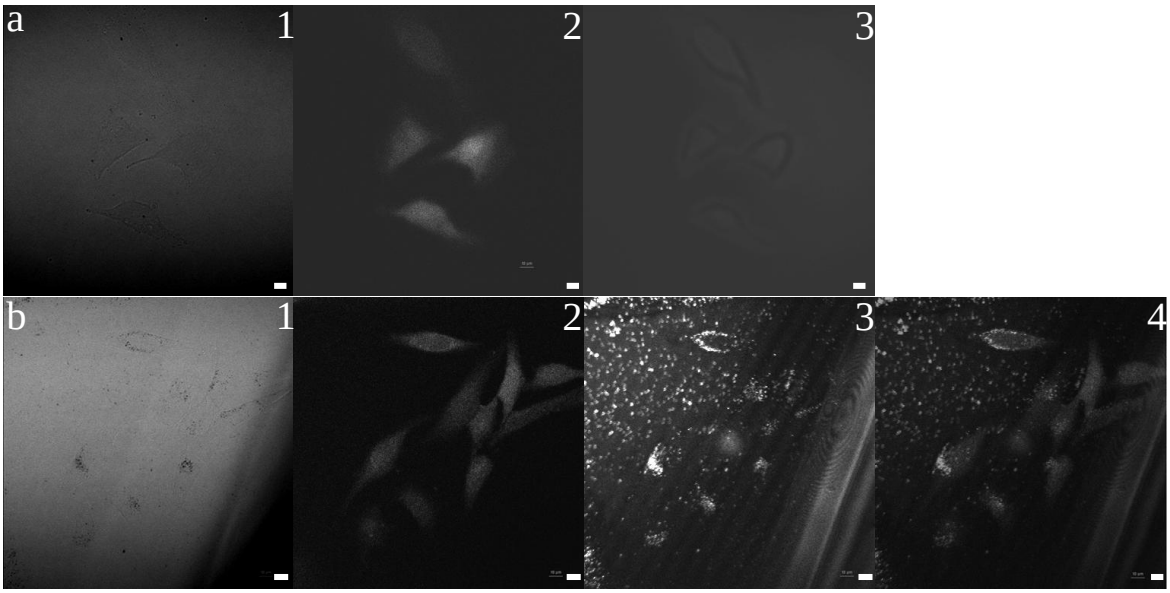

Figure 4.15 Confocal microscopy images of HeLa cells transfected for 48 h to express GFP-4C with treatment with 0.9 nM **EuL^{b}-AuNPs** for the final a) 30 minutes or b) 24 h of transfection. 1) bright field, 2) fluorescence where λ_{ex} = 488 nm and λ_{em} = 500-550 nm, 3) reflectance where λ_{ex} = 637 nm and λ_{em} = 400-700 nm and 4) overlay of fluorescence and reflectance images. Scale bar = 10 μm.

Unlike the results for **Citrate-AuNPs**, **EuL^{b}-AuNPs** appear to show large aggregates of AuNPs within cells after a 24 hour treatment with transfection factor present, apparent in both the bright field and reflectance images, whereas no aggregates are seen after only a 30 minute treatment. The aggregates appear to be located within the cells as does GFP-4C, but again the

diffuse nature of the GFP-4C fluorescence prevents the investigation into whether there is an interaction between the two species. The emission from **EuL^{b}** may have given more information about the location of the AuNPs, particularly where the lack of aggregation prevented them from being detected in bright field or reflectance modes, but unfortunately this could not be imaged. This may be due to the fact that the laser lines available for use with the microscope were not at the optimum wavelength for excitation of the complex because organic probes with longer excitation wavelengths are routinely studied using the equipment and, since the complex has a long luminescence lifetime, it emits a low number of photons at any one time making their detection difficult even with optimal excitation.

The difference in cellular uptake of **Citrate-AuNPs** and **EuL^{b}-AuNPs** may be because the surface modification of the AuNPs has affected the mechanism by which the AuNPs are taken up into the cells. In order to examine whether the presence of the transfection factor affects the uptake of **EuL^{b}-AuNPs** in the same way as **Citrate-AuNPs**, HeLa cells were incubated with **EuL^{b}-AuNPs** with and without Lipofectamine 2000 present and the cells digested and analysed for gold content using ICP-MS.

Sample	Average number of EuL^{b}-AuNPs per cell/10^{3}
HeLa cells + **EuL^{b}-AuNPs**	750 ± 195
HeLa cells + **EuL^{b}-AuNPs** + Lipofectamine 2000	680 ± 156

Table 4.4 Average numbers of AuNPs per HeLa cell as calculated from counting cells present and absolute concentration of Au present in each sample measured by ICP-MS.

ICP-MS data reveals that the average number of **EuL^{b}-AuNPs** per HeLa cell is the same within error whether transfection factor is present or not. If the presence of transfection factor

does affect the uptake mechanism of AuNPs by HeLa cells it does not affect the overall numbers of AuNPs taken up. The calculations to determine the average numbers of AuNPs per cell can be found in the experimental section.

TEM was again used to image the AuNPs more closely, and as such assess their uptake in HeLa cells more thoroughly.

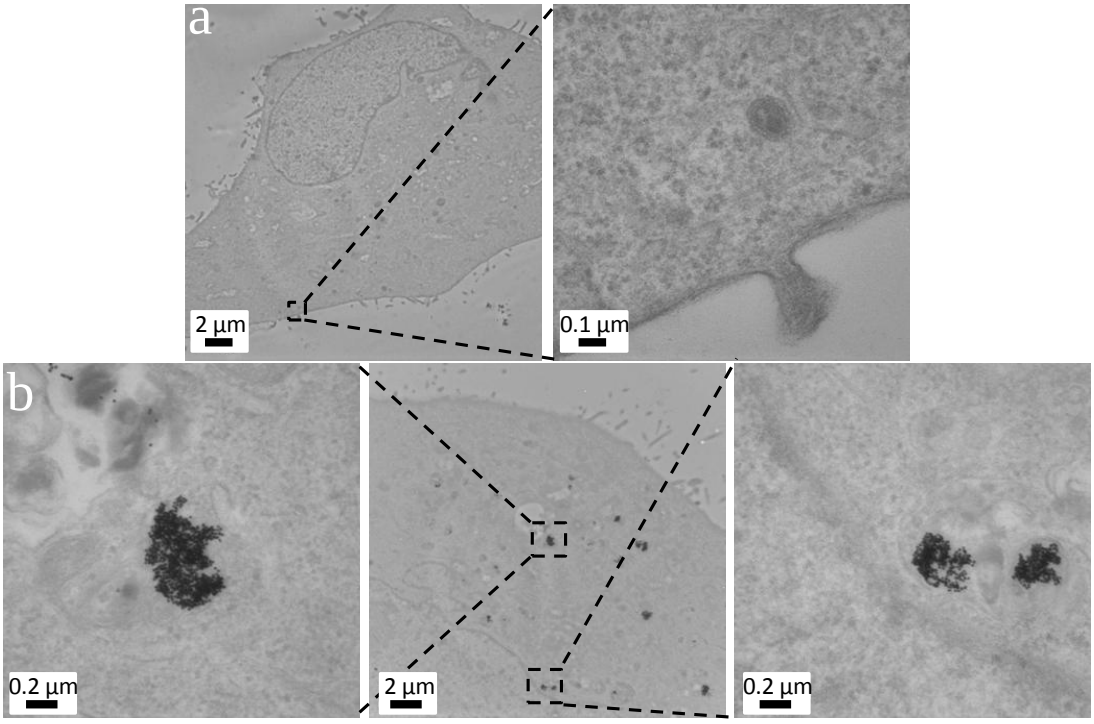

Figure 4.16 TEM micrographs of HeLa cells treated with **EuL^{b}-AuNPs** for a) 30 min and b) 24 h. Both treatments in the presence of Lipofectamine 2000.

TEM reveals that when HeLa cells are treated with **EuL^{b}-AuNPs** for 30 minutes with transfection factor present, Figure 4.16a, there is no evidence of the uptake of AuNPs into the cell. This is in contrast to **Citrate-AuNPs** which were taken up by endocytosis under the same conditions, indicating that the surface modification of the AuNPs does indeed affect cellular uptake. After a 24 hour treatment of HeLa cells with **EuL^{b}-AuNPs** in the presence of transfection factor, Figure 4.16b, there are large collections of AuNPs clearly visible within

the cell. These collections of AuNPs have diameters of up to 500 nm across their largest dimension. Some of the collections of AuNPs are contained within vesicles, however, for others it is possible that AuNPs are free within the cytoplasm of the cell. If AuNPs are free within the cell cytoplasm it is possible that an interaction between them and GFP-4C could occur, but other methods to determine this are needed.

Confocal microscopy and TEM have revealed the presence of both AuNPs and GFP-4C within HeLa cells, however, these methods have not presented the opportunity to draw conclusions about whether AuNPs do attach specifically to GFP-4C within cells. In order to gain more information about this HeLa cells were treated as for imaging purposes, but instead of being mounted were lysed in order to isolate AuNPs that had been taken up by the cells and examine whether GFP-4C is associated with the AuNPs.

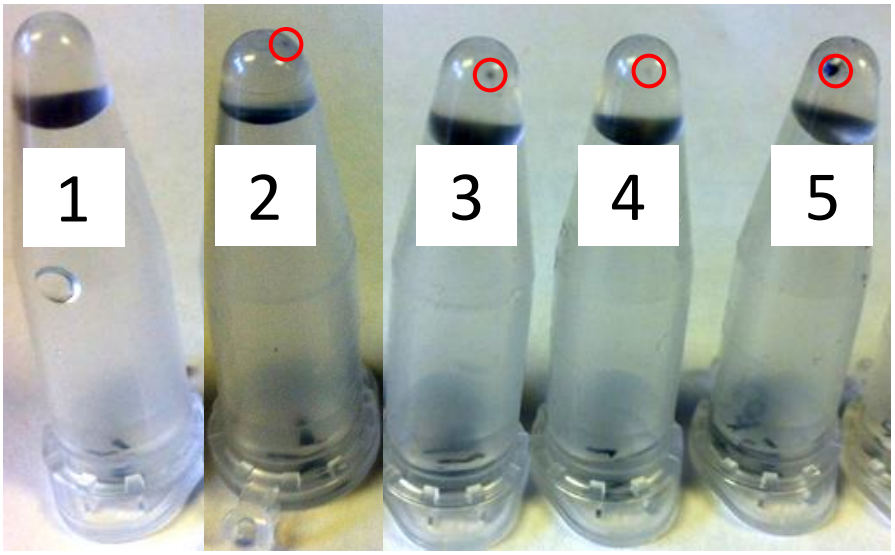

Figure 4.17 Aggregates of AuNPs, indicated by red circles, seen after centrifugation of HeLa cells after lysis. HeLa cells were all transfected for 48 h to express GFP-4C with 1) no additional treatment, treatment with **Citrate-AuNPs** for the final 2) 30 minutes or 3) 24 h of transfection or treatment with **EuL^{b}-AuNPs** for the final 4) 30 minutes or 5) 24 h of transfection.

When cell lysis is performed, the cell solution is centrifuged and the cell debris contained within the resulting pellet is discarded because the cell contents remain within the supernatant, however, in this case dark aggregates resembling clumps of AuNPs were evident in the pellet indicating that AuNPs may be present in the pellet. Both the pellet and supernatant were examined for the presence of GFP-4C by measuring its fluorescence using a steady state fluorometer.

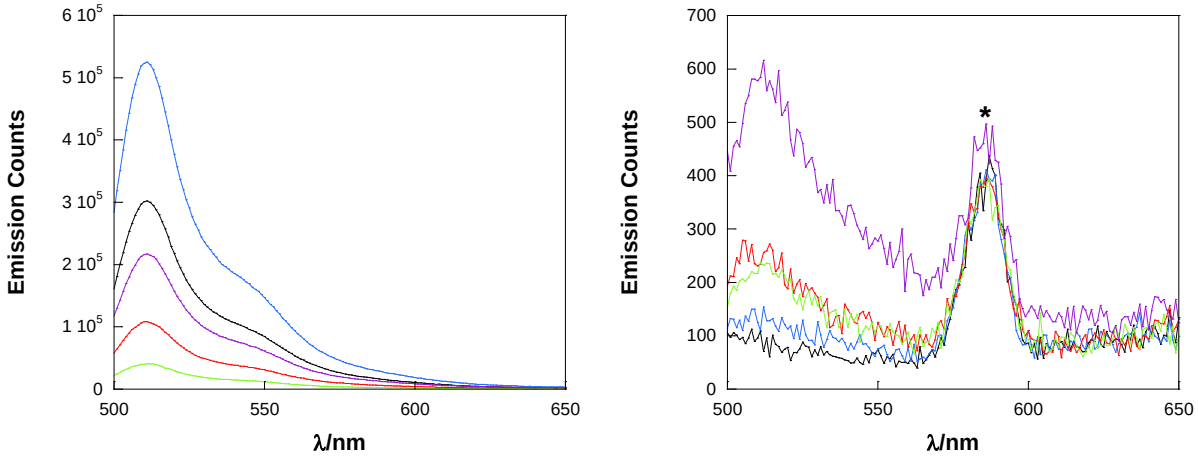

Figure 4.18 Emission spectra of GFP-4C from the supernatant (left) and pellets (right) of HeLa cells transfected to express GFP-4C for 48 h and with no additional treatment (—), treatment with **Citrate-AuNPs** for the final 30 minutes (—) or 24 h of transfection (—) or treatment with **EuL^{b}-AuNPs** for the final 30 minutes (—) or 24 h of transfection (—). In all cases λ_{ex} = 488 nm and spectra corrected for PMT response. * indicates Raman scattering of water.

The emission spectra in Figure 4.18 clearly show the characteristic emission expected for GFP with its emission peak around 510 nm, however, the emission is much more intense in the supernatant than the pellet. Indeed, the fluorescence intensity of GFP-4C from the pellet samples is so low that the Raman scattering of water can be seen at around 586 nm, as indicated by * in Figure 4.18 and seen under similar spectroscopy conditions previously.[44] This leads to the conclusion that there is more GFP-4C located within the cell cytoplasm, now

found in the supernatant, than associated with AuNPs, now found within the pellet. This is consistent with the fact that AuNPs were observed in discrete locations within the cells, however, GFP-4C was diffuse throughout the cell which would indicate that even if some of the protein was associated with AuNPs, the majority of it would not be. Certainly, the measurement of GFP-4C fluorescence within the pellet samples indicates that some of the protein is strongly associated with AuNPs. This conclusion is further strengthened by the fact that the most GFP-4C fluorescence from pellet samples is seen from samples that were revealed by TEM to have the most AuNP uptake, namely HeLa cells transfected for 48 hours with AuNPs applied in the final 24 hours of transfection. Interestingly, there is some GFP-4C fluorescence and AuNP presence in the pellet seen for HeLa cells treated with **EuL^{b}-AuNPs** for the final 30 minutes of a 48 hour transfection, however, of the cells imaged using TEM no evidence of AuNPs was observed; this may indicate that of the population of cells some take up AuNPs, whereas a significant number do not take up any AuNPs at all. TEM also showed uptake of **Citrate-AuNPs** administered in the same way, however, there is negligible GFP-4C fluorescence measured from the pellet of cells treated in this way which confirms that the containment of AuNPs within endosomes prevents their interaction with GFP-4C. Finally, cells without any AuNP treatment show no GFP-4C fluorescence from the pellet which confirms that the fluorescence measured from the other samples is not an artefact of the procedures employed.

4.3 Conclusions

The work in this chapter provides evidence of the potential for the use of luminescent AuNPs to act as protein labels. It has been demonstrated that the interaction of proteins with AuNPs differs depending on the surface coating of the AuNPs, with an anionic citrate coating allowing a strong interaction between BSA and **Citrate-AuNPs** without evidence of significant effect upon the conformation of the protein. Luminescent AuNPs coated with a charge neutral lanthanide complex, **TbL^{a}**, showed a much weaker interaction with BSA and as such affected its structure to a much smaller degree than **Citrate-AuNPs**. In addition to this the luminescence properties of **TbL^{a}-AuNPs** and **EuL^{b}-AuNPs** were unaffected by protein or cell growth media confirming their potential as luminescent protein labels in cell studies. Preliminary results indicate that **Citrate-AuNPs** and **EuL^{b}-AuNPs** are able to label a fusion protein containing the AuNP binding peptide, CCPGCC, however, the use of **EuL^{b}-AuNPs** as luminescent protein labels within cells was not demonstrated due to the inability to image europium luminescence from the treated cells. Further experiments are required to confirm the interaction of AuNPs with GFP-4C within cells which could include the expression of the protein as part of a known cellular structure and coating of AuNPs with a species able to participate in FRET with GFP-4C such as a terbium complex with improved antennas for increased luminescence intensity than that exhibited by **TbL^{a}** or **EuL^{b}**.

4.4 Experimental

4.4.1 General Considerations

Cell culture materials were obtained from either Invitrogen, Electron Microscopy Sciences or Life Technologies. Complete cell growth media was further sterile filtered after formulation.

UV-Vis absorption spectra were carried out on Varian Cary 50 or Varian Cary 5000 spectrometers. UV-Vis spectra were taken using 1 cm path length quartz cuvettes.

CD spectra were obtained using a JASCO J180 spectropolarimeter. CD spectra were recorded using 1 cm path length quartz cuvettes.

ICP-MS analysis was undertaken at the University of Warwick, UK, and conducted using an Agilent 7500cx LC-ICP-MS system. PlasmaCal calibration standard for gold was purchased from SCP science.

4.4.2 Plasmid Construct

Mammalian expression plasmid for C-terminal fusion of tetracysteine peptide (FLNCCPGCCMEP) fused to enhanced GFP was obtained from Roger Tsien, University of California, San Diego, USA. The vector used was pCDNA3.1 with ampicillin and neomycin resistance.

4.4.3 Amplification of Plasmid

A pellet of frozen DH5 α *Eschericha coli* (50 μL) was thawed on ice. The plasmid was added to water (30 μL) and briefly centrifuged and vortexed. Plasmid solution (5 μL) was added to

the bacteria and kept on ice for a further 30 min. A 45 s heat shock at 42 ºC was then applied to the bacteria mixture before being put on ice for a further 2 min. Lysogeny broth (500 μL) was added to the bacteria and the mixture shaken at 37 ºC for 1 h. 150 μL of the bacteria mixture was added and streaked across a lysogeny broth agar plate with ampicillin. The plate was left to incubate at 37 ºC for ~ 18 h. Single colonies were picked from the plate and added to separate culture tubes each containing lysogeny broth (3 mL) and ampicillin (3 μL). The culture tubes were shaken at 37 ºC for ~ 18 h. The bacteria were then collected by centrifugation and the plasmid harvested using a QIAprep Spin Miniprep Kit, QIAGEN. The purified plasmid was eluted into buffer (50 μL) and its concentration found by measuring absorbance of the solution at 260 nm.

4.4.4 HeLa Studies

4.4.4.1 Cell Culture Maintenance

HeLa cells were grown in complete media (10 mL) in T75 flasks with vented caps in an incubator at 37 ˚C containing 5% CO_2. Complete media consisted of Dulbecco's Modified Eagle's Medium supplemented with foetal bovine serum (10%) and streptomycin/penicillin (1%). Cell passage was carried out every 3-4 days by washing with PBS and detachment using trypsin followed by dilution in complete media and adding to either a fresh T75 flask or 6-well plates.

4.4.4.2 Treating Cells

1 mL of cell solution after passage was added to each well of a 6-well plate and cells incubated at 37 ˚C in a 5% CO_2 atmosphere for 24 h prior to further treatment. A glass cover slip would first be added to the well if the cells were to be used for microscopy. For

transfection a transfection mixture was made using media (50 μL per well) and Lipofectamine 2000 (1 μL per well) and allowing to stand at room temperature for 5 min before mixing with media (50 μL per well) and plasmid (2 μg per well) and allowing to stand at room temperature for 20 min. Once the cells had been incubated in the 6-well plate for 24 h the media was removed and replaced with fresh media (1 mL) before addition of transfection media to each well. The plates were then returned to incubate for 24-28 h. After 24 h of transfection the cells were either washed with PBS and fresh media added before AuNP treatment, or AuNP treatment was added directly to the cells in transfection media. AuNP treatment was administered by adding 9.4 nM AuNPs (100 μL) to each well and returning to incubate for a further 24 h. To achieve a 30 min treatment with AuNPs, AuNPs were administered in the same way 30 min before the end of a 48 h transfection.

4.4.4.3 Fixing and Mounting Cells

4.4.4.3.1 Preparation for Confocal Microscopy

Once treatments were complete media was removed from the cells and cells washed with PBS. 4% paraformaldehyde (2 mL) was added to each well and cells left at room temperature for 5 min. Paraformaldehyde was then removed and cells washed again with PBS before cover slips were placed cells down onto a drop of Prolong Gold mounting medium on a glass slide. The slides were sealed with varnish, refrigerated flat and protected from light for at least 24 h prior to imaging.

4.4.4.3.2 Preparation for TEM

Once treatments were complete media was removed from the cells and cells washed with PBS. Wells were filled with 2.5% gluteraldehyde in PBS and the plates sealed and

refrigerated for 72 h before cells being sectioned and mounted onto TEM grids by the Centre for Electron Microscopy, University of Birmingham, UK.

4.4.4.4 Microscopy of Cells

4.4.4.4.1 Confocal Microscopy

Confocal microscopy was carried out using a Nikon A1R inverted confocal microscope employing a 60x oil immersion objective and using Nikon NIS-Elements Advanced Research software version 3.2. GFP fluorescence images were gained using a 488 nm laser excitation source and detection in the range of 500-550 nm. Reflectance images were gained using 637 nm excitation source and detection in the range of 400-700 nm.

4.4.4.4.1.1 Overlaying Fluorescence and Reflectance Confocal Microscope Images

MATLAB software was used to overlay confocal fluorescence and confocal reflectance microscope images all of 512 x 512 pixels using the following code:

```
base=imread('Fluorescence Image.gif');
I=imread('Reflectance Image.gif');
base_points = zeros(4, 2);
base_points(1,1) =1;
base_points(1,2)=1;
base_points(2,1) =1;
base_points(2,2)=512;
base_points(3,1) =512;
base_points(3,2)=1;
base_points(4,1) =512;
base_points(4,2)=512;
input_points = zeros(4, 2);
input_points(1,1) =1;
input_points(1,2)=1;
```

```
input_points(2,1) =1;
input_points(2,2)=512;
input_points(3,1) =512;
input_points(3,2)=1;
input_points(4,1) =512;
input_points(4,2)=512;
TFORM=cp2tform(input_points,base_points,'affine');
registered=imtransform(I,TFORM,'FillValues', 0, 'XData', [1 size(base,2)], 'YData', [1
size(base,1)]);
figure, imshow(registered)
hold on
h=imshow(base, gray(256));
set(h, 'AlphaData', 0.2);
```

4.4.4.4.2 TEM

TEM micrographs were obtained using a JEOL 1200EX transmission electron microscope fitted with a LaB_6 filament and employing an 80 keV beam.

4.4.4.5 Cell Lysis

Lysis buffer was made by adding Triton X100 (100 μL) and 1 protease inhibitor tablet to PBS (9.9 mL). After treatments cells were washed with PBS and lysis buffer (500 μL) added to each well. Cells were then scraped from the bottom of the wells and transferred to a centrifuge tube and vortexed every few minutes for a total of 1 h. The solutions were then centrifuged to obtain cell contents in the supernatant and cell debris in the pellet. The supernatant was decanted into a clean tube and the pellets resuspended in water before being centrifuged again and the process repeated in order to wash the pellets.

4.4.4.6 ICP-MS Analysis of Cells

1 mL of cell solution after passage was added to each well of a 6-well plate and cells incubated at 37 ˚C in a 5% CO_2 atmosphere for 24 h. Following this the media was removed and replaced with 1 mL fresh media and the cells incubated for a further 24 h prior to further treatment. **EuL^{b}-AuNPs** treatment was added directly to the cells requiring treatment; AuNP treatment was administered by adding 9.4 nM AuNPs (100 μL) to each well and returning to incubate for a further 24 h. Lipofectamine 2000 (1 μL per well) was also added to the corresponding cells. After treatment the treatment media was removed, cells washed with PBS and trypsin (0.5 mL) added to each well before incubating the cells at 37 ºC for a further 5 min. Media (3 mL) was then added to each well and mixed with the contents of the well before being transferred to a 15 mL centrifuge tube. The cells were centrifuged to form a pellet, the supernatant discarded and the cells resuspended in media (1 mL per tube). Cells were counted using a haemocytometer before being centrifuged again to form a pellet. The supernatant was discarded and cells re-suspended in ICP-MS grade HCl (300 μL per tube) and HNO_3 (100 μL per tube) and placed in an ultrasonic bath at 40 ºC for 3 h. Cell solutions were then diluted with deionised water (3.6 mL per well) for analysis. The results were as follows:

Sample	Average Number of Cells	Average Au Content/ppb
Untreated HeLa cells	115000	22.09
HeLa cells + Lipofectamine 2000	75000	29.80
HeLa cells + **EuL^{b}-AuNPs**	85000	504.30
HeLa cells + **EuLb-AuNPs** + Lipofectamine 2000	80000	522.70

As an example, the working used to calculate the average number of AuNPs per cell for HeLa cells treated with **EuL^{b}-AuNPs** but no Lipofectamine 2000 is as follows:

[Au] = 504.03 parts per billion = 5.043 x10^{-4} g L^{-1}

5.043 x10^{-4} g L^{-1}/197 g mol^{-1} = 2.56 x10^{-6} mol L^{-1} of Au

It has previously been shown that for AuNPs of this size there are 106801 atoms of gold per AuNP.[34]

2.56 x 10^{-6} mol L^{-1}/106801 = 2.40 x 10^{-11} mol L^{-1} AuNPs

In the 4 mL sample: 2.40 x 10^{-11} mol L^{-1} x 4 x 10^{-3} L = 9.60 x 10^{-14} mols of AuNPs

9.60 x 10^{-14} mol x 6.02x10^{23} mol^{-1} = 5.80 x 10^{10} AuNPs in sample

5.80 x 10^{10} AuNPs/ 85000 cells = 679906 AuNPs per cell.

4.4.5 Luminescence Spectroscopy

Luminescence experiments were carried out using an Edinburgh Instruments fluorescence system, FLSPM920. The illumination source uses a 450 W xenon arc lamp. The detection system used was a Hamamatsu R928 PMT. The emission monochromator is fitted with two interchangeable gratings blazed at 500 nm and 1200 nm. Luminescence studies were carried out using quartz cuvettes with four transparent polished faces and 1 x 1 cm path length. F900 spectrometer analysis software was used to record the data.

4.4.5.1 Terbium Emission

Luminescence spectra of **TbL^{a}** containing samples were gained by excitation of the complex at 266 nm, detection of emission in the range 455-750 nm and employing a 455 nm long pass filter. Typically a 0.2 s dwell time and a 1 nm step size were employed with excitation and emission slits set to 5 nm and 3 nm respectively.

4.4.5.2 Europium Emission

Luminescence spectra of **EuL^{b}** containing samples were gained by excitation of the complex at 330 nm, detection of emission in the range 550-750 nm and employing a 550 nm long pass filter. Typically a 0.2 s dwell time and a 1 nm step size were employed with excitation and emission slits set to 5 nm and 3 nm respectively.

4.4.5.3 BSA Emission

Fluorescence spectra of BSA containing samples were gained by excitation of the protein at 280 nm, detection of emission in the range 310-450 nm and employing a 305 nm long pass filter. A 0.5 s dwell time and a 1 nm step size were employed. Excitation and emission slits were set to 5 nm and 3 nm respectively.

In order to gain details of how the tail of the BSA emission peak may create a background in the emission spectra of **TbL^{a}** containing samples native BSA was also examined under the conditions described for **TbL^{a}**.

4.4.5.4 GFP Emission

Fluorescence spectra of GFP containing samples were gained by excitation of the protein at 488 nm, detection of emission in the range 500-650 nm and employing a 495 nm long pass filter. A 0.5 s dwell time and a 1 nm step size were employed. Excitation and emission slits were set to 5 nm and 3 nm respectively. Emission data was collected over three repeats to produce a spectrum.

4.4.6 ζ-potential Measurements

ζ-potential measurements were obtained using a Beckman-Coulter Delsa Nano C particle analyser and data was recorded and analysed using Delsa Nano software. Samples were analysed using a quartz flow cell purchased form Beckman-Coulter. Measurements were taken over 10 repeats at a 15º scattering angle through a 50 μm pinhole. The Smoluchowski conversion equation was used to analyse the data.

4.5 References

1. Y. D. Álvarez, J. A. Fauerbach, J. V. Pellegrotti, T. M. Jovin, E. A. Jares-Erijman and F. D. Stefani, *Nano Lett.*, 2013, **13**, 6156-6163.

2. S. H. Brewer, W. R. Glomm, M. C. Johnson, M. K. Knag and S. Franzen, *Langmuir*, 2005, **21**, 9303-9307.

3. E. Casals, T. Pfaller, A. Duschl, G. J. Oostingh and V. Puntes, *ACS Nano*, 2010, **4**, 3623-3632.

4. S. Chakraborty, P. Joshi, V. Shanker, Z. A. Ansari, S. P. Singh and P. Chakrabarti, *Langmuir*, 2011, **27**, 7722-7731.

5. S. Dominguez-Medina, S. McDonough, P. Swanglap, C. F. Landes and S. Link, *Langmuir*, 2012, **28**, 9131-9139.

6. L. A. Dykman and N. G. Khlebtsov, *Chem. Rev.*, 2014, **114**, 1258-1288.

7. S. H. D. Lacerda, J. J. Park, C. Meuse, D. Pristinski, M. L. Becker, A. Karim and J. F. Douglas, *ACS Nano*, 2010, **4**, 365-379.

8. S. Laera, G. Ceccone, F. Rossi, D. Gilliland, R. Hussain, G. Siligardi and L. Calzolai, *Nano Lett.*, 2011, **11**, 4480-4484.

9. J. Mariam, P. M. Dongre and D. C. Kothari, *J. Fluoresc.*, 2011, **21**, 2193-2199.

10. Q. Shao, P. Wu, P. Gu, X. Xu, H. Zhang and C. Cai, *J. Phys. Chem. B*, 2011, **115**, 8627-8637.

11. D.-H. Tsai, F. W. DelRio, A. M. Keene, K. M. Tyner, R. I. MacCuspie, T. J. Cho, M. R. Zachariah and V. A. Hackley, *Langmuir*, 2011, **27**, 2464-2477.

12. J. A. Yang, B. J. Johnson, S. Wu, W. S. Woods, J. M. George and C. J. Murphy, *Langmuir*, 2013, **29**, 4603-4615.

13. J. A. Yang, W. Lin, W. S. Woods, J. M. George and C. J. Murphy, *J. Phys. Chem. B*, 2014, **118**, 3559-3571.

14. S. P. Boulos, T. A. Davis, J. A. Yang, S. E. Lohse, A. M. Alkilany, L. A. Holland and C. J. Murphy, *Langmuir*, 2013, **29**, 14984-14996.

15. M. Cui, R. Liu, Z. Deng, G. Ge, Y. Liu and L. Xie, *Nano Res.*, 2014, **7**, 345-352.

16. S. R. Saptarshi, A. Duschl and A. L. Lopata, *J. Nanobiotechnol.*, 2013, **11**, 26.

17. D. Wang, J. Ye, S. D. Hudson, K. C. K. Scott and S. Lin-Gibson, *J. Colloid Interface Sci.*, 2014, **417**, 244-249.

18. M. Yu, C. Zhou, J. Liu, J. D. Hankins and J. Zheng, *J. Am. Chem. Soc.*, 2011, **133**, 11014-11017.

19. S. Zeng, Y.-m. M. Huang, C.-e. A. Chang and W. Zhong, *Analyst*, 2014, **139**, 1364-1371.

20. T. Cedervall, I. Lynch, S. Lindman, T. Berggard, E. Thulin, H. Nilsson, K. A. Dawson and S. Linse, *Proc. Natl. Acad. Sci. U. S. A.*, 2007, **104**, 2050-2055.

21. M. Lundqvist, J. Stigler, G. Elia, I. Lynch, T. Cedervall and K. A. Dawson, *Proc. Natl. Acad. Sci. U. S. A.*, 2008, **105**, 14265-14270.

22. M. Mahmoudi, I. Lynch, M. R. Ejtehadi, M. P. Monopoli, F. B. Bombelli and S. Laurent, *Chem. Rev.*, 2011, **111**, 5610-5637.

23. C. Rocker, M. Potzl, F. Zhang, W. J. Parak and G. U. Nienhaus, *Nat. Nanotechnol.*, 2009, **4**, 577-580.

24. S. Tenzer, D. Docter, J. Kuharev, A. Musyanovych, V. Fetz, R. Hecht, F. Schlenk, D. Fischer, K. Kiouptsi, C. Reinhardt, K. Landfester, H. Schild, M. Maskos, S. K. Knauer and R. H. Stauber, *Nat. Nanotechnol.*, 2013, **8**, 772-U1000.

25. Y. Yan, K. T. Gause, M. M. J. Kamphuis, C.-S. Ang, N. M. O'Brien-Simpson, J. C. Lenzo, E. C. Reynolds, E. C. Nice and F. Caruso, *ACS Nano*, 2013, **7**, 10960-10970.

26. R. Khandelia, A. Jaiswal, S. S. Ghosh and A. Chattopadhyay, *Small*, 2013, **9**, 3494-3505.

27. A. Lesniak, A. Salvati, M. J. Santos-Martinez, M. W. Radomski, K. A. Dawson and C. Åberg, *J. Am. Chem. Soc.*, 2013, **135**, 1438-1444.

28. M. Schäffler, F. Sousa, A. Wenk, L. Sitia, S. Hirn, C. Schleh, N. Haberl, M. Violatto, M. Canovi, P. Andreozzi, M. Salmona, P. Bigini, W. G. Kreyling and S. Krol, *Biomaterials*, 2014, **35**, 3455-3466.

29. A. Davies, D. J. Lewis, S. P. Watson, S. G. Thomas and Z. Pikramenou, *Proc. Natl. Acad. Sci. U. S. A.*, 2012, **109**, 1862-1867.

30. N. J. Rogers, S. Claire, R. M. Harris, S. Farabi, G. Zikeli, I. B. Styles, N. J. Hodges and Z. Pikramenou, *Chem. Commun.*, 2014, **50**, 617-619.

31. M. De, S. Rana, H. Akpinar, O. R. Miranda, R. R. Arvizo, U. H. F. Bunz and V. M. Rotello, *Nat. Chem.*, 2009, **1**, 461-465.

32. L. Anfossi, C. Baggiani, C. Giovannoli and G. Giraudi, *Anal. Bioanal. Chem.*, 2009, **394**, 507-512.

33. S. Comby and T. Gunnlaugsson, *ACS Nano*, 2011, **5**, 7184-7197.

34. D. J. Lewis, T. M. Day, J. V. MacPherson and Z. Pikramenou, *Chem. Commun.*, 2006, **42**, 1433-1435.

35. M. A. Mahmoud, M. Chamanzar, A. Adibi and M. A. El-Sayed, *J. Am. Chem. Soc.*, 2012, **134**, 6434-6442.

36. A. C. Sabuncu, J. Grubbs, S. Qian, T. M. Abdel-Fattah, M. W. Stacey and A. Beskok, *Colloids Surf. B*, 2012, **95**, 96-102.

37. A. M. W. Reed and S. J. Metallo, *Langmuir*, 2010, **26**, 18945-18950.

38. M. S. Islam, M. Honma, T. Nakabayashi, M. Kinjo and N. Ohta, *Int. J. Mol. Sci.*, 2013, **14**, 1952-1963.

39. R. Lévy, U. Shaheen, Y. Cesbron and V. Sée, *Nano Rev.*, 2010, **1**, 4889.

40. V. Sée, P. Free, Y. Cesbron, P. Nativo, U. Shaheen, D. J. Rigden, D. G. Spiller, D. G. Fernig, M. R. H. White, I. A. Prior, M. Brust, B. Lounis and R. Lévy, *ACS Nano*, 2009, **3**, 2461-2468.

41. B. Sikora, K. Fronc, I. Kaminska, K. Koper, S. Szewczyk, B. Paterczyk, T. Wojciechowski, K. Sobczak, R. Minikayev, W. Paszkowicz, P. Stepien and D. Elbaum, *Nanotechnology*, 2013, **24**, 235702.

42. G. F. Wang, A. S. Stender, W. Sun and N. Fang, *Analyst*, 2010, **135**, 215-221.

43. G. Rong, H. Wang, L. R. Skewis and B. r. M. Reinhard, *Nano Lett.*, 2008, **8**, 3386-3393.

44. C. Xu, J. B. Shear and W. W. Webb, *Anal. Chem.*, 1997, **69**, 1285-1287.

5. Overall Summary, Conclusions and Future Work

5.1 Overall Summary and Conclusions

The use of luminescent lanthanide complexes based on a DTPA backbone have been shown to successfully label proteins *in vitro* and to maintain their luminescence properties upon doing so. The lanthanide complexes used, **LnL^{a}**, where Ln = Tb, Eu and Nd, and **EuL^{b}**, contain thiol groups for their attachment to AuNPs in addition to their interaction with **NHS-MAL** for covalent attachment to proteins. Control over the degree of labelling of the proteins was established through varying the ratio of **NHS-MAL** and **EuL^{b}** to protein during conjugation. It was found that when fewer labels are present per molecule of BSA, the protein structure is unaffected by the presence of the label as shown by CD studies. The system developed for protein labelling *in vitro*, therefore, upholds the key principles discussed in Chapter 1, specifically both the protein and the label are unaffected by the conjugation procedure.

The conjugation of the complexes to BSA was not only useful for the luminescent labelling of the protein, but it also provided a route through which these complexes could be taken up by two human cell lines which were not able to take up the lanthanide complexes in isolation. Neutrophil cells were of interest due to their use in blood flow studies, however, previous attempts by the Pikramenou group to label them with luminescent lanthanide complexes had been unsuccessful. **EuL^{a}-BSA** and **TbL^{a}-BSA** were both shown to be taken up into the cell because neutrophils treated with these proteins exhibited the corresponding lanthanide luminescence. The luminescent cells were clearly visible through epiluminescence microscopy and as such may be used in rheology studies in the future. Human ovarian cancer

cells treated with **EuL^{b}-BSA** emitted a stronger signal than untreated cells or cells treated with only **EuL^{b}** when imaged using epiluminescence microscopy, however, cells treated with a mixture of **EuL^{x}** and BSA also showed similarly high luminescence. **EuL^{x}** is able to interact with BSA as shown by the change in CD spectra of BSA when the complex is present, however, the interaction must be through non-covalent means due to the lack of thiol groups preventing covalent attachment in the same way as **EuL^{b}**. This means that both covalent and non-covalent association of these complexes with BSA can facilitate their cellular uptake. This may be of importance when it is desirable to use membrane impermeable luminescent lanthanide complexes for cellular staining because it would circumvent the need for the use of methods such as electroporation or microinjection which may perturb the cells under investigation.

EuL^{b} was used to label κ FLC in addition to BSA and when conjugated to κ FLC it was able to participate in FRET. In this case **EuL^{b}** was used as the donor species and a commercially available dye, FluoProbes 647H, was the acceptor and was conjugated to an anti-κ FLC mAb. FRET occurred when the two proteins interacted. Furthermore, the shortening of the lifetime of **EuL^{b}** in the presence of the acceptor was shown to be dependent on the concentration of the acceptor, thus demonstrating the potential application of the system for immunoassays.

The precise number of labels conjugated to BSA could not be established. The use of absorption of the conjugated species could not be used to elucidate the number of labels due to the overlap of peak absorption of the protein with the labels. Analysis by Bradford assay and MS also proved inconclusive, most likely due to the label blocking the primary amines of the protein, preventing ionisation and interaction with the reagent in the assay. ICP-MS

investigations revealed the absolute concentration of europium in samples of **EuL^{b}-BSA** and this result was used to calculate the absorption expected from the label which was then subtracted from the measured absorption of the samples to reveal the absorption arising from BSA, however, the degree of labelling calculated using this method seemed unlikely and did not concur with the absorption profile of the conjugated species. This indicates that the conjugation of **EuL^{b}** to BSA does not result in a species whose absorption properties are a linear combination of the individual species and it is for this reason that alternative methods of analysis are needed. All attempts to elucidate labelling information did confirm that the attempt to limit the number of labels per molecule of BSA was successful although the exact number of labels was not established.

The first step towards using luminescent lanthanide coated AuNPs to label proteins within cells was to develop a peptide sequence capable of preferentially binding to AuNPs which could then be expressed by a cell as part of a protein of interest. Through investigating the interactions of three peptides, CALNN, CCPGCC and **CCALNNCCALNN** with **Citrate-AuNPs** it was possible to determine the affinity of each peptide for the AuNPs. ITC, UV-Vis absorption titrations and SPR spectroscopy were shown to provide concurrent results when used to find the binding constant of peptide to AuNPs and as such not all methods were utilised for each peptide. The analyses revealed that CCPGCC had the strongest affinity for AuNPs and **CCALNNCCALNN** the weakest. This may not be intuitive from the peptide sequences as it is expected that the strongest interaction is between the thiol of cysteine and the AuNPs, however, the number of cysteine residues, and thus thiol groups, does not correlate to the strength of binding. It is fair to conclude, therefore, that in addition to the

available cysteine residues, the overall conformation of the peptide must be considered in terms of its ability to present its thiol groups to the surface to the AuNPs.

Titration of Zn^{2+} and Ni^{2+} into **CCPGCC-AuNPs** and **CALNN-AuNPs** resulted in a change in the SPR absorption of **CCPGCC-AuNPs** but not in the case of **CALNN-AuNPs**. This indicates that the metal cations are able to interact with **CCPGCC-AuNPs** but not **CALNN-AuNPs**; the most likely site of interaction between a metal cation and a peptide is through the thiol groups of the peptide which leads to the conclusion that CCPGCC does not bind to the surface of AuNPs using all of its cysteine residues which leaves one or more free for interaction with the metal cations, CALNN on the other hand uses its only cysteine residue to bind to the AuNPs and so cannot also bind the metal cations.

The effect of CCPGCC upon the luminescence of modified AuNPs was found to differ depending on the lanthanide complex used to coat the AuNPs. **EuL^{a}-AuNPs** suffered changes in their luminescence properties when the peptide was present, however, **EuL^{b}-AuNPs** did not and it was for this reason, and for the slightly lower energy excitation wavelength over **EuL^{a}-AuNPs**, that **EuL^{b}-AuNPs** were taken forward for use as protein labels within cells. In addition to their interactions with peptides, luminescent lanthanide coated AuNPs were examined in terms of their interaction with protein as they were to be used as protein labels. The fluorescence and CD spectra of BSA was affected to a lesser extent when interacting with **pTbL^{a}-AuNPs** than **Citrate-AuNPs** indicating that even partial surface coverage of the AuNPs by **TbL^{a}** limits interaction with the protein which is desired since direct interaction with the peptide binding site rather than the protein is needed for specific protein labelling. Furthermore, the luminescence properties of **TbL^{a}-AuNPs** is unaffected by the presence of

BSA and that of **EuL^{b}-AuNPs** was shown to be unaffected by dispersion in cell growth media which contains a variety of protein and salts amongst other species. These experiments confirm that luminescent lanthanide coated AuNPs are suitable for protein labelling within biological systems.

The expression of GFP-4C by HeLa cells resulted in diffuse fluorescence throughout the cells which meant that the co-localisation of the AuNPs with the protein was not established. TEM studies and reflectance confocal microscopy revealed the uptake of AuNPs by HeLa cells and the presence of transfection factor Lipofectamine 2000 appeared to facilitate uptake of the AuNPs without aggregation which presents a method for treatment of HeLa cells with AuNPs. Lysis of the cells resulted in the formation of a pellet which is likely to be aggregated AuNPs and after washing this pellet exhibited characteristic GFP emission which may suggest that some GFP-4C was indeed associated with the AuNPs. The remaining cell lysate also exhibited GFP emission which is not unexpected since GFP-4C appeared to be expressed throughout whole cell whilst AuNPs may not have had access to all cellular locations and may have been taken up in too low a concentration to bind to all of the available GFP-4C.

Overall, it has been shown that luminescent lanthanide complexes **EuL^{a}**, **TbL^{a}**, **NdL^{a}** and **EuL^{b}** are suitable as protein labels *in vitro*. **TbL^{a}-AuNPs** and **EuL^{b}-AuNPs** are able to interact with BSA without their luminescence or the structure of BSA being affected and as such also have potential as protein labels. Whilst a peptide binding study revealed that peptide CCPGCC is an ideal candidate for a specific site to bind AuNPs within cells, the results obtained for the labelling of GFP bearing this motif in cells with **EuL^{b}-AuNPs** require further confirmation.

5.2 Future Work

Whilst the use of **LnL^{a}** and **EuL^{b}** for covalent protein labelling was found to be successful it may be of interest to define the degree of labelling of the protein. So far, a technique for elucidating this information has not been found, however, the use of alternative methods such as analytical ultracentrifugation may prove more fruitful. In the case of analytical ultracentrifugation, the exact number of labels per molecule may not be determined, but a close estimate may be achieved.

In order to further investigate the interactions between GFP-4C and lanthanide coated AuNPs it may be useful to harvest GFP-4C from cells and investigate its interaction with lanthanide coated AuNPs *in vitro* to confirm whether it binds in a similar fashion as the CCPGCC motif alone. Further to this, the analysis of cell lysis materials could be extended to include the characterisation of peptides associated with AuNPs in the pellets by MS to indicate whether AuNPs bind to GFP-4C specifically or are able to bind to other proteins within the cell.

Furthermore, to establish the presence of an interaction between AuNPs and GFP-4C within cells, it may be useful to refine the transfection of the cells so that GFP-4C is located within discrete cellular compartments. This would allow the location of GFP-4C to be established more accurately and, therefore, help to conclude whether any AuNPs are in the vicinity of GFP-4C. Additionally, the AuNPs could be coated in a probe able to participate in FRET with GFP-4C which would give further information about the proximity of the two species. In terms of the lanthanide coated AuNPs themselves, the lanthanide complex used could be improved in order to aid their detection inside cells. To achieve this the antenna group of the lanthanide complex could be changed to a species such as a xanthone derivative.

The use of luminescent lanthanide coated AuNPs for protein labelling within cells will also require further investigations going forward in terms of their interaction with the cell. The uptake of AuNPs by cells could be assessed accurately by using flow cytometry detecting reflectance from the AuNPs. Toxicology assays will need to be performed in order to establish the impact of treatment with AuNPs on cell viability. In addition to this the areas of the cell accessible to the AuNPs will need to be confirmed. This may be achieved by using fluorescent stains specific for cellular structures in combination with confocal fluorescence and reflectance microscopy. Additionally, further TEM studies of treated cells should be conducted to confirm the locations of AuNPs within the cells. These investigations should be carried out at various time points during and after treatment of cells with AuNPs in order to establish the transport of the AuNPs through the cell and, therefore, which proteins the AuNPs are potentially able to label. Furthermore, these experiments should be extended to a variety of alternative cell lines to demonstrate the suitability of the luminescent AuNPs for protein labelling in a range of cells.

Appendix

A.1 Material Corresponding to Chapter 2

A.1.1 Figures Corresponding to Chapter 2

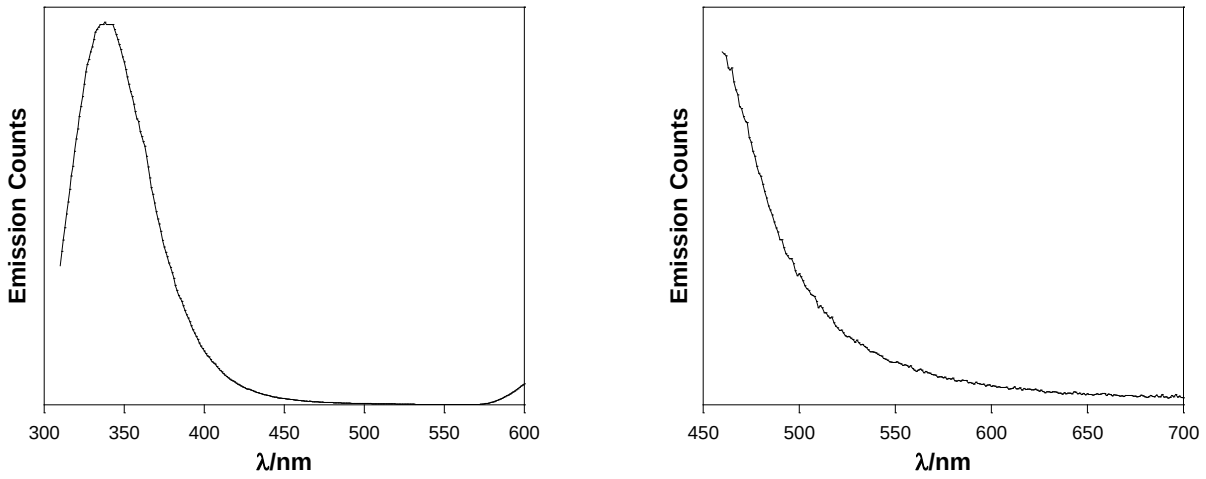

Figure A.1 Emission spectra of native BSA in aqueous solution using for emission detection a 310 nm long pass filter (left) or a 455 nm long pass filter (right). λ_{ex} = 266 nm, corrected for PMT response.

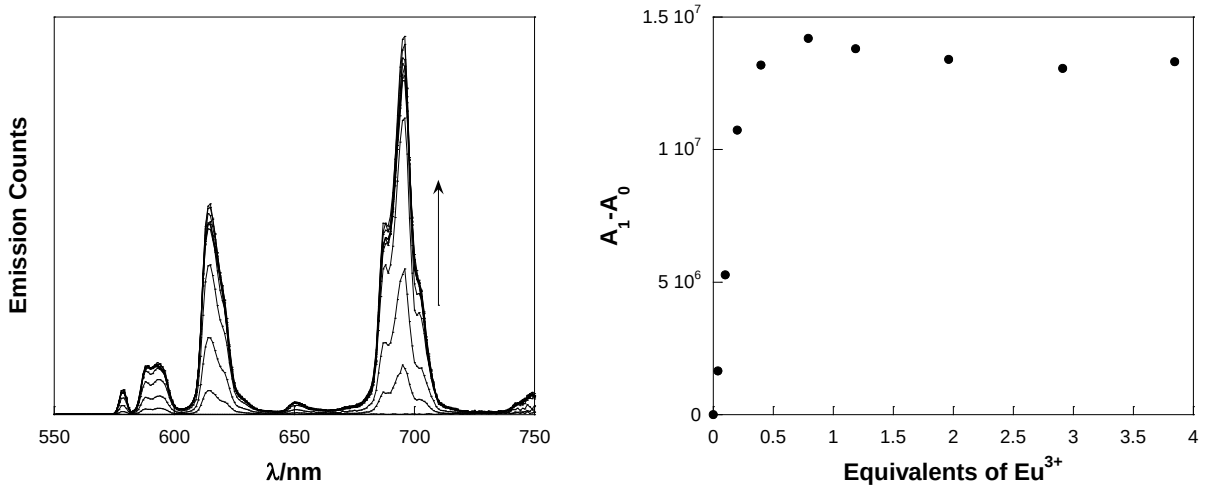

Figure A.2 Left: Emission spectra of Eu^{3+} as it is titrated into a solution of $\mathbf{H_3L^a}$. Right: Integrated emission signal of $\mathbf{H_3L^a}$, A_0, subtracted from integrated emission signal when Eu^{3+} is added, A_1. λ_{ex} = 266 nm, λ_{em} = 550-750 nm, corrected for PMT response.

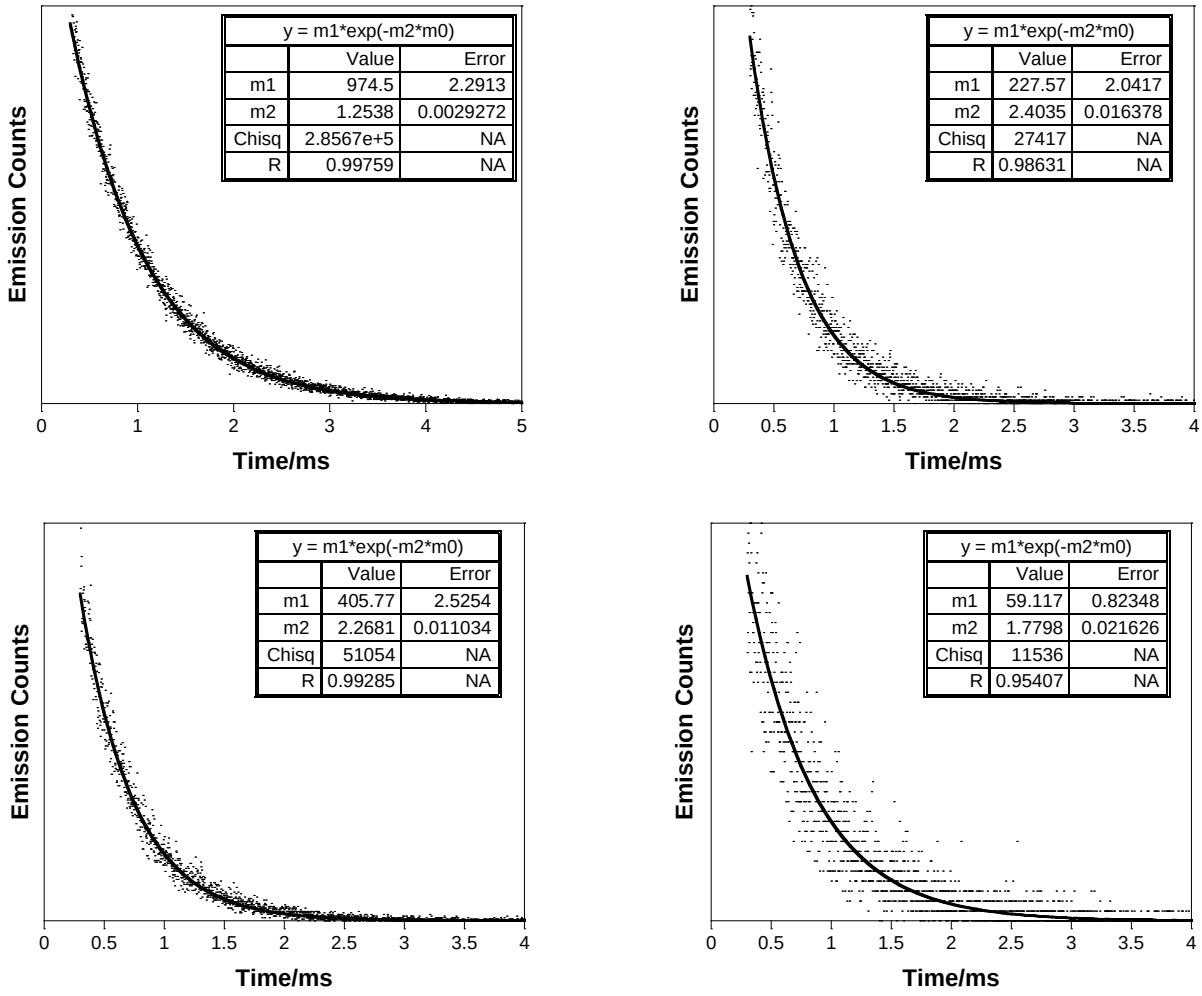

Figure A.3 Luminescence decay curves for **EuL^{b}** containing samples. In all cases λ_{ex} = 266 nm, λ_{em} = 615 nm. Top left: **EuL^{b}** in methanol; top right: **EuL^{b}** in aqueous solution; bottom left: **A-BSA** in aqueous solution; bottom right: **B-BSA** in aqueous solution.

A.1.2 Calculation of Degree of Labelling of **EuL^{b}-BSA** from ICP-MS Data

In all cases the molar extinction coefficients of BSA and **EuL^{b}** in aqueous solution were determined experimentally using solutions of each species in isolation.

A.1.2.1 Calculation of Degree of Labelling of **A-BSA** from ICP-MS Data

[Eu] measured by ICP-MS = 39.155 parts per billion = 39.155 μg L^{-1}

39.155×10^{-6} g L^{-1}/153 g mol^{-1} = 2.56×10^{-7} mol L^{-1} in submitted sample

Since 1 mL of neat sample diluted in 5 mL for analysis, neat concentration in sample is:

(2.56×10^{-7} mol L^{-1} x 5×10^{-3} L)/1×10^{-3} L = 1.28×10^{-6} mol L^{-1} in original sample

Since there is one atom of europium per label is follows that the concentration of **EuL^{b}** label in the original sample is also 1.28×10^{-6} M.

Calculated absorbance at 280 nm of **EuL^{b}**: 1.28×10^{-6} M x 1 cm x 9760 M^{-1} cm^{-1} = 0.01

Measured absorbance of sample at 280 nm = 0.15

Absorbance at 280 nm arising from BSA = 0.15 – 0.01 = 0.14

Concentration of BSA = 0.14/(42430 M^{-1} cm^{-1} x 1 cm) = 3.30×10^{-6} M

1.28×10^{-6} M/3.30×10^{-6} M = 0.39 **EuL^{b}** labels per BSA molecule

A.1.2.2 Calculation of Degree of Labelling of **B-BSA** from ICP-MS Data

[Eu] measured by ICP-MS = 19.195 parts per billion = 19.195 µg L^{-1}

19.195×10^{-6} g L^{-1}/153 g mol^{-1} = 1.25×10^{-7} mol L^{-1} in submitted sample

Since 1 mL of neat sample diluted in 5 mL for analysis, neat concentration in sample is:

(1.25×10^{-7} mol L^{-1} x 5×10^{-3} L)/1×10^{-3} L = 6.25×10^{-7} mol L^{-1} in original sample

Since there is one atom of europium per label is follows that the concentration of **EuL^{b}** label in the original sample is also 6.25×10^{-7} M.

Calculated absorbance at 280 nm of **EuL^{b}**: 6.25×10^{-7} M x 1 cm x 9760 M^{-1} cm^{-1} = 0.01

Measured absorbance of sample at 280 nm = 0.22

Absorbance at 280 nm arising from BSA = 0.22 – 0.01 = 0.21

Concentration of BSA = 0.21/(42430 M^{-1} cm^{-1} x 1 cm) = 4.95×10^{-6} M

6.27×10^{-7} M/4.95×10^{-6} M = 0.13 **EuL^{b}** labels per BSA molecule

A.2 Material Corresponding to Chapter 3

A.2.1 Figures Corresponding to Chapter 3

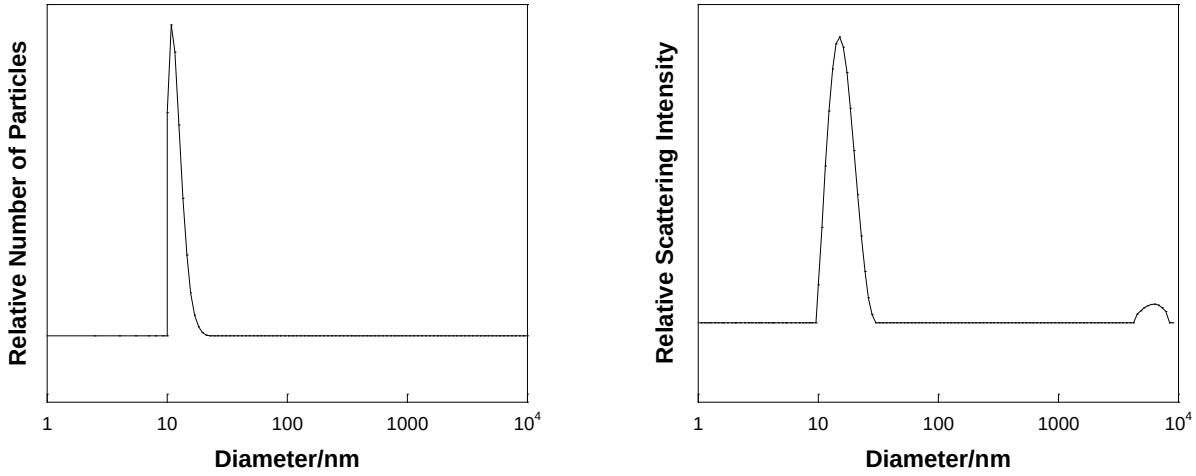

Figure A.4 DLS number (left) and intensity (right) distributions for **Citrate-AuNPs**.

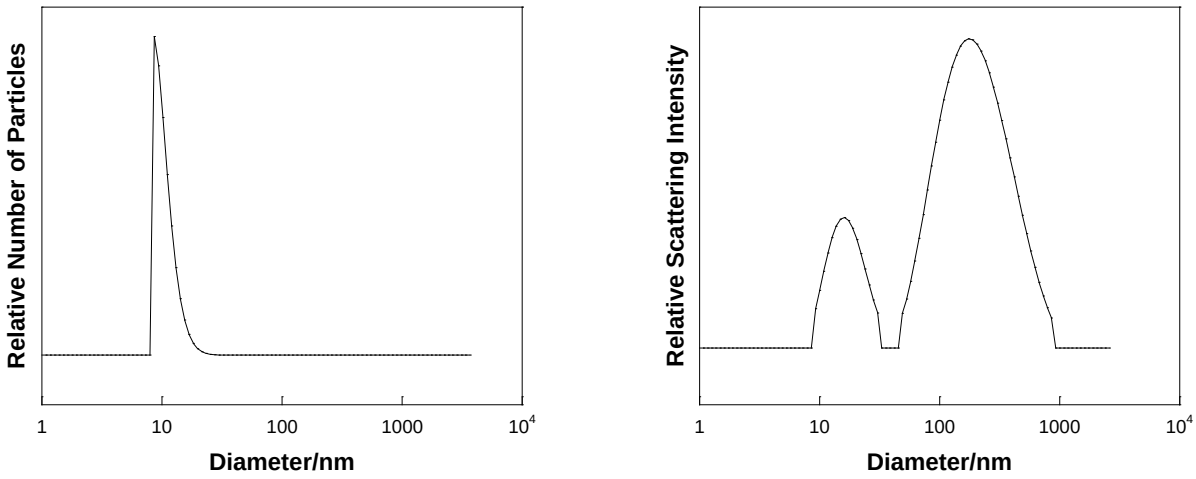

Figure A.5 DLS number (left) and intensity (right) distributions for **CALNN-AuNPs**.

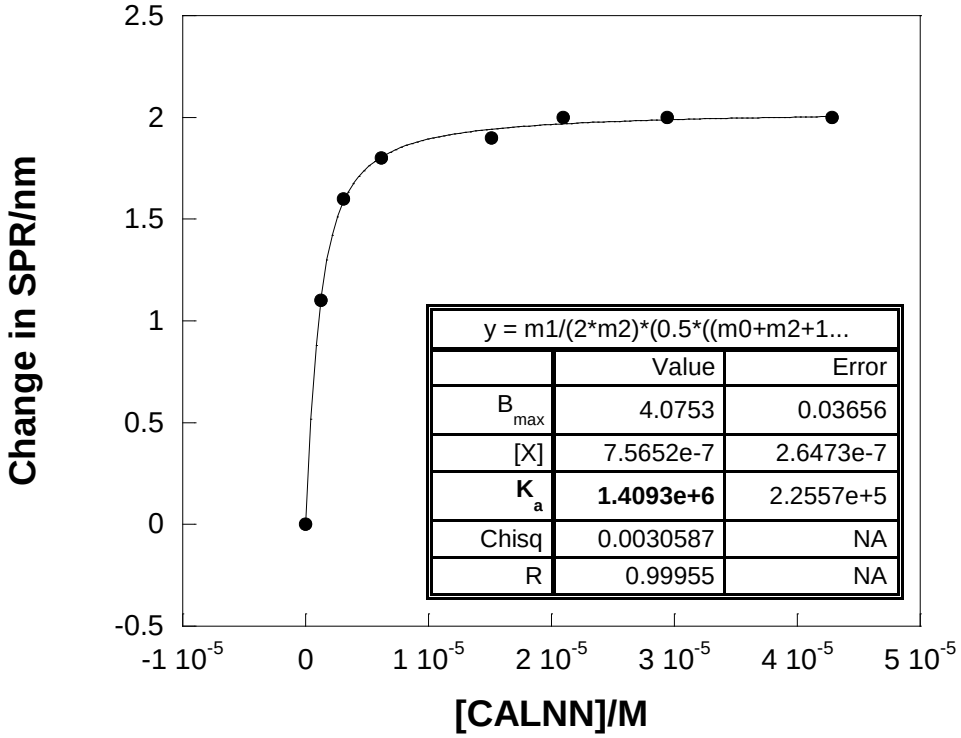

Figure A.6 Titration of CALNN into **Citrate-AuNPs** followed by absorption spectroscopy and its fit to find K_a.

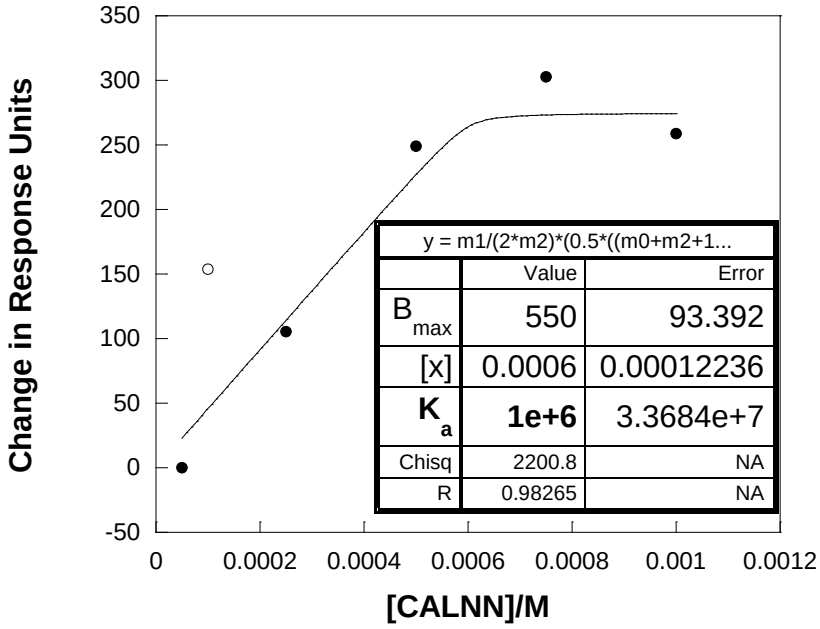

Figure A.7 Response units taken from the peak of each sensorgram as CALNN was passed across a gold chip plotted against peptide concentration and fit to find K_a.

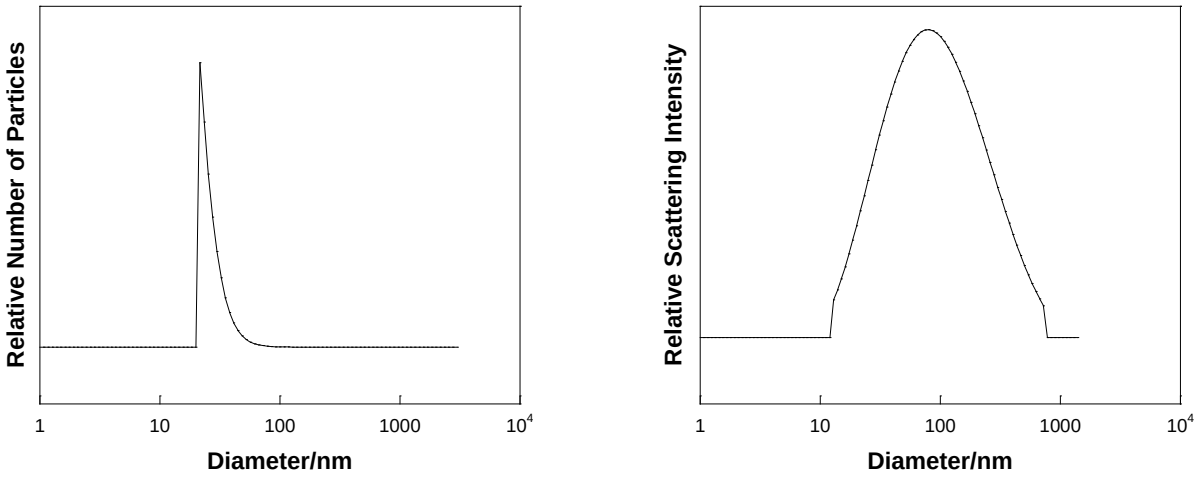

Figure A.8 DLS number (left) and intensity (right) distributions for **CCPGCC-AuNPs**.

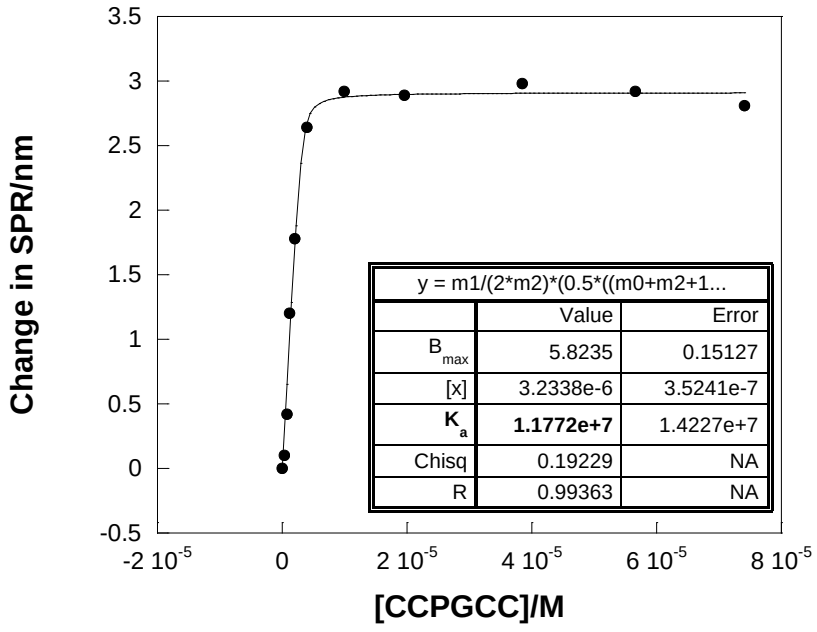

Figure A.9 Titration of CCPGCC into **Citrate-AuNPs** followed by absorption spectroscopy and its fit to find K_a.

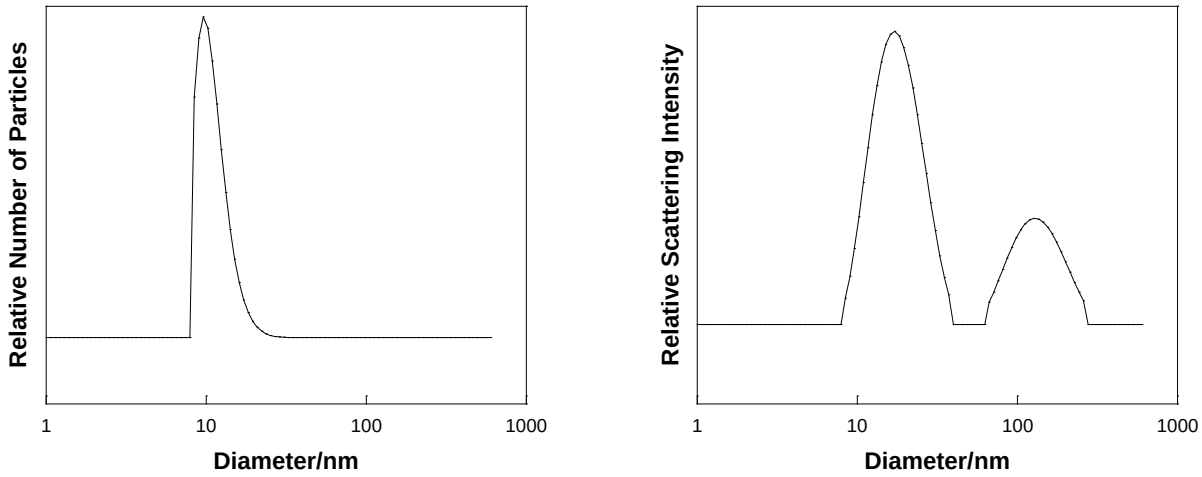

Figure A.10 DLS number (left) and intensity (right) distributions for **CCALNNCCALNN-AuNPs**.

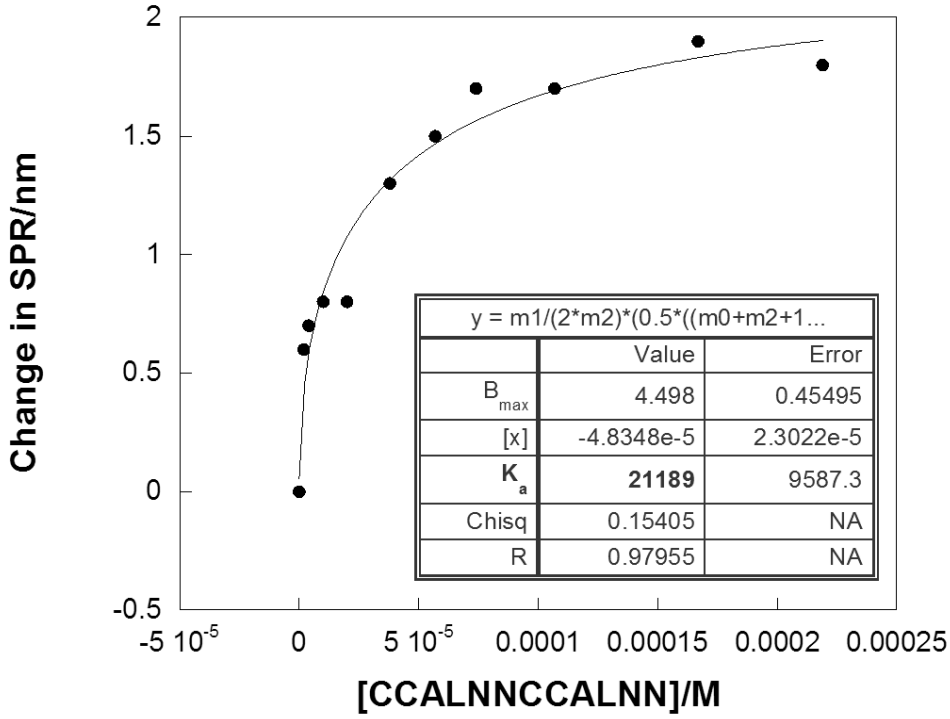

Figure A.11 Titration of **CCALNNCCALNN** into **Citrate-AuNPs** followed by absorption spectroscopy and its fit to find K_a.

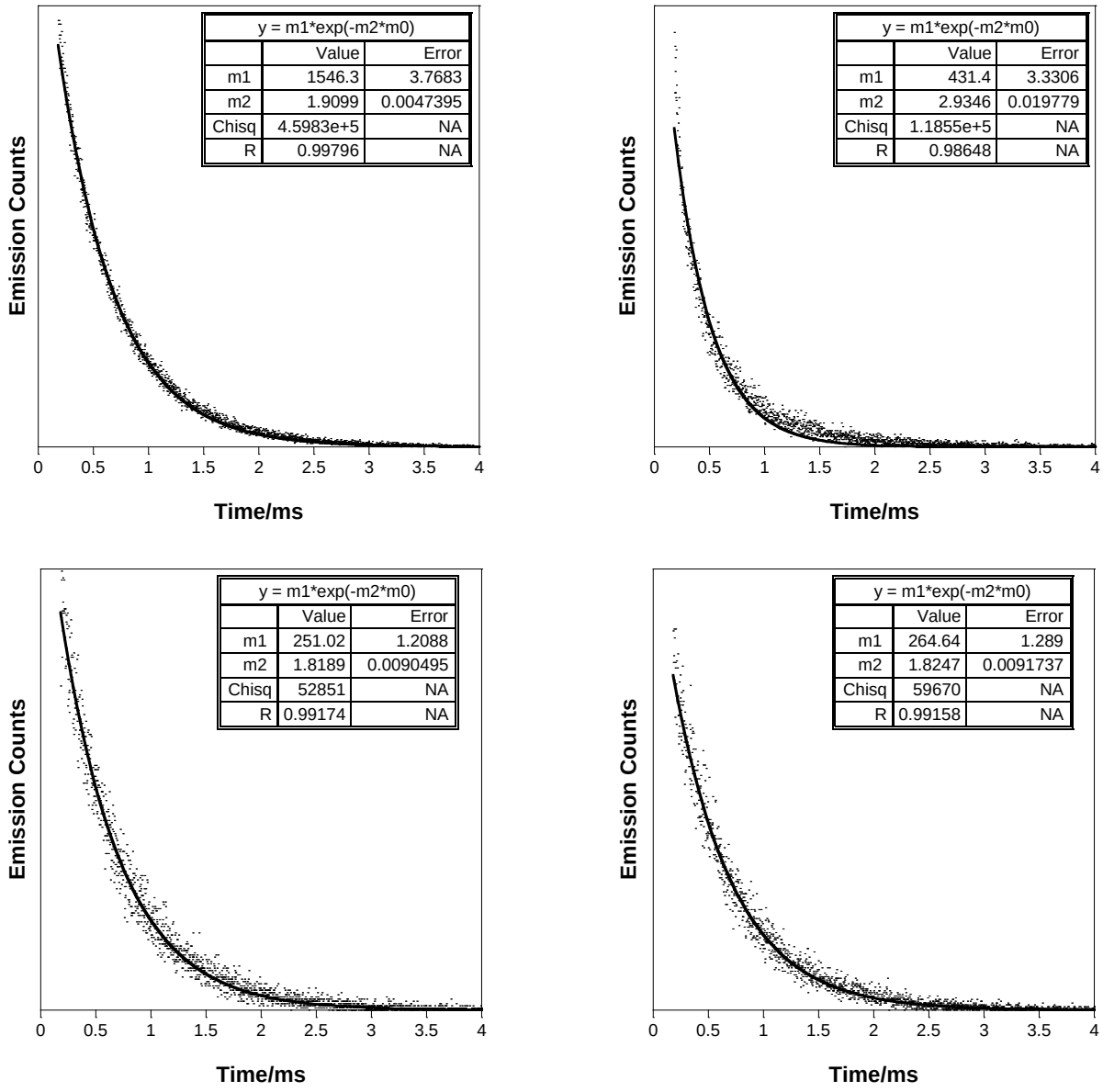

Figure A.12 Luminescence decay curves of **EuL^{a}-AuNPs** (top) and **EuL^{b}-AuNPs** (bottom) in the absence (left) and presence (right) of CCPGCC peptide.

A.2.2 Equations Corresponding to Chapter 3

$$\frac{dQ}{d[X_t]} = \frac{\Delta H \cdot V_0}{2}\left[1 + \frac{1 - \frac{[X_t]}{n[M_t]} - \frac{1}{n[M_t]K}}{\left\{\left(\frac{[X_t]}{n[M_t]}\right)^2 - \frac{2 \cdot [X_t]}{n[M_t]}\left(1 - \frac{1}{n[M_t]K}\right) + \left(1 + \frac{1}{n[M_t]K}\right)^2\right\}^{1/2}}\right]$$

Equation A.1 Equation used to in Origin 7.0 software to fit ITC data using a 1:*n* binding model where ΔH is the enthalpy change, K the binding constant, n the number of binding sites, $[X_t]$ the total peptide concentration, $[M_t]$ the total concentration of AuNPs, V_0 the effective volume of the calorimeter cell and dQ is the heat change at each addition during the titration.